The dynamic mechanical interactions associated with polyurethane baton rounds.

Atkin, Stewart Peter

THE DYNAMIC MECHANICAL INTERACTIONS ASSOCIATED WITH POLYURETHANE BATON ROUNDS

by

Stewart Peter Atkin B.Eng (Hons)

A thesis submitted to the University of Wales in candidature for the degree of Doctor of Philosophy

Department of Materials Engineering
University of Wales Swansea
Singleton Park
Swansea

DECLARATION

This work has not previously been accepted in substance for any degree and is not being concurrently submitted in candidature for any degree.

Signed..... (candidate)
Date.....6/5/02.....

STATEMENT 1

This thesis is the result of my own investigations, except where otherwise stated. Other sources are acknowledged by footnotes giving explicit references.

Signed..... (candidate)
Date.....6/5/02.....

STATEMENT 2

I hereby give consent for my thesis, if accepted, to be available for photocopying and for inter-library loan, and for the title and summary to be made available to outside organisations.

Signed..... (candidate)
Date.....6/5/02.....

SUMMARY

This thesis examines the important materials issues related to the design, improvement and biomedical assessment of baton rounds. In particular, it focusses on the time-dependent mechanical interactions between polyurethane and bone. The project initially deals with the mechanical behaviour of the polyurethane elastomers used for baton rounds. Using a variety of mechanical and environmental exposure tests, a better understanding is gained of the mechanical properties required for consistent performance. In particular, the importance of rebound resilience is identified when relating quasi-static quality control tests to impact behaviour.

The thesis then concentrates on the dynamic mechanical properties of bone, with particular consideration to the measurement of shear modulus, which has been identified as a key parameter for modelling of baton round impacts. A combination of re-analysis of previously reported data and torsional testing of bovine scapulae samples has yielded a good understanding of the shear behaviour of bone and the effect of test rate. In addition, various synthetic bone materials have been characterised, in an attempt to design a bone simulant material that could be used for impact trials. This work has established the basis for a successful simulant based on fibre composites and polyurethane foam.

The final section of the thesis comprises a brief examination of various options to design energy attenuating baton round systems that will further reduce the potential for head injury.

TABLE OF CONTENTS

CHAPTER 1 INTRODUCTION

Baton rounds, more commonly known as "plastic bullets", are used by both police and armed forces all over the world for the purpose of crowd and riot control. They are designed to act as a deterrent to violence, to protect police officers and military personnel and control and reduce the threat from violent demonstrators. Baton rounds are classed as non lethal weapons (NLW's) and are not intended to cause serious injury or death. Strict guidelines exist regarding the use of baton rounds including, for example, a no-head-shot policy.

However, accidents happen, and over the many years that baton rounds have been used by British Forces some serious and permanent injuries have occurred, including death.

The purpose of the first phase of this research project, funded by the Defence and Evaluation Research Agency (DERA), Chemical and Biological Defence, Porton Down, is to investigate the materials used in the production of baton rounds in order to gain a greater understanding of their properties. The aim of this was to then select a range of suitable materials, which could be used in the next generation of baton rounds. There would then be a more comprehensive understanding of the impact effects of these rounds, and therefore, a lower probability of serious injury or fatality.

Polyurethane elastomers were the preferred material used for baton round applications, and the first phase of this project was to concentrate mainly on investigating the dynamic properties of various polyurethanes and related polymers. Studies would also include environmental experiments to test the ability of the materials to withstand exposure to the elements such as ultraviolet light, water, and heat.

One of the initial problems with plastic bullets was a lack of understanding of how they respond under different conditions. This applied to everything from the initial material manufacture and processing, to storage, to firing, and to impact. This project aimed to investigate and gain a fuller insight into all of these areas.

Material selection with regard to both firing and injury properties was also of utmost importance. In order to ensure a snug fit in the barrel, correct biting of rifling grooves, and good accuracy the rounds needed to be as hard as possible. This was so that the dimensions could be made to higher tolerances, less allowance needed to be given for thermal expansion in the barrel and the round could move through and exit the barrel with maximum efficiency and minimum energy loss. The round would also be able to fly more smoothly through the air and have a greater degree of accuracy.

However, the harder the round, the less contact time there would be with the object it was impacting. Therefore the energy would be dissipated in a shorter time, and there would be more damage to the person it hits. Therefore, from a medical viewpoint, in order to ensure minimum casualties the batons should be made as soft as possible.

Here existed a problem between producing a round that was as hard as possible from a ballistics point of view, but was as soft as possible from a medical point of view. It was hoped that a suitable compromise could be achieved.

After considering the materials used in the baton rounds, the next step was to look at the effects of impacts onto the area of the body of greatest concern; the head. The second phase of this study commenced with a full review of published literature on the properties of bone, and concentrated on experiments conducted on human and primate bones. Strength and stiffness values were of particular interest. The review also included the analysis of a series of experiments undertaken by a DERA contractor several years ago. These experiments looked at the properties of the human skull and compared them to those of bovine scapula. The similarity found between the two sets of bone later resulted in bovine scapula being used as a physical model for baton round impact tests. However, a call came for a move from using animal bones, to the use of synthetic bone for the impact tests. The development of a bone analogue of the human skull was thought to be easier to work with and give more accurate and reproducible results.

The physical model research initiated with a search for commercially available synthetic bones from both North America and Europe. It was hoped that a suitable material could be found via this means, instead of going through the lengthy process of trying to produce a synthetic material from scratch. Following a comprehensive search, two companies were

identified as producing potential matches. Material was then ordered from both companies with the intention of testing them to identify the mechanical properties.
In parallel with the work on bone substitutes, it was deemed necessary to conduct further tests on bovine bone samples in order to obtain mechanical property values against which the synthetic bones could be compared. Strip and disc shaped samples of bovine scapula were obtained from DERA for use in a variety of mechanical tests at Swansea. The desired results were obtained. It was then apparent which behaviour the selected synthetic bones would have to exhibit in order to be considered as a human skull impact model.

Following these experiments, the same tests were then carried out on the two sets of synthetic bones and recommendations regarding their suitability were put forward. Also, suggestions for slight changes in the combinations of materials used by one of the companies, to result in an ideal candidate material, were also put forward.

During the project both physical and finite element computer models were to be looked at, with both parts being developed side by side. The physical model work being undertaken within this project, and the finite element model to be produced by Fluid Gravity, a computer modelling company who were contracted to DERA. Unfortunately, the computer modelling has yet to be completed and so some of the later results presented in this thesis can not be analysed to their full potential as no comparison with finite element modelling is yet possible.

In the final stages of the project, progression was made to study new, novel energy attenuating systems for the next generation of baton round. Several suggestions had been put forward by DERA and comments were made regarding their potential benefits. Some sample rounds had been produced and selected mechanical testing was carried out on these. Based on this, predictions were made to the impact forces and response of the rounds with different combinations of composite rounds.

In short, the purpose of this project was to gain a full understanding of the different aspects of the mechanical interactions of baton round impacts against a human head. Then using this information it was intended to develop a physical head impact model from synthetic bone to test the qualitative effects of the impact of both the current baton round, and the next generation baton rounds. Working in conjunction with DERA and Fluid

Gravity these results could also be used to help develop a computer model, giving quantitative results for the effects of impact with the human head. The results could help towards ensuring that any baton round impacts against the head would lead to as minimal injury as possible, avoiding serious injury and death.

Inevitably, as an externally-funded project, which forms just part of a larger development, there was a compromise between academic research and the requirements for DERA. Although the thesis presented here consists of several sections, there is commonality concerning the dynamic mechanical interaction between the materials involved.

Chapter 2 presents a general background and literature review to the project, covering both historical and recent developments. Chapter 3 then focuses in detail on the properties of the polyurethanes used for current baton rounds. In chapter 4, attention turns to the mechanical properties of bone, with a separate review of relevant literature and a description of the tests on bone conducted within this project. In chapter 5, a study of potential synthetic bone simulants is described. Chapter 6 contains a brief look at energy-attenuation systems, which will be the next stage of baton round development. The separate phases of the project are brought together in a concluding Chapter.

CHAPTER 2 PROJECT BACKGROUND

2.1 INTRODUCTION

Non Lethal Weapons (NLW) have been used in the United Kingdom for over 30 years. Blunt (non penetrating) impacts by a low mass projectile are a very effective way of causing short term incapacitation and help prevent aggressors from committing violent acts, particularly in riot or crowd-control situations. In the UK the NLW of choice is the baton round.

It is of utmost importance that NLW applications offer a low risk of causing serious injury or death, whilst at the same time imparting a suitable incapacitating force on the target. This has proved a very difficult balance to achieve and has resulted in the call for detailed research to be undertaken to model, both by physical means and computer modelling, the effects of baton round impacts. Of greatest risk to targets from this projectile is an impact to the head. If a head impact occurs serious injury and even death can result. Nearly all recorded deaths from baton rounds are due to head impacts.

DERA recognised in 1997 that the problem of head impacts needed serious address. A projectile that delivers sufficient force to a person's torso to induce a short term incapacitation would be highly likely to cause serious injury if the impact was received on the head, especially if no energy attenuation systems were incorporated into the baton rounds. Development work undertaken for and by DERA included gradual redesign of the baton round geometry, materials and firing system to attempt to minimise the risk of serious injury. In order to assess the performance and injury-potential of new baton round designs, there is a need for the capability to model the impact of a baton round. To look into this further a physical head impact model was required to study the effects of the low mass, high velocity baton rounds on the human skull. It was hoped that in the short term a qualitative physical model could be developed and in the medium term a computer model could provide more detailed, quantitative analysis.

Sadly any head impact models that had previously been developed were designed to focus on the effects of head impacts in automotive and aeronautical accidents. The

biomechanical interactions in these types of impacts are very different from those of baton round impact.

2.2 BATON ROUND HISTORY

As previously mentioned, the non-penetrating projectiles used in the UK are baton rounds and have been used almost exclusively for riot and crowd control situations in Northern Ireland. The earliest baton rounds were developed in the USA for the purpose of practice rounds for tear gas projectiles. These were made of wood.

In the 1950's the Royal Hong Kong Police Force began to realise the benefits of using wooden rounds in crowd control situations. They began using baton rounds made of teak with a metal core, for anti riot purposes, and this continued into the 1960's. The Hong Kong Police deployed these rounds by firing them towards the target, aiming to strike the ground ten to fifteen meters in front of the target [1]. The idea was the rounds would glance off the ground and up at the target. As the rounds were made of wood, when they bounced off a hard surface such as a road, they tended to fracture and splinter, causing serious injury on impact. During its use in the 1950's and 60's one person was reportedly killed and several major casualties resulted. This round was not considered appropriate for use in Northern Ireland.

In 1970 a similar design of round was introduced in Northern Ireland, made of hard rubber. It was used for civil disturbances, predominantly in Belfast and Londonderry. As with the Hong Kong police, the Army adopted a similar technique of bouncing the round off the ground in front of the rioters so it would bounce up and strike in the lower extremities. It was hoped that this would avoid potential impacts to the head. The projectile was meant to supply a "painful slap" to the human target from a range of 50 meters, and was hoped to discourage stone and petrol bomb throwers, but not cause serious injury. This round was highly inaccurate and unstable in flight. It also caused some fatalities.

In 1973 it was replaced by a PVC plastic bullet baton. This time the Rules of Engagement (ROE) stated the baton should not be bounced off the ground but instead, aimed and fired

directly at the torso. This round was designed to introduce new levels of improved accuracy and therefore the resulting change in ROE was hoped to reduce accidental head impacts. However over the period 1973 to 1987 thirteen deaths due to plastic bullets had been reported [2], seven of these being children. Many more serious injuries such as brain damage, eye injury, and pulmonary contusions were also reported [3].

However, it was also considered important to put into context the number of deaths from baton round impacts with the necessity of controlling riot situations. Over 50,000 rounds had been reportedly fired up to 1997 to maintain public order. A survey conducted in 1983 [4] looked at injuries caused by both plastic and rubber bullets. Of those admitted to hospital 2 deaths occurred due to rubber bullets (one of which was not included in the survey), giving about 1 death for 16,000 rounds fired. 29,000 plastic bullets were fired and 7 deaths occurred (3 of which were not included), giving a rate of 1 death for every 4,000 rounds fired.

The next round to be adopted by the armed services in Northern Ireland was the L5A5 plastic baton round, made of polyurethane. It is the predecessor to the L5A6 round which is described later in this report. The L5A5 round had a mass of 130g and measured 100 mm (length) x 37 mm (diameter) [5].

2.3 HEAD INJURY

The anatomy of the human head can be described as being comprised of five main structures. These are the scalp, skull, meninges, brain and tentorium.

- The scalp is comprised of five layers of tissue which cover the outer bone layer of the skull.
- The skull is the bone matter comprising of inner and outer tables of hard cortical bone, sandwiched by a softer, spongy, cancellous layer.
- The meninges form three layers separating the brain from the inner part of the skull. The most outer layer is the dura matter, and this lines the inside of the skull. The middle layer is the arachnoid, which is thin and transparent. And finally the third layer, the pia, is firmly attached to the brain cortex. In the

subarachnoid space between the arachniod and the pia layers, circulates the cerebrospinal fluid (CSF).

- The brain consists of the right and left hemispheres (the cerebrum), the cerebellum, and the brain stem.
- The tentorium is a fibrous partition layer that the brain partially sits upon.

One of the most important injury mechanisms with regard to head injury is that of the coup / contre coup. Three main characteristics of the brain-skull anatomy are responsible for this type of injury:

- The incompressibility of brain tissue
- The rigidity and internal contours of the skull
- The susceptibility of the brain to shearing forces.

The first two points mentioned above are responsible for contusions and haematomas (bleeding) on the brain surface. Usually in a brain injury, two contusion sites are formed. The first being at the site of the impact and is known as the coup injury. The second occurs on the opposite side of the head to the coup injury. It is caused by the moving of the brain away from the site of impact, compressing against the opposite side of the head and then, consequently, bouncing back to its original position. Both the compression and bouncing back can also cause bleeding at the suture points if the dura matter has been ripped away from the inside of the skull.

The injuries due to shearing forces can result from rapid movement or rotation of the head following, for example, a whiplash injury.

All of the injury mechanisms mentioned can result in a swelling of the brain, which can lead to a compression of critical areas of the brain stem which control cardiac and pulmonary function. These functions will eventually cease, causing death.

Three specific types of head injuries are skull fracture, diffuse brain injuries and focal injuries [6].

2.3.1 Skull Fractures

Baton round impacts to the head will commonly cause skull fracture. Many skull fractures, will occur as the primary injury, followed by direct brain damage. However, skull fracture does not necessarily mean brain damage will occur, and conversely serious brain damage can occur without skull fracture. Skull fracture can be divided into four categories [7]:

1. Linear (non-depressed) fractures, are commonly seen as hair line fractures on x-rays. Brain injury and possible haemorrhaging can occur as a result of linear fractures.

2. Depressed fractures occur as a result of a high intensity, sharp blow which then pushes fragments of bone into the meninges, and can cause tearing of the dura matter. These commonly need surgery to elevate the bone back into position.

3. Open skull fractures following the laceration of the scalp, again can lead to tearing of the dura matter, the brain becoming visible and the seeping out of CSF. These wounds are particularly nasty as they can easily allow infection to enter.

4. Basal skull fractures are fractures that occur at the base of the skull, deep inside the head. These cannot be as easily diagnosed as the other three mechanisms above, and again can lead to infection, this time from inside the body. One possible way of confirming this type of fracture is if CSF begins to leak from the nose or ears.

The face, and particularly eyes, are very vulnerable to damage from blunt impacts. Loss of sight can occur due to fractured bone piercing the eye, the retina becoming torn from the back of the eye, and sometimes a crushing of the eye ball. Reduced levels of vision can also occur if eye muscles and nerves become trapped or pinned in a fracture.

There are further potentially life threatening injuries to the head area such as damage to the cervical spine and the thyroid cartilage. The cervical spine surrounds and protects the spinal cord. If this is damaged paralysis and sometimes death can occur. If the thyroid cartilage is crushed, the throat tissues will swell, leading to inhibited breathing and possible suffocation.

2.3.2 Diffuse Brain Injuries

This occurs following a rapid movement of the head which causes significant interruption of brain activity throughout most of the brain. Two main types of diffuse brain injury are 1) Concussion and 2) Diffuse axonal injury (DAI)

Concussion, following a head impact, is the temporary loss of neurological function. This may or may not be associated with unconsciousness following the impact and usually leads to no permanent damage.

DAI is also known as brain stem injury. This is characterised by a comatose state and can last, days, weeks or even indefinitely. This type of injury results mainly in widespread microscopic damage that is inoperable. Recovery can occur but may never be full.

2.3.3 Focal Injuries

Focal injuries occur in a relatively localised area, but are characterised by macroscopic damage and are made up of contusions, haematomas and haemorrhages. Contusions occurring in the cerebral region are typically those of the coup/contre coup genre, described earlier.

Intracranial haemorrhages can vary greatly in size, location and intensity of bleeding, and typically occur in either the meningeal or brain regions.

Lacerations of the brain as well as haemorrhaging are the tearing of brain matter. If this happens there is little chance of recovery from the injuries.

2.4 HEAD IMPACT MODELS

Listed below are various head impact models that existed in 1997, when DERA started their initial search for a suitable model to assess the results of baton round impacts to the human head.

a) Human volunteers

For certain types of head impact, human volunteers have been used. An example of tests where human volunteers have been used is when researching head impacts from contact sports such as boxing. Obviously the levels of injury inflicted, and consequently studied, were very low. It would be most ideal, but obviously not possible, to use live humans for baton round impact research due to the intense and possibly fatal results.

b) Human cadaver models

Many studies of head impacts using human cadavers have taken place over the years. These have involved tests on full, complete cadavers, skulls, or material-filled skulls. The vast majority of testing has been conducted within the automotive industry [8] to study head injuries during crashes. This is, unfortunately, not particularly representative of a baton round impact (as previously mentioned).

Also, there exists a relative difficulty in gaining possession of human cadavers for testing. The majority of cadavers used have been from elderly and infirm individuals, however the majority of baton-round fatalities that have occurred follow an impact to young skulls. It is thought that an impact to a child's head would be worse than an adult's, and is known that the mechanical properties change with age. This is due to a change in the balance of collagen and mineral in the bone. Therefore, tests on cadavers from children would be useful to gain more comprehensive comparisons of bone properties with age.

Many of the studies undertaken use embalmed cadavers, which also alters the mechanical properties of the tissues. And other tests involving skulls or material filled skulls use skulls that have been dried, not fresh wet bone [9-11]. Dry bone is much more brittle than wet bone.

c) Animals

Animal models have been used in the past to predict brain injury from head impacts. Primates have the closest similarity in skull shape and design to humans. However, bone properties have been shown to vary considerably from primates to humans, so the use of this type of model for the purpose of blunt trauma testing is limited and considered too dissimilar to the human skull to be accurate. There are also important ethical issues in using animals for this type of testing.

d) Physical models

Physical impact models can be divided into two categories:

1) Anthropomorphic dummies, which are primarily used for crash assessment in the aeronautical and automotive industry.
2) Material filled shells which are used to better understand injuries to the head.

The crash test dummies are made of a robust plastic with metal inserts. They are a similar weight to humans and are filled with many pressure-, force- and other electrical sensors to model impacts throughout the body. Whilst they are an invaluable modelling tool in the automotive and aeronautical industry, their suitability for modelling low mass, low momentum and high velocity NLW impacts, is doubtful. During car and aircraft crash testing the dummies impact, at a relatively low speed, with a large, high momentum, immovable object and are not designed for the type of impact associated with baton rounds.

Many head impact models have involved the use of a material filled shell [12]. They generally have provided qualitative information about the movement of fluid in the shell, following a low speed blunt impact, and compared this to the effects seen in human head impacts.

The problem with this type of model is the unrealistic relating of the material in the shell to the inside of the human skull. To match the mechanical behaviour of the biological tissues of the human head would prove to be extremely difficult. These models can be, however, useful for qualitative analysis of injury mechanisms.

e) Computer models

Due to a continuous increase in both speed and power of computer systems, the possibilities that can be reached by use of computer models are much greater than ever before. Many researchers have used computer models (normally based on finite element methods) to predict injury levels from head impacts. Once again the vast majority of research into head impacts has been undertaken within the automotive and aviation industry.

Finite element models allow many complex shapes and structures to be represented by dividing the structure into individual, easily manageable elements, then predicting how they relate to each other under various conditions (such as during an impact). They allow both space and time factors to be treated individually.

However, biological materials are particularly difficult to model due to the fact that they are anisotropic, non linear, inhomogeneous and strain rate dependent. Due to this, none of the models developed to date provide any accurate quantitative information, especially that can be related to baton round impacts. Also, due to the complexity of a large deformation, such as in skull fracture, that is strain rate dependent and non linear, the computer model codes would have to be very specialised.

The impact models that do already exist, generally use one of three processors to model the events. These are: Lagrangian, Eulerian, and Arbitrary Lagrangian Eulerian (ALE).

Lagrangian processors are used mainly for modelling behaviour in solids. Each element always represents the same piece of material and they move with the movement of the material.

Eulerian processors have a grid which is fixed in space, and the material can flow through the elements. It is possible for more than one material to flow through any one element at the same time. This type of solver is used primarily for modelling behaviour of liquid and gas.

Arbitrary Lagrangian Eulerian (ALE) combines both types of processor techniques listed above. This is useful for modelling the interaction between solids and liquids/gases.

Some of the models that have been developed vary in complexity from models that are relatively simple, such as fluid filled shells, to 2 and 3-D complex geometry models. The most common model is based on 2-D shapes. This is easier to develop and involves a great deal less complexity and computing power than 3-D models. 3-D models are usually produced following the development and understanding of 2-D behaviour.

One potentially useful model to DERA for modelling brain injury associated with baton round impacts has been produced by Wayne State University, Detroit, Michigan, USA. The model was constructed over several years by Ruan et al [13] from the university's Bioengineering Centre. It uses a 2-D configuration and maps the interior of the head, including membranes and others internal structures with varying mechanical properties. DERA contacted the university to enquire about the possibility of using the model, but, partly, due to associated costs, it was decided not to follow this route.

Many modellers have succeeded in modelling the internal structure of the head, with varying degrees of accuracy. Dimasi et al [14] modelled the internal structure of the head using multiple layers of material with different properties. Also, by using Computer Tomography (CT) imaging Bandak et al [15] were able to collect both geometric and density characteristics of the skull, and convert this from the 2-D CT images into a 3-D structure.

However, combining accurate modelling of the head with the effects of an impact from NLW applications is highly complex, requiring a great deal of time and expense to research and develop. For this reason DERA have focussed on the production of finite element models that predict skull fracture and do not (yet) address brain injuries.

2.5 BOVINE SCAPULA MODEL

A physical model for studying baton round impacts was developed by the Trauma and Surgery group of CBD at Porton Down. This model was developed following work conducted by Professor David Taylor and J.S. Whamond of the Royal College of Surgeons for Trauma and Surgery, CBD, Porton Down [16]. Their work investigated the possibility of using bovine scapula as an analogue the human skull.

It had previously been identified that should a baton round impact and fracture either the frontal or temporal regions of the skull, death was more likely to occur than if an impact was sustained on any other region. To simulate both these regions of the skull required a relatively large area of flat bone which has as similar a structure and properties to the human skull as possible.

The study carried out by David Taylor compared the biomechanical properties of both wet (fresh) and dry bovine scapulae with wet (fresh) and dry samples of human skull. Analysis of the findings, and further information regarding this study can be found later in this report. It was found that bovine scapula was likely to be a good analogue in studies of blunt impact to the human skull for all regions except the temporal region. In this area it would underestimate the risk of damage due to the temporal regions more significant weakness in comparison with the rest of the skull.

The bovine scapulae model was consequently developed and the test program initiated. Samples were prepared for testing by embedding the bovine scapulae in ballistic gelatine. Two scapula samples were embedded side by side in each gelatine block which therefore allowed two sets of results to be obtained from each block - one per scapula. The gelatine blocks measured approximately 34 x 50 x 15 cm. The layer at the point of impact was then reduced to approximately 5mm thickness to give a more realistic comparison with the soft tissues of the human head. The impactor initially used for the program was an aluminium cylinder of the same diameter of the baton rounds (37mm). It is important to note that these tests provided only a qualitative insight into the risk of skull fracture from baton round impacts. Each scapula was then assessed after impact and graded on the type of impact, i.e whether fracture occurred or not, and the type of fracture present.

However, an impact sustained to the head would generate both stress and shear waves, which would be likely to induce the coup/contre coup injuries previously discussed. These effects were not able to be considered or measured by the scapulae model so a simple finite element computer model was developed [17]. The model considered a cylindrical impactor, colliding with an infinitely wide isotropic plate, and not a plate of varying thickness, stiffness and which was anisotropic (as the scapulae were).

The model showed the expected coup/contre coup style injuries due to areas of high strain on both the top and bottom surfaces of the model - as seen in head impacts. The areas of damage were limited to circular regions slightly larger than the diameter of the impactor. At higher impact velocities the concentration of strain under the perimeter of the impactor would increase and lead to a shear plug formation. This was similar to the effects observed in the physical tests, although a non-failing material model was used. Therefore it was not possible to measure skull fracture or crack initiation and propagation.

2.6 SUMMARY OF IMPACT MODELLING

It was clear that neither a physical or computer based model, alone could accurately predict the effects of NLW blunt impacts to the human skull. What was deemed necessary was a parallel development of both types of model. The physical model would be able to provide a better understanding of skull fracture, whereas the computer model would be able to predict brain injury from the stress waves produced from an impact.

The bovine scapulae model had proved useful but inconsistent. Bovine scapulae is a biological material, requiring suitable facilities in which to store and test it. Also, as with all biological materials, there would always be an inherent variability between samples. Further problems were to arise from the difficulties in obtaining scapulae due to the "beef on the bone" ban and issues relating to BSE. It was therefore recommended that a non-biological analogue of human cranial bone was to be researched and developed. The analogue was required to have the appropriate high strain rate properties of cranial bone, and preferably the ability to be produced in a spherical shape similar to the human skull, instead of being flat, as with the scapulae. This problem resulted in the initiation of the second part of the project outlined in this thesis.

The computer modelling problem was forwarded to Fluid Gravity, a specialist computer modelling firm who worked in conjunction with both DERA and Swansea University to develop an accurate simulation for baton round impacts. The model was designed to look at the stress distribution as a function of time in the skull material following a baton round impact. Combined with a fracture model, the points of highest stress and strain could be used to predict where, when and if fracture would occur. Results from the work undertaken at Swansea, which are contained in this thesis, were forwarded to Fluid Gravity to aid them in the development of the computer model.

2.7 BATON ROUND MATERIALS SELECTION

At the beginning of this project the baton round used by the police and armed forces was the L5A6 round. The project was initiated with the aim of investigating materials-related aspects of the L5A6 round and the next stage of development, the XL21 round. This work arose following some previous testing, carried out at Swansea [18], which highlighted significant consistency irregularities of the L5A6 rounds. The problems warranted the attention to materials and manufacturing consistency to prevent similar occurrences in the XL21 development.

In an attempt to overcome some of the problems relating to the L5A6 round, in the XL21 development, a fairly wide ranging examination of the material options for the baton round was commissioned.

The L5A6 rounds were made from castable polyurethane. Although this gave reasonably good performance, one of the main problems highlighted was a variation in properties between different batches of plugs. These properties were also seen to gradually vary with time. The most critical property to be affected was that of stiffness. As the stiffness of the round increased, the firing characteristics changed. The force from the explosive charge on firing had less effect on the expansion of the round in the barrel. Therefore the biting of the round on the rifling grooves in the barrel was less. This led to a decrease in the frictional force, causing exit velocity from the barrel to be increased, and the round accuracy to be reduced. Both effects seen lead to a greater chance of injury on impact.

To improve the consistency, a review of the choice of plug material was undertaken. Also, thought was given to the size, weight and exit velocity of the rounds as well as an investigation into the consistency of the explosive charge.

The materials selection process was designed to look not only at the mechanical properties of possible candidate materials but also the ease of manufacture and the shelf life stability. It was intended, following this part of the work, to focus on a small number of the most suitable candidate materials. Trial rounds were then made from these, with mechanical characterisation and firing trials to follow.

2.7.1 Property Requirements

The following shows the initial proposed specifications for the XL21 baton rounds:

1.	Projectile mass	95g
2.	Muzzle velocity	78 m/sec
3.	Muzzle energy	285 Joules
4.	Diameter	37.49 mm
5.	Maximum length	99 mm
6.	Colour	Black
7.	Hardness	IRHD 80-90 (Approx modulus of 30 MPa)
8.	Resistant to fracture on impact	
9.	Operating temperature	-21°C to +46°C
10.	Non-toxic	
11.	Crimped end closure, preferably with no sealant	
12.	Resistant to high gas temperatures on firing (typically 1500°C for 0.1 sec)	
13.	Shelf life	3 years.

Based on both the criteria above and experience with the L5A6 plugs, a list of important material criteria was specified. It was noted that some criteria were more critical than others, so priorities became necessary regarding the relative importance of each one.

2.7.1.1 Material Density

Due to the size specifications of the XL21 rounds and a required mass of 95g, the minimum allowable density was calculated to be $0.87g/cm^3$. It was decided that to allow for materials of higher density and, yet, match the same criteria, either the plug length could be reduced or a central region of the cylinder could be given a smaller diameter. This would be possible providing there are two driving bands, one at each end of the round, that are 37.49mm in diameter to ensure correct sizing in the barrel.

It was calculated that a sensible maximum density to set was of $1.4g/cm^3$. This was set to accommodate all reasonable shape variations, and the material density range of $0.87g/cm^3$ to $1.4g/cm^3$ encompasses virtually all solid polymers [19]. Therefore no major restrictions are placed on choice of material.

2.7.1.2 Colour

The rounds were specified to be black in colour. No problems could be foreseen as most polymers could be supplied in this colour, some being "off-the-shelf" while others would necessitate a mixing process to incorporate a black pigment - usually carbon black. If a mixing process was necessary some concerns were displayed over reproducibility, although the carbon black pigment would have the advantage of reducing any likely property changes due to UV exposure.

2.7.1.3 Stiffness

Stiffness of the rounds is considered to be the single most important factor. This is for two reasons. Firstly, it effects the consistency and accuracy on firing, and secondly, effects the severity of impact.

When a baton round is fired, an explosive charge at the rear of the round is ignited. The rapidly expanding gases of the charge exert a compressive force on the round, causing it to expand laterally in the barrel. The expansion causes the round to bite against the rifling grooves inside the barrel and as it moves down the barrel, to spiral. If the round is not stiff

enough the expansion will be too excessive, and cause the round to increase friction against the side of the barrel, reducing muzzle velocity. In extreme cases the expansion could cause the baton round to jam in the barrel.

To compensate for a less stiff material it was thought possible to reduce its diameter so that the extra expansion on firing could be offset. This however, could lead to potential problems if the stiffness of rounds varied even slightly, which would in turn effect the degree of expansion. Sometimes it may not be sufficient, on other occasions it may be excessive.

It was therefore decided that for the most reproducible firing, the stiffer the material the better.

As far as the influence of stiffness on injury levels is concerned, the opposite is true. The stiffer the round the more severe the impact injuries would be. The best information regarding baton round impacts at the time suggested that an impact to the abdomen has a timescale of about 3 ms and causes an "acceptable" level of injury. An impact to the head however, has a timescale of impact of about 1ms and can exert much more serious levels of injury. Using calculations from the theory of Hertzian impact of an elastic sphere (the baton round) onto an elastic body (the head) [20], and based on experience of the L5A6 round, it was decided to set a nominal level of plug stiffness of around 30 MPa. Rounds of higher stiffness would still be reviewed as an increase in injury levels due to a stiffer round could be acceptable if the round was so much more accurate that the chances of a head impact occurring were significantly reduced.

2.7.1.4 Impact Toughness

This criteria simply says that the candidate material should not break up on impact with a hard surface, and not leave any sharp edges. Therefore the material should have high toughness under impact over the suggested temperature range.

2.7.1.5 Temperature effects

Operating temperature of the XL21 round was set between -21°C and +46°C. If the material undergoes any changes in stiffness or dimension over this temperature range,

then the firing characteristics would be effected. Stiffness changes can be characterised by the Heat Deflection Temperature (HDT), which is the temperature at which the stiffness is reduced to half its ambient value. It was decided that this parameter would give a good indication of whether a change in stiffness with temperature would be a problem.

With regard to dimensional changes, this would be determined by the materials thermal expansion coefficient. This figure was therefore needed to be as small as possible. The thermal expansion coefficient of polyurethane is 150 x 10^{-6} /°C, which is one of the highest values found in polymers. As this material was already being used successfully within the mentioned temperature parameters, it was considered unlikely that any polymer in contention would have too high a value. However, if a material with a lower value could be found it was thought it would be an advantage and lead to greater consistency when firing.

2.7.1.6 Toxicity

Material toxicity was also a potential hazard. Both operators and targets of the round should not be put in danger of toxic gases should the rounds be, for example, burnt in a fire.

2.7.1.7 High temperature resistance on firing

When the rounds are fired, the explosive charge igniting can lead to temperatures up to 1500°C being reached. These temperatures however only last for a fraction of a second, and experience from the L5A6 round showed negligible levels of degradation. The end caps used were made of low density polyethylene, which is one of the least temperature resistant polymers, and were not unduly affected by the firing, so this was not a problem of great concern.

2.7.1.8 Resilience

If the round were to be fired and strike a solid object, such as a wall, the rebound resilience would ideally need to be kept low, to avoid potential rebound problems.

2.7.1.9 Shelf Life

Over time, properties such as stiffness and dimensions were required to be as consistent as possible, both between individual rounds in the same batch, and from batch to batch. This also had to be true for rounds from the same, and different suppliers, and also when in storage for up to three years.

2.7.1.10 Manufacturing

In total, five possible routes of manufacturing were considered. These were casting, injection moulding, machining from commercially supplied rod, extrusion from granules followed by machining and compression moulding. Casting was the method used for the L5A6 baton rounds and was relatively simple. However, to achieve consistency care had to be taken over uniform mixing, temperature distributions and avoiding bubble formation.

Injection moulding would produce good consistency but there was an issue over the ability to successfully injection mould the relatively thick baton round, without generating voids or sink marks on cooling. Machining would also ensure high levels of consistency, as long as the selected material was available in rod form. Extrusion could be used if the rods were not available, but consistency would be reduced slightly. Compression moulding could be used for non castable or injection mouldable rubbers.

2.7.1.11 Cost

A specified cost of £2.50 per plug, including both material and manufacturing costs was set.

2.7.2 Candidate Materials

Firstly, it was decided to attempt to avoid so called "trade named" materials that were only available from a single supplier. This would mean that any problems relating to sudden changes in materials availability could be avoided. However, nearly all commercially available polymers are trade names, and the properties of two supposedly identical polymers from different manufacturers could be very varied. Due to, for example, degree

of branching, crystallinity, and additives. Bearing this in mind it could be seen that tight specifications would need to be produced for material and baton round production.

The materials that were considered are:

Polyurethane
Conventional rubbers
Thermoplastic elastomers
Ethyl vinyl acetate (EVA)
Plasticised Poly vinyl chloride (PVC)
Low density polyethylene (LDPE)
Medium density polyethylene (MDPE)
Ionomers
Polypropylene (PP)
PTFE
PVDF
Nylon 11
Nylon 12
Acetal
ABS

All other materials were either too stiff or not tough enough, and were therefore rejected.

Following classification of the fifteen polymers, and research into which ones met the necessary criteria, it was decided that only nine were suitable for continued investigation. These were: Polyurethane, TPE, EVA, LDPE, MDPE, PP, Nylon 11 and 12 and ABS.
The others were rejected for reasons to do with consistency of moulding, density and stiffness too high, material cost, impact strength too low, and poor temperature performance.

The nine materials selected for further investigation were split into two types: Softer elastomeric materials that would need to be cast or moulded, and harder thermoplastic materials which could be machined from extruded rod. It was thought that the best consistency could be achieved with the harder thermoplastics, although a doubt existed

over the potentially unacceptably high stiffness levels of these materials. It was decided to produce trial rounds and then note their performance during firing trials, before discounting them.

2.7.3 Firing Trials

Following the initial material selection, plugs were produced from ABS, Acetal, Polypropylene, and a Nitrile Rubber. The firing trials were conducted at DERA, Porton Down over a range of low, ambient and high temperatures. This was primarily to test for expansion in the barrel and if the accuracy was consequently affected, and to see if the rounds would survive an impact without fracturing.

The tests showed that the stiffer rounds did indeed exhibit greater firing consistency and accuracy, as expected. However, only two materials survived all the tests: ABS and medium density polyethylene.
Throughout this program, work was also being conducted by DERA to characterise head impacts using the scapulae models previously discussed. The aim was to better understand the effects of head impacts and assess what were acceptable levels of injury, following baton round impact. Time scale of impacts could be measured, and a clearer idea of maximum allowable levels of plug stiffness could be ascertained.

To help answer the question of acceptable material stiffness high strain rate tests were conducted on cylinders of the stiffest and least stiff materials in contention (acetal and polyurethane respectively). These test were performed at strain rates of 5.5×10^{-3} s^{-1} and 9 s^{-1}, with the aim of assessing the strain rate sensitivity of the materials.

The tests showed that the variation of stiffness with rate for both materials was not great and that the acetal was more reproducible than the polyurethane. From these results, and other modelling work being conducted by DERA it was deemed that the stiffness of the acetal rounds was too high, and subsequent modelling defined the maximum baton round stiffness to be set at about 50 MPa. With this in mind, the materials selection program was forced to shift away from the harder thermoplastics (as they all had unacceptable levels of stiffness) and focus on the softer elastomers.

Therefore, only four materials were left in contention. These were: polyurethane, TPE, EVA and nitrile rubber. Plugs were manufactured from each of these materials and further material characterisation was conducted. The tests that were performed were:

Compression tests on unconditioned rounds

Dimensional changes on rounds conditioned at -10°C and +50°C

Compression tests on the conditioned samples

Water absorption rate at room temperature

Rebound resilience

2.7.4 Summary of Softer Material Tests

The results of the tests showed that there would definitely be advantages in moving from polyurethane to one of the other three elastomeric materials. Principally, these benefits would come in terms of greater consistency which were due to both the thermoplastic nature of TPE and EVA, and also in their slightly higher stiffness. The TPE and nitrile rubber in particular showed much less variation of properties and dimension with temperature than the polyurethane.

One effect that was observed in the polyurethane and thought to be of benefit was as the temperature rises, the plug softened and expanded in the barrel, giving greater friction on firing. However, with an increase in temperature, the explosive charge exerted more force on the round when fired. These two effects were seen to offset each other, but in a fairly non reproducible fashion.

Despite the advantages found in the three new materials, there remained some significant drawbacks. The nitrile rubber failed low temperature attrition tests and there were doubts over its batch to batch reproducibility. With regards to the EVA it was seen to have the largest variation with temperature and its density was so low that problems with plug design became apparent. Due to this, both materials were shelved, leaving TPE as the only alternative to polyurethane.

The only problem posed by the TPE was of a very high rebound resilience, but work could have been done to alleviate this. It was finally decided to continue working on the TPE option for possible future use, but not to use it for the XL21 rounds.

After these tests were conducted a new thermoplastic polyurethane emerged as the strongest contender, over the L5A6 polyurethane. This was to be produced by PPL (Polyurethane Products Ltd), and at the start of this project a large batch were already being manufactured. In addition to this a large number of thermosetting polyurethane plugs were also being produced by an alternative supplier (Marbill). It was thought that the PPL rounds would enable an ironing out of the previous inconsistencies due to it being made of a thermoplastic. It was considered that with carefully controlled manufacturing the Marbill rounds could be as consistent as those from PPL, but it would be more difficult to achieve.

Further testing of both PPL and Marbill rounds was commissioned, which is the point at which this project began.

CHAPTER 3 PROPERTIES OF POLYURETHANES FOR BATON-ROUND USE

3.1 INTRODUCTION

This phase of the project was conducted primarily to gain a better understanding of the important materials properties required for polyurethanes for baton rounds. One of the most important aspects of this relates to the stiffness of the round, and how it varies with loading rate. There is a requirement for a minimum stiffness in order to attain good firing accuracy and reproducibility. Conversely, there is a maximum stiffness allowable in order to prevent unacceptably injurious impacts. This necessarily leads to a balance between these two requirements for optimum performance. One problem, however is that the stiffness is generally tested at low rates, whereas the conditions on firing impart much faster loading, and those on impact can be even faster. There was therefore a need to investigate these effects more fully, as well as the related effects of temperature. This phase of the study involved some in-depth testing of the dynamic behaviour of several different types of polyurethanes, both thermosetting and thermoplastic. This also generated further materials data to be used for finite element modelling.

Another aspect that was studied in depth within this second phase was the effect of long-term storage, in particular the effects of prolonged elevated temperature, UV and water exposure. Encouragingly, this work showed that the polyurethanes in question were all reasonably stable.

3.2 BACKGROUND

3.2.1 Polyurethane Systems

A polyurethane polymer can be described as a material containing, amongst other chemical groups, a repeating urethane group. The urethane group is shown below in Fig 3.1.

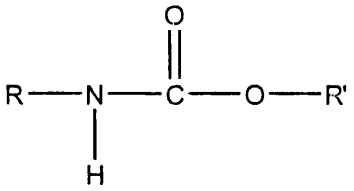

Fig 3.1 A urethane linkage

The urethane linkage can either be produced by means of addition polymerisation or condensation polymerisation. The most important reaction is that between a diisocyanate and a diol, as shown below in Fig 3.2.

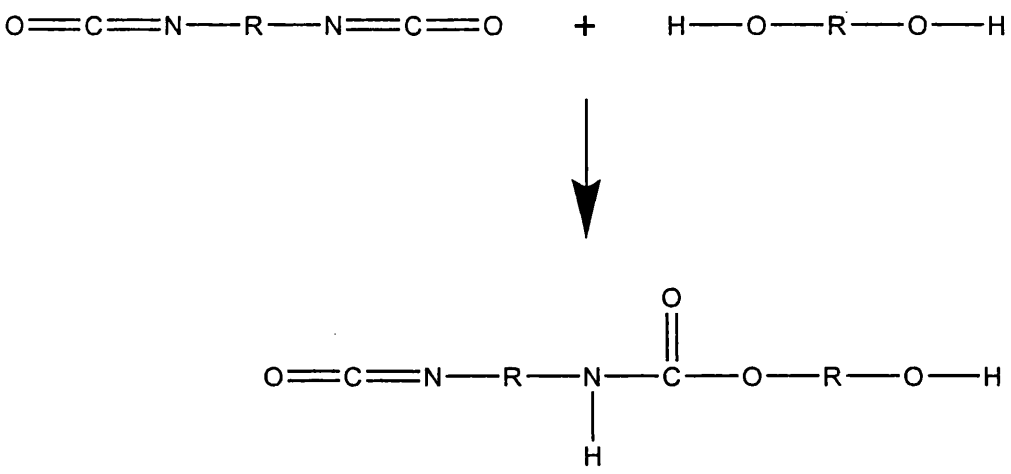

Fig 3.2 The Reaction Between a Diisocyanate and a Diol to Produce a Urethane Link

There is a wide range of polyurethane materials currently available [21], and they can be categorised as follows:

Linear polyurethanes

Castable polyurethanes

Millable polyurethanes

Thermoplastic polyurethanes

Cellular polyurethanes

Sprayable polyurethanes

Poromeric polyurethanes

Spandex fibres

The linear, castable and thermoplastic polyurethanes are the most applicable to this report, so are the only ones that shall be considered here.

Linear polyurethanes were the first commercially available solid polyurethanes. They were prepared by an addition reaction between aliphatic diols and aliphatic diisocyanates. No crosslinking between the chains occurred and no trifunctional compounds were added to cause branching. Therefore the chains only consisted of urethane groups joined by short hydrocarbon chains.

Castable polyurethanes were the first to be used to any significant degree and they account for the largest proportion of solid polyurethanes. They can be divided into three main groups. These are unstable prepolymers, stable prepolymers and one-shot systems.

The chemical basis of the three groups is very similar. They each contain three major ingredients: A long chain polyol, either a polyester or polyether, an aromatic diisocyanate, and a chain extender in either the form of a short chain diol, water or a diamine. In both cases of the prepolymer systems, the polyol is first extended with diisocyanate to yield an isocyanate-terminated prepolymer. A small excess of diisocyanate is added which allows crosslinking to occur at the urethane or urea groups.

There are two principle types of polyurethane materials [22]. These are 1) polyester-based, and 2) polyether-based. The polyether-based type is the most important with regard to solid polyurethanes, and these can be in the form of polypropylene glycols (PPG's) or polytetramethylene glycols (PTMEG's). The materials used in this project are primarily the polyether-based PPG's and PTMEG's. PTMEG's are non-branched polyether polyol backbones, and PPG's are polyether polyol backbones with pendant chains.

The structure of PPG and PTMEG is shown in Figure 3.3 below:

Figure 3.3 The structure of PPG (left) and PTMEG (right)

The polyurethane types used in this study then contain isocyanates of either a toluene diisocyanate (TDI) or a diphenylmethane diisocyanate (MDI) base. The purpose of the diisocyanate groups is to enable increased modulus and hardness. This is, however, coupled with a decrease in tensile strength and elongation at break.

The structure of TDI and MDI is shown in Figure 3.4 below.

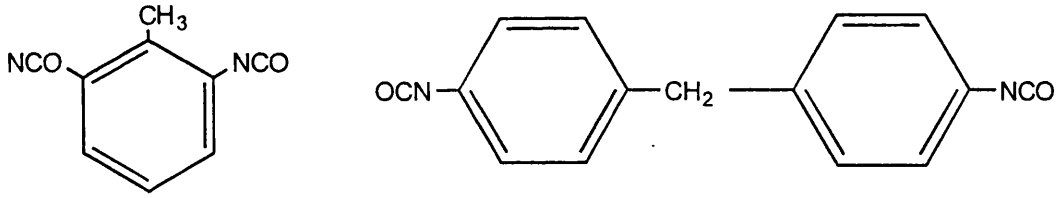

Figure 3.4 The structure of TDI (left) and MDI (right)

The reaction to form the prepolymer is given schematically in Figure 3.5 below.

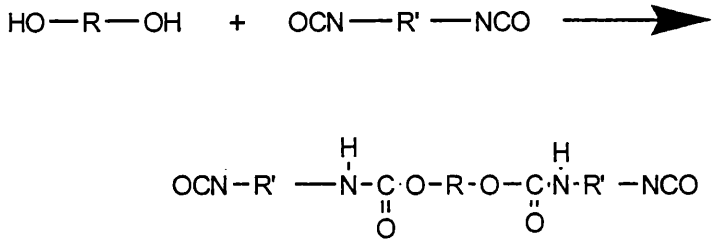

Figure 3.5 The reaction to form polyurethane prepolymer

The chain extension then occurs, most commonly with methylene-bis-ortho-chloroaniline (MbOCA), shown in Figure 3.6.

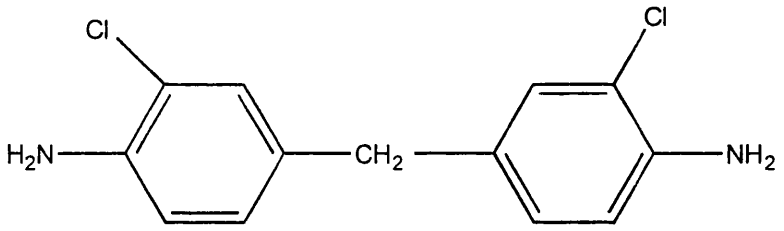

Figure 3.6 The structure of MbOCA

The chain extension reaction is shown schematically in Figure 3.7 below.

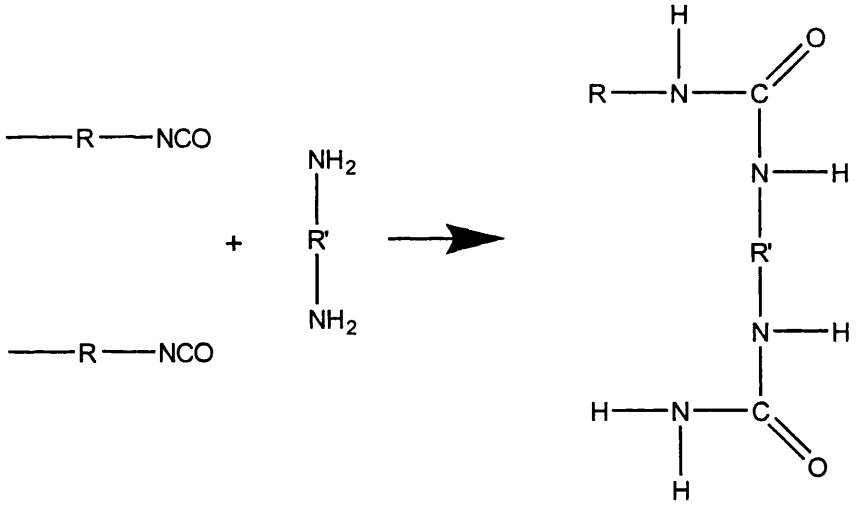

Figure 3.7 The chain extension reaction.

The resultant properties of the polyurethane will depend on the exact proportions of the polyol, diisocyanate and chain extender, and a wide range of properties (hardness, strength, resilience etc) are possible. In general, however, using the bulkier PPG and MDI will give rise to harder materials with higher Tg's and lower resilience [23]. Polyester-based polymers also tend to be somewhat harder and are often more used as mouldable rigid polurethanes and thermoplastics.

The one-shot system has a similar network structure but is formed via a slightly different process. The long chain polyol and the chain extender are mixed with no chemical reaction occurring. The diisocyanate is then added and both crosslinking and chain extensions occur almost immediately.

Thermoplastic polyurethanes are chemically very similar to the castable type mentioned above, including the use of a slight excess of diisocyanate to allow crosslinking. The properties are also very similar and their processing ability means they can be injection moulded, blow moulded, extruded and calendered.

3.2.2 Dynamic Behaviour of Polymers

For this study, the effects of loading timescale on the mechanical properties of polyurethanes was important as the loading rates on firing and impact are considerably higher than those normally used for testing. Most polymers exhibit a certain amount of viscoelasticity, or time-dependent mechanical behaviour and this will certainly play a major part in baton round behaviour.

Polymeric materials exhibit both viscous and elastic behaviour with the degree of each component determined by the temperature and timescale. With higher temperatures and lower strain rates, more viscous behaviour is observed, whereas at lower temperatures and higher strain rates, more elastic behaviour is observed. Polymers are generally therefore termed as being viscoelastic.

Viscoelasticity is exhibited in polymers due to the time taken for certain chain motions and rearrangements to take place [24]. Although the polyurethanes considered here are essentially rubbery in nature and so their behaviour is dominated by rubber elasticity [25], with little or no viscous behaviour, the chain rearrangements leading to strain do take a finite time. Therefore, the faster the rate of loading, the stiffer the materials tend to be.

In addition to this effect, there is also the consideration of the glass transition temperature, Tg. This is essentially the temperature at which main chain motion is virtually eliminated.

As the temperature is reduced, the material changes from a rubbery solid to a stiffer glassy solid as the temperature is decreased through the glass transition. For rubbery polyurethanes, the value of Tg is below room temperature. As the material changes in nature, there is an associated increase in hysteresis, or energy loss. The glass transition is also somewhat affected by the loading rate; a faster rate will give a higher value of Tg due to time-temperature effects. Therefore, as the temperature is decreased, or the rate increased, the material will become stiffer and less resilient.

The dynamic behaviour of polymers are most commonly exhibited when the polymer is subjected to cyclic deformation. These cyclic deformations can be divided into two classes of dynamic motion. These are firstly free vibration, and secondly forced vibration. The first involves the material being set into oscillation and the wave amplitude being allowed to decay naturally. This will produce a sinusoidal wave with a continuously decaying amplitude. The second involves oscillation being kept constant by an external force, and will have a constant continuous amplitude.

Under dynamic stressing, the response of elastomers is also a combination of viscoelastic and elastic behaviour and there is a time lag before the material takes up the associated strain. The time delay is due to a need for the atomic vibration energy to overcome the intermolecular attractions within the structure. In dynamic applications, this time lag means that the strain is not in phase with the sinusoidal stress wave but follows behind. There is an associated loss of energy with each cycle, which is converted into heat. The phase angle difference between stress and strain is known as delta, and the commonly used term of tan δ represents the ratio of energy lost to stored energy [26].

The typical variation of stiffness and tan δ with temperature and testing frequency (hence rate) is shown in Figure 3.8 for a typical rubbery polymer [27].

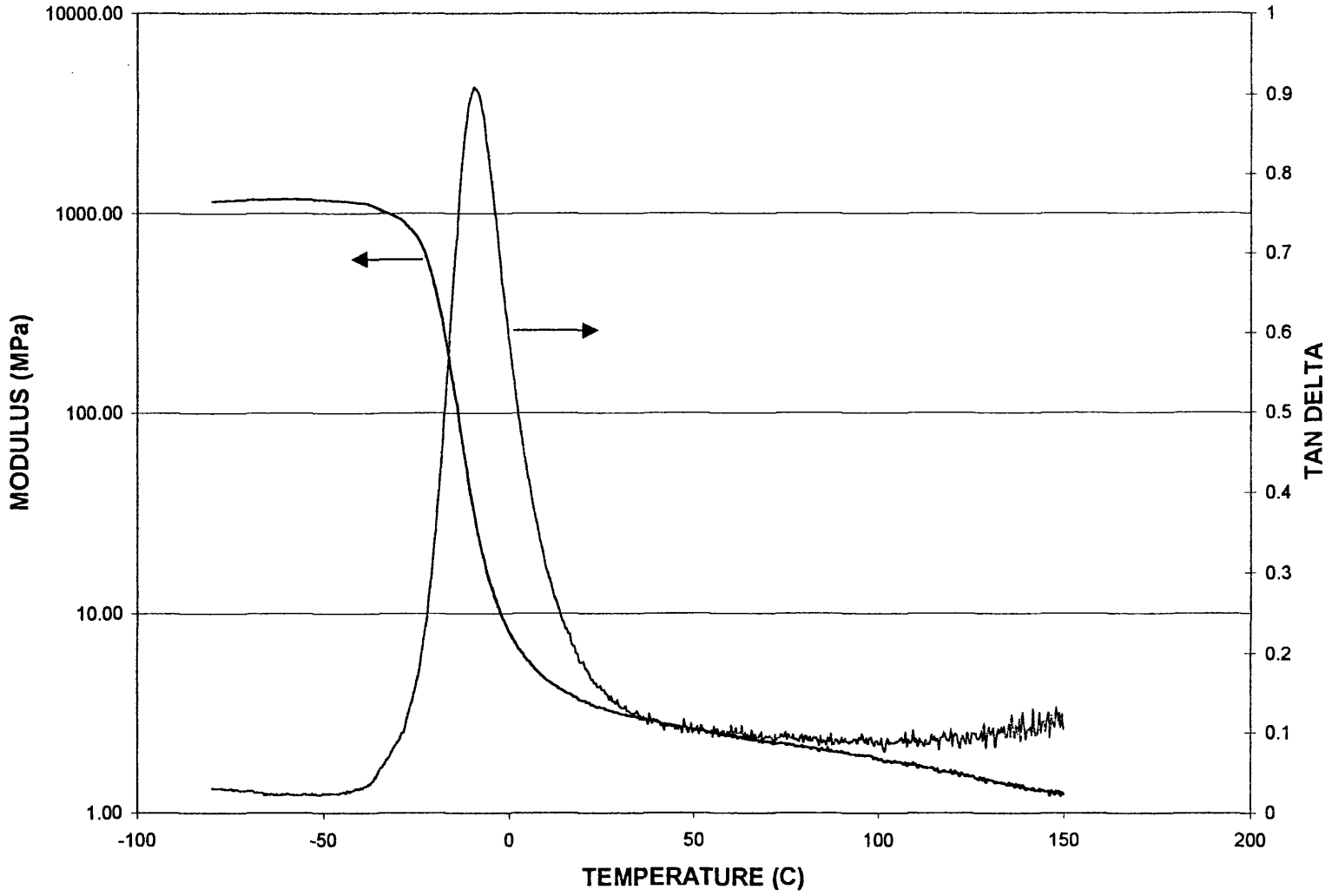

Figure 3.8 Typical DMTA results (for a silicone rubber) showing how the modulus and tan delta vary through the glass transition.

3.2.2.1 Rebound Resilience

The energy loss described above can be measured by the use of rebound resilience. This is a fairly simple dynamic test which uses an indentor to impact the test piece and rebounds freely after impact. The material is therefore subjected to only one half-cycle deformation.

The rebound resilience is defined as the ratio of energy of the indentor before impact to its energy afterwards. This is expressed in terms of percentage with 100% rebound resilience being where no energy is lost. i.e when the indentor rebounds to its original position after impact. There are two commonly-used methods of measuring rebound resilience, which unfortunately give systematically different results, due to differences in time of impact and size of impactor [26]. These are described below.

The Lupke pendulum (shown in Figure 3.9) consists of a horizontal rod with a hemispherical end, suspended on wires so that it is free to swing in the arc of a circle. The test piece is normally a disk of 29 mm diameter and 12.5 mm thickness.

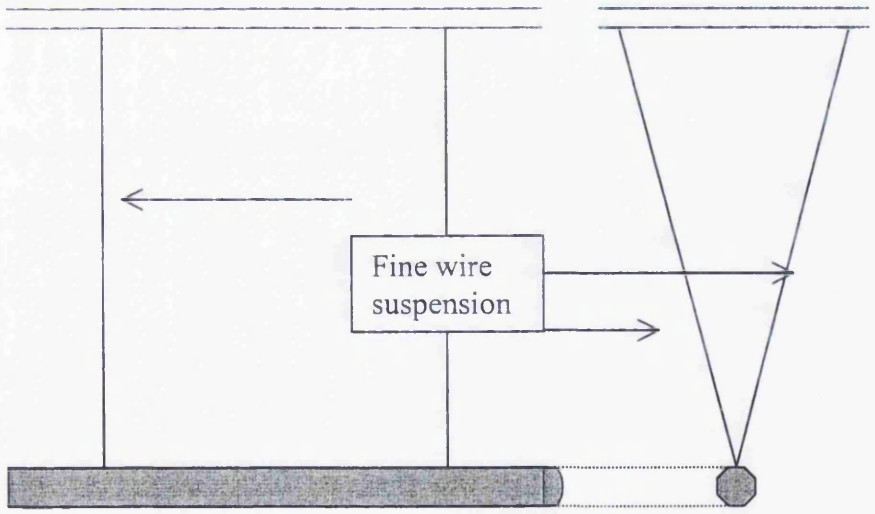

Figure 3.9 The Lupke Pendulum

The Schob pendulum (shown in Figure 3.10) is a simpler rod system, pivotted at the end, but with a relatively heavy indentor end. The sample is normally 6 mm thick.

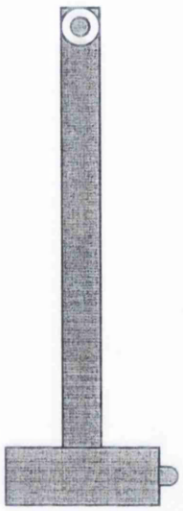

Figure 3.10 The Schob Pendulum

3.2.2.2 The Effects of Temperature

When the temperature is changed, all physical properties of polymers are affected, to a greater or lesser extent. If these temperature changes are large enough, long term, irreversible effects are observed. These effects are predominantly due to chemical changes within the material structure and are generally known as ageing.

If the temperature variation is not large enough to cause chemical changes, short term, reversible effects occur. These are physical alterations and are more, or less extreme depending on the degree of temperature change. For this reason, where possible it was important to try to design experiments to observe material characteristics over a range of temperatures.

a) High temperatures

When polyurethanes are subjected to temperatures above ambient temperature they can undergo two distinct processes. The first is a physical process of general bond strength reduction, which causes an overall decrease in mechanical properties. It is generally seen in polyurethanes over a range from room temperature to 70 or 80 degrees C and is completely reversible when the temperature is reduced back to ambient.

The second process occurs at higher temperatures (upwards of 70 to 80 C) and involves permanent chemical change within the structure. Once again there is a gradual decrease in properties. However it should be mentioned that Young's Modulus can increase with an increase in temperature as age hardening occurs. Then as temperature continues to increase, degradation of bonds will occur, leading to a reduction in modulus. This will be discussed in more detail later.

As the vibrational energy of the atoms is increased with increasing temperature the time lag seen with cyclic deformation (discussed above) will decrease. Therefore less energy will be lost when the material undergoes a deformation and an increase in rebound resilience will be observed.

b) Low Temperature

As with high temperature exposure, changes in properties occur in polyurethanes when they are subjected to low temperature. However, regardless of how much the temperature is reduced, no permanent degradation occurs and all effects are reversible. With a decrease in temperature, an increase in stiffness (modulus) is observed, as is an increase in tensile strength, hardness and tear strength. In contrast to the effects of increasing temperature there is less energy in the system to allow a large amount of atomic vibration. Therefore a decrease in rebound resilience occurs.

This increase in stiffness with decreasing temperature may lead to brittleness at around -70 to -80 degrees C and also cause the recovery from an applied deformation to be less responsive.

3.2.2.3 Glass Transition Temperature (Tg)

When a polymer in the molten state undergoes cooling it eventually reaches a stage where flow is reduced and viscosity increases. The polymer then takes on a more rubbery form. As temperature is reduced further a stage known as the Glass Transition temperature is reached, where chain movement is restricted further, a large increase in modulus is observed, and the polymer loses its rubber-like characteristics, passes through a leathery state and becomes a polymer glass. After a move through the glass transition region other physical properties such as electrical, thermal and mechanical all change significantly.

3.2.2.4 The Effects of Strain Rate

Dynamic properties also lead to a strong dependence on strain rate. The effects of increasing or decreasing strain rate are inter-related with the effects seen when decreasing or increasing temperature. Increasing strain rate gives the same effects as a reduction in temperature, due to less molecular mobility and hence, decreasing strain rate has the same effect as increasing temperature. This leads to the possibility of determining fast rate properties indirectly, by measuring slower rate behaviour at lower temperatures. In order to do this, the 'time-temperature equivalence' must be established, by performing a range of tests over accessible timescales and temperatures.

3.3 MATERIALS TESTED

Throughout the course of this part of the project, a range of tests were conducted on a total of 13 different polyurethane materials. These materials were a mixture of polyester-based, polyether-based and thermoplastic polyurethanes. The polyether-based materials were either polypropylene glycols (PPG's) or polytetramethylene glycols (PTMEG's). They contained either toluene diisocyanates (TDI's) or diphenylmethyl diisocyanates (MDI's).

These materials were supplied from a variety of sources in both sheet and baton round form. The sources were Polyurethane Products Ltd (PPL), Marbil, Baule and DuPont.

They also came with a range of information regarding chemical content, processing history, rebound resilience and hardness values. A list of each material together with the information supplied is shown below.

The values of rebound resilience and hardness supplied by the different sources were, unfortunately not taken from the same standard scales. For example, resilience tests were conducted by both Baule and RAPRA. Baule use DIN53512 which specifies the Schob pendulum method (see Fig 3.10), and RAPRA use BS903, Part A8, which specifies the Lupke pendulum method (Fig 3.9). Even though both pendulum methods are accepted

they do not give the same levels of rebound resilience for a given material. The Lupke method always gives a higher value than Schob. This is due to the velocity of the pendulum on impact, the size/mass of the indentor and, hence, striking energy.

RAPRA used hardness tests in accordance with BS 903, Part A26, Method CN 1995, IRHD (International Rubber Hardness Degrees). Unless stated, all hardnesses are quoted as IRHD values.

L5A6

This was the round in service when the project began. The standard round is cylindrical in shape, whereas the rounds supplied for testing were variants, which had been machined into the shape of the new XL21 rounds, with a more rounded nose, driving bands at the front and rear, and a thinner cylindrical section in the centre, as shown in Fig 3.11. This was to enable differences in material to be assessed independently of the geometry of the round.

These rounds were manufactured by PPL from a polyester-based polyurethane and were supplied by DERA. They were straw-coloured. RAPRA Lupke rebound resilience values were quoted as 50%, with hardness at 90.

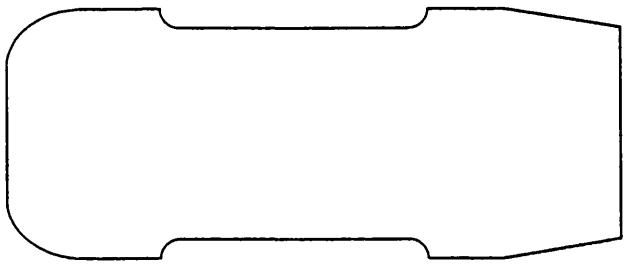

Figure 3.11 The XL21 Baton Geometry (Schematic).

L5A7

This round was a virtually identical replacement for the L5A6, and was also produced by PPL. In this case, the original L5A6 shape was retained, which is a less rounded cylindrical form. They were also straw-coloured.

Marbil

This round was an early XL21 contender. It was produced by Marbil and had a quoted resilience of 20%. However, subsequent tests by RAPRA, showed these values were closer to 30% Lupke. Hardness was measured at 92. The polyurethane used was a TDI based PPG and the colour was deep red with a gloss finish.

Marbil New

This was a reworked version of the original Marbil XL21 round. The shape was the same, but the driving bands had been centreless ground to give better contact with the rifling grooves inside the barrel. The colour was Burgundy red / dark purple.

PPL

An XL21 contender, the PPL round was a TDI based PTMEG. Resilience was quoted as 50% from PPL, but subsequent testing from RAPRA showed figures averaging 64%. Hardness was quoted at 95 by PPL but was later determined by RAPRA to be 90. Colour was light red with a matt finish.

PPL New

This XL21 round was also a TDI based PTMEG but was catalysed to speed the curing process. Initial resilience values appeared to be around 35% Schob, but RAPRA testing showed them to be 50% Lupke. Hardness was recorded as 94. These rounds were the same burgundy red / dark purple colour as the Marbil New although the finish was matt. The plug was moulded and had not been subject to a grinding process.

PPL New 2

A newer version of the PPL round in the same colour as PPL New, but the entire round had been centreless ground. Also a TDI based PTMEG.

PPL New 3

The same round as PPL new 2 in every respect but these were taken from a different batch.

Hytrel

This material which is a polyester–based thermoplastic elastomer was produced by DuPont and was supplied in sheet form. Dimensions were approximately 150 x 100 x 2 (mm). Colour was light yellow.

PU Thermoplastic

This was another sheet material supplied by DuPont. Dimensions were also 150 x 100 x 2 (mm). This was a polyurethane thermoplastic elastomer material and was clear in colour.

MTQ

The MTQ 25130 material was supplied by Baule in sheet form of dimensions approximately 250 x 250 x 4 (mm). The material was an MDI based PTMEG. Hardness values of between 60 and 95 Shore A are possible, but although the material supplied was specified as Shore A 90, no values were taken for the sheet supplied. Colour was white. Schob resilience was quoted as 56%.

TG

TG 448 was also supplied by Baule with dimensions approximately 250 x 250 x 4. This was a TDI based PPG and was processed with 4,4'-methylene-bis (2-chloroaniline) (MBOCA). This results in an elastomer with a 95 Shore A hardness. Colour was cream. Schob resilience was quoted as 47%.

TT142L supplied from Baule in sheet form with the same dimensions as both the MTQ and TG materials. This material was reported as being the same as the original PPL (TDI / PTMEG polyurethane, Hardness 92 – 94, resilience ~ 50%) and was greeny cream in colour.

3.4 TESTING METHODS

3.4.1 Infra-red spectroscopy

IR analysis of a selection of rounds was carried out to assess the levels of residual isocyanate (NCO) within their structure. These tests were conducted using a Perkin Elmer FTIR spectrometer.

Two sets of results were taken. The first was for a batch of 10 L5A7 rounds supplied by PPL. At the same time, analysis was carried out on PPL, PPL new 2, PPL new 3, Marbil and Marbil new XL21 rounds.

The second set was four rounds from four batches of PPL rounds (total of 16 rounds), and 30 rounds supplied by Pyrotechnik Silberhutte in Germany. These were all of the L5A7 specification.

Potential surface hardening of the rounds was the major concern, especially the effects with storage for several months or years. Ideally, all the isocyanate (NCO) would be converted into urethane links during the curing process, however if incomplete cure occurs, the remaining NCO can react with moisture, especially at the surface and cause additional hardening to occur over time. Therefore the presence and magnitude of any NCO peaks on the IR spectra was of most importance.

The rounds were sectioned through the middle, and a transverse section was analysed. It was unlikely moisture would have been able to diffuse throughout the entire width of the rounds with the environmental exposure they had experienced. Therefore if excess NCO

had been present following processing, there would still be signs of this in the centre of the rounds. Excess NCO on the surface would have reacted within a few hours and at the time of testing would, obviously, not be present. However, for completeness, the outer surface of a selection of rounds was analysed.

3.4.2 Compression Tests

Compression tests were conducted for the primary purpose of gaining an understanding of the response of the polyurethane rounds to varying strain rates. They were also used to compare the response to testing temperature.

Tests were carried out using a servo-hydraulic tensile/compression testing machine at compression rates of 0.5, 5 and 50mm min^{-1}. The maximum displacement was set at 6mm in all cases. Temperature was kept at room temperature for the majority of tests (23°C) with some samples being tested immediately after conditioning at -10°C. Humidity was kept constant at 50%.

The strain rates that occur within the rounds during impact were not reproducible using the equipment available, so testing was conducted at lower rates with the aim of extrapolating results to gain a realistic understanding of behaviour on impact. From the results of each experiment a graph of force vs displacement was plotted. This generally gave a straight line graph, from which the gradient was taken and used as a measure to compare plug stiffness at the different rates.

3.4.3 DMTA Tension Tests

Dynamic mechanical thermal analysis (DMTA) tests were conducted in tension with small rectangular sections of seven materials for the purpose of further investigating the effects of rate on stiffness. These materials were: PPL, PPL new, PPL new 2, Marbil, TT, TG and MTQ. Tests were isothermal, at room temperature, and were carried out at small strain amplitude at four frequencies of 1, 3, 10 and 30Hz for a period of 5 minutes. This was

sufficient time to gain an accurate measurement of both material stiffness and tan δ (a measure of the degree of energy loss) for each frequency.

The data of most interest was the modulus values for each material at both 1 and 30Hz. As with the compression tests, the differences in stiffness at the lower frequencies being tested were a good indication of the effects of rate on stiffness at the 1kHz impact frequency. If there was little difference in stiffness between 1 and 30Hz, it was most probable that, relatively, there would not be a vast increase at 1kHz. Whereas if there is a large difference between 1 and 30Hz, extrapolating to 1 kHz would be likely to show considerable stiffness increases.

3.4.4 DMTA Tests

The Dynamic Mechanical Thermal Analyser can be used for many forms of test to obtain a range of information regarding the dynamic properties of the polyurethane materials. The machine can record modulus, and tan δ values over time with increasing, decreasing or constant temperature.

During the course of development work at DERA, it became clear that the rebound resilience of the rounds was of some importance. Therefore, the main interest in this section was to see how the rounds would behave on impact. As the frequency of testing of the DMTA could not reproduce the strain rates inflicted on impact, lower frequencies were used with the potential to extrapolate to frequencies equivalent to impact.

With typical baton round impacts, the time of contact is about 1ms which is equivalent to a test frequency of 1 kHz. Accurate results of the polyurethane response could only be obtained up to 100 Hz. Depending on the type of test being carried out it was decided to use a range of frequencies from 1 – 100 Hz. This range covers two orders of magnitude, so extrapolating by 1 more factor of ten from 100 Hz to 1 kHz, was expected to give fairly accurate results.

The machine can be set up in a number of testing states including tension, compression, three point bending, single cantilever and dual cantilever. Throughout the project all types of the aforementioned head set-ups were tried but the most favoured were tension and compression.

The main use of the DMTA was for testing the material responses from temperatures as low as -80 to +60°C. Over this range, both modulus and tan δ were recorded, which included their behaviour around the glass transition temperature.

3.4.5 Thermal Expansion

Problems were experienced by DERA with the PPL new 2, XL21 round during firing trials. The baton material was expanding at elevated temperatures and drastically increasing bore friction to the extent that at temperatures of + 40°C, rounds were actually sticking in the barrel.

It was thought that as this did not occur previously with the moulded batons, the problem was due to the slightly rougher centreless ground finish, coupled with there being no mould release silicon compounds on the surface.

Therefore it became important to establish a profile of the expansion coefficient for the PPL new2 baton for the temperature range + 15 to + 56°C.

The DMTA was used for this, and was set up in tension mode. Tests were carried out over the range -60 to +80°C, in TMA (thermo-mechanical analysis) mode. This produced inaccurate results with excessive noise, so testing was repeated in Creep mode. Noise was eliminated and a clear plot was produced. A force of 0.1N was applied, which was small enough to allow the DMTA head to expand/contract with the sample over the temperature range, but was not large enough to significantly deform the sample. The temperature was increased at a rate of 1°C per minute. Testing was carried out on PPL new2 and a polycarbonate control sample.

3.4.6 Environmental Tests

The ability of each baton material to be able to withstand "acceptable" levels of exposure to a range of environments, without significant changes in properties was of utmost importance. Therefore a series of environmental tests was designed and implemented. These covered three main areas of potential harmful exposure. They looked at the effects of high temperature, ultraviolet light, and water.

The tests could be used as a guide to predict shelf life of the rounds and to what degree this would be affected by effects of the environment during storage. Examples of possible problems are:

1) Being stored in metal containers in direct sunlight in a hot country, where the temperature inside the box could easily rise in excess of 50 or 60°C.
2) Long term exposure to direct sunlight if they are stored in a container with no lid can cause UV degradation.
3) Moisture effects from something as extreme as being left out in the rain, to being stored in a country with high humidity.

These examples could all cause permanent degradation of the polyurethane rounds.

Tests were performed on samples of MTQ, TG, TT, Hytrel, PU thermoplastic and PPL new2. Eight rectangular strip samples of each material were prepared. Dimensions were approximately 25 x 5 x 2 mm. Initial tests were performed on all samples using the DMTA to establish values of modulus and tan δ at 25°C. Two samples were used for each of the three types of conditioning test (described below), and the remaining two samples were left in the open air in the laboratory as control samples. These two specimens were re-tested after a two week period.

3.4.6.1 High Temperature

Samples were left in a dark, preheated oven at 50°C for an initial 7-day period. Following this, they were re-tested to see what, if any, effects had occurred. They were then heated for a further 7 days at the same temperature and tested once again.

3.4.6.2 Ultraviolet light

Samples were initially exposed to 24 hours of UV light using an ultraviolet lamp producing a peak wavelength of 265nm after which modulus and tan δ values were recorded. The samples were then exposed for a further 24 hours and were then re-tested. They were then left under the UV lamp for a further 72 hours and final values were taken in the DMTA.

3.4.6.3 Water Exposure

These samples were immersed in a beaker of water for a 7-day period. They were then removed, lightly hand dried with tissue, and tested in the DMTA. They were then left in the open air in the laboratory for a further 7 days and then re-tested. This was to determine whether there had been any permanent effects of the water exposure that had not recovered after drying.

Table 3.0. Showing which samples underwent which type of testing.

	IR	Compression	DMTA Tension	DMTA	Thermal Expansion	UV	High Temperature	Water Immersion
L5A6		X		X				
L5A7	X							
Marbil	X	X	X	X				
Marbil New	X			X				
PPL	X	X	X	X				
PPL New		X	X	X				
PPL New2	X	X	X	X	X	X	X	X
PPL New3	X	X		X				
Hytrel				X		X	X	X
PU Thermoplastic				X		X	X	X
MTQ			X	X		X	X	X
TG			X	X		X	X	X
TT			X	X		X	X	X

3.5.1 Infra Red Analysis

If NCO is present within a material, an infra-red spectroscopy scan would be expected to show a small peak at 2270 cm^{-1}. This is to the right of the two sharp peaks at 2370 cm^{-1}, which are produced due to the presence of carbon dioxide.

3.5.1.1 L5A6 results.

One round (44), with a hardness of 89, showed a significant NCO peak. By comparison with a previous set of IR analysis, this level of NCO was probably large enough to cause surface hardening. The IR trace of this round can be seen in Fig 3.12.

Three rounds (62, 21 and 34), with hardness values of 87.5, 88 and 90 respectively, all showed some NCO, as shown in Fig 3.13, but at around half the levels of round 44. These levels would not be expected to cause any significant surface hardening.

Three further rounds (3, 6 and 76), with hardnesses of 90, 89.5 and 88.5 respectively, did show NCO peaks but the levels were only just detectable. The levels should not lead to any measurable changes in properties. An IR trace from round 6 can be seen in Fig 3.14.

The remaining three rounds (59, 77 and 91) (hardness 89, 89.5 and 87.5 respectively) showed no presence of NCO at all, as seen in Fig 3.15.

From the results of these tests it is clear that there is some degree of variability with the levels of residual isocyanate present. The worst rounds cause concerns over the likelihood of surface hardening on storage. There is also no visible relationship between the level of NCO present and the recorded values of hardness, i.e a high NCO level accompanying a low level of hardness due to incomplete curing.

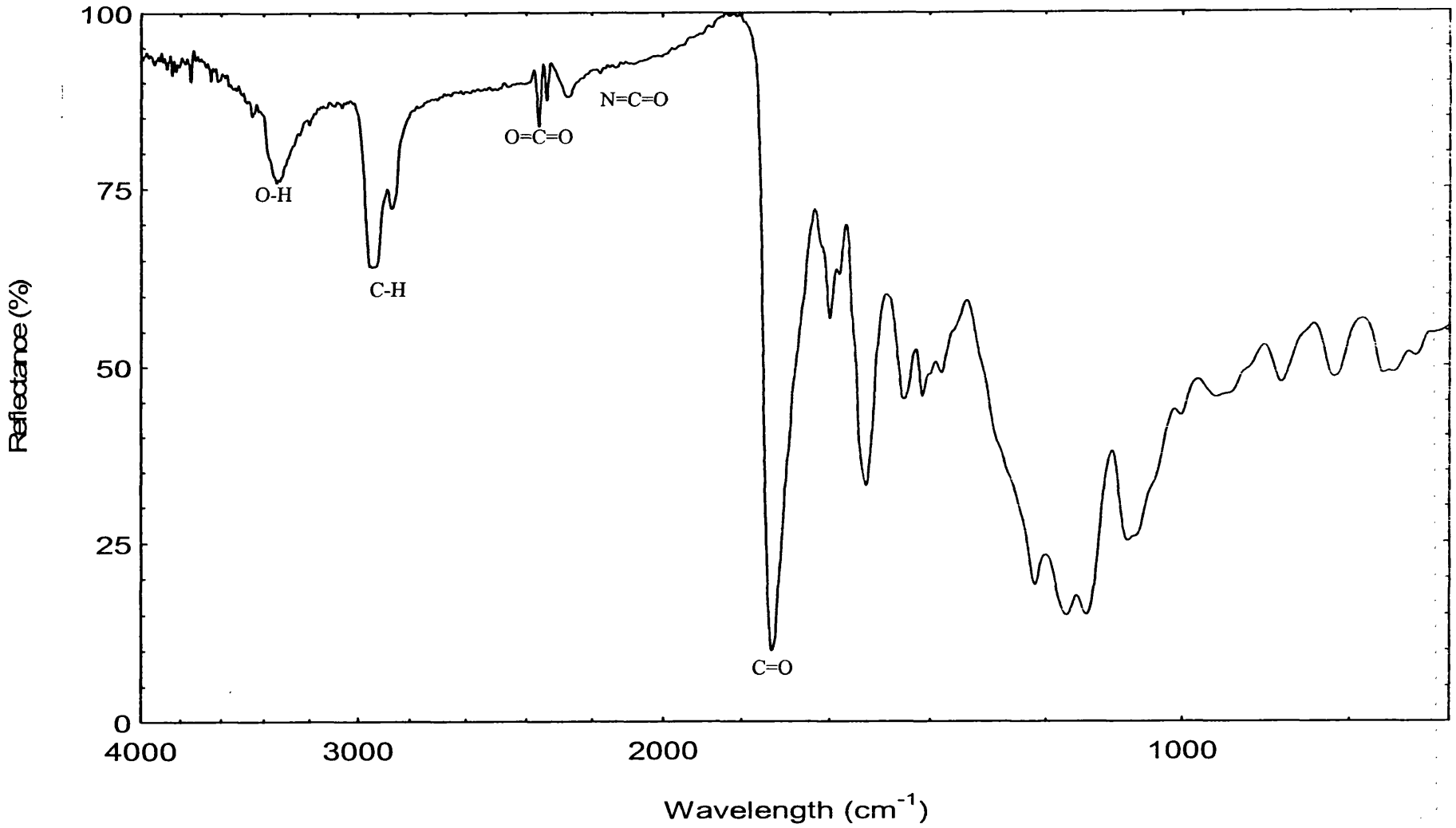

Fig 3.12 Infra Red plot of Round 44 showing a significant NCO peak

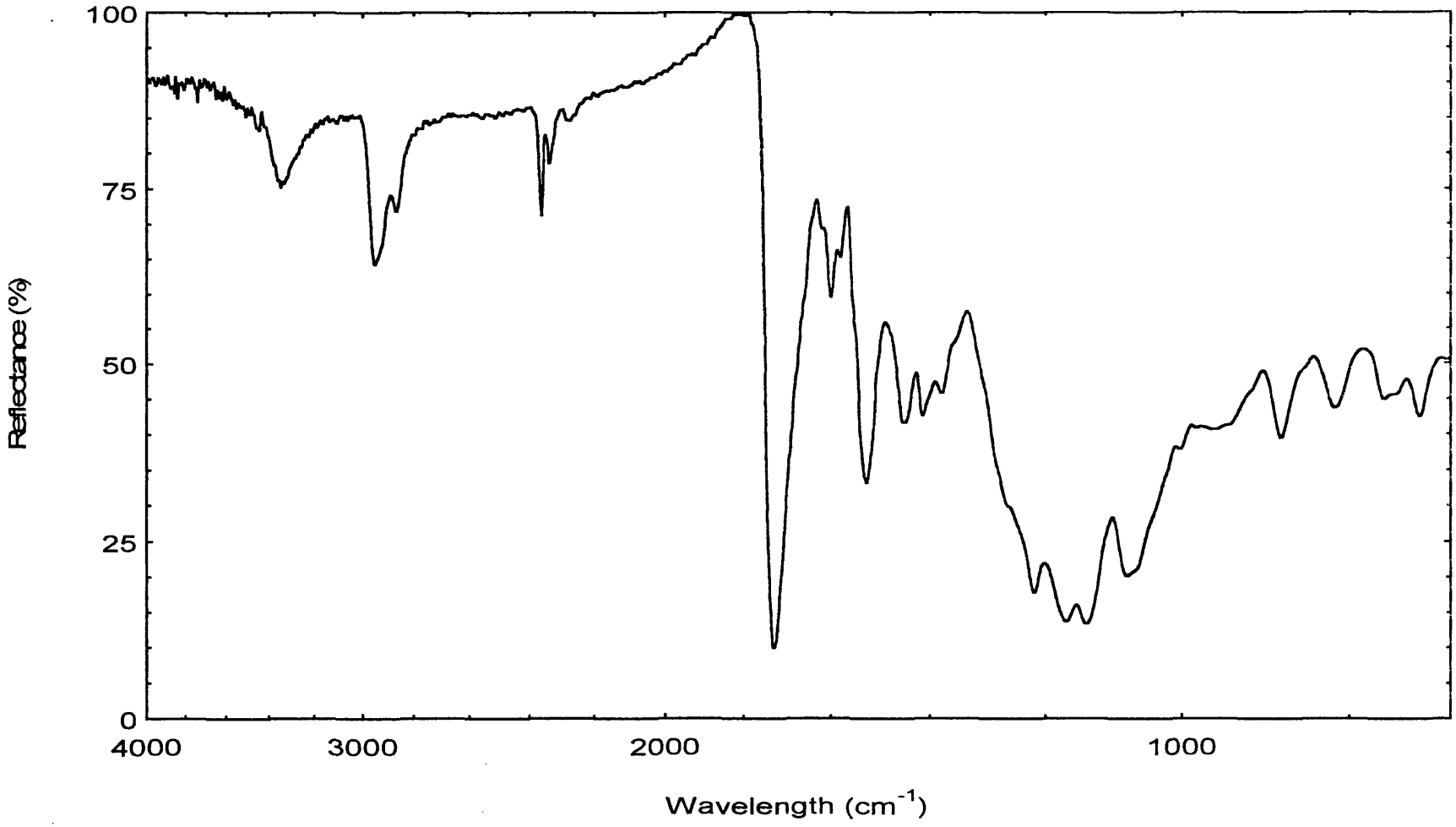

Figure 3.13 Infra Red plot of Round 62 showing a noticeable NCO peak

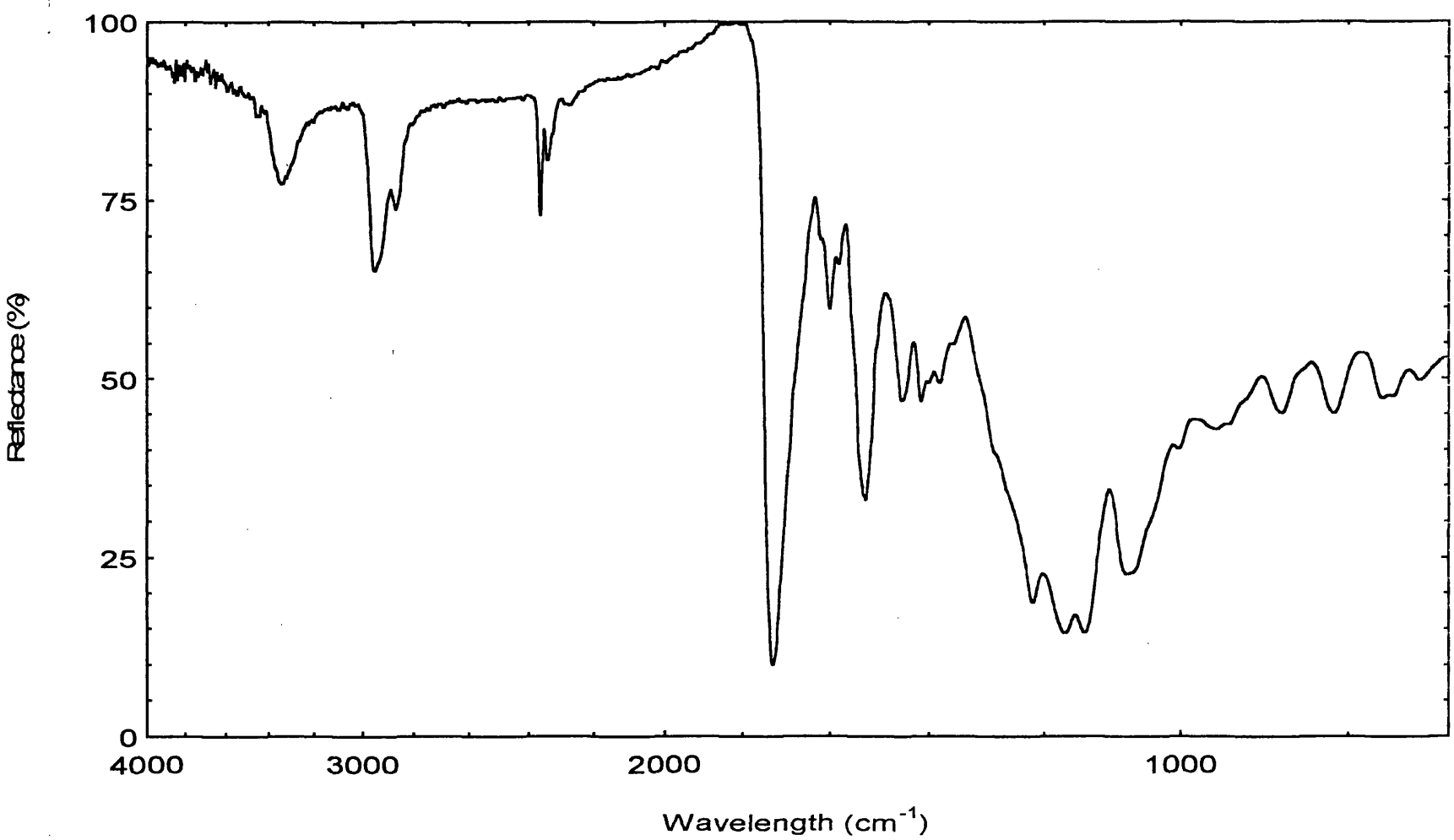

Figure 3.14 Infra Red plot of Round 6 showing a small NCO peak

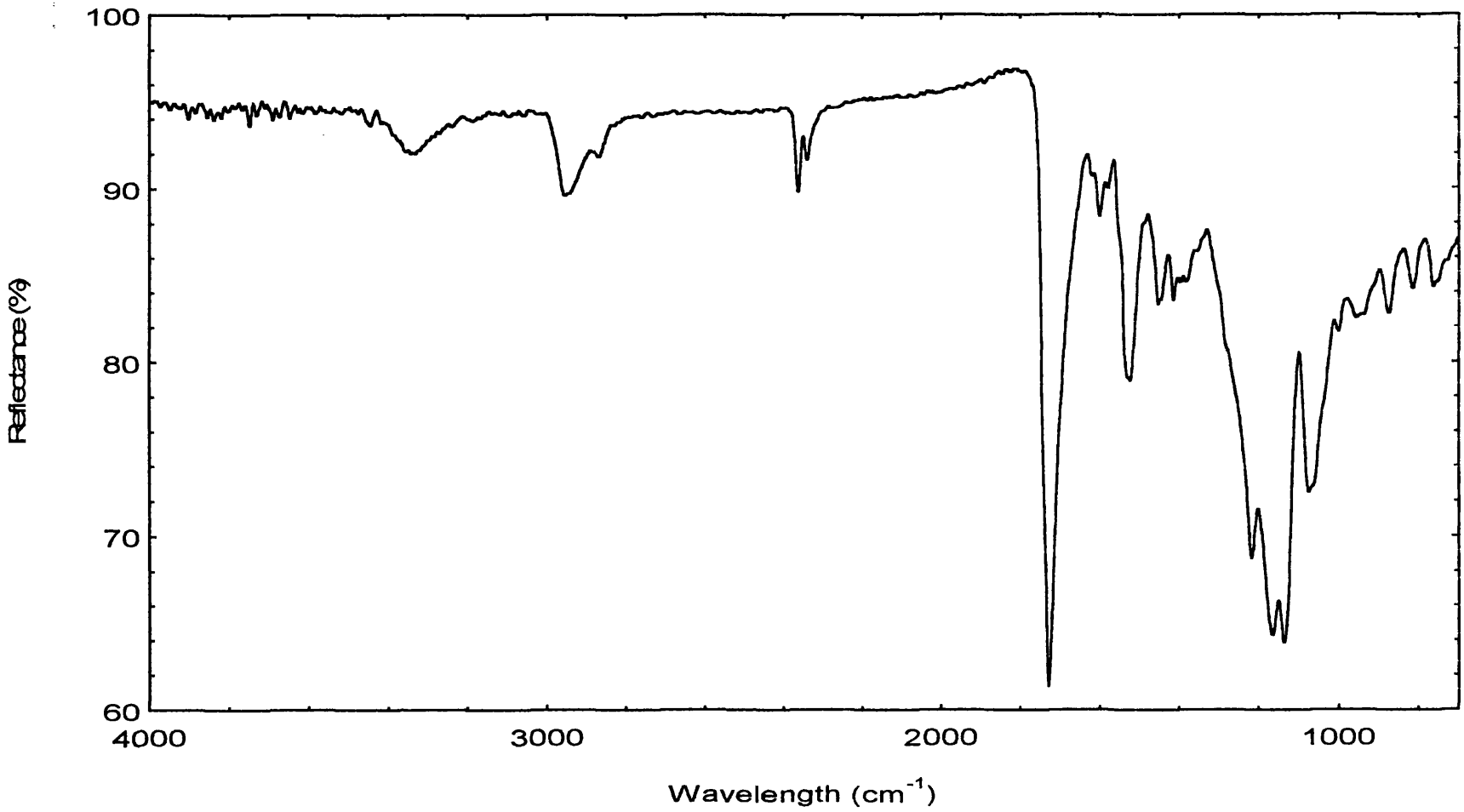

Figure 3.15 Infra Red plot of Round 91 showing no NCO peak

3.5.1.2 L5A7 Results

As a result of concerns raised from the L5A6 results, IR tests were performed on the next batch of L5A7 rounds. Of the second batch of 16 PPL rounds, 12 were tested. Only one of these showed any presence of NCO, and the level was so small it was not considered to be significant. From the 30 Pyrotechnik Silberhutte rounds, 20 were tested. Four rounds were found to contain minimal quantities of isocyanate. Once again, these findings were considered insignificant, as the levels of NCO found would not have any effect on surface hardening. These results show that the L5A6 results above are likely to be due to problems at the start of a small batch, but nevertheless, IR testing was introduced into the specifications for the L5A7 rounds.

3.5.1.3 XL21 Rounds

Of the five XL21 rounds tested, the three variants from PPL showed no presence of NCO at all, as shown in Figure 3.16. Both Marbil and Marbil new showed trace amounts, but these were so low they could be mistaken for background scatter.

3.5.2 Compression Tests

Concerns had arisen at DERA over the measured hardness values of the PPL and Marbil rounds compared to the effects of the rounds on impact. The PPL round came with a quoted hardness of 95 IRHD, and the Marbil with a hardness of 92 IRHD. However, results from firing trials showed the Marbil rounds to be far more devastating on impact than those supplied by PPL. So even though the Marbil rounds appeared to be softer at slow loading rates (during hardness tests), they were harder at fast loading rates, producing more damage on impact.

The most probable reason for this was that the Marbil material was far more sensitive to changes in rate than the PPL. At low rates of deformation, such as during a hardness test, the material was softer, yet at the higher rates, on impact, it stiffened to a greater extent than the PPL round. This could be explained by the Marbil round having a higher glass transition temperature.

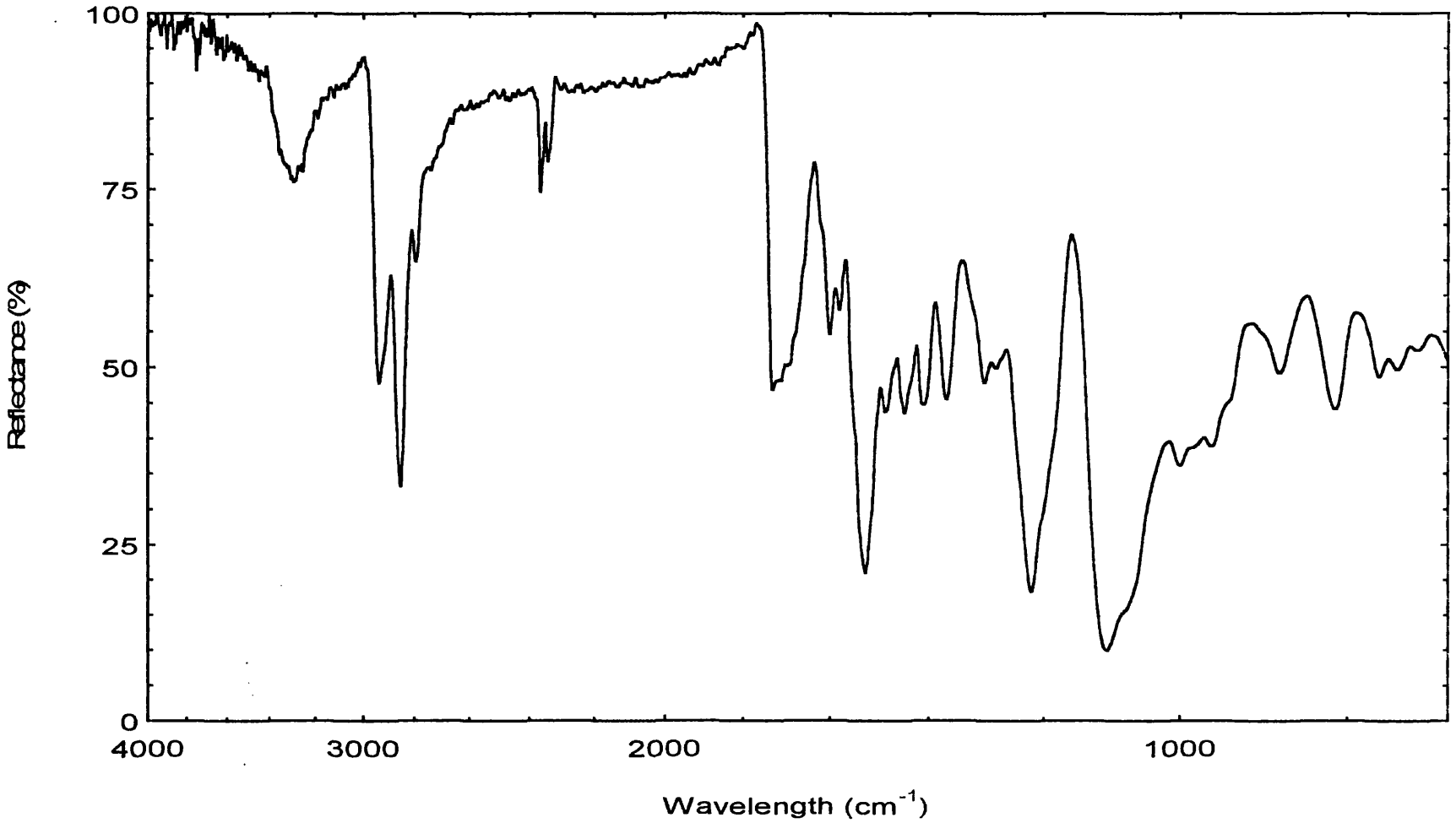

Figure 3.16 Infra Red plot of PPL Round 3 showing no NCO peak

If this idea were correct, the Marbil round would have a Tg that is closer to room temperature and the modulus curves for the different rates would be further apart than those of the PPL round. Therefore there would be a greater difference in modulus values between the fast and slow rates of the Marbil rounds compared to those associated with the PPL batons. When extrapolating to the higher rates seen on impact (of 1 ms^{-1}) the difference in modulus will be exaggerated further.

Following this idea further, the larger modulus range associated with the Marbil round could also be explained by the resilience of the material. If we only consider the Marbil and PPL rounds, the resilience value of the Marbil is taken as being 20% Schob and 30% Lupke, whereas the PPL has a resilience of 50% Schob and 64% Lupke. Therefore the Marbil round can be considered to have low resilience and the PPL, high resilience.

This idea is presented graphically in Figure 3.17 below, where it can be seen that the stiffness of low resilience rounds increases more dramatically with rate than rounds of high resilience. Therefore, low resilience rounds of the same hardness (at low rates) will have much higher stiffness at the high rates of impact. It is even possible for low resilience rounds of lower hardness to be stiffer at the faster rates. There is a balance to be struck between a high enough stiffness at firing rates for accuracy, and low enough stiffness at impact rates to minimise injury potential. From Figure 3.17, it can be seen that this will be more easily achieved with a high resilience round, especially as this will give a smaller difference in stiffness between the low rates of hardness testing and higher rates of impact.

In order to investigate this effect, the compression tests at different rates were performed. Initially, tests were conducted on three types of round; the Marbil, PPL and L5A6. Three samples of each round were tested at the three rates previously mentioned. Tests were carried out at room temperature and then repeated at -10°C (samples stored in a freezer and tested immediately on removal).

Following this, the same tests were carried out on two of the PPL new batons, both at room temperature and -10°C.

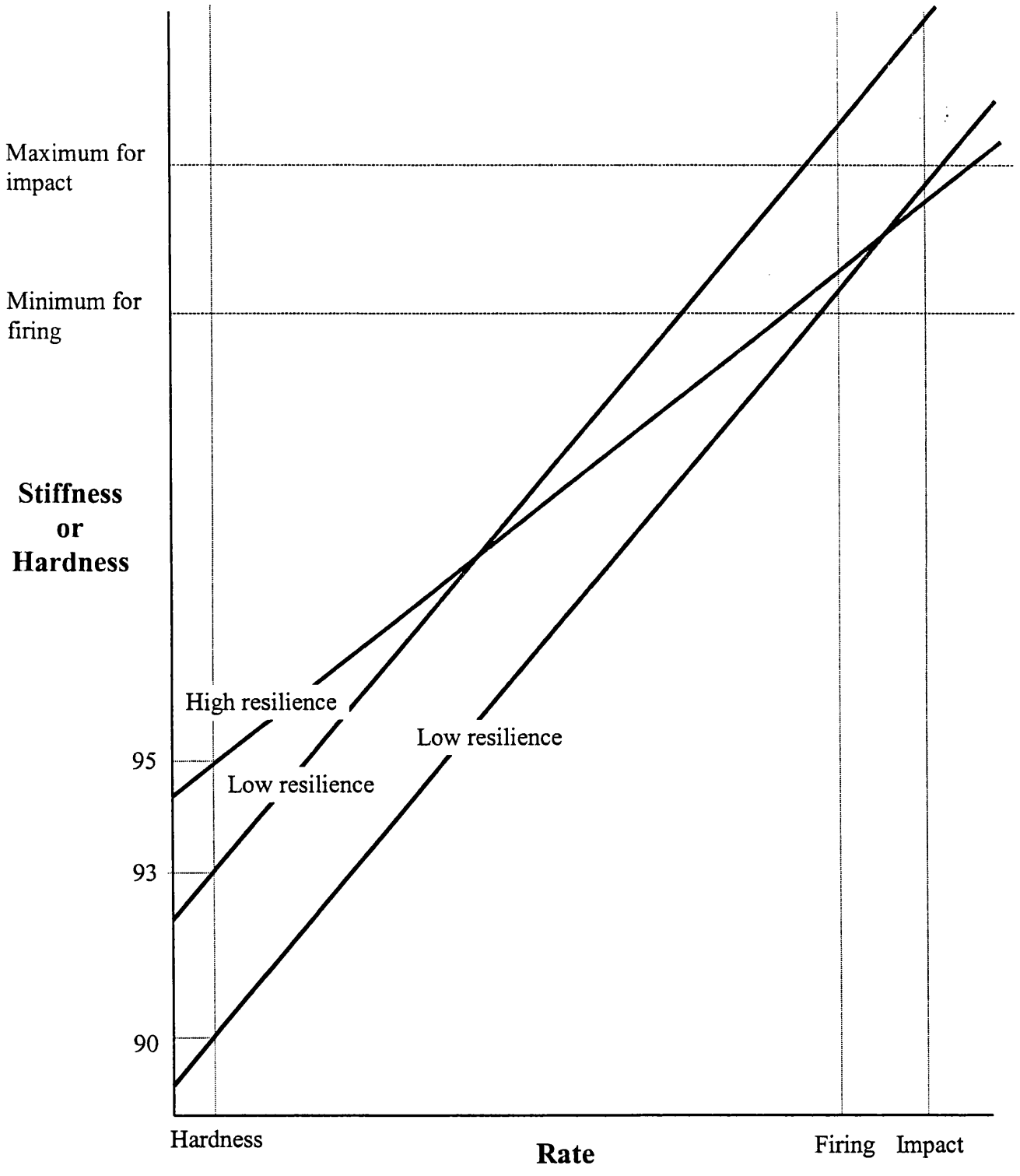

Figure 3.17 The effects of resilience on the variation of stiffness with rate.

Some months after the completion of this set of tests, new batches of PPL new2, PPL new3 and Marbil new arrived. Once again three batons were tested, at the same rates, but this time only at room temperature.

The graphs that were plotted directly from the test data were load vs displacement. The gradients of the plots were taken and this gave a measure of the material stiffness, with a steeper gradient corresponding to a higher material stiffness.

Figure 3.18 shows the results for the first batch of results at both room temperature and at –10C. Figure 3.19 then shows results for all the rounds just at room temperature, where the effect of testing rate can be seen more clearly. From these, it can be seen that the Marbil round is most affected by both temperature and rate. The PPL rounds generally show least variation with temperature and rate, except for the PPL new batch. The L5A6 rounds show little effects of rate, and moderate effects of temperature.

These results can be reasonably well correlated with resilience; the PPL rounds are generally of high resilience except for the catalysed PPL new, which had lower values. The Marbil rounds were of lower resilience and showed a greater effect of testing rate and temperature. From the first set of compression tests, the low resilience rounds showed more significant effects of rate changes than those of higher resilience.

These results confirm the proposed ideas discussed above and show that in order to have as little variation in stiffness with rate and temperature, a high resilience (or low glass transition temperature) needs to be specified.

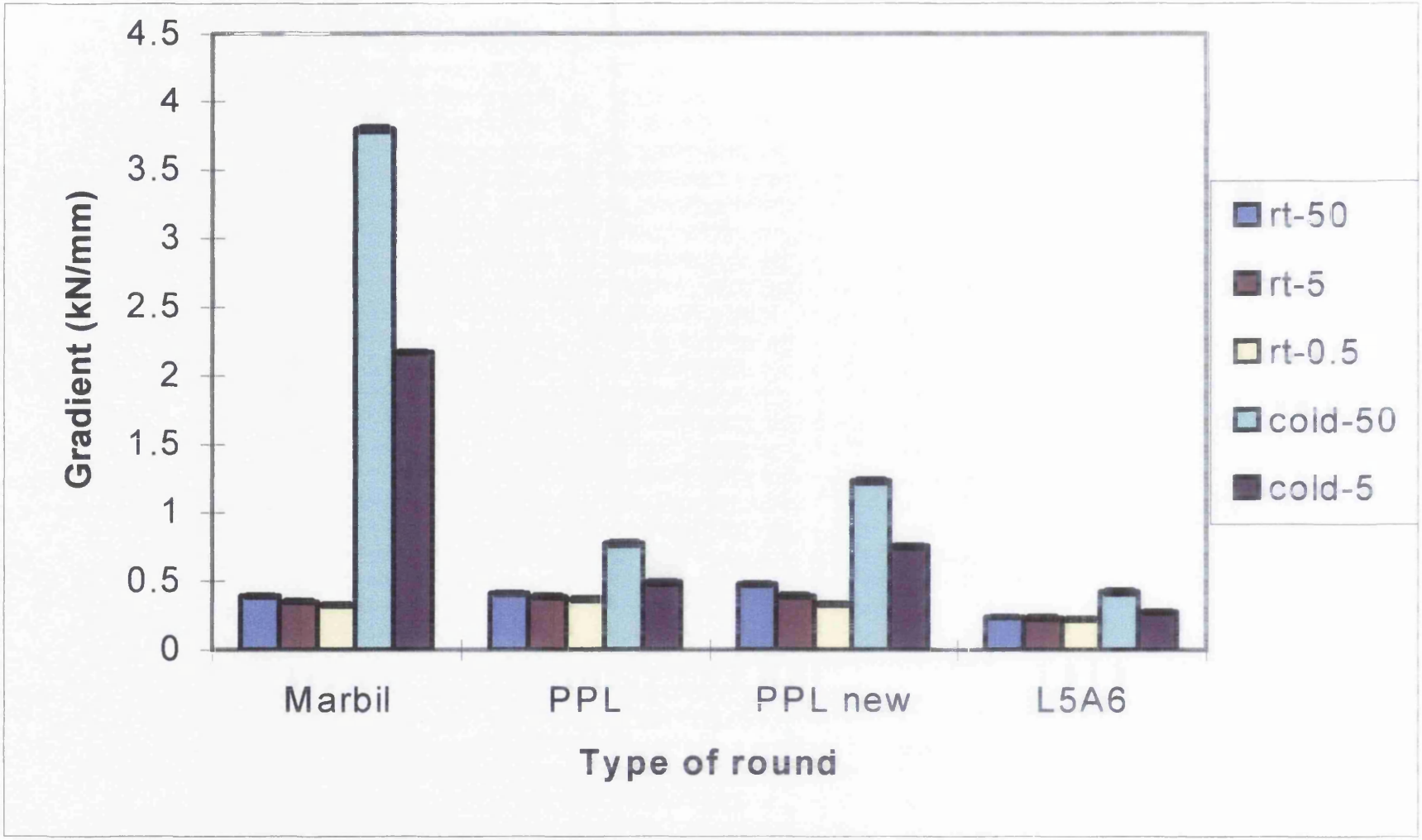

Figure 3.18 The Effects of Rate and Temperature on Compressive Stiffness

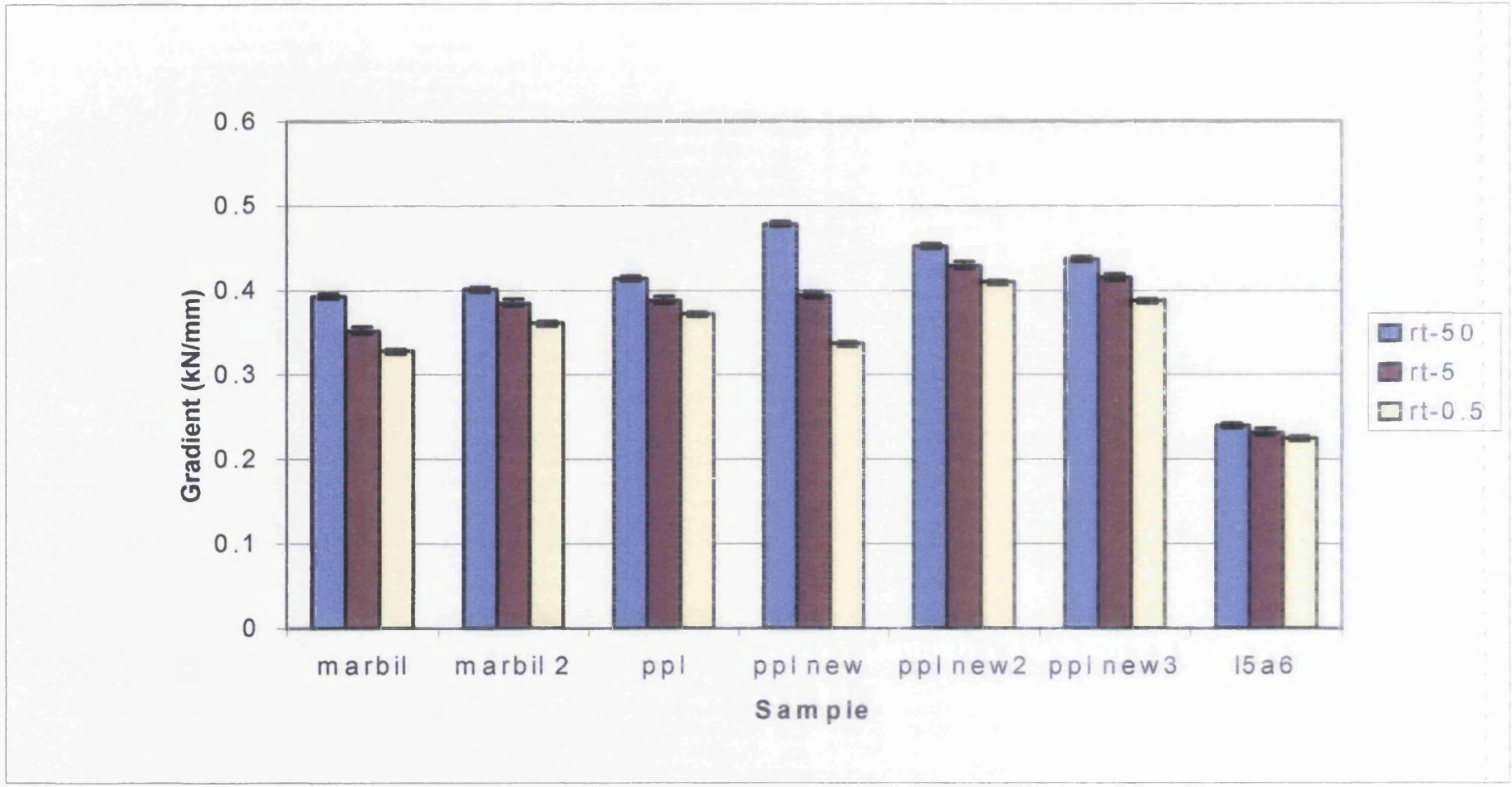

Figure 3.19 The Effects of Rate on Compressive Stiffness of all the Polyurethanes

3.5.3 DMTA Tests - The Effects of Test Rate

Similar tests to assess the effects of loading rate were performed using the DMTA. This has the advantage that it also gives values of damping, which should correlate well with resilience.

These tests were initially carried out in various different modes to establish which mode of testing would be the most accurate. Three of the most suitable testing set-ups were tried. These were Tension, Dual Cantilever Bending, and Three Point Bending. (Single cantilever had been tried prior to this, and deemed unsuitable due to erratic results).

Table 3.1 below shows a summary of these results for a range of the polyurethanes. The table shows values of the ratio of stiffness at 30 Hz to stiffness at 1 Hz. These values (listed as E(30)/E(1)) indicate the relative steepening effect of testing rate. Also listed are the values of tan δ (energy lost) at the two test frequencies, which should be similar for all three set-ups. It is clear that for each material tested in both dual cantilever and three point bending, the values of tan δ are significantly higher than for tension. It is clear that excess energy is being lost in these two test modes than in tension. The most probable reasons for this are due to slipping in the grips and/or friction. It was concluded from this that tension was the most reliable form of testing.

Table 3.1 The effects of testing rate and test geometry on stiffness and damping for various polyurethanes.

Sample	Resilience (Schob %)		Mode of Testing: Tension	Dual Cant	3 Pt Bending
PPL	50	E(30)/E(1)	1.22	1.23	1.48
		Tanδ (30)	0.13	0.168	0.43
		Tanδ (1)	0.07	0.08	0.13
PPL New 1	35	E(30)/E(1)	1.4	1.7	1.48
		Tanδ (30)	0.2	0.314	0.315
		Tanδ (1)	0.145	0.234	0.175
PPL New 2		E(30)/E(1)	1.19		
		Tanδ (30)	0.119		
		Tanδ (1)	0.063		
Marbil	20	E(30)/E(1)	1.8	2.09	1.66
		Tanδ (30)	0.3	0.457	0.47
		Tanδ (1)	0.17	0.326	0.22
TT	50	E(30)/E(1)	1.2		1.17
		Tanδ (30)	0.125		0.22
		Tanδ (1)	0.075		0.143
MTQ	56	E(30)/E(1)	1.17		1.24
		Tanδ (30)	0.095		0.25
		Tanδ (1)	0.068		0.08
TG	47	E(30)/E(1)	1.26		1.29
		Tanδ (30)	0.128		0.245
		Tanδ (1)	0.103		0.13
			Most reliable form of testing.	Possible slipping in grips.	Possible problems with friction

Considering the values for the tensile set-up (the first column in Table 3.1), the following points can be drawn. The values show that the MTQ round (with E30/E1 = 1.17) is least affected by rate at room temperature. It also has the second lowest tan δ value at 1Hz (0.068) and has the second smallest range of tan δ between 1 and 30Hz.

PPL new 2 is the next least affected by rate, with E30/E1 = 1.19. It also has the lowest 1Hz tan δ value. The tan δ at 30Hz is higher than the MTQ material but overall the properties of the two materials are quite similar. The behaviour of the PPL new 2 round in the compression tests and the small effects of rate on its stiffness indicate that MTQ would have similar (favourable) characteristics if it were formed into a baton.

The results of the compression tests for both Marbil and PPL new are backed up by the DMTA tests, with both rounds having a considerably higher E30/E1 ratio than the other specimens. Marbil is most affected by rate at room temperature, followed by the PPL new round. Marbil has an E30/E1 = 1.8, and PPL new = 1.4.

Except for PPL new 2, the three sheet materials, which all have a high resilience, outperformed all of the baton materials. The tests have shown that the effects of rate are lower for materials of high resilience. This backs up the earlier argument brought about by the compression results.

It can be seen that the values of E30/E1 and tan δ at 1 and 30Hz for both PPL and TT are very similar. They were supplied from two different sources and were said to be the same material, although without stronger evidence than word of mouth, it was not possible to be completely sure. However, the values recorded in this experiment are a strong indication that they are, in fact, the same. The slight differences in values that exist can be put down to sample preparation and machine set up before testing. It is also possible that the processing of the materials (the PPL into baton form and the TT into sheet form) had an influence on the results.

The PPL new 2 round appears to be the best candidate, based on these two sets of experiments. This is then followed closely by MTQ, then TT (PPL) and TG. The Marbil and PPL new rounds are unacceptably sensitive to rate change and should not be considered further.

3.5.4 DMTA Tests – The Effects of Temperature

In order to explore the link between the effects of test rate, the rebound resilience and the effects of temperature, further tests were performed using the DMTA to determine the way in which stiffness varies with temperature. These tests could also determine the glass transition temperature (Tg), and it was expected that a material with a low Tg would have a high rebound resilience at room temperature, a low variation with rate and a low variation with temperature. All of these properties are desirable in a baton round material, and so further confirmation of this would be considered useful.

Tests were conducted using the DMTA in temperature sweep mode. The samples were deformed cyclically in tension at 1 Hz while the test temperature was ramped from –80 C to + 60 C. Values of modulus and tan δ were continually recorded. Figure 3.20 shows typical results for the Marbil material. It can be seen that as the temperature increases, the modulus falls, most steeply over the glass transition region. The value of tan δ rises to reach a peak in this same region. The temperature of this tan δ maximum, which corresponds to the steepest drop in modulus, was used as the glass transition temperature, Tg. For the Marbil round, it can be seen that this occurs at about +7 C. An equivalent curve for the MTQ material is shown in Figure 3.21, from which it can be seen that there is a much lower value of Tg, at around – 65 C.

A summary of glass transition temperature values that were obtained from DMTA temperature sweep experiments is shown in Table 3.2 below.

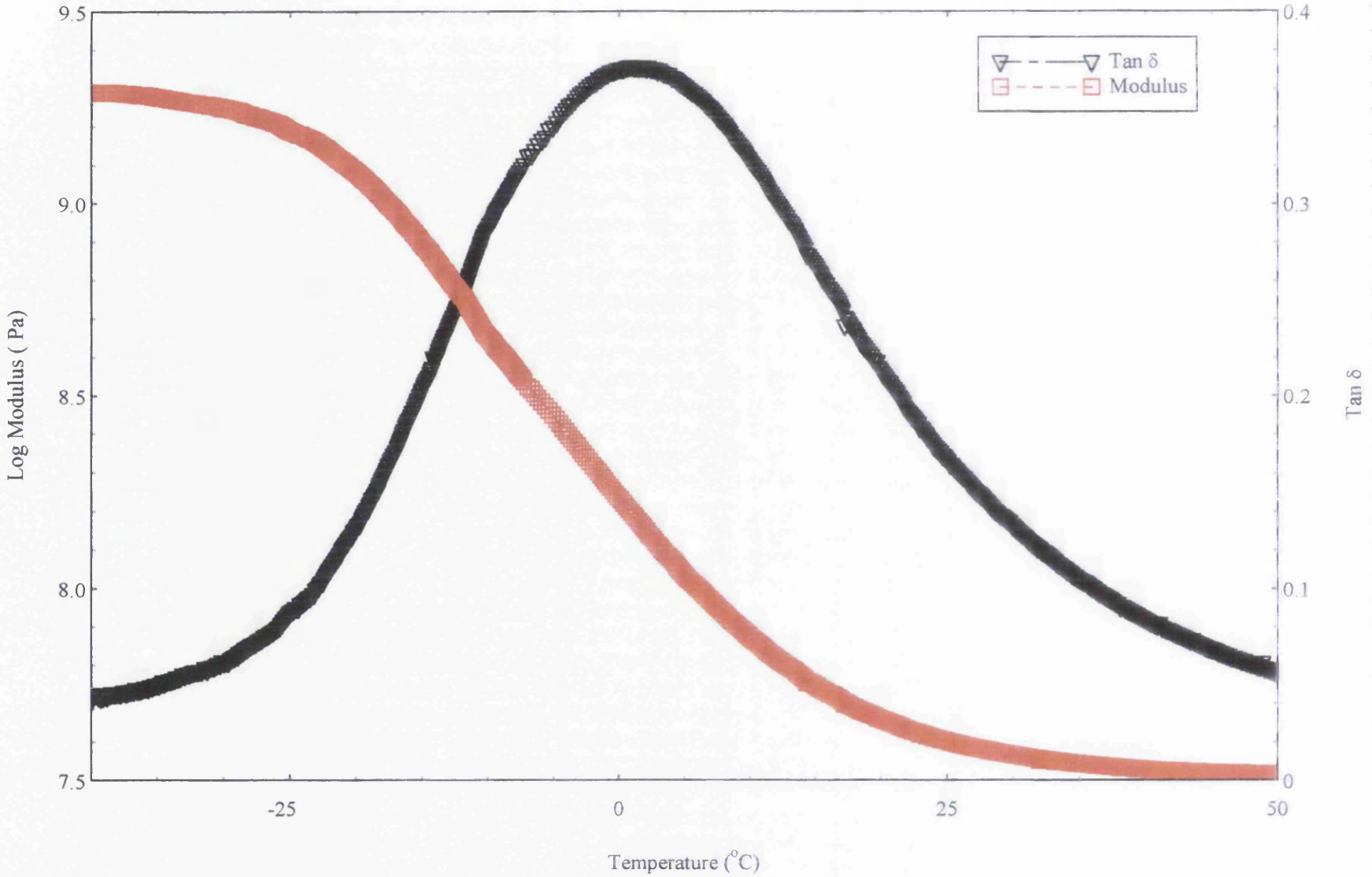

Figure 3.20 Modulus and Tan δ for Marbil sample at 1 Hz

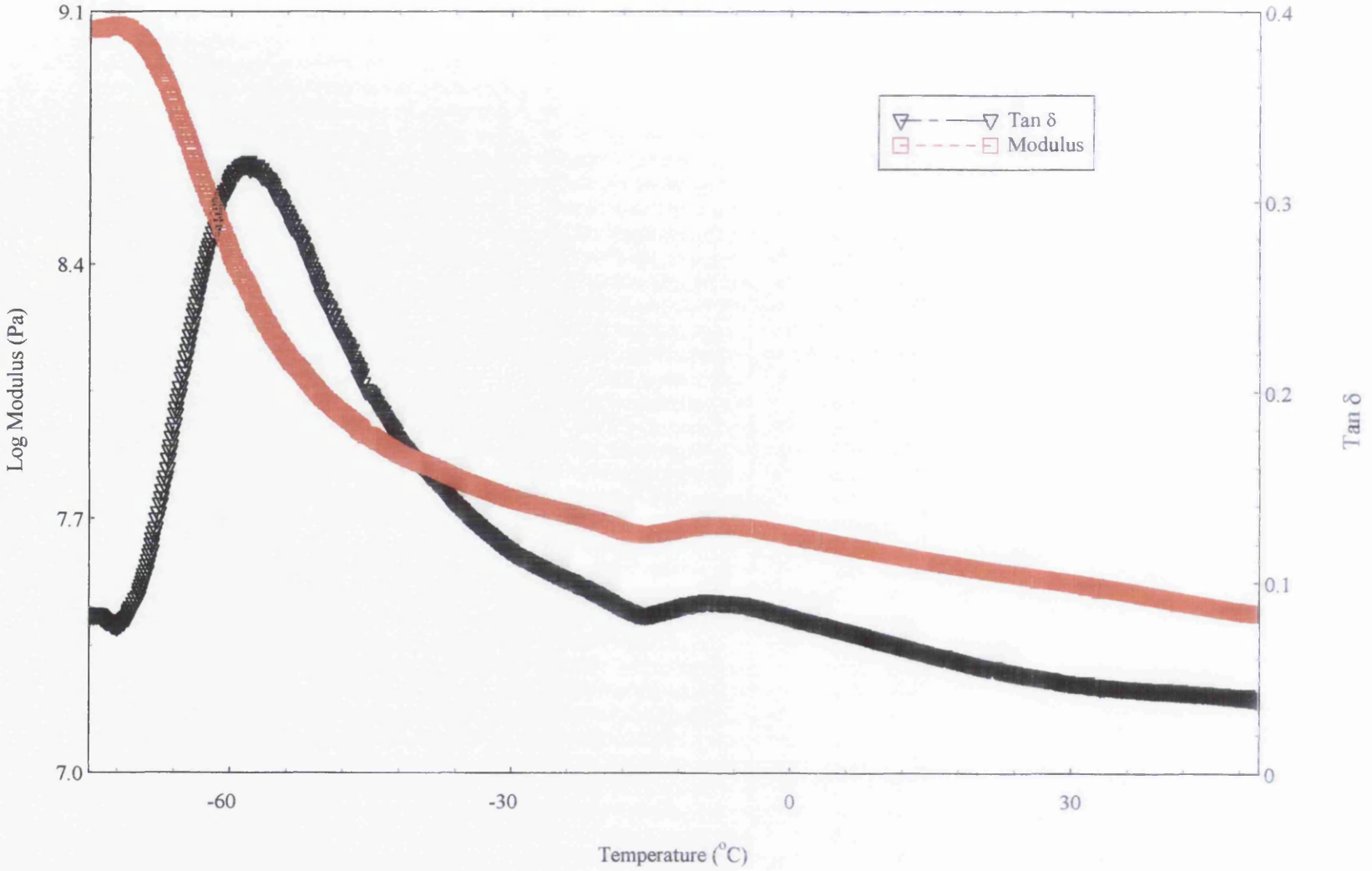

Figure 3.21 Modulus and Tan δ for MTQ sample at 1 Hz

Table 3.2 Glass Transition Temperatures, Listed Along with Resilience Values.

Baton Type	Glass Transition Temperature at 1Hz (°C)	Resilience (Schob, %)
L5A6	-28	50
Marbil	+7	20
Marbil new	-50	
PPL	-28	50
PPL new	-32	35
PPL new2	-50	
PPL new3	-53	
Hytrel	-67	
PU Thermoplastic	-65	
MTQ	-65	56
TG	-50	47
TT	-32	50

It can be seen that, in general, the rounds with the highest Tg, such as the Marbil material, have the lowest resilience values and those with the lowest Tg, such as the MTQ material, have the highest resilience. This is because the further from the Tg the batons are, the further away they are from the transition state, and the more the behaviour follows rubber (visco)elasticity. The correlation is not perfect, however, which demonstrates the complex nature of the dynamic behaviour of polymers. From all the results above, it is generally the case that the resilience gives a better indication of the effects of test rate than the value of Tg does. It therefore seemed sensible to use resilience as a specification for future rounds, but also to consider Tg (ideally a low value) when choosing the polyurethane material.

3.5.5 Assessing the Properties of Baton Round Materials at Realistic Testing Rates

The following section presents further results on the effects of strain rate on the modulus of two of the polyurethane materials; the L5A7 material, and the PPL new2 XL21 material. The purpose of these tests was to provide the important materials properties at realistic rates for the purposes of computer modelling of baton round impacts. Various test methods were employed, with the aim of ensuring good results by correlation of different methods, as well as to use the effects of low temperature to provide some information about the strain rates not directly accessible.

The most significant results are shown in Figure 3.22 below. These were performed in compression using dynamic mechanical test equipment. The compression modulus was measured for a range of strain rates from 5 x 10^{-3} to 10 s^{-1}. For each material, seven samples were tested. The results for some of these are not shown for clarity, but the band of results shown on the graph indicates the spread of results obtained. It can be seen that both materials have a similar and gradual increase in stiffness with increasing strain rate. The L5A7 material has less spread in results. The solid lines on the graph indicate the average values. All tests were performed at 23°C, and it should be noted that at lower temperatures, higher values of stiffness will result.

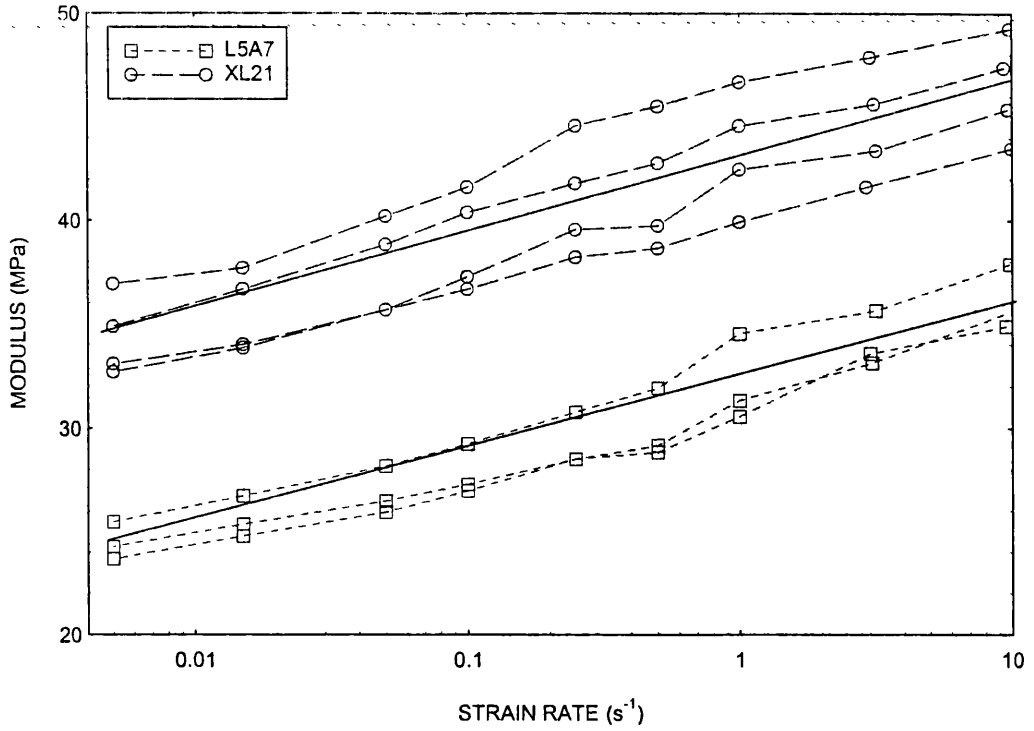

Figure 3.22 The effects of strain rate on the modulus of L5A7 and XL21 materials.

While these tests were performed at small strains (less than 0.5%), other tests were conducted to higher strains of about 30%. For both materials, the gradient of the stress-strain curve decreased with increasing strain. For the L5A7 material, this was a very gradual change; for the XL21, there was a more pronounced decrease in gradient at about 10% strain. Some tests were also performed in tension and bending to ensure reproducibility of modulus measurements, which was achieved.

The strain rate of 10 s^{-1} was the highest measurable. There is a need for values of the stiffness at higher rates, and so an estimation of this was performed using time-temperature equivalences. The basis behind this is that a reduction in temperature is equivalent to an increase in rate (as there is less scope for molecular motion in both cases).

Tests were performed on strip samples in bending at three rates (indicated by testing frequency) at temperatures ranging from -10 to 25°C. These are shown in Figures 3.23 and 3.24 for the L5A7 and XL21 materials respectively. The modulus is higher at low temperatures for both materials, as they approach the glass transition region. As this

region is at a lower temperature for the XL21 material than for the L5A7 material, the increase in stiffness at low temperature is more pronounced with the L5A7. These graphs also give information on the temperature-sensitivity of modulus, if needed.

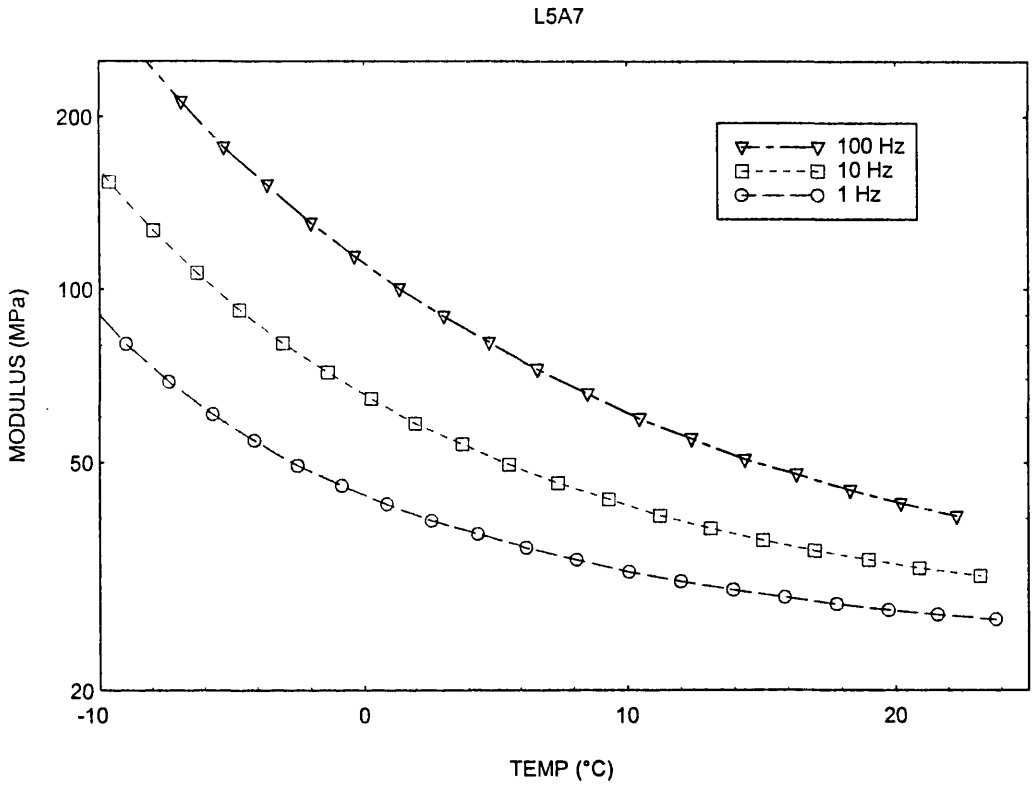

Figure 3.23 The modulus of the L5A7 material versus temperature and frequency.

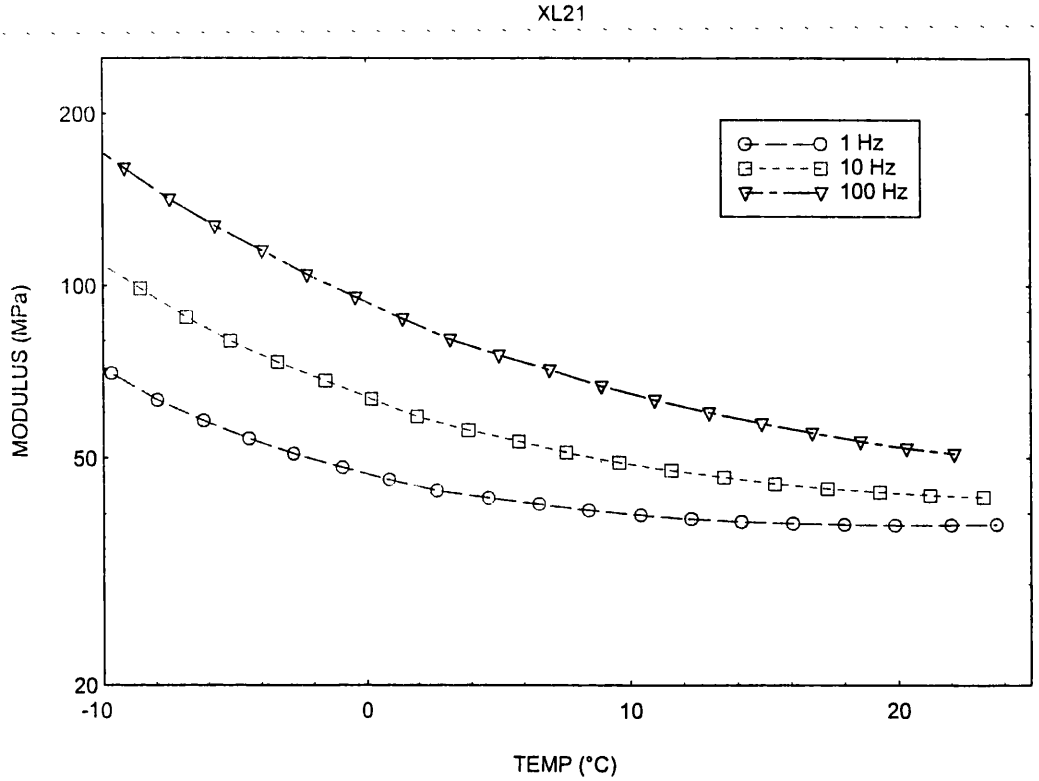

Figure 3.24 The modulus of the XL21 material versus temperature and frequency.

The curves can be made to superimpose by shifts along the temperature axis, with about 8°C being equivalent to one decade of test rate. This amount is similar to values found for a wide range of polymeric materials. By using this scaling factor, it is possible to estimate the behaviour at higher frequencies. For example, the stiffness at 1 kHz at 23°C is equal to that at 100 Hz at 15°C. By using this method, values of stiffness were estimated for rates as high as 1000 s^{-1}. These are shown on Figure 3.25, from which it can be seen that the increase in stiffness with rate accelerates, but more so for the L5A7 material, reflecting its higher glass transition temperature. These values, although giving some indication of the behaviour at higher rates are only estimates, and should be treated with more caution than the directly measured values.

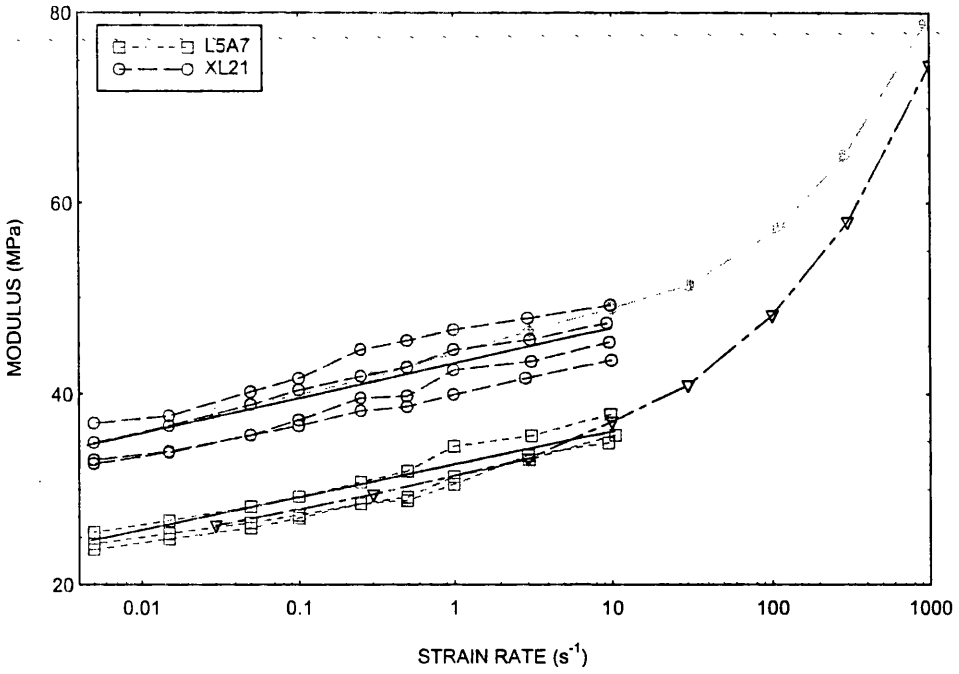

Figure 3.25 An extrapolation of modulus values to higher strain rates.

3.5.6 Thermal Expansion Tests

Results from the thermal expansion tests conducted using the DMTA for PPL new2 and Marbil rounds are as follows.

Specimen	Thermal Expansion Coefficient / °C
Marbil	182×10^{-6}
PPL new2	207×10^{-6}

When conducting the tests the specimens were initially set up in tension. Unexpected results were obtained for all samples using this set up. One of the unexpected effects on the graphs produced was in the form of dips, within the range -20 to +20°C. It was possible that this was due to slipping in the grips, or crystallisation of some parts of the

material structure. However, the most likely reason was due to the effects of water within the material. The polyurethanes used had a high absorption rate and could have had water within the system. As the temperature increased to close to zero this would lead to ice within the polyurethane beginning to melt and cause the displacement variances.

Heat treatment prior to testing was thought to be a possible solution, so various levels of heat treatment were initiated to see if the blips and dips could be either reduced or completely removed. This was seen to have an effect, and the dips were reduced considerably.

Another problem observed from the DMTA-produced graphs was a series of small steps in the displacement axis. There were two possible reasons for this occurrence. One was that this jerky displacement was a physical event and occurred as a result of flexing within the material structure, and the second, was that it was due to a machine-related event, occurring due to stepper motor gear backlash. If the former was the case, then the displacement losses should be added together to give the true displacement. However, if the latter was the case then the steps should be averaged out.

To test which was true, a sample of polycarbonate was tested under the same conditions. This is a much stiffer polymer and was not expected to have any of these stepped effects. Therefore if, at the end of the test the final displacement on the graph was the same as that shown on the specimen in the grips of the DMTA (measured with calipers), then the results should be averaged as the problems are machine related. Or, if the displacement figures were lower on the graph than in machine grips the effects are material related, and should be added.

The findings were that the effects were machine-related; probably due to the gearing in the stepper motor. Therefore the edges were averaged out and the thermal expansion coefficients were calculated.

3.5.7 Environmental Exposure Tests

3.5.7.1 High Temperature Exposure (Heat Ageing)

Results for the heat ageing experiments are shown below in Figures 3.26 to 3.29. Figure 3.26 shows the variation in modulus after ageing for MTQ, TT and TG samples (2 of each). It can be seen that all except the two TG samples show a small degree of hardening after 7 days, whereas the TG samples both decrease in modulus. After 14 days MTQ and TT continue to increase in modulus. TG has now increased in modulus as well, to near the original values.

Figure 3.27 shows the values of tan δ for these materials after thermal ageing, from which it can be seen that all samples show a decrease in tan δ after 7 days. After 14 days, however, the tan δ values for the MTQ have increased to the original values and TT has increased to above the original values, whereas tan δ for TG has decreased even more.

The increase in modulus and an initial decrease in tan δ seen with the MTQ and TT can be put down to the high temperature leading to an accelerated curing of any remaining TDI groups within the structure i.e making the material stiffer and more resilient.

The TG material was more heavily cross-linked to begin with and therefore any further heat treatment would not lead to increases in stiffness. With this material after 7 days and with the others after 14 days, the heat ageing eventually leads to permanent degradation of bonds, which gives a further increase in modulus and an increase in tan δ.

Figs 3.28 and 3.29 show modulus and tan δ values for the heat ageing experiments for Hytrel, PU Thermoplastic and PPL new2. It can be seen that Hytrel shows a small and steady decrease in modulus after both 7 and 14 days. PU Thermoplastic shows a more significant drop after 7 days (the same amount as Hytrel after 14 days) but then remains constant after 14 days. Both these samples are showing signs of permanent chemical degradation. PPL new2 is significantly stiffer to begin with than the other two samples. With heat ageing it stiffens by a small amount after both 7 and 14 days.

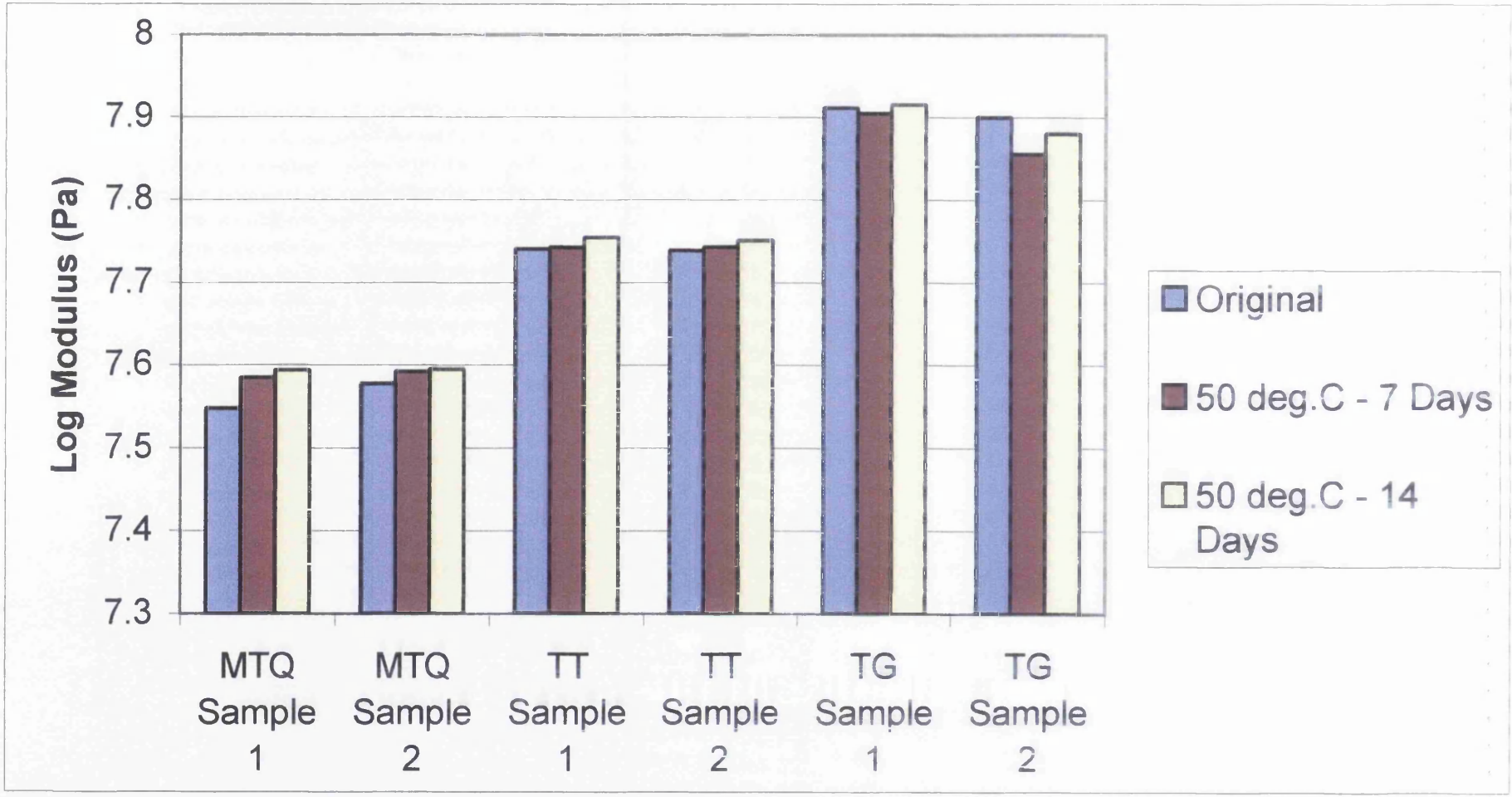

Figure 3.26 The Modulus of MTQ, TT and TG after Thermal Ageing

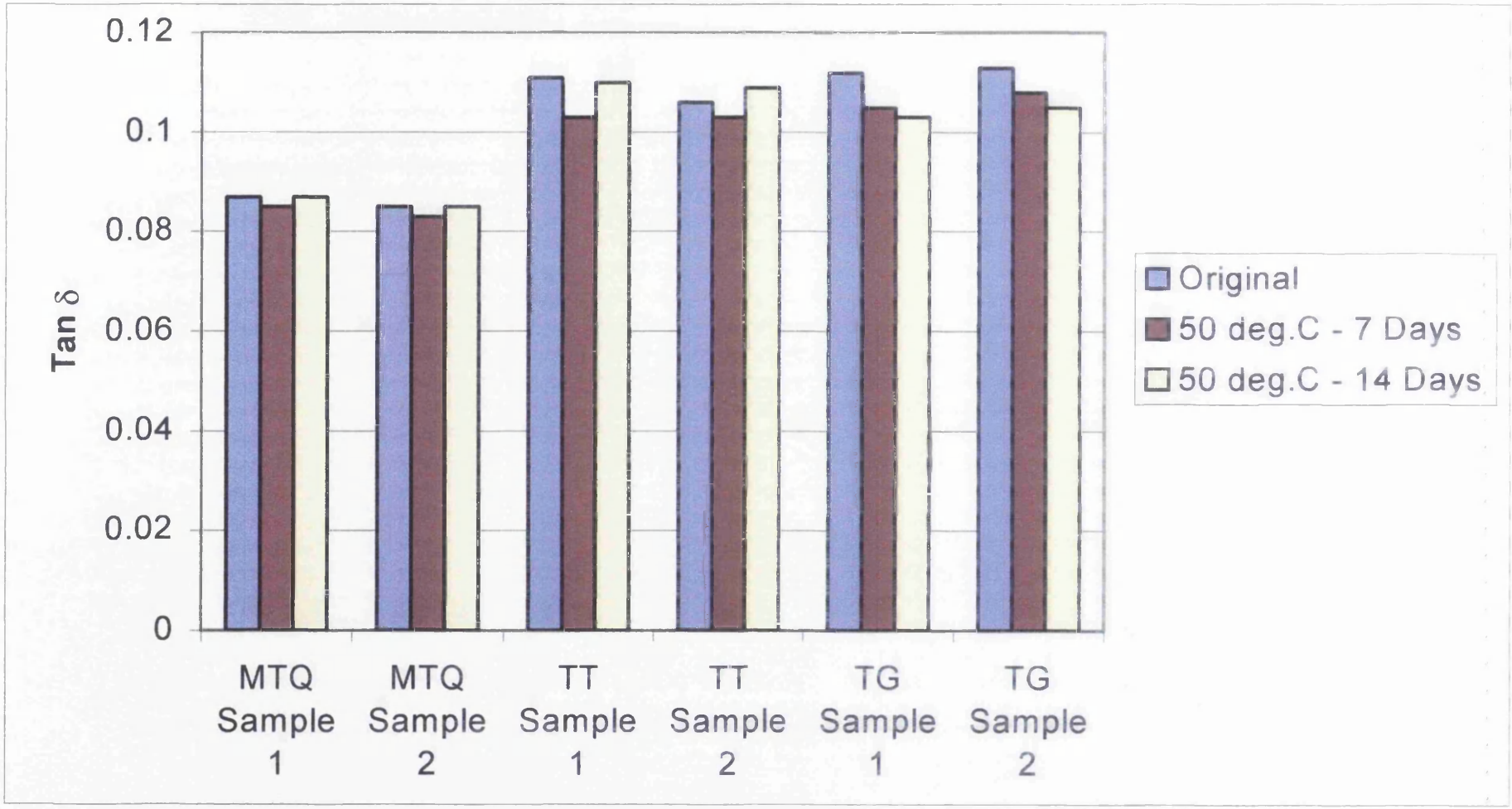

Figure 3.27 The Tan δ of MTQ, TT and TG after Thermal Ageing

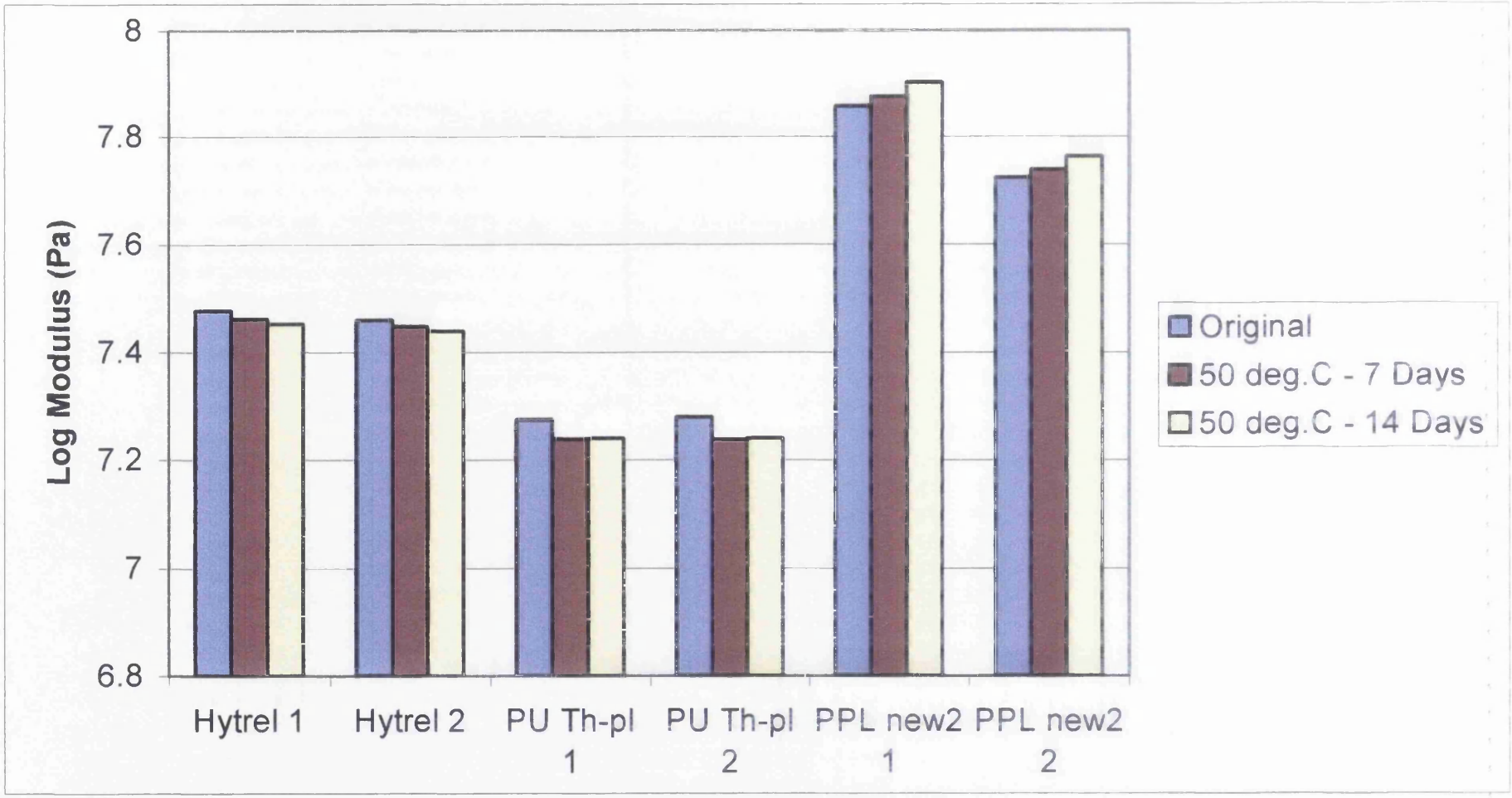

Figure 3.28 The Modulus of Hytrel, Polyurethane Thermoplastic and PPL new2 after Thermal Ageing

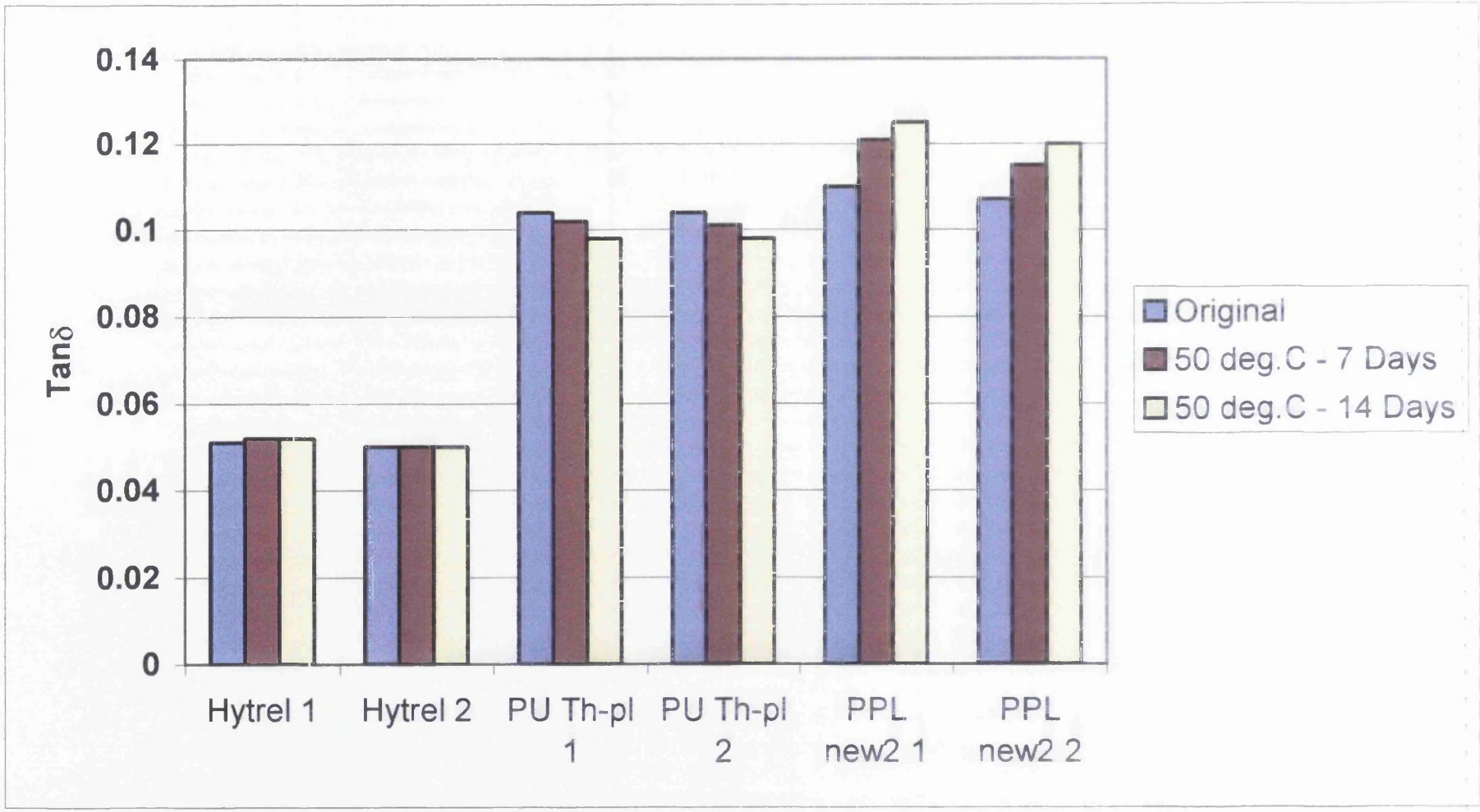

Figure 3.29 The Tan δ of Hytrel, Polyurethane Thermoplastic and PPL new2 after Thermal Ageing

The tan δ for Hytrel remains unchanged after 14 days. That for PU Thermoplastic decreases a small amount after 7 days, then again after 14 days. Tan δ for PPL new2 increases a reasonable degree after 7 days, then a further small amount after 14 i.e there is an initial large decrease in resiliance and thereafter the following decrease is small.

From these, it can be seen that there is potential for further hardening due to incomplete cure (seen with the TT, MTQ and PPL new2), as well a change in stiffness (up or down, but accompanied by an increase in tan δ) due to chemical degradation (seen with TG, Hytrel and PU thermoplastic). It should be emphasised, however that the changes seen are relatively small, given the severity of the thermal ageing treatments.

3.5.7.2 UV Exposure

The UV exposure test results are shown below in Figures 3.30 to 3.33. Figure 3.30 shows the effects of UV exposure on the modulus for MTQ, TT and TG. Figure 3.31 shows tan δ values for these materials. From these, it is clear that there is no generally clear pattern for behaviour of any of the materials. MTQ is the most consistent, exhibiting a small decrease in stiffness after 24 hours, followed by an increase to just above the original values after 48 hours, then a more marked increase after 120 hours. This occurs for both samples tested. Tan δ values show a consistent increase with exposure. This behaviour is consistent with a gradual hardening due to cross-linking.

Both samples of TT and TG show no major similarities in their behaviour as exposure time is increased. Instead, they show random increases/decreases. An explanation for this random behaviour can be found by looking at the molecular effects of ultraviolet light. When exposed to UV, polyurethanes can suffer from chain breakage. With time the chains can either stay broken or re-cross link. Both mechanisms can operate at the same time, but one will always dominate the other. This is determined by a number of complex factors that shall not be discussed here. The dominant mechanism is the one that will be observed, which is why some of the values of modulus and tan δ increase, whilst others show a decrease.

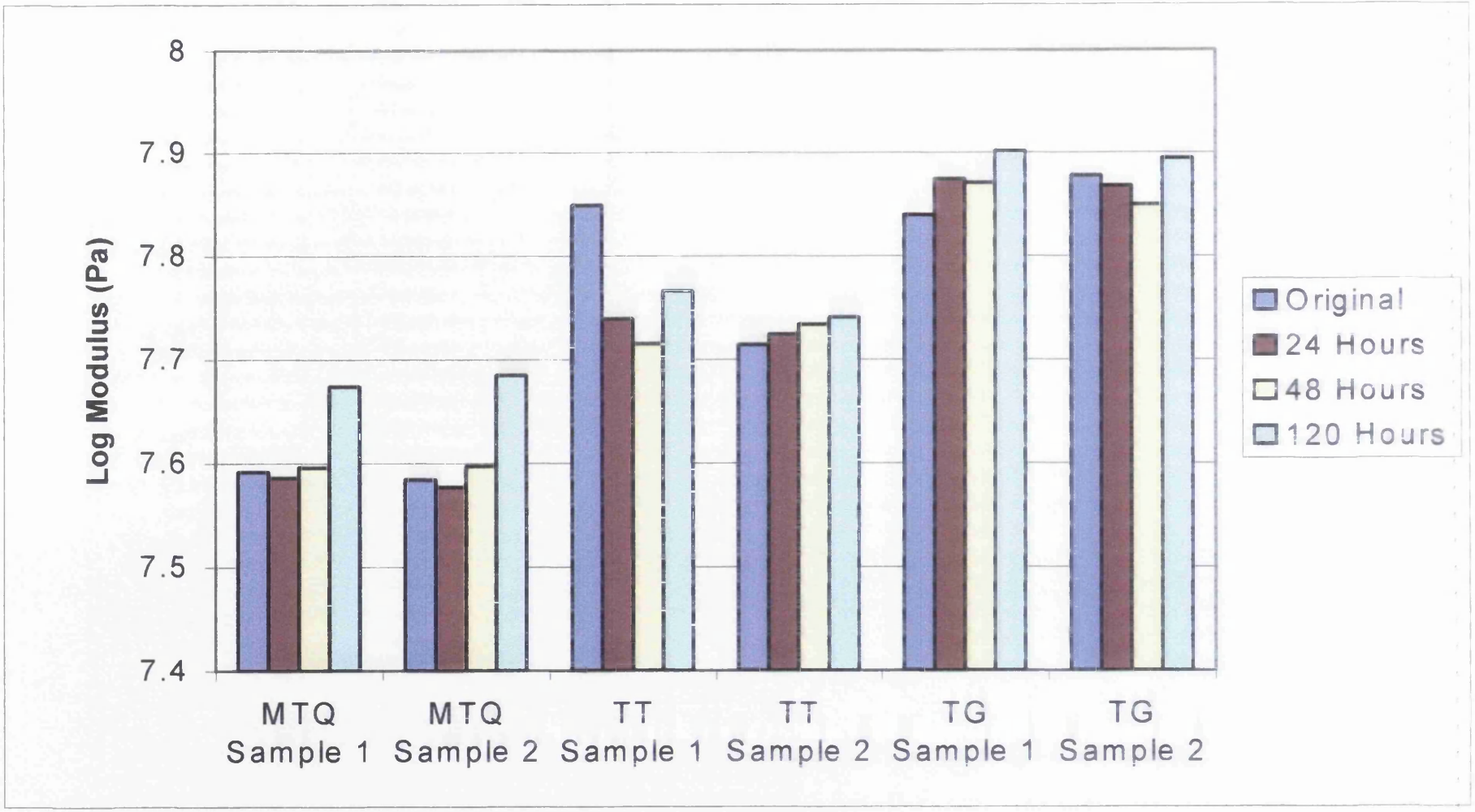

Figure 3.30 The Modulus of MTQ, TT and TG after UV Ageing

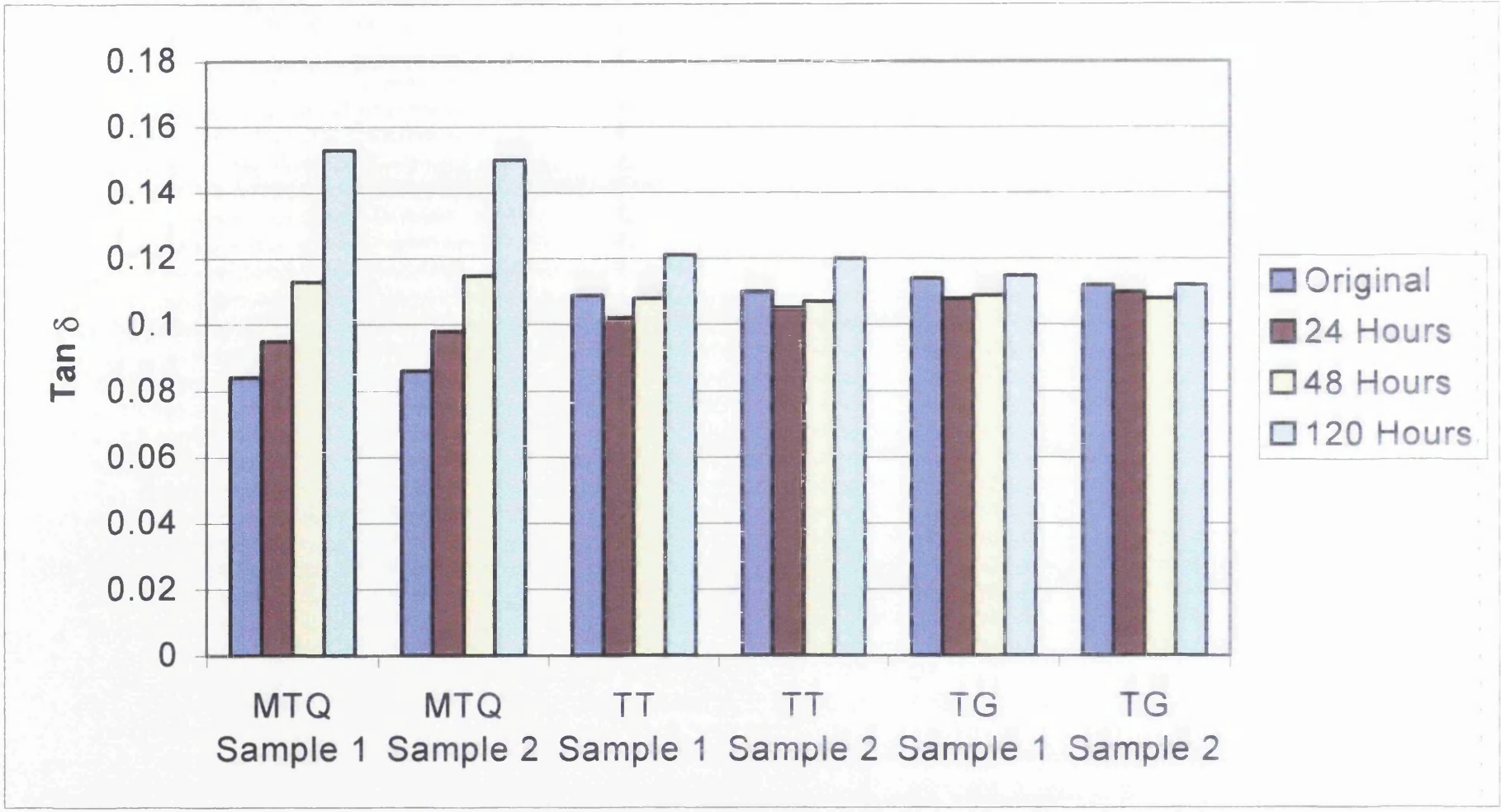

Figure 3.31 The Tan δ of MTQ, TT and TG after UV Ageing

The results for Hytrel, thermoplastic PU and PPL new2 are shown in Figs 3.32 and 3.33. It is clear that Hytrel shows a steady decrease in modulus over the 120 hours of exposure (especially after the first 24 hours). This is accompanied by an increase in tan δ, and is evidence for permanent chain breakage.

One sample of PU Thermoplastic shows a large initial decrease, then it fluctuates up to 120 hours. The other sample shows a steady modulus decrease throughout. This is accompanied by a tan δ increase.

PPL new2 shows a general increase in modulus, accompanied by an increase in tan δ except for the longest exposure, when there is a slight decrease.

There is more consistency in this set of UV exposure experiments than those mentioned above, but it is clear across the six specimens that the process of bond breaking, then either further breaking or re-crosslinking is occurring. The dominant mechanism varies for each sample, but as with the thermal ageing, it should be emphasised that the changes are slight, given very severe UV ageing (equivalent to well over a year's continuous sunlight exposure).

3.5.7.3 Water Exposure

The values of modulus and tan δ for MTQ, TT and TG after water immersion are shown in Figs 3.34 and 3.35. It is clear that the effects of immersing the samples in water for 7 days then drying them in air for a further 7 days were very similar across the whole range of samples tested. For all three materials, both modulus and tan δ decrease after the 7 day immersion. Then after the drying in air, the values increase again to either just below, just above or equal to the original values.

As the samples are immersed, water can diffuse in and cause a small degree of plasticisation. The chains are allowed to move more easily and the frictional losses when the chains move are reduced. The water molecules between the chains act almost like a lubricant and result in the material becoming more flexible. This is the reason for the

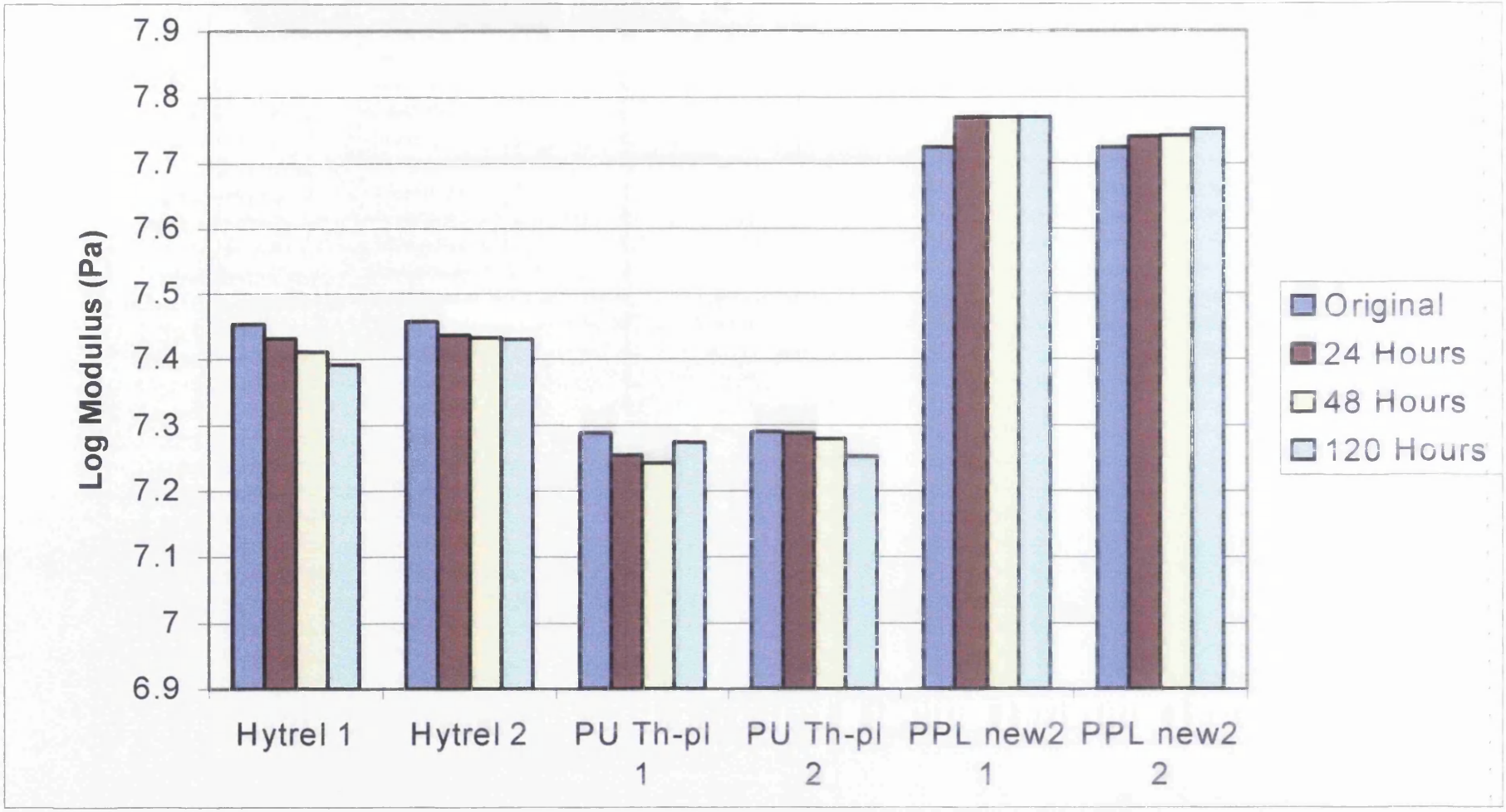

Figure 3.32 The Modulus of Hytrel, Polyurethane Thermoplastic and PPL new2 after UV Ageing

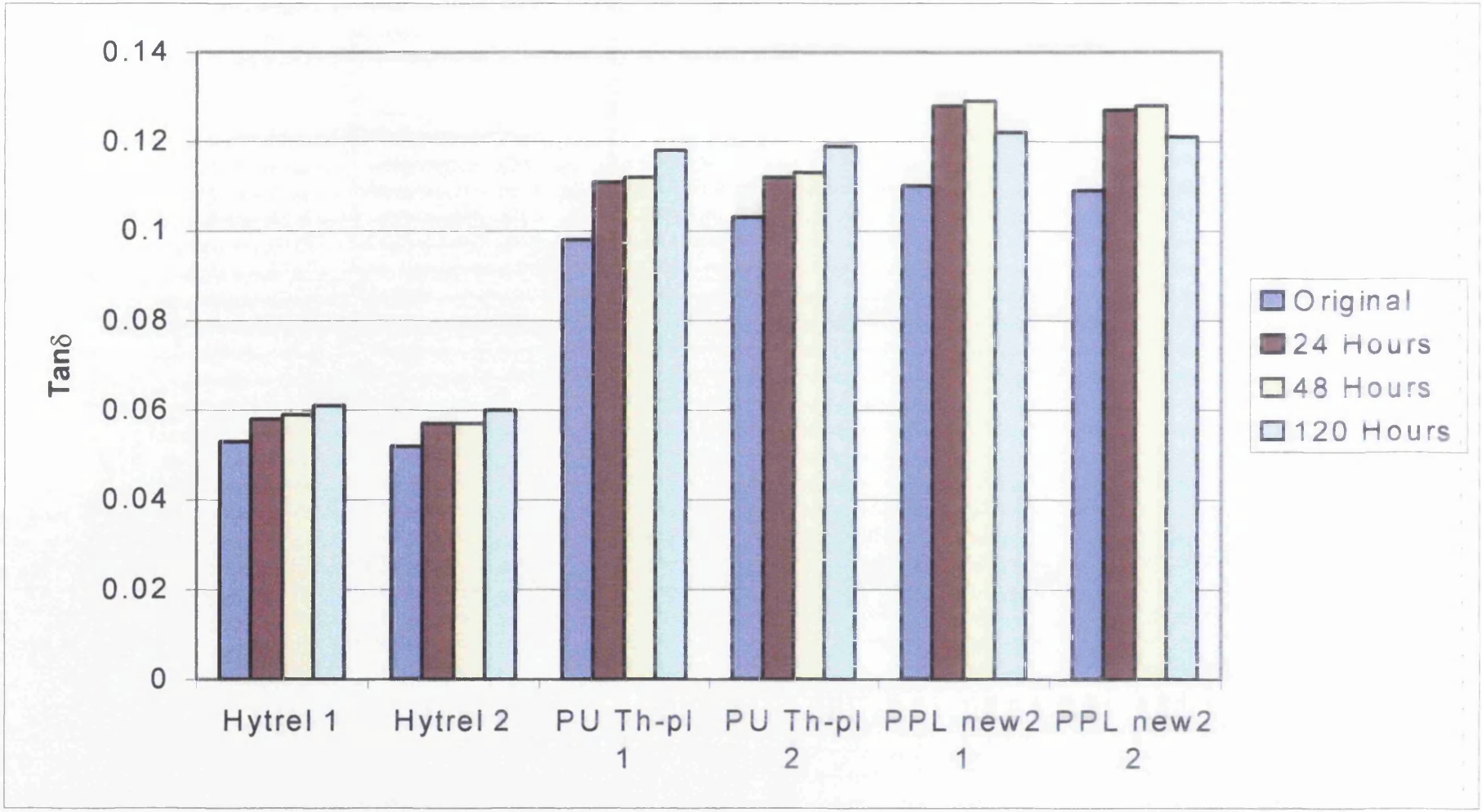

Figure 3.33 The Tan δ of Hytrel, Polyurethane Thermoplastic and PPL new2 after UV Ageing

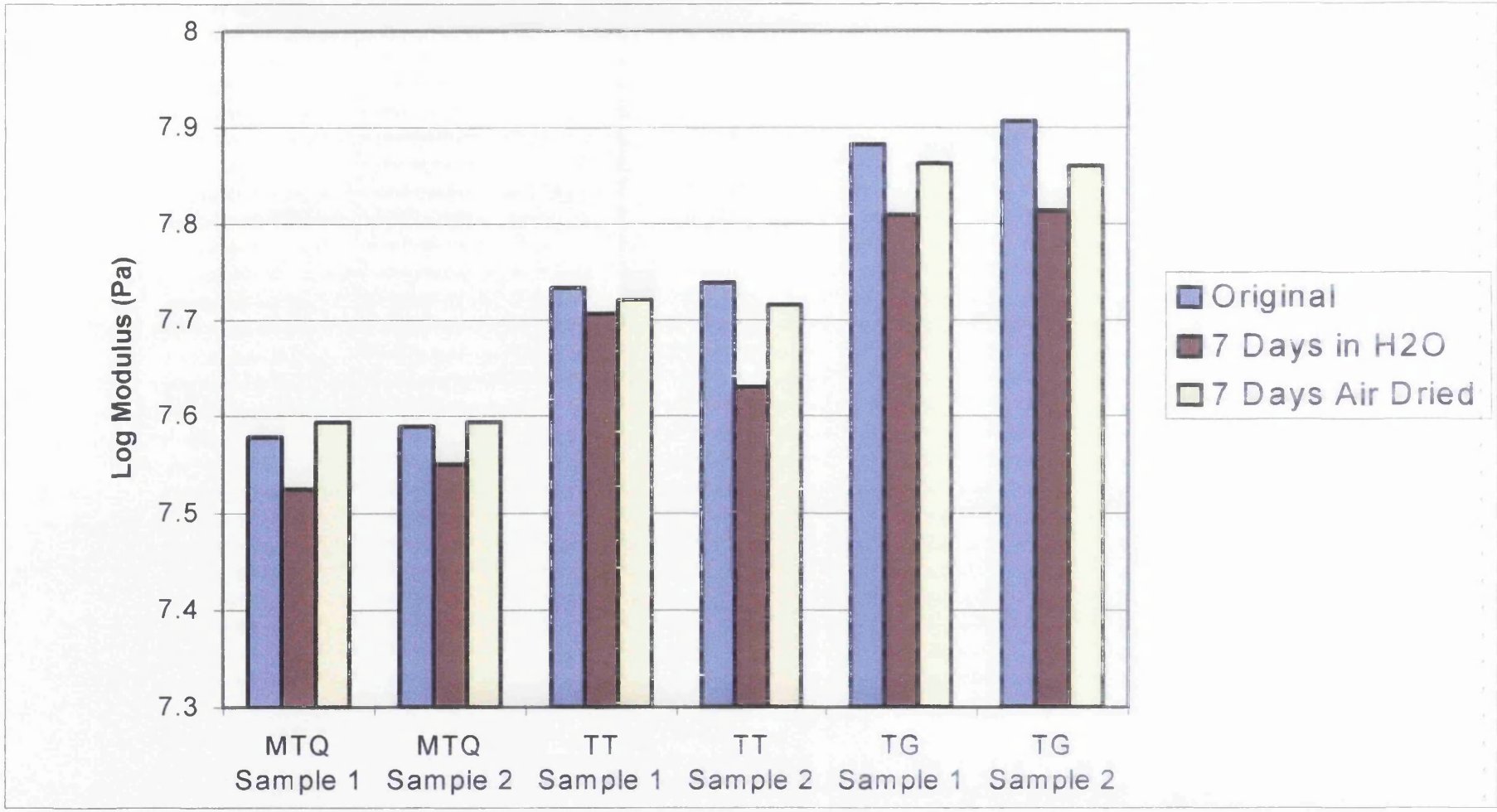

Figure 3.34 The Modulus of MTQ, TT and TG after Water Immersion

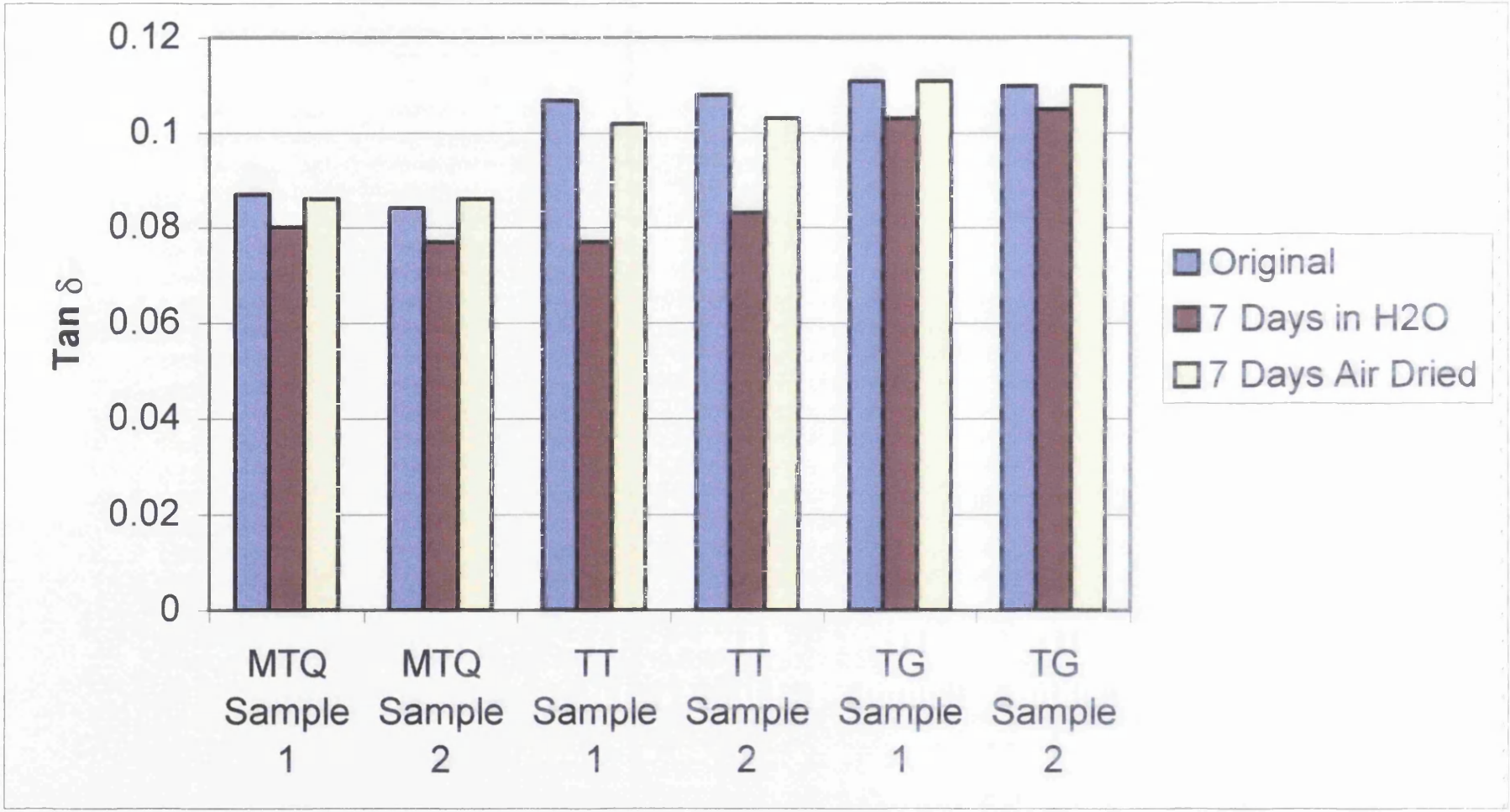

Figure 3.35 The Tan δ of MTQ, TT and TG after Water Immersion

initial decrease in modulus and tan δ. However, after the samples are allowed to dry in air, the water molecules are driven off the sample. The easy chain movement is restricted and frictional forces increase. More energy is lost from the system, leading to an increase in tan δ to close to the original level.

After the 7 day drying period all samples, except the MTQ, show the modulus to be slightly less than the original values. MTQ shows values marginally in excess of its initial values. This implies that the MTQ sample has undergone a minimal degree of hardening. This can be explained by the probability of a slight excess of TDI left in the material after initial curing on manufacture.

TDI reacts with MbOCA to give cross-links. There is approximately 95% MbOCA to 100% TDI in the initial polymer mix, so when curing takes place it is sometimes possible to have an excess of TDI left in the system. Exposure to water can cause the remaining TDI to react, leading to an increase in hardness. However, considering the timescales and levels of exposure, the resulting increase in hardness is not of particular concern.

Both TT and TG samples show a slightly lower modulus after drying than before exposure. This could be due to some water molecules remaining in the samples. More time may be needed for the water to fully be driven off.

The results of water immersion for Hytrel, PU Thermoplastic and PPL new2 are shown in Figs 3.36 and 3.37 below. Hytrel shows a slight decrease in modulus after 7 days immersion in water. This is combined with an increase in tan δ, i.e the sample is softer and less resilient due to the ingress of water. Then after 7 days drying, the modulus returns to the original values, as does the tan δ, showing that no permanent hardening has occurred.

The PU Thermoplastic shows a drop in modulus after immersion in water, which then remains constant after drying in air. This is strange as it implies the material has either not had sufficient time or heat to drive off the water, or it has undergone permanent softening.

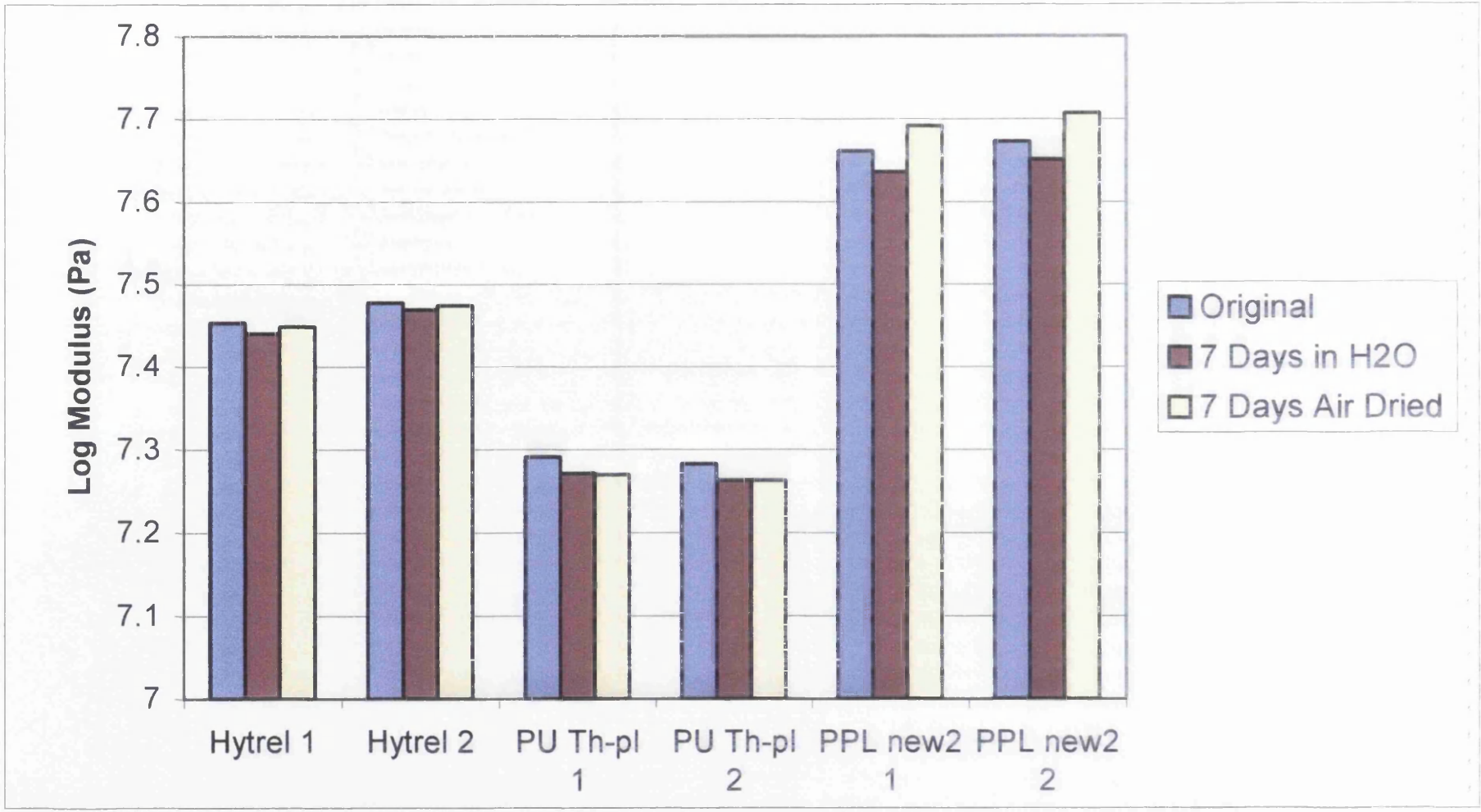

Figure 3.36 The Modulus of Hytrel, Polyurethane Thermoplastic and PPL new2 after Water Immersion

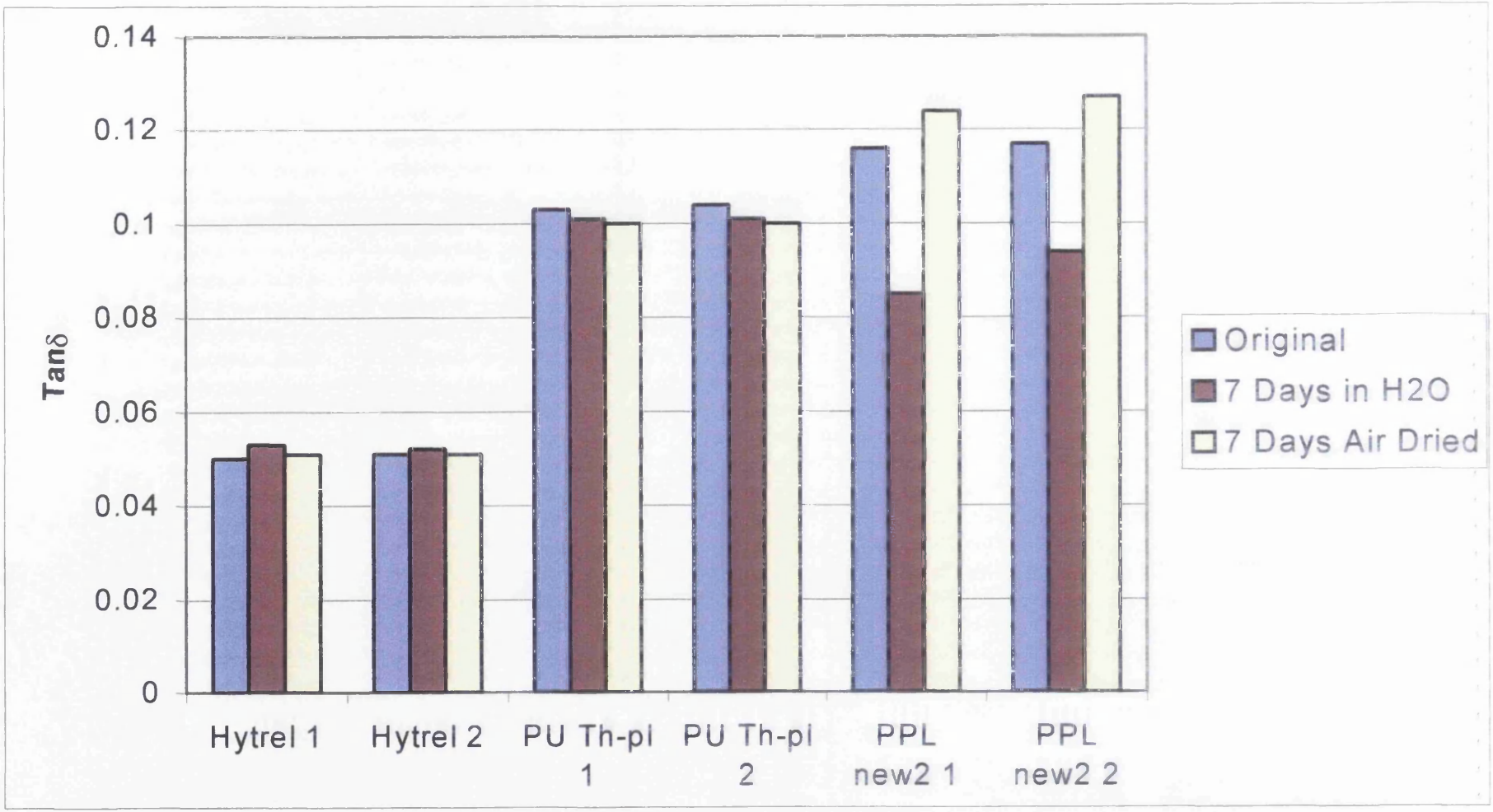

Figure 3.37 The Tan δ of Hytrel, Polyurethane Thermoplastic and PPL new2 after Water Immersion

It also shows a steady decrease in tan δ which means less energy is being lost per cycle, and it is becoming more resilient.

The PPL new2 samples also show a decrease in modulus and at the same time a significant drop in tan δ, which means the material becomes softer and much more resilient. After the drying time, the modulus increases to above the original level, as does the tan δ. Therefore this sample had suffered hardening which is most likely to be due to curing of excess isocyanate.

3.5.7.4 Summary of Environmental Tests.

In conclusion of the environmental exposure tests, it is clear that there were small effects due to prolonged heating, UV exposure or water contact. Most of these effects were fairly consistent between the thermosetting polyurethanes and are reasonably well explainable. The two thermoplastic materials show slightly different effects. Despite this, the effects of environmental exposure are relatively small and should pose no real problems when storing rounds made from these materials.

3.6 SUMMARY OF CHAPTER 3

From the work described above, it is clear that the understanding of the polyurethanes that could be used for baton rounds has progressed considerably. This work has shown that material specification is not a simple process, but there are now clear indications of what materials issues are important. The key points arising from this study are as follows:

- The rebound resilience is an important property. As all polymers will become stiffer at faster rates, this fact has to be accounted for in material specification. It has been shown that for polyurethanes of high rebound resilience, the effects of rate are least significant. With materials of low resilience, the stiffness at impact rates could be unacceptably high. It has been proposed that a resilience of at least 50% (measured by the Schob method) or 60% (measured by Lupke) should be required.

- There was no systematic variation of rebound resilience with polyurethane type, and so there was no need to specify exactly which type of polyurethane is to be used, as long as it is of high resilience.

- The glass transition temperature is another measure of this behaviour. A low glass transition temperature will generally give high resiliences, as well as least effect of test temperature on properties. Given the difficulty in measuring this property, it was not thought appropriate to be included as a specification.

- The infra-red analysis method had again proved successful in picking up uncured NCO, which may lead to delayed hardening. This was built into the specifications for the L5A7 rounds. No excess NCO was detected with any of the XL21 rounds, and so this may not be necessary for the polyether based polyurethanes.

- Environmental exposure tests showed only slight changes on exposure to prolonged high temperatures, UV radiation or water immersion. These results showed that the polyurethanes are generally stable materials and so can be stored for moderate lengths of time with confidence.

- Thermal expansion tests have shown that all the materials have relatively high values of thermal expansion (between 180 and 200 x 10^{-6}). These high values may cause problems with firing at high temperatures, but unfortunately, there is little that can be done to the materials to reduce the values.

CHAPTER 4: MECHANICAL PROPERTIES OF BONE

4.1 LITERATURE REVIEW ON THE DYNAMIC PROPERTIES OF BONE

The area of work covered in this literature review is essentially concerned with the properties of human skull bone at fast rates. The number of published papers in this area was found to be very limited, so the study includes important findings from other types of bone. It was seen that many of the important issues seem to be common to all types of bone.

The issue of comparing experiments conducted by different workers can be a very complex task and the variation of results can be explained by many variables such as testing set up, size, shape and type of sample used, strain rate etc. For the purpose of this report it was necessary to discuss the most important variables as separate issues. If this was not done, the properties seemed to vary wildly and it would have been very hard to select values to be used for modelling. The key variables were divided into the following groups:

- Density (and hence ratio of compact / cancellous bone)
- Location and orientation
- Testing rate
- Testing geometry (tension, compression or bending)
- Sample condition (fresh, dry or re-wetted)

With regard to the type of sample, for example, many workers have tested bone not only from humans but bovine and primate too. Some investigators have studied whole sections of cranial bone modelled as a layered sandwich structure [28-31]. Others have focussed on the mechanical properties of just the compact or cancellous regions as independent structural elements. Wood [32], Reilly and Burnstein [33], Tanabe and Kobayashi [34] concentrated only on compact bone, whereas Carter and Hayes [35], Schoenfeld, Lautenschlager and Meyer [36] focussed only on cancellous bone.

4.1.1 Density Factors

The classification of bone as being compact or cancellous is an issue relating to porosity. This is the proportion of the volume that is occupied by non-mineralised tissue. Compact bone has a porosity of between 5 and 30% and cancellous bone has a porosity ranging from 30 to 90% [37].

Cancellous bone and cortical (compact) bone can be expected to have different mechanical properties due, mainly, to significant structural differences between the two. Cortical bone is macroscopically a uniform solid whereas cancellous bone is a non-uniform three-dimensional array of bony trabeculae with interconnecting spaces containing bone marrow [36].

McElhaney et al [28] found that the structure of the human skull was a well-defined shell of compact bone separated by a core of spongy, cancellous bone (the diploe). Compact bone surrounds and reinforces the sutures. The thickness of the spongy core increases towards the centre of the bone away from the sutures. The cancellous region is extremely variable in structure with marrow spaces normally ranging from 3mm diameter down to microscopic size.

The density of bone is the most important factor in determining strength. McElhaney et al [28] found positive correlations between bone density and the compressive strength and modulus of elasticity. As density increases, so does the strength and modulus. They hypothesised that the compressive strength was proportional to the 4^{th} power of the density, and the Young's modulus was proportional to the 3^{rd} power of the density i.e the density cubed. This was called the "porous block model", and assumed that the two different types of bone have the same microscopic properties but varying microscopic structure.

However, work carried out by Carter and Hayes [35 and 37] found the compressive strength to be proportional to the density *squared*. This relationship was found to be true

for the whole range of bone densities found through the human skeleton from very compact compact bone to very porous cancellous bone.

The most reasonable explanation for the difference in findings between Carter and Hayes and McElhaney et al can be attributed to the difference in samples tested. McElhaney et al looked at human cranial bone as a two-phase structure - testing both inner and outer tables of compact bone with the trabecular diploe layer between them. Whereas Carter and Hayes only tested the trabecular region. The differences in the two structures could be responsible for the different findings.

The re-analysed results from David Taylor's work (discussed later) showed that both the strength and stiffness increased with decreasing sample thickness (and hence increasing density). However, the stiffness increased more markedly than the strength and this suggests that the cubed factor for stiffness and squared factor for strength is probably more universal.

The squared relationship between compressive strength and density fits both theoretically and experimentally with work previously carried out by Patel [38] on rigid cellular plastics.

The similarity comes when comparing failure modes in the two materials. Cellular struts and walls in the plastics fail by buckling and bending, and studies have shown that, in compression, one of the major modes of failure of cancellous bone is also by buckling and bending [39-41].

Patel found that the physical structure of trabecular bone is similar to that of open-celled rigid plastic foams and aerated (porous) concrete. In these materials the apparent density is the most important factor affecting material properties.

In agreement with the findings of McElhaney et al, Carter and Hayes also believe that the compressive modulus of bone tissue was proportional to the density cubed.

However, both groups of workers found there to be a considerable degree of scatter in their data and McElhaney et al discussed the mechanical responses of cranial bone to be

strongly influenced by the structural arrangement of the cancellous bone. Properties such as compressive strength and Young's modulus are structural properties, and therefore the scatter in the data can be attributed to variations of the porosity of the traebeculae.

McElhaney et al's porous block model showed that small porosity changes in bone of relatively low density result in only small changes in strength and modulus, whereas small porosity changes in bone with a relatively high density result in large changes in strength and modulus.

Due to the differences in morphology and mechanical properties of both compact and cancellous bone many researchers have studied these two bone types as separate materials. However, since the early seventies some researchers have looked at cancellous bone as a porous structure comprised of bone tissue with the same microscopic mechanical properties of compact bone [35]. Work conducted by Galante et al [42] and Gong et al [43] showed that the compositions and true tissue densities (mass of mineralised tissue per volume of mineralised tissue) of both compact and cancellous bone are very similar. In addition, four separate studies between 1970 and 1975, found that the microscopic material properties of both cancellous and compact bone are also similar [40,41,44,45].

These findings indicate that it could be possible to model bones as composite structures which have both a solid and fluid phase. The solid phase being the mineralised bone tissue and the fluid phase being a mixture of bone marrow, blood, blood vessels, nerve tissue etc. They also indicate that the main assumption of McElhaney et al's porous block model i.e with the bone having the same microscopic properties but different structure, is correct.

Carter and Hayes [37] examined the compressive response of both human and bovine trabecular bone, with and without the bone marrow in situ. They measured both the apparent densities (wet weight / initial specimen volume) and tissue densities (wet weight / bone tissue volume) of trabecular bone. They found that the apparent densities varied from 0.07 to 0.97 g/cm^3, but that the tissue densities were approximately equal to that of compact bone (1.6 to 2.0 g/cm^3). They concluded that all bone can be mechanically viewed as a single material of variable density.

4.1.2 Location & Orientation

The location and orientation of samples of bone would be expected to have some effect, even after the effects of density variations have been accounted for. Various studies have investigated effects such as the orientation of samples around the skull, the effects of sutures and the entire skull geometry, as well as effects on long bones, where orientation would be expected to play a more significant role. These studies are discussed below.

McElhaney et al [28] conducted experiments in various testing set-ups on the human skull and the Rhesus monkey. Samples were taken from the frontal, right and left parietal and occipital regions of the skull. For the human skull, no significant differences were found for the modulus and ultimate strength due to loading in various tangential directions. Tangent sections of the inner and outer tables of compact bone and the trabeculae were studied and it was concluded that skull bone is reasonably isotropic in directions tangent to the skull surface.

Wood [32] conducted tensile tests on human cranial compact bone, and as with McElhaney et al, used specimens taken from the left or right temporal and parietal bones or the frontal bone. He tried to determine whether the bone samples were transversely isotropic - having equal properties in all directions tangent to the surface of the skull. To achieve this he measured the modulus of 55 samples and plotted these values against the angle taken between the sagital suture and the long axis of the specimen. The results conclude that there is no apparent relationship between the modulus and orientation. He too found the modulus to be the same in all directions tangent to the skull surface.

Tests were performed to determine if there were any noticeable patterns between location (left/right side of the body), age, type of bone (parietal, frontal, temporal), and layer (inner and outer table). The results showed that there were no significant differences based on age, side of body, type of bone or layer, for breaking stress or breaking strain. So all the bones tested can be considered equally strong and the strength is not affected by age.

Also the modulus of elasticity was the same for the three bone regions tested and for both sides of the skull. It was found that the modulus for young people was significantly higher

than that for old people (15.8 and 14.8 GPa at a strain rate of 1 sec^{-1}) However, this difference was considered to be unimportant.

Jaslow [46] looked at the mechanical properties of cranial sutures. She compared the differences in mechanical bending strength and energy absorption on samples of cranial bone taken from goats that contain sutures, to those without sutures.

Most samples of cranial bone with sutures had lower bending strength than pure cranial bone. This can be explained by the presence of collagen in the sutures. Tests conducted by Elliott [47] and Blanton and Biggs [48] summarised several results for mechanical properties of collagen and reported values of collagen strength between 14 and 200 MPa with a mean value less than 100 MPa. This mean is less than half of the bending strength of cranial bone measured by Jaslow [46] as 259 MPa. This value is in agreement with the findings for cortical bone from bovine femora (Currey [49], Burstein et al[30]) of 247 MPa and 266 MPa respectively, and goose femora from McAlister and Moyle [50].

There was reduced strength of the suture due to the presence of collagen which caused most sutures to fail before the surrounding bone. Failure strengths of as low as 50% that of non sutured bone were observed.

With regard to energy absorption it was found that bone containing sutures absorbed more energy under impact loading than cranial bone without sutures. Jaslow indicated that energy absorption during bending depends largely on the presence of collagen in the sutures and this is backed up by the findings of Wainwright et al. [51] who reported that collagen can absorb at least 100 times more energy than bone per unit volume.

Some interesting work has been carried out on the biomechanics of skull fracture by Yoganandan et al [52]. They looked at both quasistatic and dynamic, impact loading of various areas of the human skull as a whole unit. As with McElhaney et al [28] and Wood [32], these researchers tested the response of different areas of the skull including vertex (the top central area), parietal, temporal, frontal and occipital regions. Unlike the other workers who machined specimens from the various parts of the skull these tests were conducted on the whole skull. The results showed that the fracture patterns were complex and were dependent on the anatomical location of the loading site. It was found that

fracture widths were narrower at the site of impact compared to other regions further away.

As an example, one of the specimens that was impacted at the vertex showed no damage at the loading site. However, fractures of the frontal bone and frontal sinus were found. A greater widening of fractures was found at sites more remote from the vertex. An earlier study by Gurdjian and Webster [53] noted similar findings.

Yoganandan et al [52] found too that during quasistatic loading there were consistently occurring fractures of the inner and outer tables. When force-displacement curves were plotted it was found there were multiple peaks corresponding to the fracture of the two tables. A specific example shows a peak at 3.4 kN and 6.9 mm displacement, which is the point at which the outer table fails. Then there is a secondary peak (the ultimate force) at 4.5 kN and 9.1mm displacement, which is where the inner table reaches its load carrying capacity, and fracture occurs. Such characteristics were not observed during dynamic loading and are most probably due to the high rate of testing leading to simultaneous fracture of both inner and outer tables.

In a separate study by Dechow et al [54], the mechanical properties of two regions of the skull were looked at. This time the specimens were taken from both the supraorbit (the site behind the eyebrows) and the mandible (the jaw bone). In contrast to the studies previously mentioned Dechow et al found there to be a definite difference in mechanical properties and directionality. He found that bone from the mandible was stiffer than the supraorbit (11.3 to 19.4 GPa, compared to 10.9 to 15.2 GPa), and the bone from the lower border of the mandible shows less directional variation in material properties than bone from the supraorbital region. The bone from the mandible was found to be stiffer than the supraorbit in the longitudinal direction, but not in the transverse or normal directions, resulting in greater directionality in the mandibular bone tissue.

The results of this study suggest that the greater stiffness of the mandibular region is an evolution factor, based on the need to chew and eat. The properties of the jaw have adapted to the forces required to bite and chew food, with regard to both strength and directionality.

In contrast to the lack of male/female variation in skull properties, Duma et al, [55] found that there is a difference in mechanical properties between male and female long bones. They found that female long bones contain a lower degree of minerals compared to males, and reported that female bones are therefore weaker.

Schoenfeld, Lautenschlager and Meyer [36] who tested the mechanical properties of human cancellous bone in the femur reported too that no significant correlation between strength and location was found. Their tests showed that there was a degree of scatter in the strength values obtained from compression loading. This scatter was found to be consistent with all femurs tested and not the result of differences between femurs. They stated that the relatively strong and weak regions of cancellous bone observed appeared on a random basis, and are probably the result of structural variations of the trabeculae.

4.1.3 Strain Rate

Strain rate is the most important factor to consider in this study. Results between different workers have generally been in agreement, and many of their findings are fairly conclusive.

Carter and Caler [56] derived a model of monotonic tensile fractures for human bone. They predicted that bone accumulates damage over time when stressed and the bone fractures after a certain amount of damage has accumulated. Low strain rates should result in more time for damage to accumulate than at higher strain rates so therefore lower strain rates should result in lower strength. Their model predicts that:

$$\text{Ultimate stress} = 87 \times \text{stress rate}^{0.053} \qquad 4.1$$

and converting stress rate directly to strain rate gave,

$$\text{Ultimate stress} = 147 \times \text{strain rate}^{0.055}. \qquad 4.2$$

Carter and Caler looked at work previously carried out by Burstein et al [57], on human bone, and Crowninshield and Hope [58] and Wright and Hayes [59], on bovine bone, and showed that the data produced concurred well with their model.

Currey [60] reanalysed the work previously conducted by Carter and Caler [56] in an attempt to see how conclusive the model really is when considering a series of questions and queries raised by Currey about the findings. In this study, 35 bovine femora specimens were tested wet, in tension, at room temperature. (Carter and Caler tested human bone at 37°C). The strain rates used ranged from 10^{-4} s^{-1} to 0.16 s^{-1}. (Carter and Caler tested at strains up to $5x10^{2}$ s^{-1}.)

Currey found the exponent to the loading rate (both stress and strain) to be 0.091 and 0.090 respectively, which is significantly higher than that of Carter and Caler of 0.053 and 0.055, respectively. The high value was largely put down to a high degree of scatter in the results. It was considered that the mineral content of the bone tested was a significant factor in the variation of values. A forward stepwise regression was used to separate the effects of loading rate and mineral content and this led to an improved agreement of the values of exponent in the equations. Currey's exponent reduced to 0.067 after allowing for mineral content, and therefore reducing the scatter of results.

Carter and Caler [61] produced evidence that Young's modulus is strain rate dependent. They produced an equation to the effect:

$$E = 21.4 \times \text{strain rate}^{0.050} \qquad 4.3$$

However, the data from Currey's experiments found the value of Young's modulus to be barely, if at all, dependent on loading rate. This disagrees with the findings of other workers such as Carter and Caler, but could be put down to the fact that the tests performed by Currey were at constant strain rate whereas the tests performed by Carter and Caler were at constant stress rate. Also, the modulus of bone can be fairly difficult to measure, which could have led to discrepancies in the results.

Two studies carried out by Carter and Hayes [35,37] as previously mentioned, tested the compressive behaviour of cancellous bone with the bone marrow both removed and in

situ. A range of strain rates were used from 0.001 to 10 /sec. They found that the influence of strain rate on strength and stiffness was similar in the cancellous bone they tested, to compact bone tested by other workers. They reported that both the strength and stiffness were proportional to the strain rate raised to the power of 0.06.

Over the range of strain rates (0.001 to 10 /s) it was observed that the trabecular bone without the bone marrow in situ more or less doubled in strength and stiffness. Following the aforementioned allowances for specimen densities Carter and Hayes acknowledged the importance of strain rate, but said (for bone without marrow in situ) it was no more important than the composition of the bone tissue and the orientation of the trabeculae. The apparent density was said to be a much more important factor than strain rate.

Trabecular bone tested with the bone marrow in situ was found to show no increase in strength, stiffness or energy absorption at rates between 0.001 and 1 /sec. However, specimens tested at strain rates of 10/s showed a distinct increase in strength, stiffness and energy absorption. These results agree with the findings of two sets of other workers. Firstly, Swanson and Freeman [62] showed that trabecular bone is not hydraulically strengthened by the presence of marrow under low to moderate loading conditions such as walking. Pugh et al [40] found that the presence of marrow in unconfined specimens did not influence the viscoelastic behaviour of cancellous bone.

Carter and Hayes' results from specimens tested at rates of 10/s suggest that under these higher loading conditions during severe, traumatic compressive loading the bone marrow in vivo absorbs considerable energy. He also stated that the energy absorption was due to a restriction of marrow flow through restrictive boundaries, and not through the trabecular pores themselves. For example, in the skull the inner and outer tables of compact bone act as restrictive boundaries and limit the outflow of marrow during trabecular bone fracture.

Wood [32] concentrated research on mechanical response of human cranial bone in tension. He tested 120 specimens of skull at strain rates ranging from 0.005 to 150/sec. His findings were much the same as Carter and Hayes [38], McElhaney et al [28] and Currey [60] in that he found that the modulus of elasticity, breaking stress and breaking strain were all rate sensitive. Of the mechanical properties determined the modulus values were the most consistent for all the specimens at a given strain rate. In agreement with the

other workers he also found the energy absorbed to failure was not affected by rate. Modulus, breaking stress and breaking strain all increased in response to higher strain rates.

However, in contrast to these findings Wright and Hayes [59] found that strain rate had a significant effect on the energy absorption capacity of bone. They also found that bone specimens tested at higher rates generally absorbed much more energy during failure. These results though, disagree with all of the other studies looked at so far and the difference in findings can be explained by the fact that they used inconsistent specimens such as whole bones or different sized specimens which makes comparison of results much more difficult.

In a similar set of experiments to Carter and Caler, and Currey, McElhaney [31] set out to test the dynamic response of bone and muscle tissue at loading rates ranging from relatively static (0.001/sec) to fast rate (1500/sec). His purpose was to show that biological materials exhibit a high strain rate sensitivity. He tested femurs from both human and steer subjects in the wet state. He found that a critical velocity was reached at strain rates between 0.1 and 1/sec. This is where the mechanical properties of a material exhibit a large variation over a small range of strain rates. He found that the properties most affected were the energy absorption capacity and the strain to failure. Also the type of fracture observed before and after the critical velocity was different. Before critical velocity, at low strain rates (up to 1/sec) a shear fracture was seen. McElhaney reported that these were similar to the cone fracture associated with the sheared fracture surface of concrete. Above the critical velocity (at strains above 1/sec) the fracture surface was represented by vertical splintering with many small pieces being formed.

In the previous study conducted by Jaslow [46] on the mechanical properties of cranial sutures it was found that in samples where the sutures were highly interdigitated and slow loading rates were used (0.8mm/s), some cases showed that the sutured bone was as strong as unsutured bone. When faster loading rates were used (9.7mm/s) it was found that the sutures fractured at a lower strength, which seems to disagree with all of the previous studies mentioned above. These results can be put down to the structural variations in the bone sutures compared to the non-sutured bone.

4.1.4 Sample Condition

No papers have been found that directly compare the differences in mechanical properties of wet bone, dry bone and re-wetted bone. Wood [32], McElhaney [31], McElhaney et al [28], Carter and Hayes [35,37], Currey [60], Burstein et al [30] and Reilly and Burstein [33] all used fresh samples that were taken from the human or animal on the day or shortly after its death. These samples were then either machined and tested, or frozen, or refrigerated with saline solution to keep the samples in a moist condition.

Even with careful storage, such as in a freezer, drying will occur during sample preparation. Special care needs to be taken to obtain samples representative of living bone, to test them as soon after death as possible, and to ensure little or no drying occurs.

It is generally held that stiffness and strength will be higher in the fresh state than after drying, but exactly how much is unclear. Re-wetting is certainly detrimental to both strength and stiffness.

4.1.5 Testing geometry

The geometry in which bone testing is carried out can lead to differences in values obtained with regard to mechanical properties. The main testing geometries are compression and tension, with bending used less. Many workers have conducted and compared test results for tension and compression. There are some general differences between these two geometries in the results they produce. Generally, bone is slightly stiffer, and slightly weaker in tension compared to compression. Yielding is also more likely to occur in tension.

McElhaney et al [28] carried out experiments in tension and compression. They found differences in Young's modulus between the two testing set-ups. Typical values for various mechanical properties of both human and animal bone can be found in Tables 4.1 and 4.2.

They also found that in both tangential compression and radial compression, a distinct variation of results was observed. Tangential compression gave a modulus more than twice that of radial. Ultimate strength was higher in tangential compression but both ultimate strain and energy absorption capacity were higher in radial. This, however, is largely due to orientation effects of the bone as previously described.

Very little difference was found in either of the two testing set-ups between human and primate cranial bones.

The effects of bending are a little less clear. Bending strengths are often higher than would be expected from a tensile test, due to the effects of the sandwich structure. This was examined by Hubbard [29]. He explained that as bending deformation causes a change in the curvature of a layered panel and is resisted by a normal stress distribution, the loading changes through the structure from tensile in one face to compression in the other. The forces developed in the relatively low stiffness core are insignificant when compared to the stiffness in the faces.

The effects of shear loading have not received much attention, with only a few studies looking at shear moduli or Poisson's ratio. The only work found that measures these values for human skull samples is David Taylor's work where Poisson's ratio was measured. As is discussed later, however, the accuracy of these values is open to question and the measured value of 0.45 seems very high.

All the other studies that have looked at shear stiffness have measured the shear modulus and calculated the Poisson's ratio from this and the tensile modulus. The majority of these studies have used ultrasonic tests, passing high frequency longitudinal and transverse waves through samples and measuring the modulus from the wave velocities. These include studies on rat cortical bone [63,64], whalebone [65], human femurs [66,67] and human mandibles [68].

Although this covers a wide range of types of bone, there are a few general features that can be drawn out. The tensile modulus values quoted are generally higher than have been measured mechanically, with values between 10 and 40 GPa. The higher values would be expected from the high strain rates associated with the ultrasonic test method. Shear

moduli lie typically between about 3 and 12 GPa, giving Poisson's ratios between 0.25 and 0.37.

There is some suggestion from the results that Poisson's ratio is a little higher for compact bone than for cancellous bone, but that it is relatively insensitive to location, orientation or strain rate.

Other studies looking at shear effects have been quite varied and include the use of microhardness [69], where a Poisson's ratio of 0.3 was assumed in order to calculate tensile moduli of between 7 and 25 GPa. Computer tomography has also been tried [70], but this yielded very low values for stiffness of human pelvic bone, and so should be treated with caution.

An interesting study used bend tests of various span lengths coupled with a mathematical extrapolation to generate the shear modulus of various cortical bone samples [71]. In this study, it was found that the shear modulus was only $1/20^{th}$ of the tensile modulus, giving an unreasonable value for Poisson's ratio of –0.9. This effect was probably due to a combination of experimental errors being amplified during the extrapolation process as well as some early fracture occurring during the testing.

Only one study has been found that looks at shear strength. In this [72], the shear strength of sheep bone was found to lie between 7 and 15 MPa, i.e. of a similar magnitude to the tensile strength.

4.1.6 Summary of Values

Tables 4.1 and 4.2, below, give a summary of the values of bone strength and stiffness from various studies. It can be seen from these that there is a fair degree of spread, due to the differences in the variables discussed above. The purpose of these tables is to give an idea of the 'typical' values that could be used for modelling. From these and a review of the literature, typical values for human skull, of about 4 mm thickness, at a rate of about 10^{-2} s^{-1}, could be taken to be :

Tensile stiffness : 8 - 10 GPa

Tensile strength : 80 – 100 MPa

Tensile strain to failure : 1%

Poisson's ratio : 0.3 – 0.35

Shear modulus : 3 - 4 GPa

Table 4.1 A summary of strength values from the literature

Source	Tensile Strength (MPa)	Compressive Strength (MPa)
REILLY & BURSTEIN [33]	133	
CURREY (Bovine) [60]	112	
McELHANEY (Bovine) [31]		175.9 - 365.7
McELHANEY (Human) [31]	91.3	150.4 - 317.4
SAHA & HAYES (Bovine)	101	
HAYES & CARTER [39]	99	
WOOD [32]	48-127	
McELHANEY et al [28]	79.35 (compact bone)	73-97
McELHANEY et al [28]	43.5	41 (cancellous only)
SCHOENFELD et al [36]		0.145 - 13.5 (cancellous)
SCHOENFELD et al [36]		68.95 (compact)

Table 4.2 A summary of modulus values from the literature

Source	Young's modulus (GPa)
REILLY & BURSTEIN [33]	17
McELHANEY (Bovine) [31]	18.63 – 42.09
McELHANEY (Human) [31]	15.18 – 40.71
RAFTOPOULOS [67]	17.09-18.32
HUBBARD [29]	9.7
WOOD [32]	10.3-22.1
McELHANEY et al [28]	2.42 - 5.59
DUMAS [55]	24.4 +/- 3.9
DECHOW et al [68]	11.3-19.4 (Mandible)
DECHOW et al [68]	10.9-15.2 (Supraorbit)
SCHOENFELD et al [36]	0.344 (cancellous)
SCHOENFELD et al [36]	6.895 (compact)
YOGANADAN [52]	0.467 - 1.29 (quasistatic)
YOGANADAN [52]	2.46 - 5.87 (dynamic)

4.2 COMMENTS ON AND RE-ANALYSIS OF PREVIOUS BONE TEST DATA

A series of tests were commissioned by DERA several years ago with the aim of determining the similarity in mechanical properties and mechanical behaviour between bovine scapula and human skull. The purpose of these tests was to see whether bovine scapula could be used as an accurate and reproducible physical model to measure the responses of the human skull under baton round impact conditions. These tests were carried out by medical surgeon, David Taylor from Queen Mary and Westfield College, London (only available as internal DERA report).

Some of the results from his tests appeared a little ambiguous and some key calculations had not been made, so it was considered necessary and beneficial to re-analyse some of the raw data.

4.2.1 Analysis of Strength Values

David Taylor's analysis was based on taking the maximum force and dividing by either the sample width (to give a value in kN/cm) or by the sample cross-sectional area (to give a value in kN/cm^2). Neither of these values is the true maximum stress for the 3-point bending geometry. The values that David Taylor had calculated will depend on the geometry of the sample, which does vary, particularly between the human and bovine samples.

The effects of sample size are illustrated below in Table 4.3, where values have been calculated for 5 different sample sizes, assuming a constant modulus (of 10GPa) and failure strength (of 100 MPa, failure strain of 1%). These values show that although the material properties are the same, DT's results would have been considerably different.

Table 4.3 The effects of sample size on properties calculated in various ways

Length	Width	Thickness	Max Displ.	Max Force	Strain (%) {DT}	Strength (kN/cm) {DT}	Strength (kN/cm^2) {DT}
50	20	2.5	1.6667	166.6	3.33	8.49	34.0
70	20	2.5	3.2667	119.1	4.66	6.07	24.3
50	15	2.5	1.6667	125.0	3.33	8.49	34.0
50	20	2.0	2.083	106.7	4.17	5.44	27.2
50	20	3.0	1.389	240.0	2.78	12.23	40.78

These show that the sample thickness has the most effect, width has no effect and length is in between.

David Taylor did list values of maximum tensile and compressive stresses and strains, which are almost correct, except that they are the average stresses and strains across the sample, and not the maximum values in the centre, which are important. The maximum values are considerably larger.

The correct formulae for maximum stress and strain (on the outer surface, below the central support) are :

Maximum stress

$$\sigma = \frac{3FL}{2bt^2} \qquad 4.1$$

Maximum Strain

$$\varepsilon = \frac{6\delta t}{L^2} \qquad 4.2$$

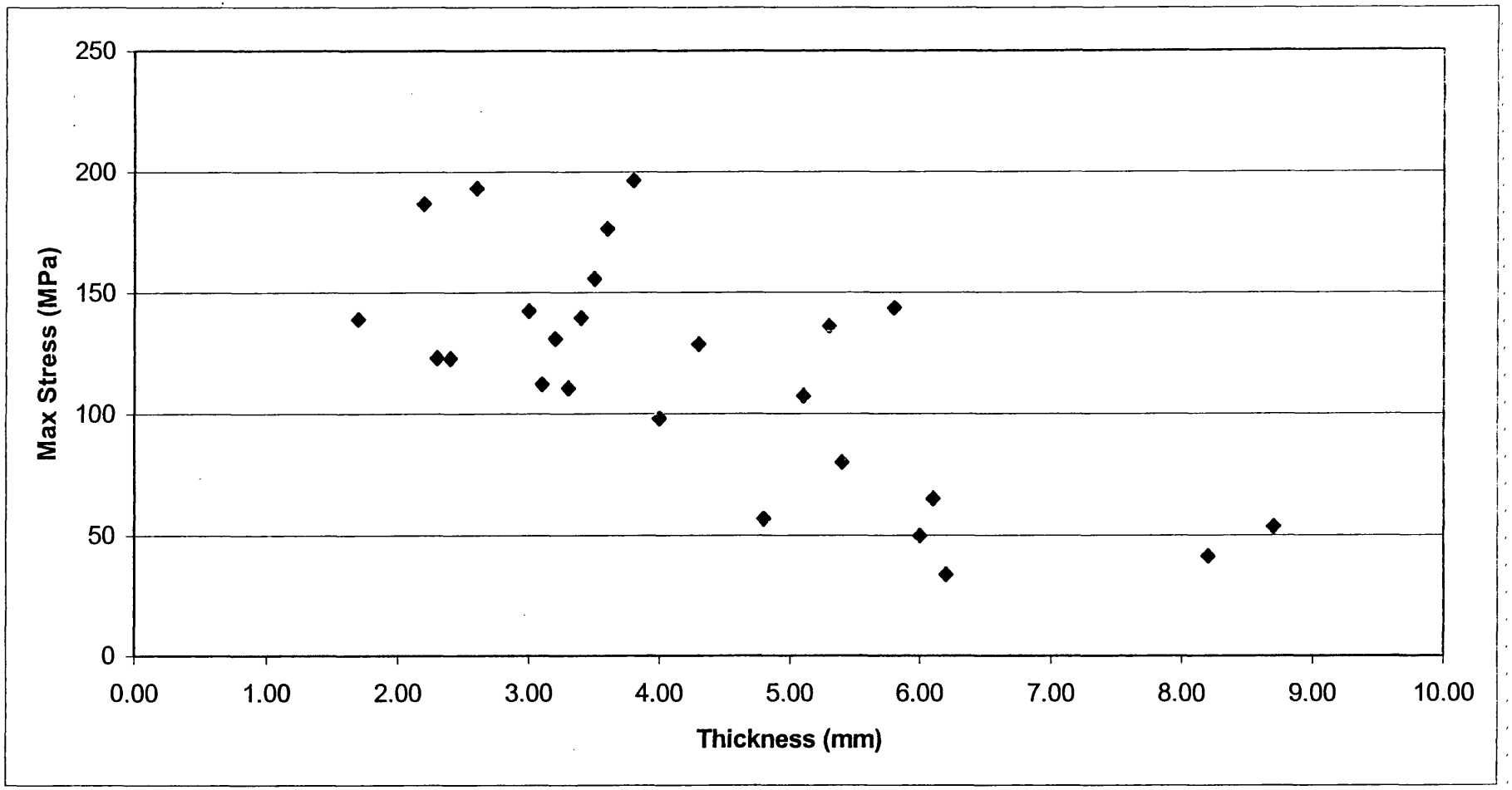

Figure 4.1 The maximum stress versus thickness for dry bullock scapula experiments.

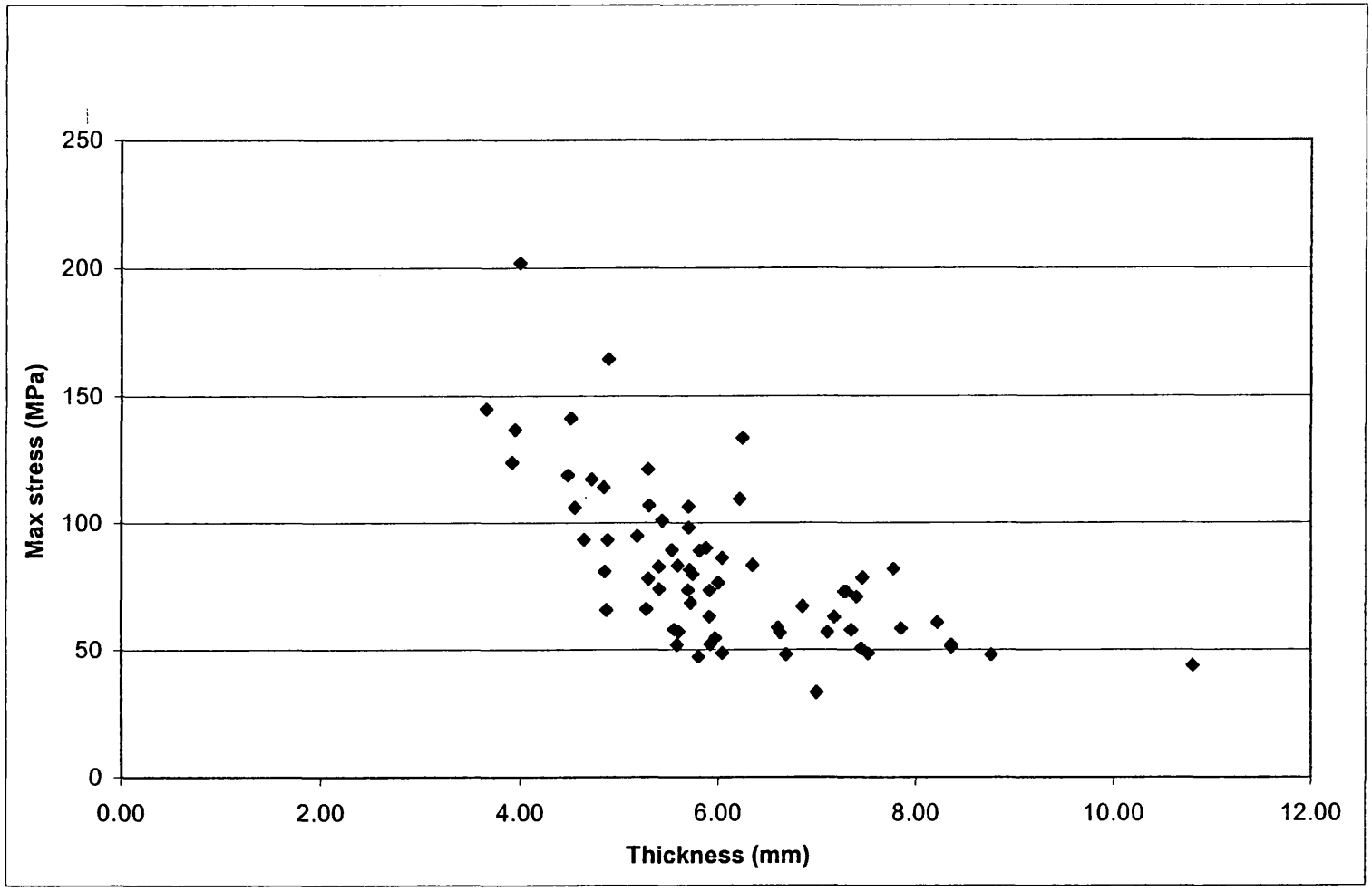

Figure 4.2 The maximum stress versus thickness for wet bullock scapula experiments

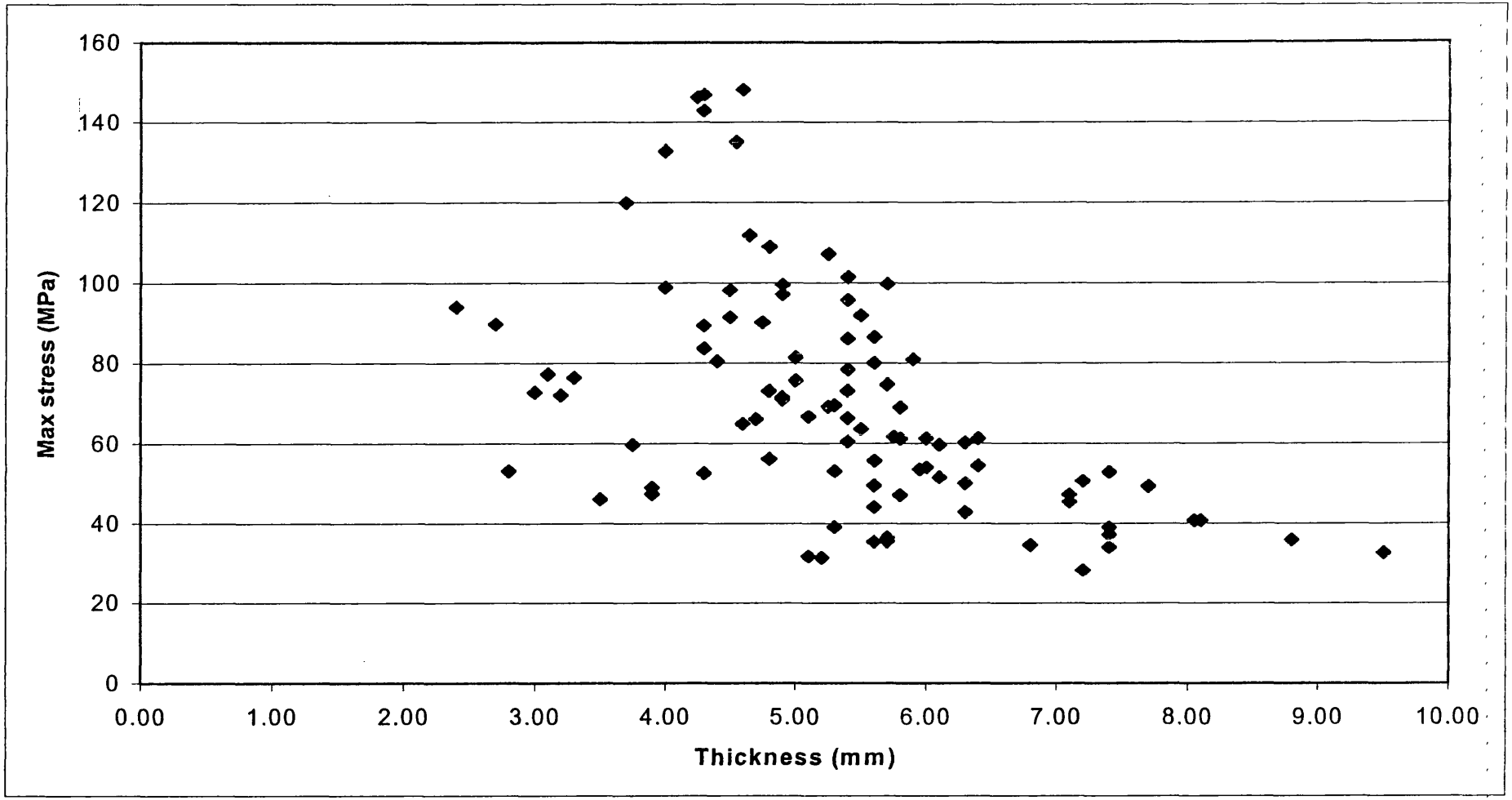

Figure 4.3 The maximum stress versus thickness for dry human skull experiments

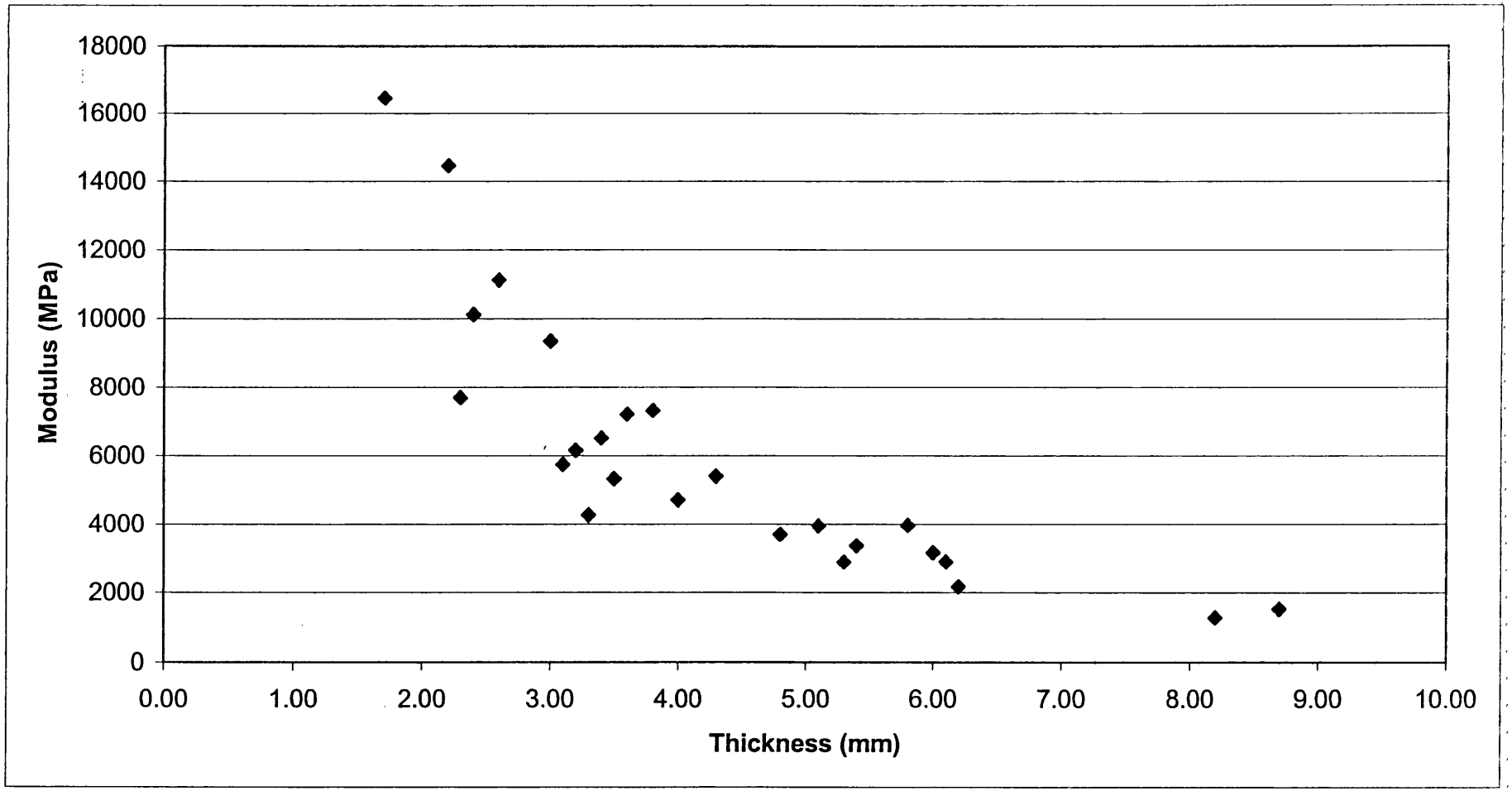

Figure 4.4 The flexural modulus versus thickness for dry bullock scapula experiments

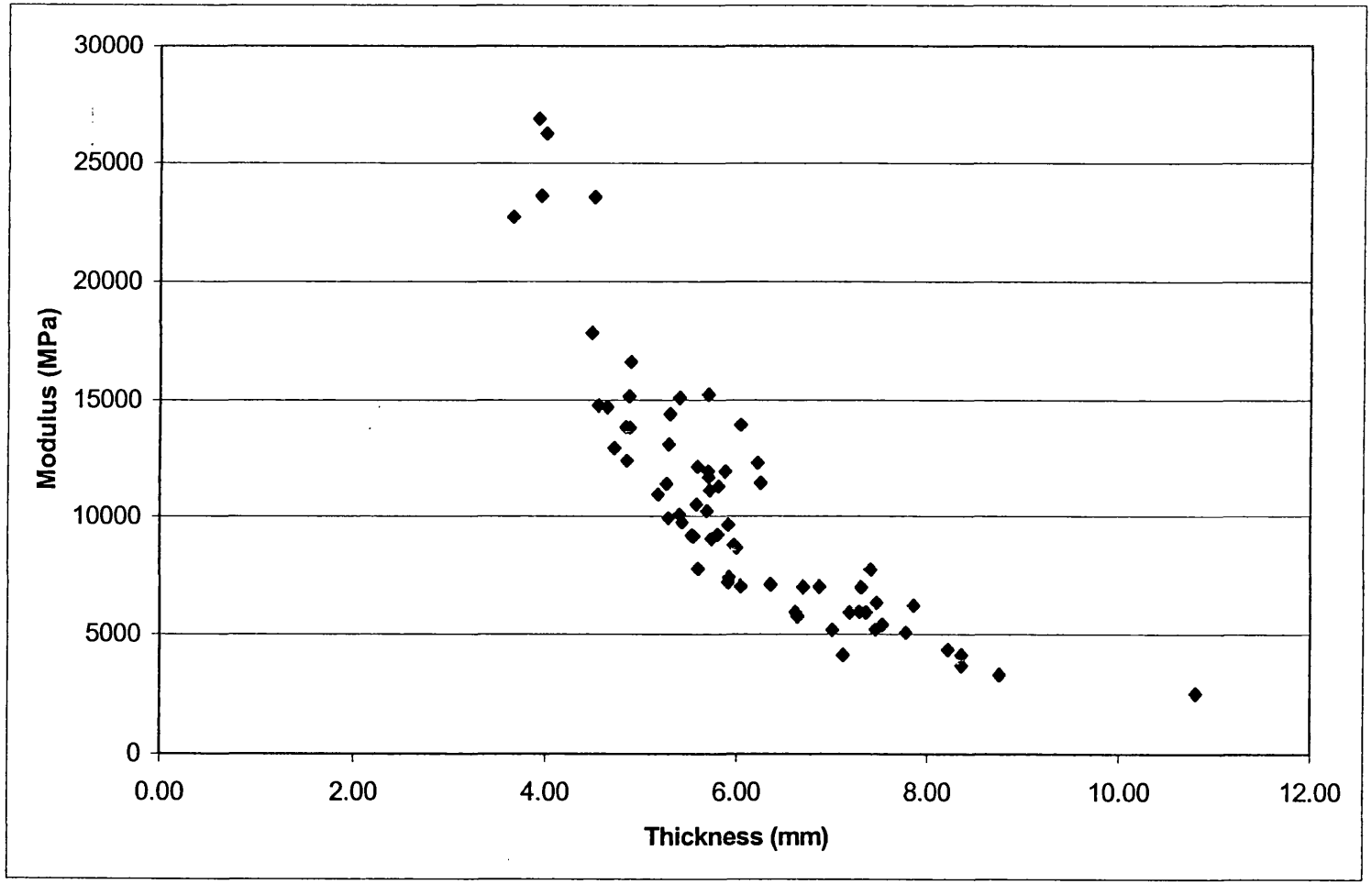

Figure 4.5 The flexural modulus versus thickness for wet bullock scapula experiments

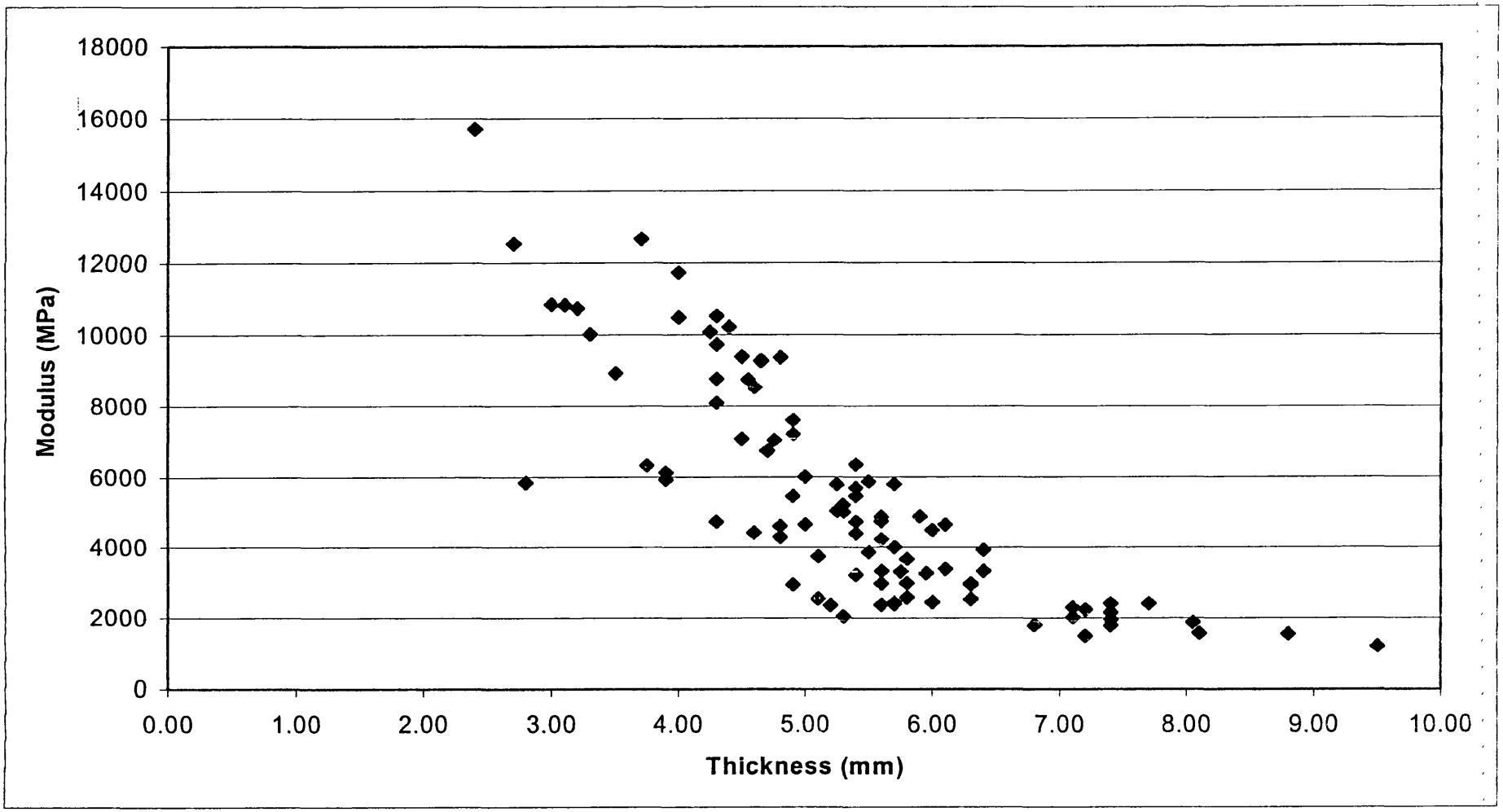

Figure 4.6 The flexural modulus versus thickness for dry human skull experiments

somewhere between 2 GPa and 15 GPa. In reality, the stiffness depends strongly on thickness and for a thickness of 4 mm (for instance), lies between 5 GPa and 11 GPa, a much smaller spread.

Other features from the stiffness values include:

- A very similar range of stiffness for dry scapulae and dry skull samples.
- Significantly higher stiffnesses for the wet scapulae samples.

Unfortunately, data for wet skull samples has not been made available, so an amount of intuitive guesswork is required to put these results firmly into context, but some key points can be made as follows:

- The values of thickness, strength and stiffness are sufficiently similar between bovine scapulae and human skull to confirm that the use of bovine scapulae will give broadly similar results to skull impact.
- The effects of thickness complicate the picture. It was considered possible to take these into account in some way to produce a more accurate physical model.
- As the modulus of dry scapulae and skulls are very similar, the impact stresses generated on bones of similar thickness will be similar.
- As the strength of dry scapulae is higher than dry skull, (and it is feasible to guess that wet scapulae will be stronger than wet skull) it suggests that scapulae impact will be slightly less likely to cause a fracture than would occur with a skull impact.
- To obtain greater consistency in results, it may be possible to take thickness effects into account, either by adjusting the impact velocity, or by only selecting target areas of a certain thickness. Further consideration needs to be given to this point, but it certainly gave potential for better confidence in interpreting scapulae impact results.

4.3 SHEAR BEHAVIOUR OF BONE

Leading on from the literature review of bone, the analysis of David Taylor's work and in discussions with DERA and Fluid Gravity, it seemed that there was a lack of information on, and therefore a need to determine, the shear modulus. As there was very limited information on this parameter in the literature, this seemed the most important avenue to pursue with further testing. There were several possible methods by which this could be done, and summary information on them is given below.

4.3.1 Orientation

As bone is an anisotropic material, the shear modulus (and Poisson's ratio) will vary with orientation. This was considered to be an important issue; if values were measured in one orientation and modelling required values for a different orientation, discrepancies may have arisen. As the modelling was to treat the bone as an isotropic material, it was thought it would be more appropriate to try and measure an 'average' shear modulus.

An illustration of this effect is given below in Fig 4.7. Orientation 1 was considered as being probably the easier to measure, whereas Orientation 2 may have been the more appropriate for modelling purposes.

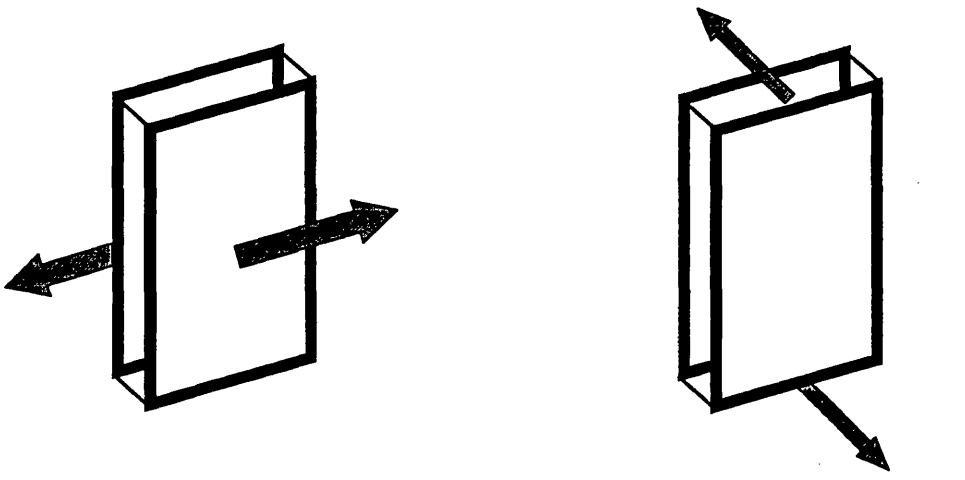

ORIENTATION 1 ORIENTATION 2

Figure 4.7 Possible orientations for shear testing

The two basic methods of determining the shear modulus are either by measuring the Poisson's ratio during a tensile test when measuring the Young's modulus, or by directly measuring the shear modulus. The relationship between these values is :

$$E = \frac{2G}{(1+\upsilon)} \qquad 4.3$$

4.3.2 Measuring Poisson's Ratio

The simplest method of measuring Poisson's ratio is to measure the lateral contraction during a tensile test. Poisson's ratio is then defined as the ratio of lateral contraction to longitudinal extension. The key issue to be addressed is the need for accuracy of measurement. As the lateral contractions are even smaller than the extensions (which are also fairly small), in order to generate an accurate value of Poisson's ratio, high precision strain measurements are usually needed. An example of the problems with this can be seen with David Taylor's brief attempt to measure Poisson's ratio using a simple visual measurement system. The accuracy obtainable with this gave a variability in υ of +/- 0.1, which covers the range of υ for most materials.

There are various methods of measuring the lateral contraction, as indicated below.

a) Strain gauges. These offer advantages in allowing simultaneous measurement of the strain in two perpendicular directions. The main disadvantage is the need to fix them securely to the material. This would pose serious problems for the use of bone, especially in the 'wet' state, and probably precludes their use.

b) Contact extensometers. These clip-on systems give reasonable accuracy and are fairly easy to use. Normally, the contraction in width of the sample would be measured. This would equate to Orientation 1 illustrated above. In order to investigate Orientation 2, the thickness change would be needed, which was thought to be harder to measure.

c) Optical extensometers. These give similar accuracy to contact extensometers, but do not touch the sample. They are harder to set up and the equipment is more costly.

4.3.3 Measuring Shear Modulus, G

4.3.3.1 *Measurements in simple shear*

The simplest method of measuring G is to perform a simple shear geometry, as illustrated below in Fig 4.8. By measuring the applied force and resultant deformation angle, the shear modulus can easily be calculated.

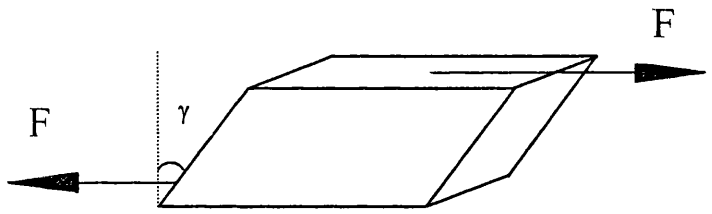

Figure 4.8 Simple shear geometry

The main problem that this method would have present would be ensuring the force could be applied with no slippage. It may have been possible to do this by gluing the sample to the shear plates, but then the shear modulus of the adhesive would have played a part in the deformation. This method works well for soft materials where the forces are low and deformations high, but for stiff materials it is rarely successful.

4.3.3.2 *Torsion testing*

This method (BS 2782 153A) uses a strip sample and measures the torsional stiffness, which can be converted directly into the shear modulus. This would give an average measure, as it combines Orientation 1 and Orientation 2. The rate of testing would depend on the test equipment, but would be similar to standard tensile tests (strain rates of up to 0.1 s^{-1} possible). Suitable testing equipment would be needed to apply torsional loads and measure angular displacements and such equipment was available at Swansea. It was thought that this would be a promising method.

4.3.3.3 *Ultrasonic testing*

This method (BS 2782 323E) relies on the fact that the wave velocity is proportional to the modulus. In order to achieve measurable signals, frequencies of above 0.5 MHz are used. By using longitudinal waves, the longitudinal modulus can be measured. By using transverse waves, the shear modulus can be measured. By combining these, all the elastic constants can be determined. This method has the advantage of giving comprehensive information, potentially in any orientation. This meant that values for Orientation 1 and 2 could be measured independently, as long as a transducer smaller than the sample thickness could be used. The high frequencies mean that the tests are effectively very high strain rate tests. The equipment for making these measurements, did not exist in Swansea at the time, so if this method were to be pursued, it would have been necessary to purchase the equipment and do some initial setting-up trials.

4.3.4 Measuring Other Properties.

Effects of biaxial testing. To date, virtually all tests have used uniaxial testing (tension, compression or simple bending). Bearing this in mind, it was thought to be sensible to consider biaxial testing, as this was appropriate to the conditions that were being modelled. This would also indirectly assess any Poisson's ratio effects, which are often hard to measure. It was also thought that biaxial tests could be performed reasonably well via a disk or plate testing approach. This is similar to a standard method of measuring the shear strength (BS 2782 340A). The shear strength was thought to be probably not needed as this type of failure is unlikely to occur in practice. The disk test method has been used successfully for metallic samples [73,74], especially where limited material is available, and also for polymers [75]. It has the advantage of easily giving biaxial stress states and yields certain values related to stiffness and strength. The main drawback is that as there is a complex stress and strain distribution, it is very difficult to obtain direct values for modulus and strength.

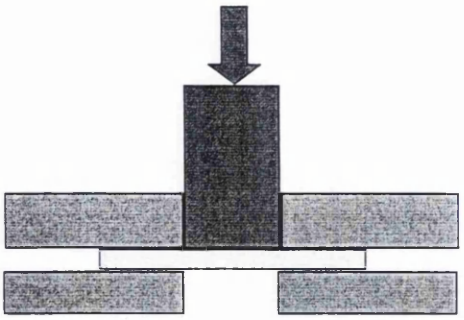

Shear strength testing

Fig 4.9

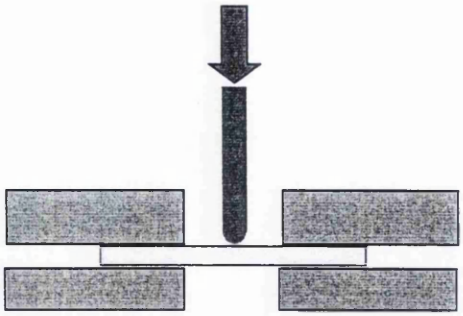

Biaxial stress testing

Fig 4.10

In order to obtain the most useful mechanical property data, it was decided to conduct both torsion tests and tension tests on strip samples of bovine scapulae. In this way, the tensile and shear behaviour would be measured, hence indirectly yielding values for Poisson's ratio. In addition, it was decided to conduct biaxial stress disk tests. The biaxial tests also were to be performed on bovine samples, using the disk bend test set-up illustrated above. The purpose of these tests was to investigate the effects of biaxial testing as well as to provide a semi-complex loading situation to compare with finite-element predictions.

4.4 MECHANICAL PROPERTIES OF BOVINE SCAPULAE

4.4.1 Introduction

This part of the report describes a detailed assessment of the mechanical properties of bovine scapulae samples, in order to provide data and validation for finite element modelling purposes. It has been highlighted previously that there is a lack of available information on the shear modulus (and hence Poisson's Ratio) for bone, and especially how these vary with rate.

This study was instigated to address this need. A review of methods available for determining shear modulus and Poisson's Ratio has been given above. The method that was chosen was to use torsional testing of strip samples. This was used as it conveniently gives data on the average properties of an entire sample. This is needed as the modelling is to be performed using the approximation of an 'average' isotropic material. This method also allows tensile and shear modulii to be determined at a range of strain rates, and hence allows determination of how Poisson's ratio varies with rate.

The approach that was used was to measure tensional and torsional stiffness at different rates, using small deformations (less than 0.5 %). This permitted several tests to be performed on each sample. After this, the samples were tested to destruction in bending at different rates, to give values of failure strength and flexural modulus as a function of rate.

4.4.2 SAMPLES

The samples of bovine scapulae were provided by DERA. The scapulae were frozen soon after being obtained from the abattoir. The samples were machined into parallel-sided strips at RMCS Shrivenham. There was some difficulty in producing samples of uniform thickness. Samples machined transverse to the central ridge had extremely variable thickness that would have caused great difficulty in testing. Therefore all samples were machined parallel to the central ridge. Although these still had some variation in thickness, they were suitable for testing. The samples were machined while

still frozen and were re-frozen after machining. The trabeculum was removed after machining.

The samples were about 100 mm in length, 15 mm width and thickness between 2 and 5 mm. The samples were predominantly of compact bone, with approximately 25 % spongy bone. Generally, thicker samples had a higher proportion of spongy bone. Two or three samples were provided from each scapula, and in total, some 50 samples were used. The samples were designated with the codes SA1, SA2, SA3, SB1 etc, where the letters refer to the scapula from which the samples were taken and the number is the particular sample from that scapula.

Before testing, the samples were immersed in saline solution for 24 hours to thaw and hydrate totally. The samples were then tested in air, where some drying of the samples inevitably limited the time available for testing. Because of this, the samples needed to be re-immersed in saline (for up to a further 24 hours) after tension and torsion testing but before bend testing.

4.4.3 Test Methods

All testing was performed on an ESH servo-hydraulic testing machine at a standard room temperature of 23 C. Before testing, each sample's dimensions were measured using vernier calipers. As the thickness of each sample was not constant along its length, it was necessary to record the thickness at 5 mm intervals along the sample length.

4.4.3.1 Tensile Testing

The samples were clamped in the testing machine to give a free gauge length of 60 mm. The samples were then deformed at one of 5 testing rates, to a strain of just under 0.5 %. The testing rates used corresponded to strain rates of 10^{-3}, 3 x 10^{-4}, 10^{-4}, 3 x 10^{-4} and 10^{-5} s^{-1}. The testing rate was limited by the speed of accurate data capture, with the fastest tests taking about 5 seconds.

The force was continually recorded from a load cell, and the displacement recorded from the cross-head displacement. The displacement needed to be calibrated to account for

machine compliance. It was decided to avoid the use of extensometers or strain gauges, due to the difficulty of attaching them to the variable-section samples.

A typical force / displacement graph for a tensile modulus test is shown in Figure 4.11, from which it can be seen that there is a reasonably good straight-line fit to the initial part of the data. The gradient of this line was used to calculate the tensile modulus E as below:

$$E = \left(\frac{F}{d}\right) x \left(\frac{GL}{w.t}\right) \qquad 4.5$$

where F/d is the force / displacement gradient, GL is the gauge length, w is the sample width and t the sample thickness. As the sample thickness varied along its length, a simple average of the 12 readings that were taken at 5 mm intervals was used.

4.4.3.2 Torsion Testing

Torsional testing was performed on the same samples, using the same grips, but with a rotational displacement. The tests were adjusted to give the same strain rates and maximum strains as with the tensile tests.

A typical graph of torque / rotation is given in Figure 4.12. This shows an even better straight-line fit than for the tension tests. The gradient of this line was used to calculate the shear modulus, as described below.

For torsional testing, the calculation of modulus is more complex as the stress and strain vary across the sample, with a maximum at the corners of the sample going to zero in the middle of the sample [76-78]. The shear modulus can be derived from these tests using the following equation:

$$G = \left(\frac{T}{\vartheta}\right) x \left(\frac{GL}{k.w.t^3}\right) \qquad 4.6$$

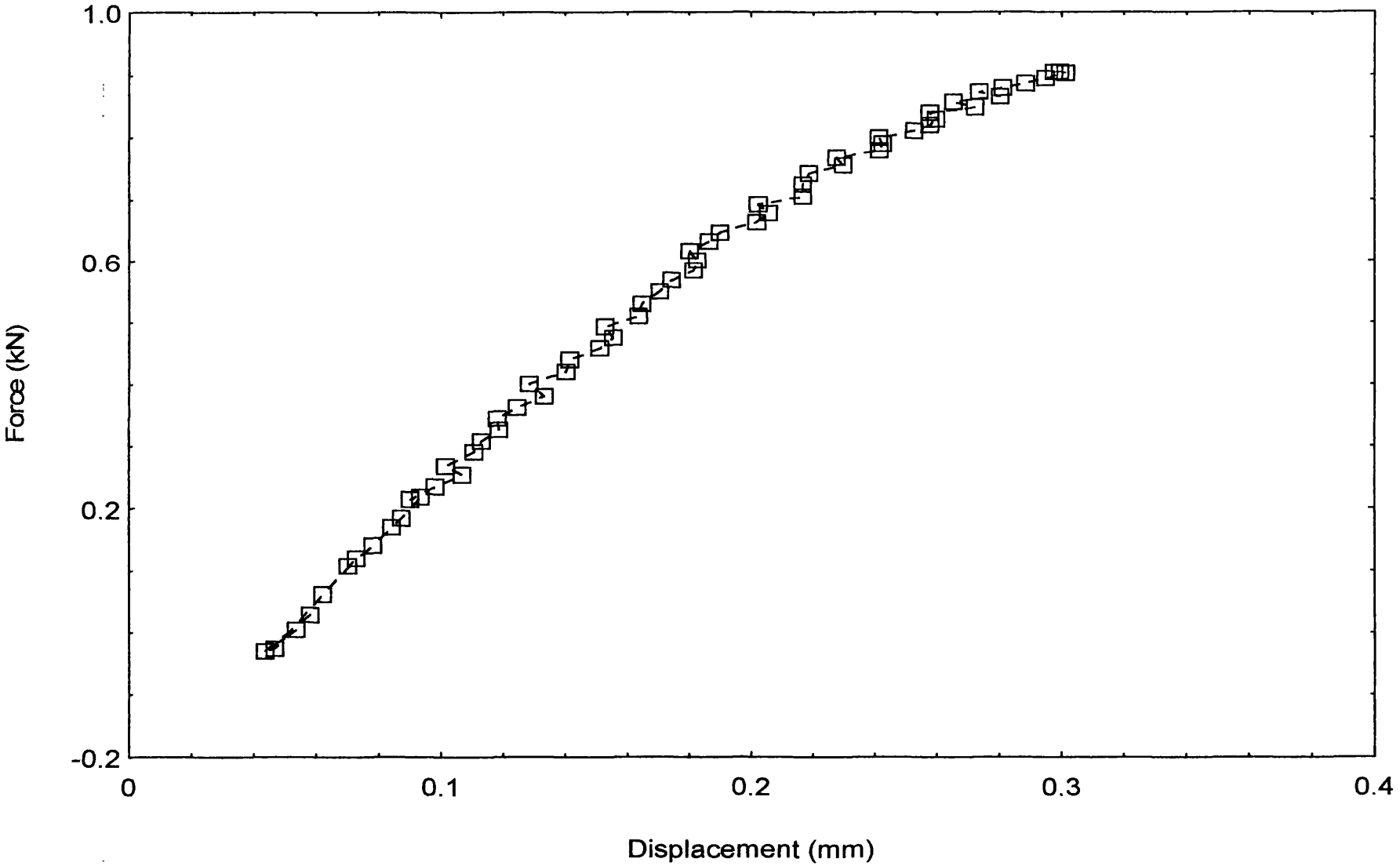

Figure 4.11 Typical Force / Displacement curve for a tension test

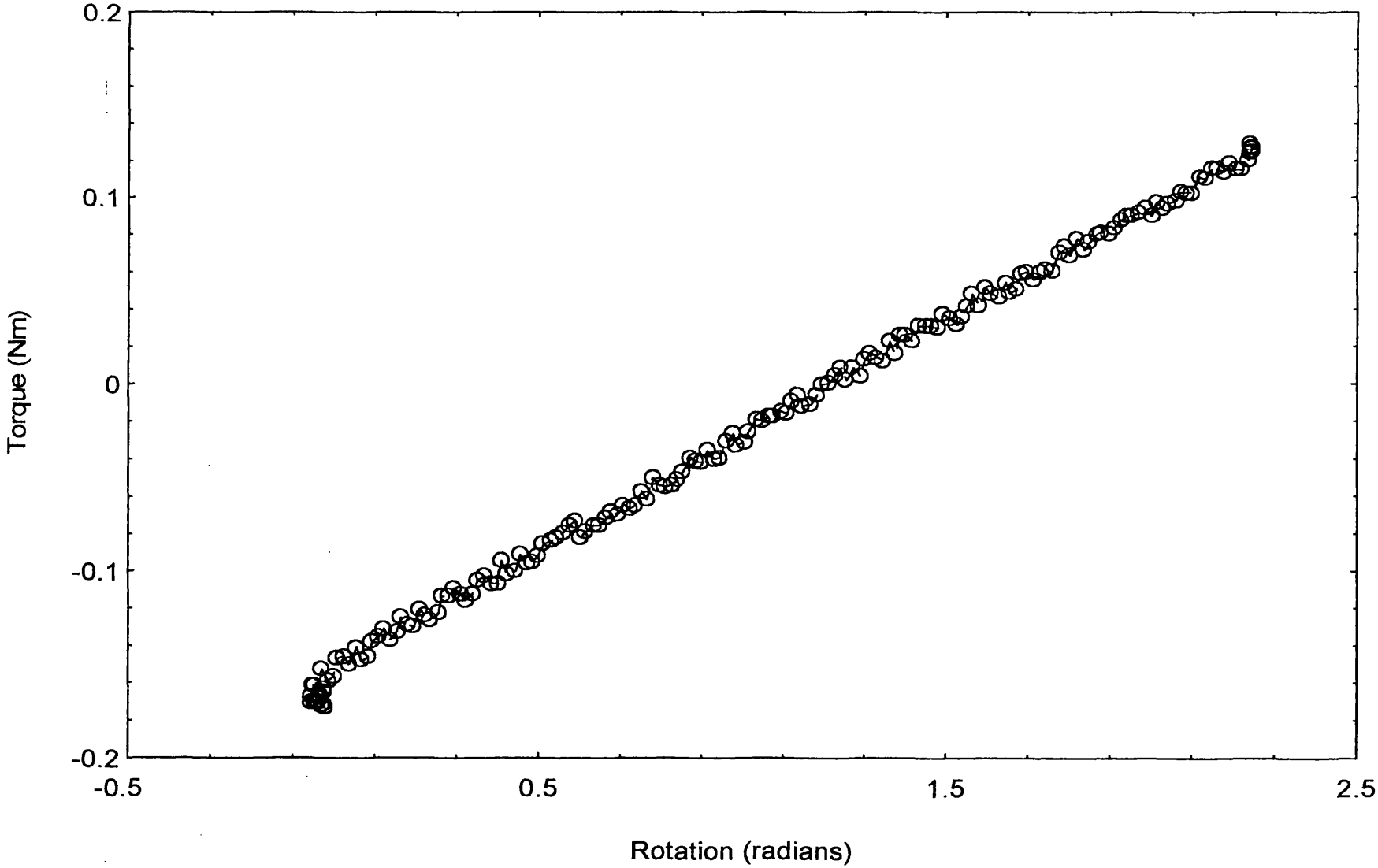

Figure 4.12 A typical torque / rotation curve for torsion test

where T/θ is the torque / rotation gradient (with θ in radians), GL is the gauge length, w the sample width, t the sample thickness and k is a slowly-varying function of the sample geometry.

For samples where the width/thickness ratio is greater than 5, k can be approximated to:

$$k = \frac{1}{3}\left(1 - \frac{0.63.w}{t}\right) \qquad 4.7$$

This equation was used for all samples, with an average value of thickness for each sample.

An additional complication arises because the sample thickness is not constant. For the tension tests, where the modulus is simply dependent on 1/t, an average value of t is appropriate. For the torsional tests, however, this is not the case, as the dependency on t is $1/t^3$. This means that the thinner sections of the sample will twist disproportionately compared to the thicker sections. In order to account for this, equation 4.6 was modified to become :

$$G = \left(\frac{T}{\vartheta}\right) x \left(\frac{1}{k.w.}\right) x \sum \frac{\Delta GL}{t^3} \qquad 4.8$$

where the summation was performed for each 5 mm section of gauge length for which a separate thickness was measured.

A final complication arises with torsional testing due to the clamping, which provides an artificial constraint to the twisting of the sample. It is possible to account for this by doing tests with samples of different gauge lengths, but this process is very long-winded for a large number of samples. This process was performed for three initial samples, from which it was found that a sensible approximation was to reduce the effective gauge

length by 2 mm at each end. This is effectively saying that the first 2 mm at each end are constrained from free rotation by the grips.

4.4.3.3 Order of Testing

For each sample, three tension and three torsion tests were performed, each at a different rate. The standard rate of 10^{-4} s^{-1} was used for all samples, with two of the other rates in addition. In order to reduce the likelihood of any systematic effects of drying or viscoelasticity, the order of testing was varied with each sample. After each test, the sample was allowed to recover for a short time before the next test.

It was found that the samples did dry out during the testing process, and so some initial tests were performed to determine how long a test period could be used. The tension and shear modulii were measured as a function of time out of saline. It was found that after about 30 minutes, noticeable effects were observed. These were more pronounced for the tension tests. The reason for this is that these will have a greater contribution from the central spongy region, which will be more affected by drying. For torsion tests, the central region is under the least stress and so is far less significant than the outer compact regions which are not affected by drying as much. As a result of these findings, all testing was performed within 30 minutes of removal from saline.

4.4.4 RESULTS

4.4.4.1 Tension

The complete set of tensile modulus results (some 140 tests) are shown in Figure 4.13 as a function of sample thickness. This plot is included to determine whether the thickness has a systematic effect (with thicker samples generally having a greater proportion of spongy bone). It can be seen from this graph that there is considerable scatter from sample to sample, that values lie generally between 3 and 10 GPa, and that there is a very slight increase in modulus with decrease in thickness. As this variation with thickness is very slight, it was decided not to 'normalise' the data to a constant thickness, as has been done in other studies.

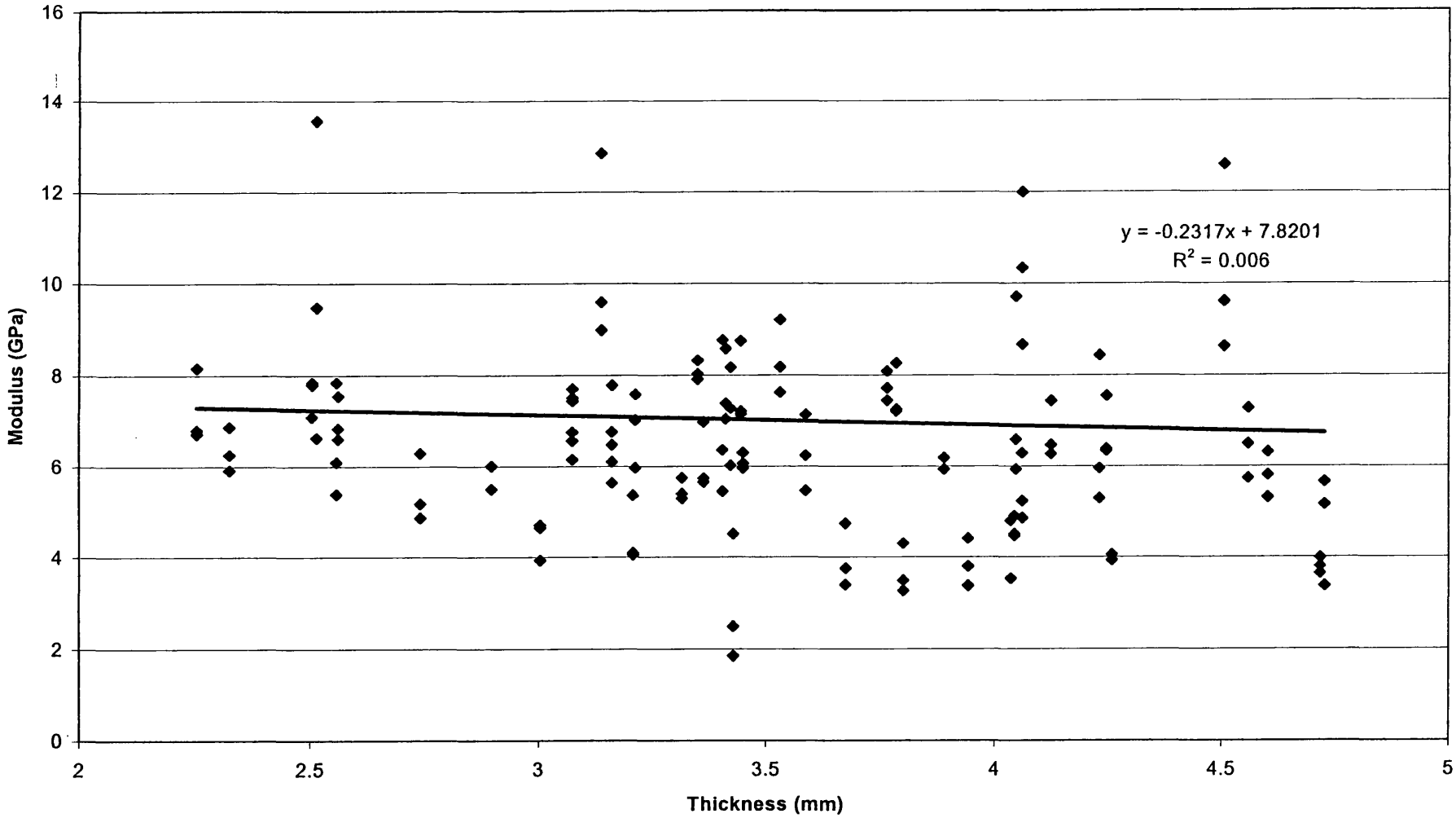

Figure 4.13 The tensile modulus versus thickness for bovine scapulae samples

The effect of testing rate is shown in Figure 4.14. From this it can be seen that the dominant feature is the sample to sample variation, and that there is no dramatic variation with rate. There is a very small increase in modulus as the rate increases, which can be fitted to a power-law curve to give the following best-fit equation:

$$E = 9.41 \times (\text{Rate})^{0.05} \qquad 4.9$$

The exponent of 0.05 is similar to values found by other workers.

4.4.4.2 Torsion

The values of shear modulus are plotted against sample thickness in Figure 4.15. This again shows considerable sample to sample variation, with values generally between 1.5 and 3.5 GPa. There is only a slight variation with sample thickness, with a slight increase in modulus as the thickness decreases.

Figure 4.16 shows the modulus values plotted against rate. This is very similar to the tensile modulus behaviour, with a very slight increase in modulus with rate, which can again be fitted to a power law:

$$G = 2.57 \times (\text{Rate})^{0.008} \qquad 4.10$$

The exponent here is considerably lower than that found in tension. This is what would be expected for the following reason. Spongy bone will be more rate dependent than compact bone as it is more akin to a viscoelastic material. For the tension tests the whole sample contributes to the stiffness, whereas with the torsion tests, the outer regions contribute more than the centre, and so the effect of the spongy bone will be less significant.

4.4.4.3 Poisson's Ratio

Attempts were made to correlate pairs of individual tests in tension and torsion to generate values of Poisson's Ratio, but as the order of testing was deliberately varied with each sample, this process introduced considerable scatter. Instead, the average values of tensile and shear modulus were used to generate values of Poisson's Ratio and some information on how this varies with rate.

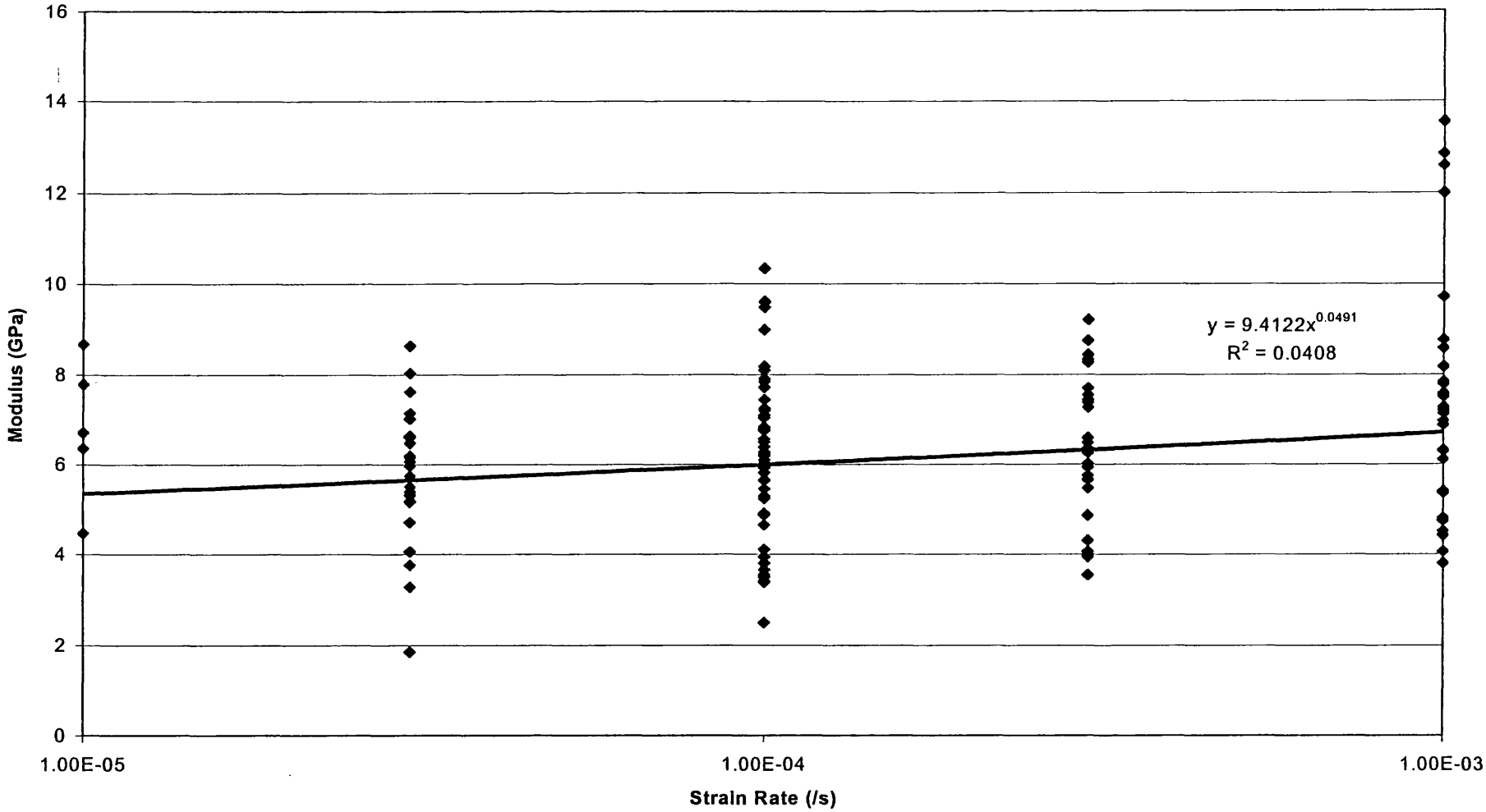

Figure 4.14 The tensile modulus versus rate for bovine scapulae samples

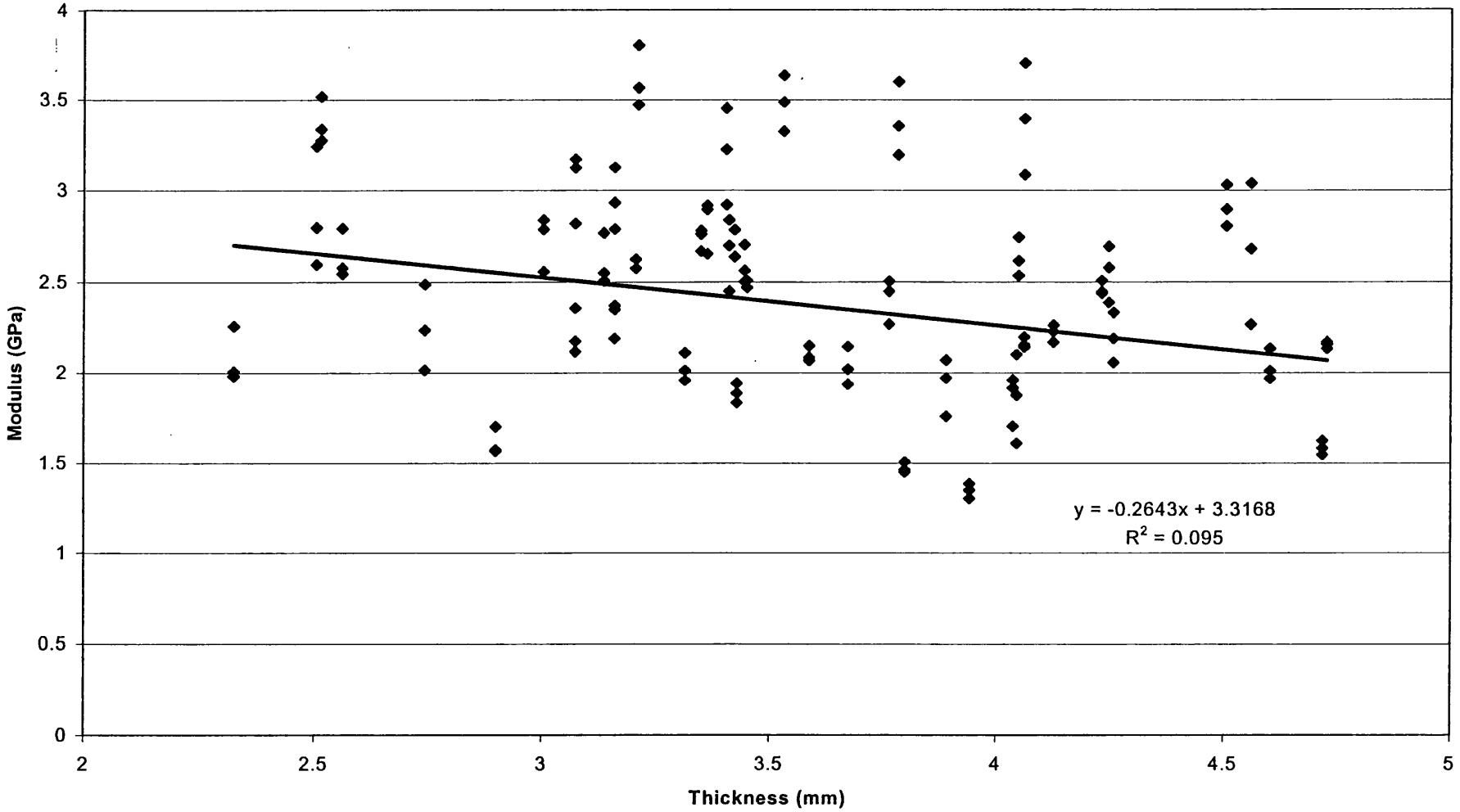

Figure 4.15 The shear modulus versus thickness for bovine scapulae samples

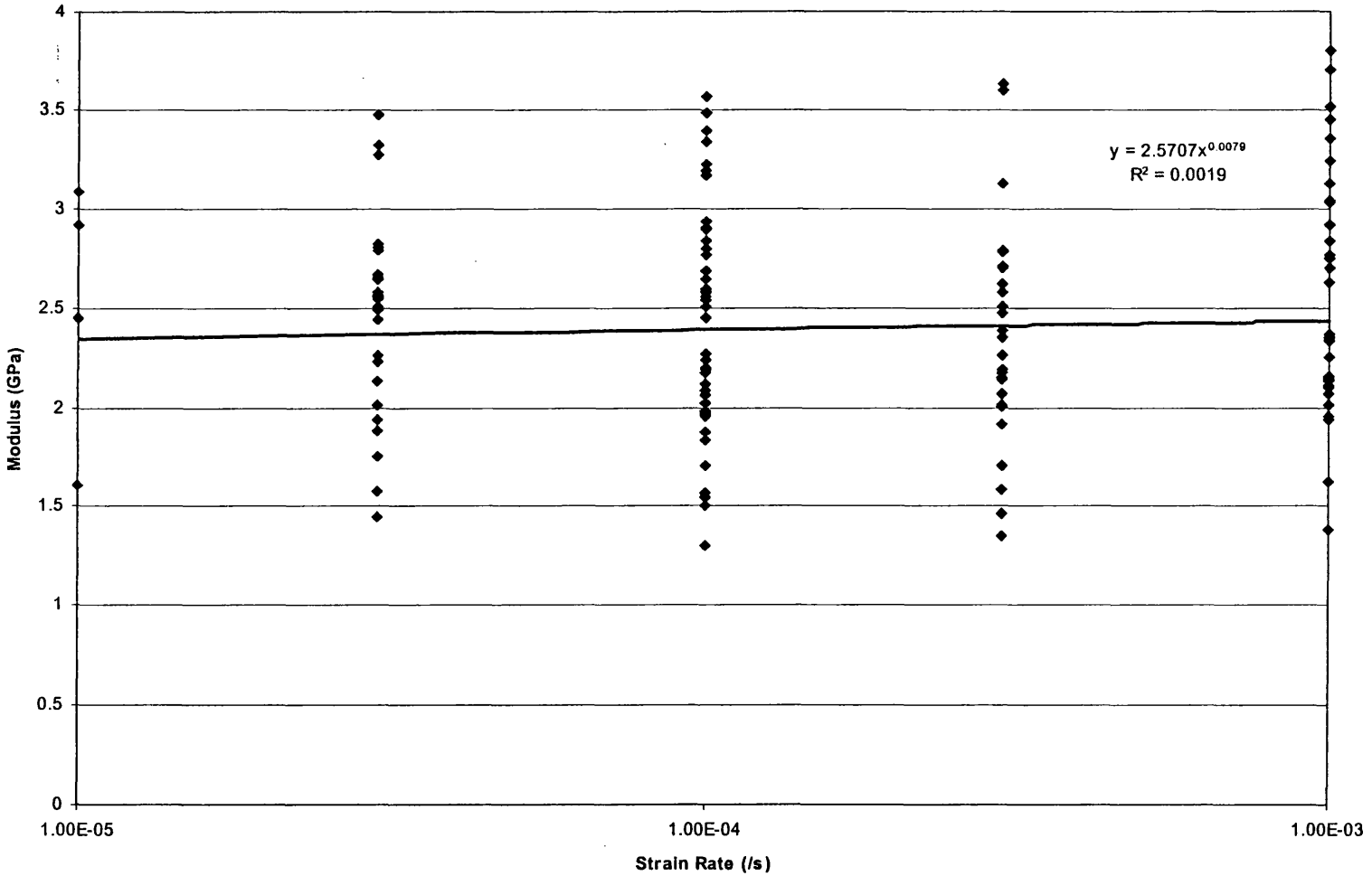

Figure 4.16 The shear modulus versus rate for bovine scapulae samples

Poisson's Ratio is given by :

$$\nu = \frac{E}{2G} - 1 \qquad 4.11$$

Therefore, comparing equations 4.9, 4.10 and 4.11 gives us a variation for Poisson's Ratio as follows:

$$\upsilon = 1.831 \text{ x } (\text{Rate})^{0.04} - 1 \qquad 4.12$$

This shows that Poisson's Ratio varies with rate, increasing as the rate increases. A summary of values at different strain rates is given below in Table 4.4.

Table 4.4 A summary of the stiffness properties of bovine scapulae samples at different strain rates

Strain Rate (/s)	E (GPa)	G (GPa)	υ
10^{-5}	5.35	2.35	0.155
10^{-4}	5.99	2.39	0.267
10^{-3}	6.71	2.43	0.389
10^{-2}	7.51	2.48	0.522
10^{-1}	8.41	2.52	0.670
1	9.41	2.57	0.831

The υ values at high rates seem rather high but it should be noted that these are extrapolations from low rate tests and ideally should be verified experimentally.

4.4.5 BENDING TESTS

After tensile and torsional tests, samples were re-immersed in saline and then tested in three-point bending mode within a further 24 hours. This was to provide a measure of the fracture strength of the samples, and incidentally, an additional measure of modulus.

Samples were tested using a three-point bend jig with a span length of 51 mm. Three different testing rates were used, corresponding to strain rates of approximately 10^{-2}, 10^{-3} and 10^{-4} s^{-1}. For this geometry, the maximum stress, strain and modulus can be calculated from the equations below:

Stress : $$\sigma = \frac{3FL}{2wt^2} \qquad 4.13$$

Strain : $$\varepsilon = \frac{6\delta t}{L^2} \qquad 4.14$$

Modulus : $$E = \frac{FL^3}{4wt^3\delta} \qquad 4.15$$

Where F is the force, L the span length, δ the displacement, w the sample width and t the sample thickness. As the strain is dependent on the sample thickness, the strain rate varied slightly from sample to sample.

Figure 4.17 shows a typical force / displacement curve for a slow rate test, while Figure 4.18 shows a curve for a fast rate test. It can be seen from these that there is an initial straight line region, with a gradual curve to the maximum force, followed by a gradual failure. With some tests, the failure was fairly rapid and complete after the peak force, while with others, there was a much slower failure process, with the sample gradually bending with many small cracks developing. For this reason, the values of strain to failure were not reported as they would not show any useful information.

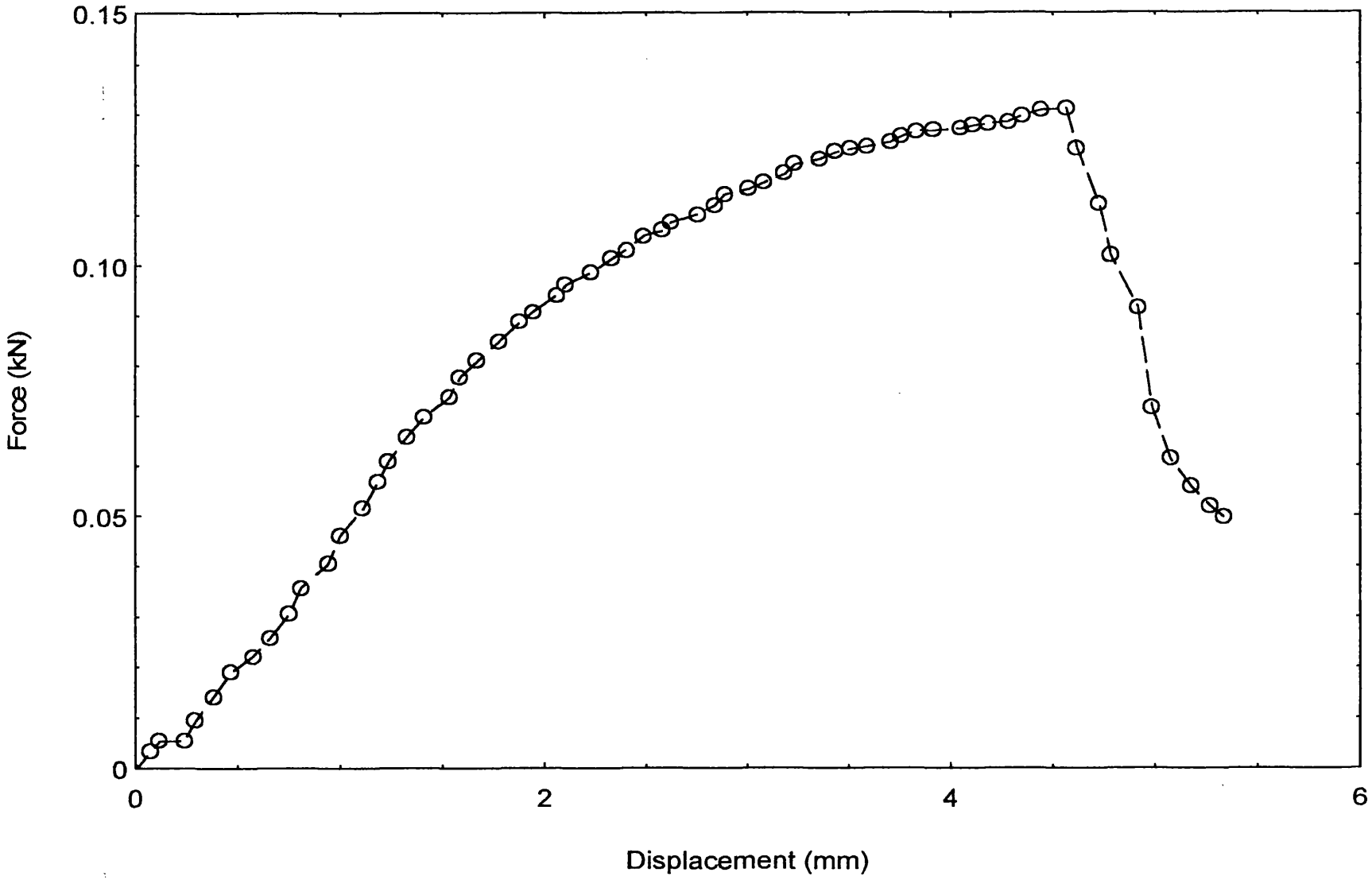

Figure 4.17 A typical force / displacement curve for a bending test at a slow rate (1mm/min)

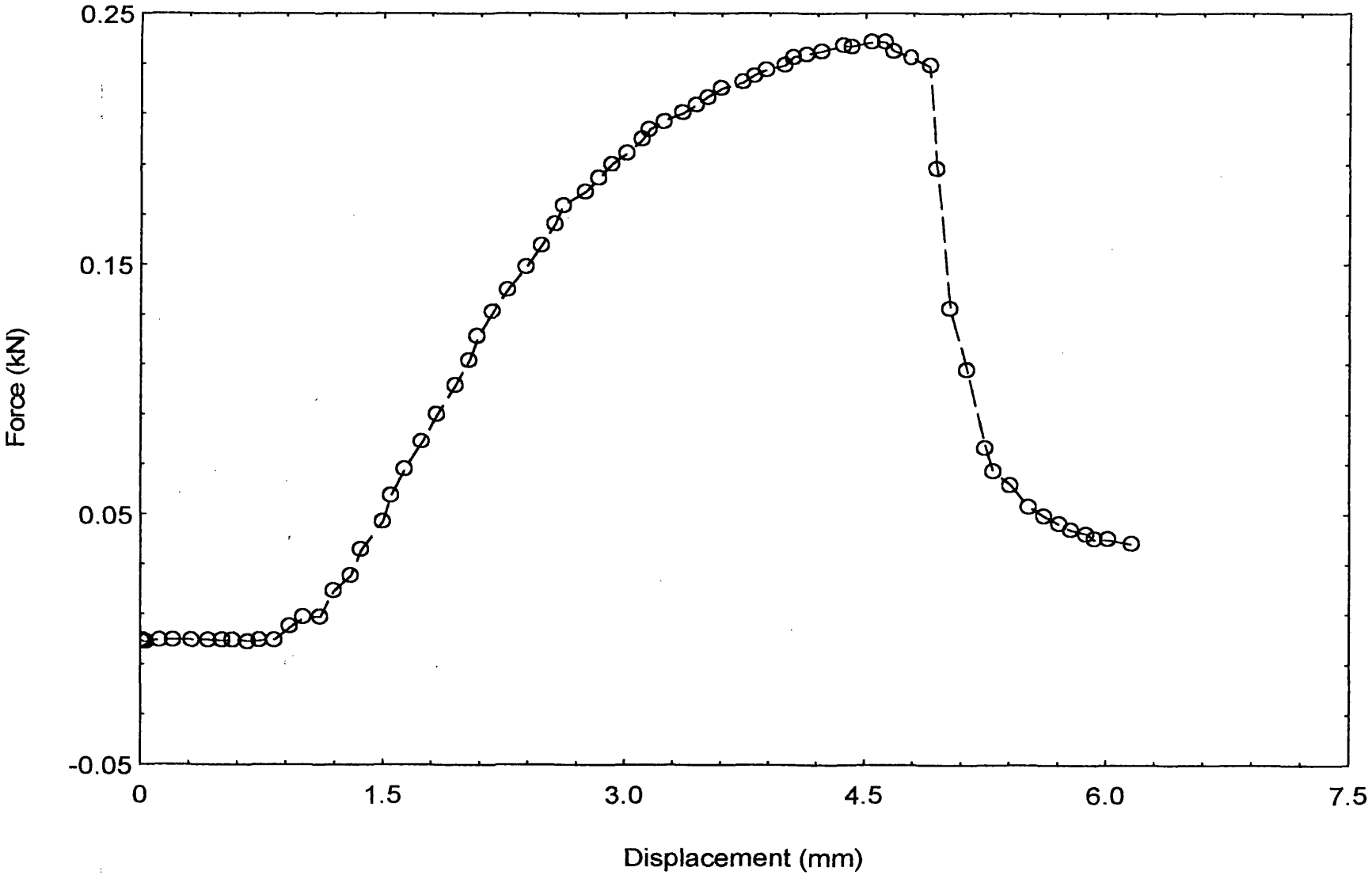

Figure 4.18 A typical force / Displacement curve for a bending test at a fast rate (50mm/min)

From each graph, the value of maximum stress at failure was calculated, as was the flexural modulus E_f. These are shown plotted against strain rate in Figure 4.19 and 4.20 respectively.

Figure 4.19 shows that the failure stress increases quite strongly with increasing rate. If this is fitted as a power-law variation, the equation is:

$$\text{Maximum Stress} = 180 \times (\text{Rate})^{0.063} \quad \text{(MPa)} \qquad 4.16$$

Again, this value of exponent is similar to those found for failure stress by other workers.

Figure 4.20 shows that the flexural modulus also increases with strain rate, but much less markedly, with a power-law variation of:

$$\text{Flexural Modulus} = 7.95 \times (\text{Rate})^{0.033} \qquad 4.17$$

The exponent is similar to that found for tensile and shear modulii. The values of flexural modulus are slightly lower than for tensile modulus, as expected, as bending deformation has some shear component.

Values of strain to failure have not been calculated from bend tests, as some samples exhibited considerable ductility before finally failing. To use the maximum strain recorded would therefore give dangerously large values, and it is perhaps more appropriate to use a 'yield strain' as the strain beyond which the material starts to deform permanently and more easily. By comparing the values of modulus and maximum stress, this 'yield strain' is of the order of 1.5 %.

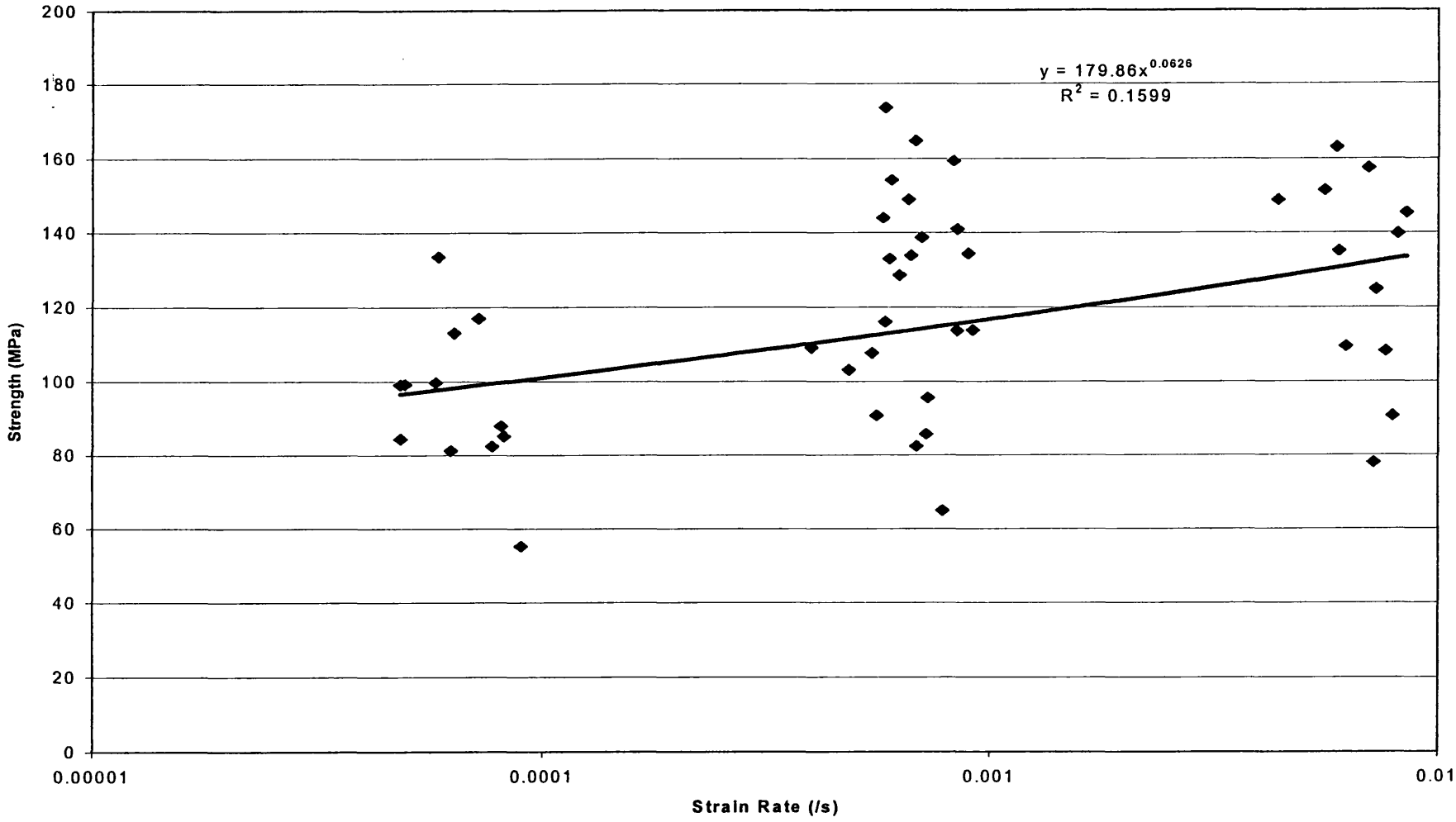

Figure 4.19 The flexural strength versus rate for bovine scapulae samples

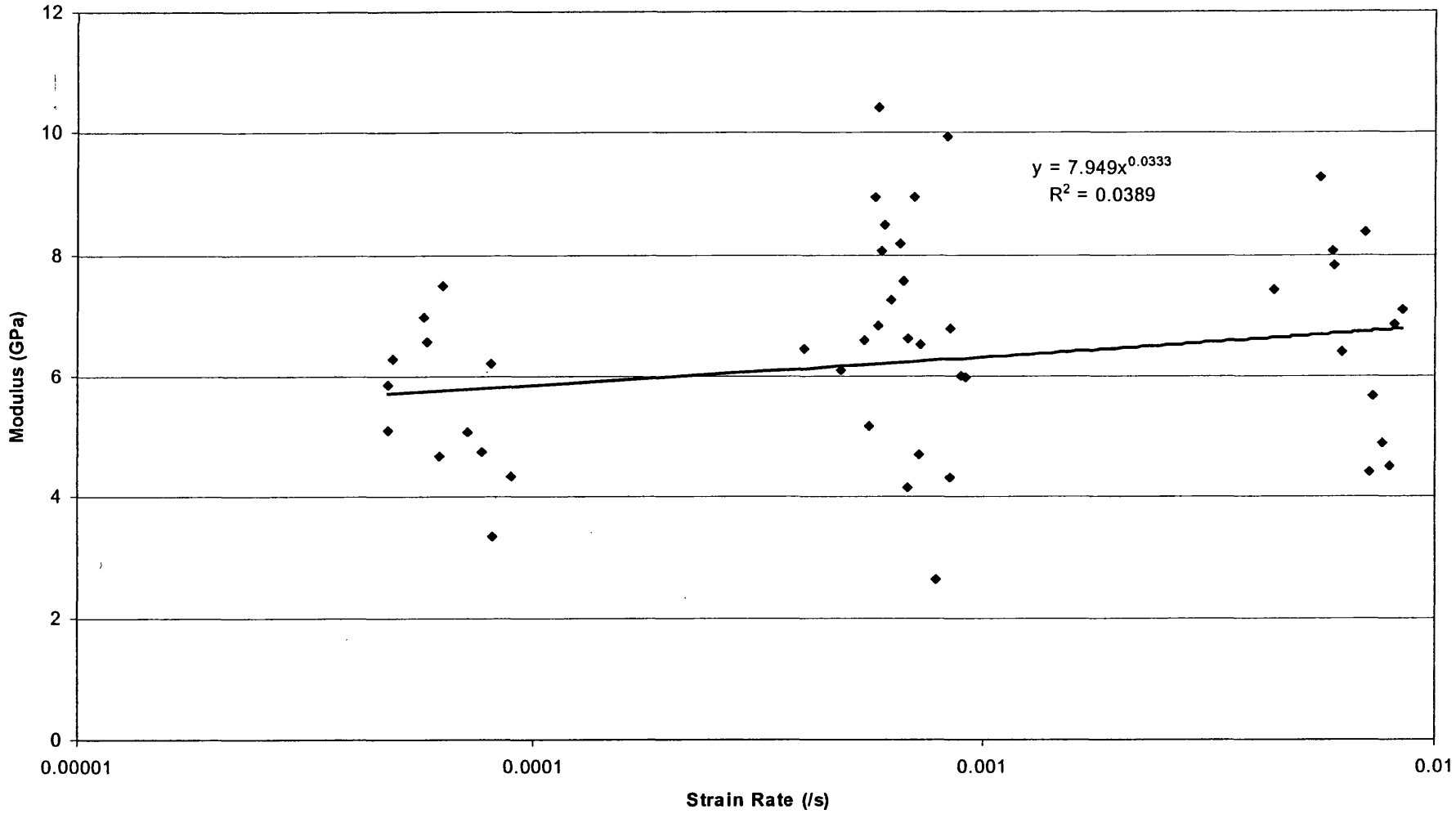

Fig 4.20: Bending Modulus vs Rate

4.4.6 CONCLUSIONS TO MECHANICAL TESTING

The test results described above show that the most significant feature of the mechanical properties of these materials is the sample-sample variability, but that if sufficient tests are performed, the underlying features can be deduced.

The tensile and flexural modulus values produced here are all in reasonable agreement with previous studies. For instance, David Taylor's work gave modulus values of between 5 and 10 GPa for bovine scapulae. The effects of rate observed here are also similar to those found elsewhere, with exponents of 0.03 to 0.04 being commonly reported.

The values for shear modulus cannot easily be compared to other studies, as none have been reported. The values produced seem sensible, and show a very similar variation with testing rate.

The value of Poisson's Ratio calculated from the tests show that this lies in the range of 0.29 to 0.36, and increases only very slightly with strain rate. The few studies that have looked at Poisson's Ratio of bone have shown that it has very little dependency on strain rate, and so these findings seem to be in good agreement. It should be noted that as bone is a composite sample, it is somewhat of an approximation to quote a single value of Poisson's Ratio, but that if modelling is to be performed using an isotropic material, then it is necessary to make this approximation.

The failure stress found from bending tests is also in good agreement with David Taylor's results, where an average value of 110 MPa was found, compared with the values of 110 – 130 MPa seen here. There is a stronger variation with strain rate, with an exponent of about 0.066. This is also in reasonable agreement with previous studies which generally show that strength varies more strongly with rate than does stiffness.

4.5 BOVINE SCAPULAE DISC TESTS

4.5.1 INTRODUCTION

This part of the report describes an assessment of bovine scapulae through the use of disc testing. A need for controlled biaxial testing became apparent, that produced measurable results in a similar testing configuration to that of baton round impact tests carried out by DERA. The results of the disc tests were intended to be used to aid in the validity of the finite element computer model, developed by Fluid Gravity Ltd, Aberdeen. This makes predictions on the effects of baton round impacts on bovine scapula, and has been previously discussed.

It should, however, be noted that the finite element model was developed for fast (impact) rates of around 68 ms^{-1}, onto an unconstrained target. With the disc tests the fastest rates achieved were only 6 m min^{-1} (almost 3 orders of magnitude slower), however as the disc is constrained failure occurs sooner (relatively) than in a free impact. Taking strain rate as an important consideration it can be estimated that the disc tests achieved a strain rate of about one tenth of that seen during impacts. In addition, the disc tests operate at a constant displacement (constant velocity), which are not representative of baton round impacts. Despite these differences it was thought that modelling of the disc tests would be a useful exercise as they allow a well-instrumented half way point between conventional mechanical tests and the full impact conditions. Although there were differences in strain rate, the biaxial bending nature of the loading would provide a good test of any modelling.

4.5.2 EXPERIMENTAL PROCEEDURE

50 disc samples of bovine scapulae were machined and prepared by RMCS, Shrivenham. They were taken from the animal within an hour after death and frozen. They were machined frozen and remained so, until they were needed for testing. The scapulae samples were machined into discs with a diameter of 100 mm. The discs were not isotropic, and ranged in thickness at their centre from 2.44 to 7.82 mm. Due to the broad range of thicknesses it was decided to divide the 50 samples into five groups of ten. Group

1 would contain the ten thinnest samples, Group 2 the next ten thinnest, up to Group 5, containing the ten thickest. Each thickness group was then divided in two as there were two different types of test to be conducted.

The samples were defrosted in a 0.9% saline solution and refrigerated for 24 hrs. Prior to testing they were removed from the fridge, transferred to a room temperature saline solution and left to reach room temperature for between 2 and 6 hours.

The disc tester was purpose built for these experiments. It was machined from steel and can be seen below in Fig 4.21. The samples sit inside the test jig and are fixed in place firmly as the jig is screwed closed. Rubber O-ring seals are situated both above and below the sample to aid in a more secure fitting. The samples were not of uniform thickness so the rubber seals allowed for more uniform gripping, and helped in reducing the stress concentrations in the areas of greatest thickness where contact with the upper and lower surfaces of the test jig occurred.

The indentor, that was forced onto the centre of each sample at a constant rate, had two differently shaped ends. These were designed flat and spherical. The spherical end was a hemisphere of 25mm diameter. The flat end was rounded at the edges (to a radius of 3mm) to reduce any severe stress concentration at the edges. This is similar in design to the new XL21 baton round (which has a slightly larger corner radius). The two indentor shapes were used to see what difference, if any, there would be in the impact effects of baton rounds with differently shaped noses. ie flat, or spherical designs.

The machine used to apply the constant displacement was a servo hydraulic tensile machine, which was set up in compression mode. The head of the servo hydraulic would move down onto the indentor which had been placed gently onto the surface of the clamped specimen. The maximum displacement was set to 20 mm as it was noted in trial tests that the majority of failures occurred at 10 mm or less. Four testing rates were used, over almost 4 orders of magnitude. The rates were 10, 100, 1000 and 6000 mm/min. 6000 mm/min was the fastest operating speed of the machine and test data recording equipment. Throughout each test a constant record of force against displacement was taken. This allowed the maximum force (at first fracture) and the initial (steepest) gradient of force / displacement to be determined for each test.

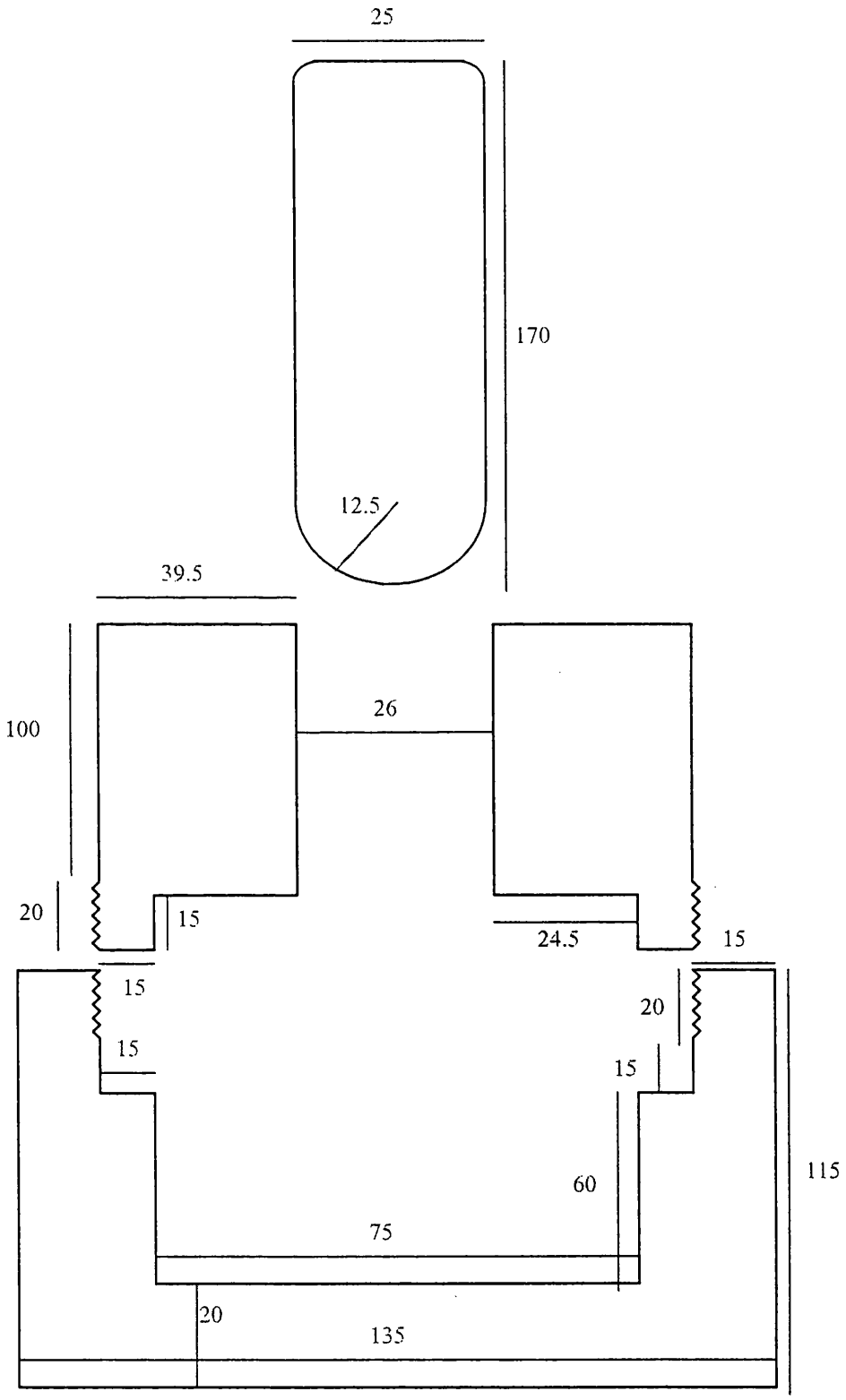

Figure 4.21 The disk testing apparatus (all dimensions in millimetres)

After the completion of each test a note was made of the type of fracture observed. These were classified into 6 groups and related to the severity of fracture.

4.5.3 RESULTS

A plot for each test showing Force (kN) and Displacement (mm) was produced. These were then plotted in groups depending on testing rate and thickness group. Eight graphs were created showing the variation of force and displacement for the 5 thicknesses at each of the four testing rates, for both the flat and spherical indentors. These are shown below in Figs 4.22-4.29.

One graph was plotted showing force at fracture versus rate for all samples tested to compare the effects of both indentors. Then a plot of the average values of each rate was produced. These are shown in Figs 4.30 and 4.31.

The same was then done for peak gradient versus testing rate, and is shown in Figs 4.32 and 4.33.

The classification of samples into groups a - f, relating to the severity of fracture observed after testing is as follows:

a: Single diametric crack on lower surface
b: Single diametric crack right through
c: as a, but also diametric crack on top
d: as a, but with perpendicular crack on lower surface
e: complex cracking, starting with diametric crack on lower surface
f: complex cracking, starting around edge of indentor

Digital photographs were taken of a selection of tested specimens, and outline the differences in severity of failure observed. These can also be seen below in Figs 4.34 - 4.39. A summary of the type of failure observed for each sample is given in Table 4.5

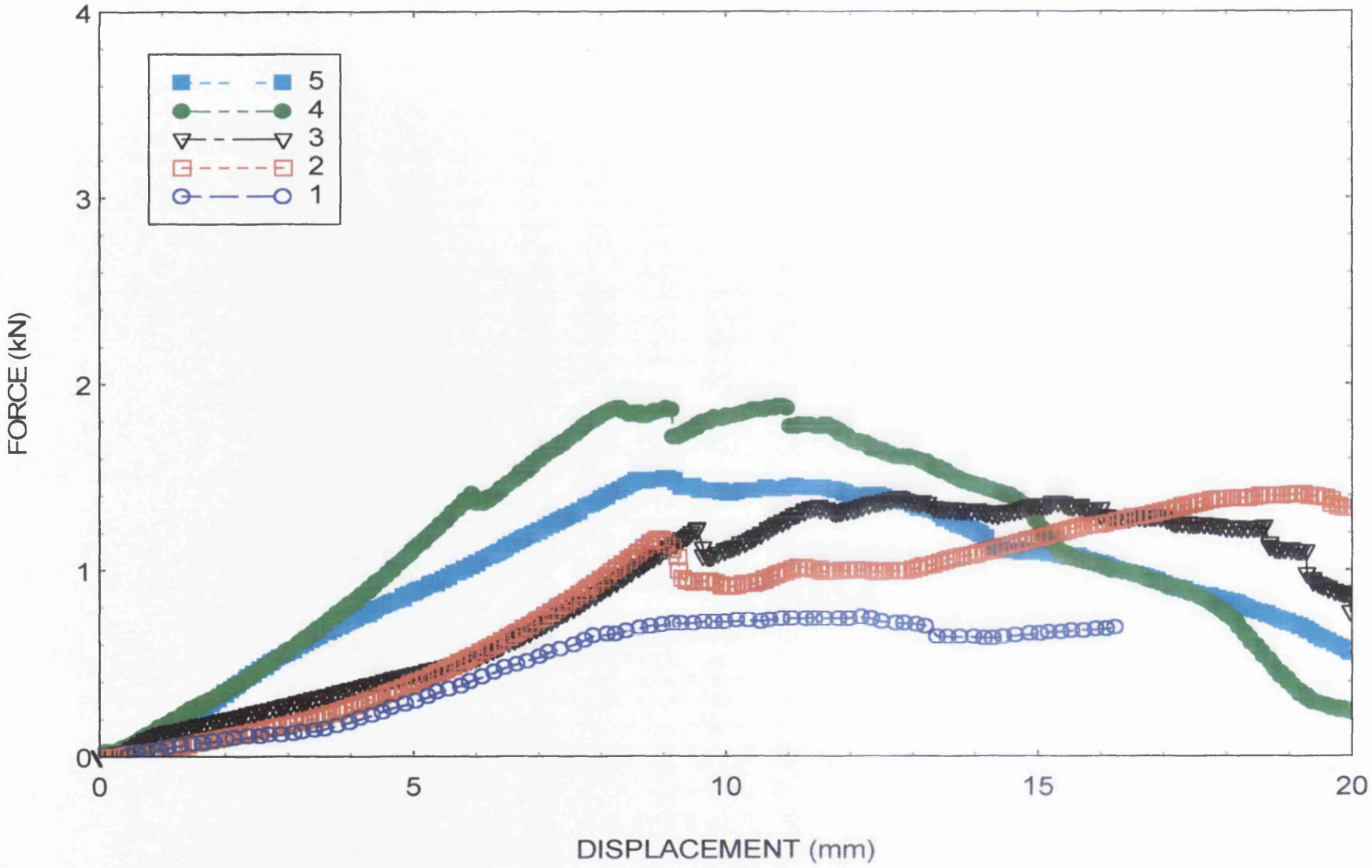

Figure 4.22 Disk test graphs of samples from different thickness groups using a spherical Indentor at a rate of 10 mm/min

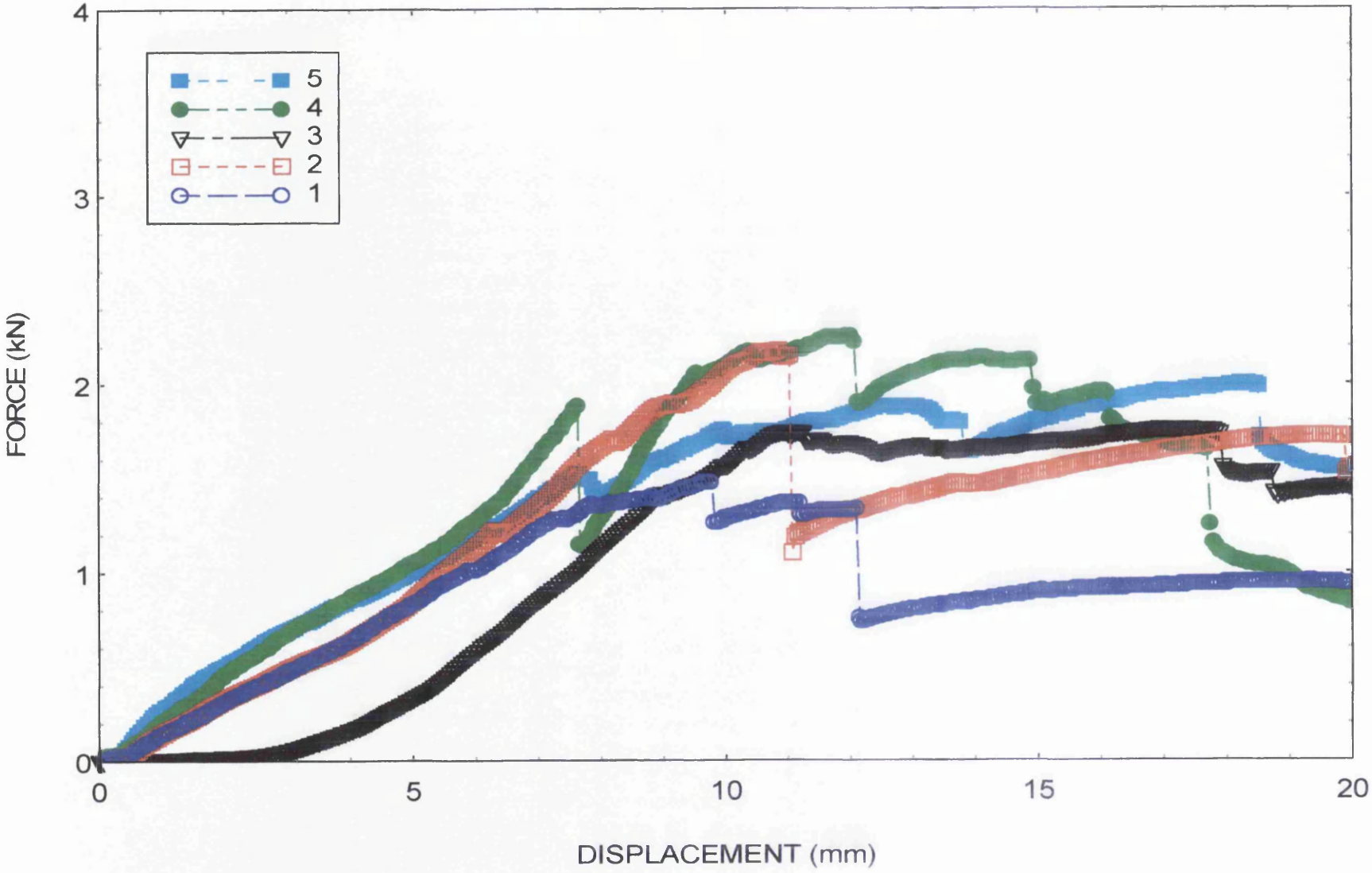

Figure 4.23 Disk test graphs of samples from different thickness groups using a spherical Indentor at a rate of 100 mm/min

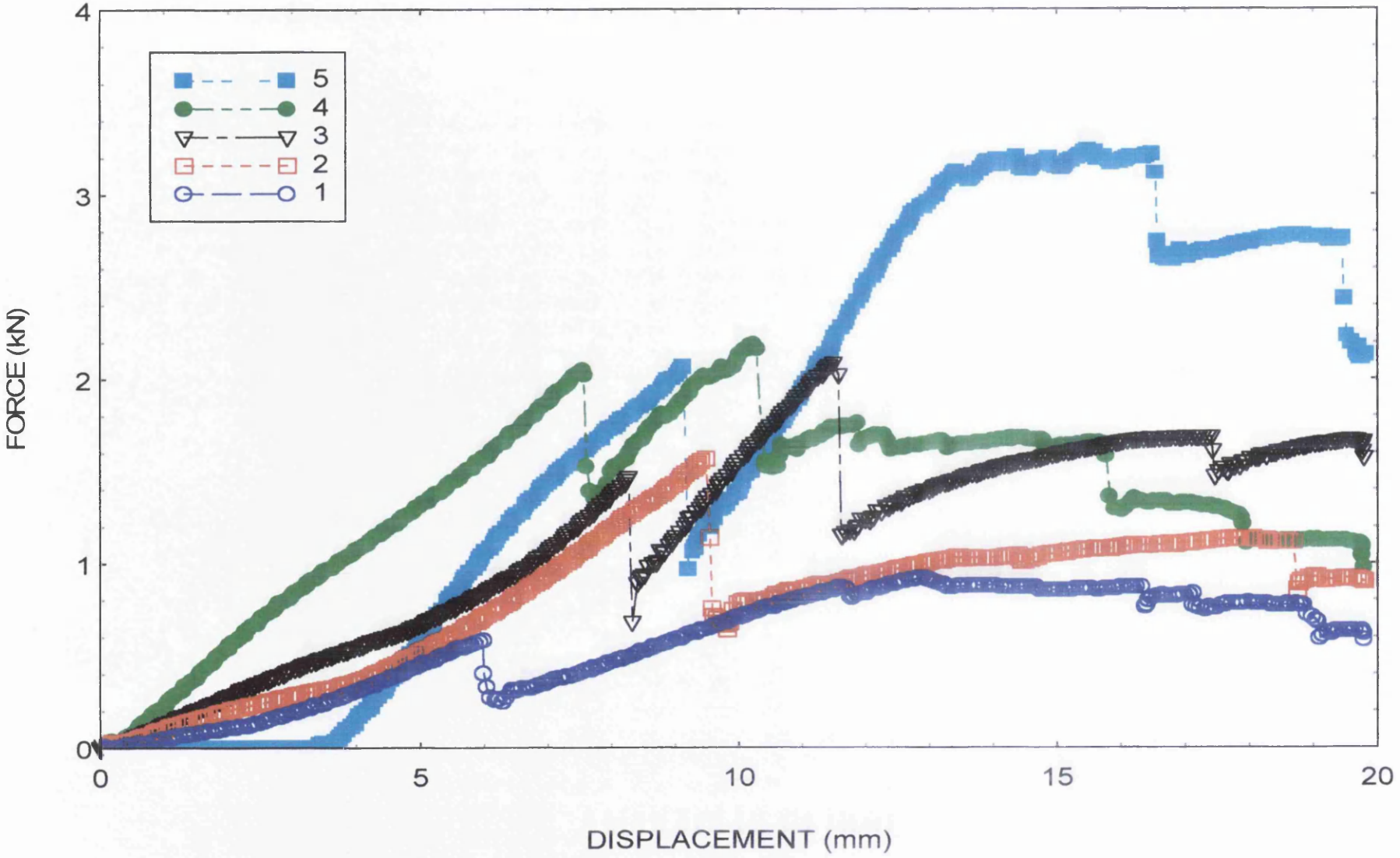

Figure 4.24 Disk test graphs of samples from different thickness groups using a spherical Indentor at a rate of 1000 mm/min

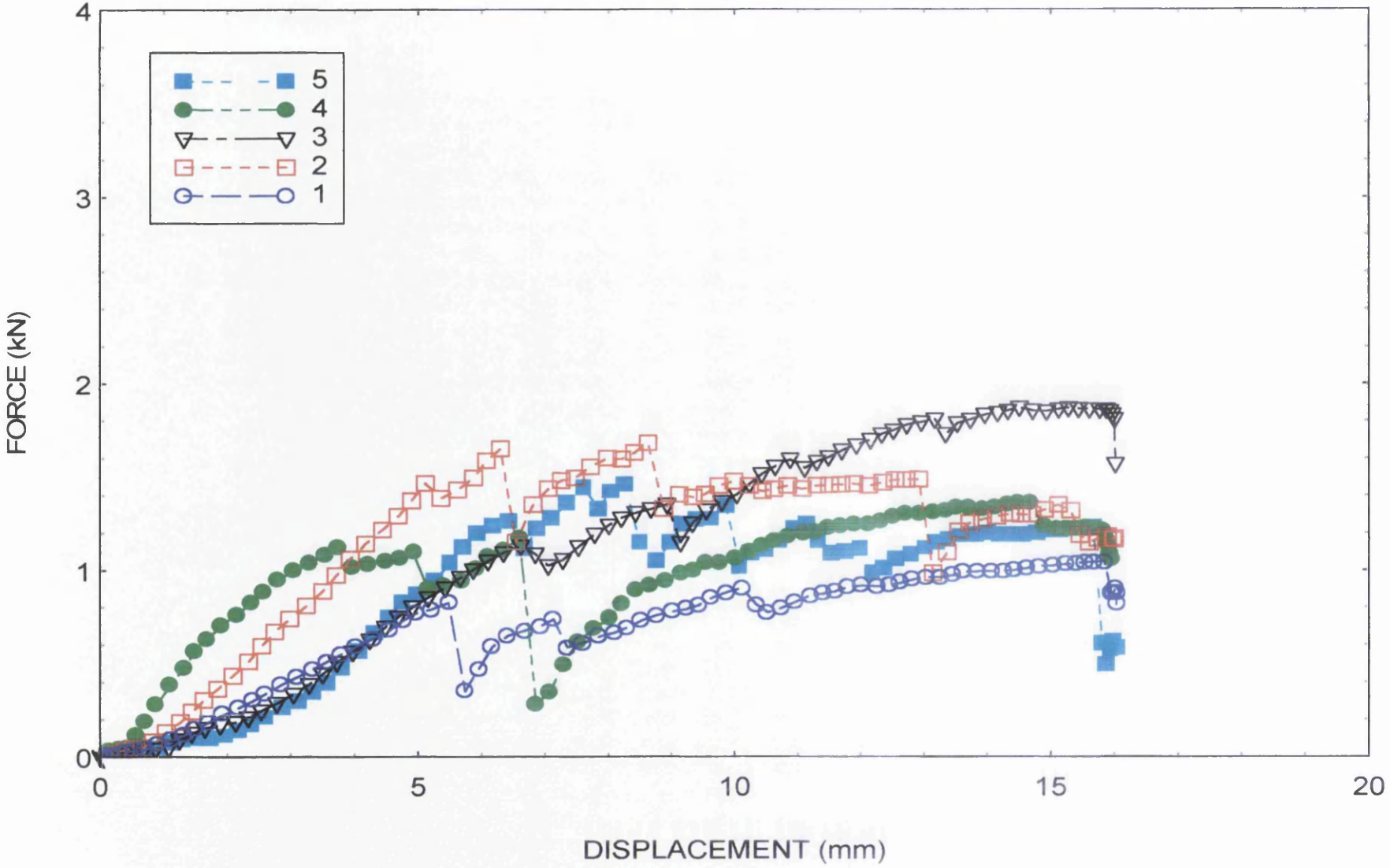

Figure 4.25 Disk test graphs of samples from different thickness groups using a spherical Indentor at a rate of 6000 mm/min

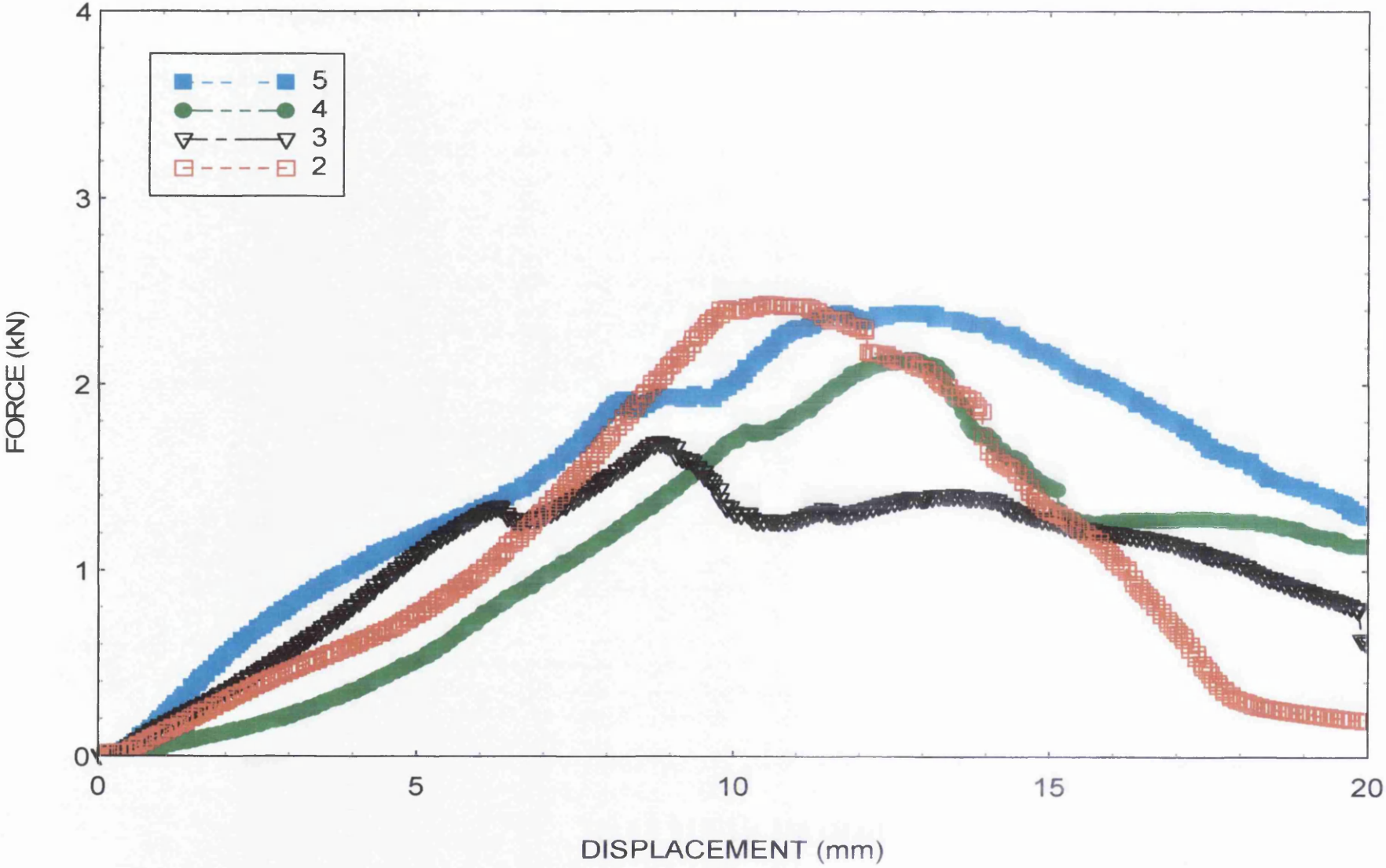

Figure 4.26 Disk test graphs of samples from different thickness groups using a flat Indentor at a rate of 10 mm/min

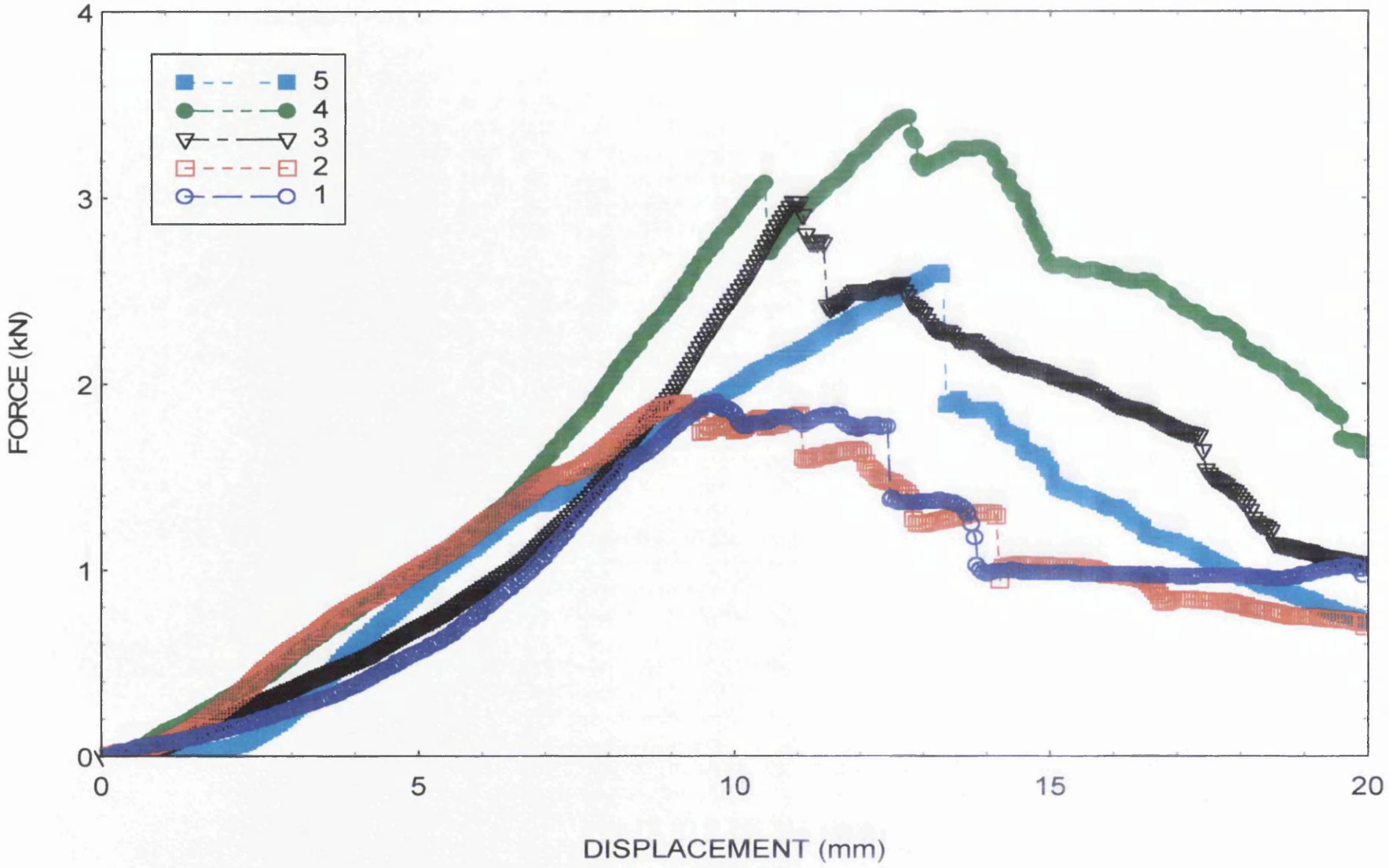

Figure 4.27 Disk test graphs of samples from different thickness groups using a flat Indentor at a rate of 100 mm/min

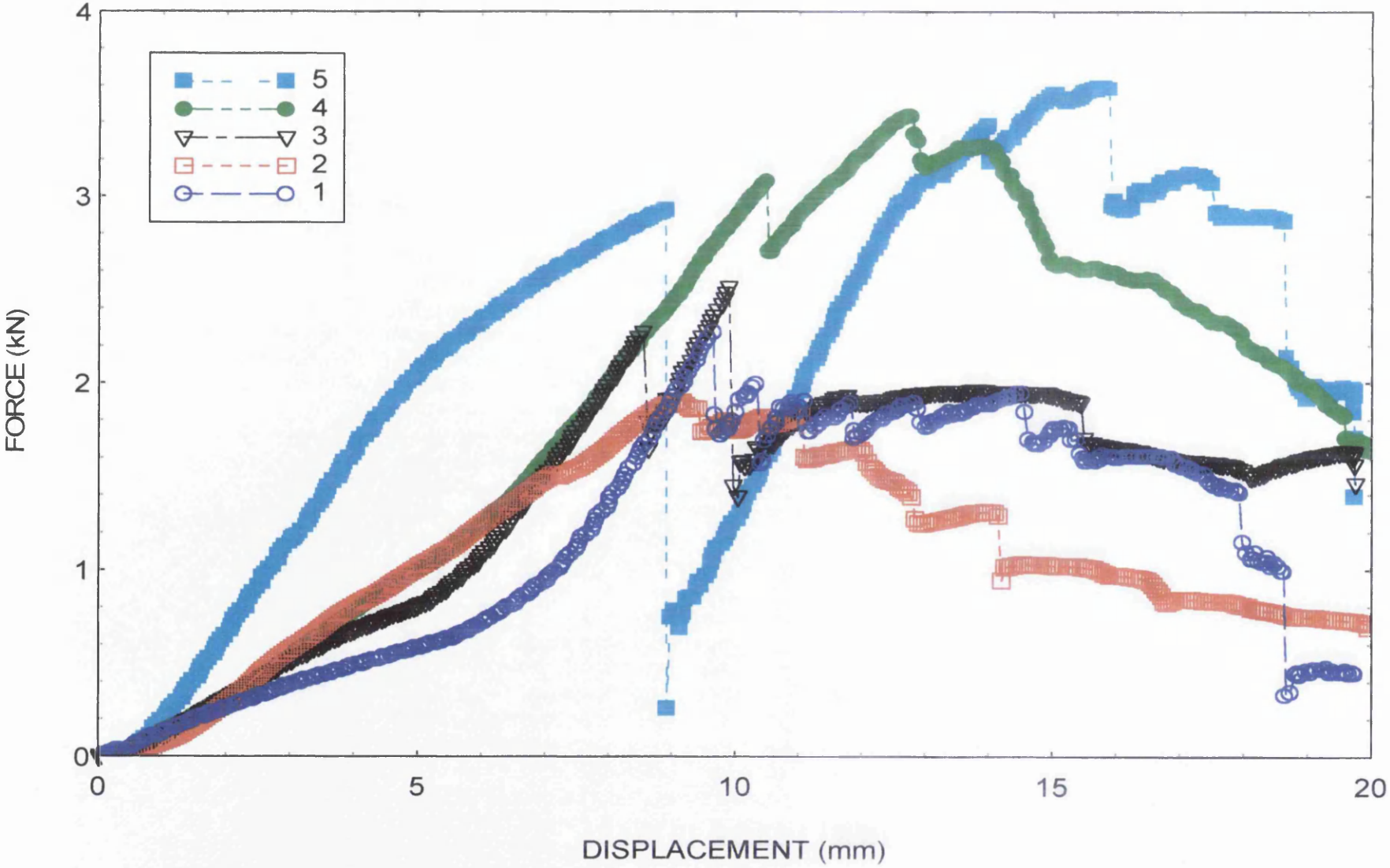

Figure 4.28 Disk test graphs of samples from different thickness groups using a flat Indentor at a rate of 1000 mm/min

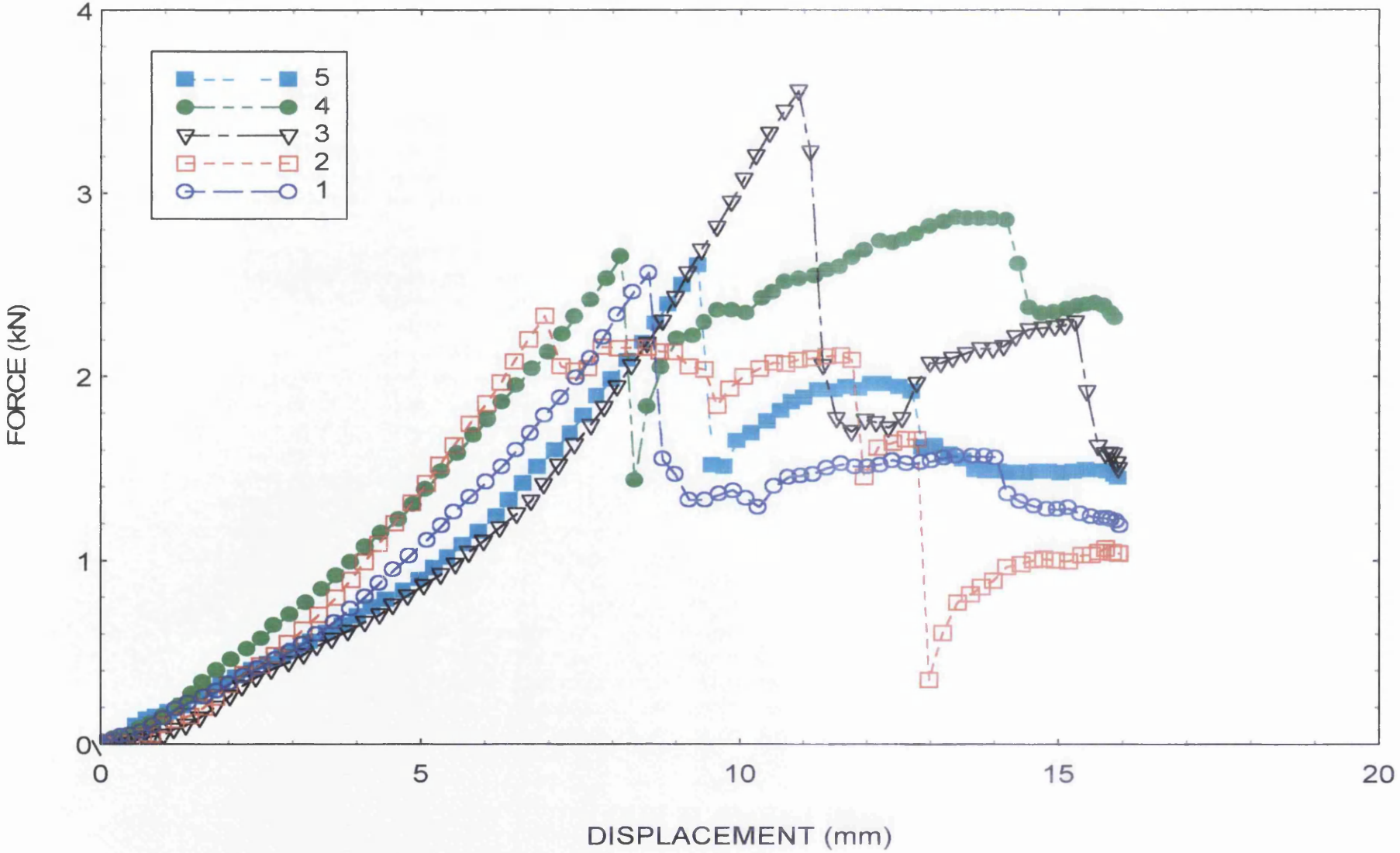

Figure 4.29 Disk test graphs of samples from different thickness groups using a flat Indentor at a rate of 6000 mm/min

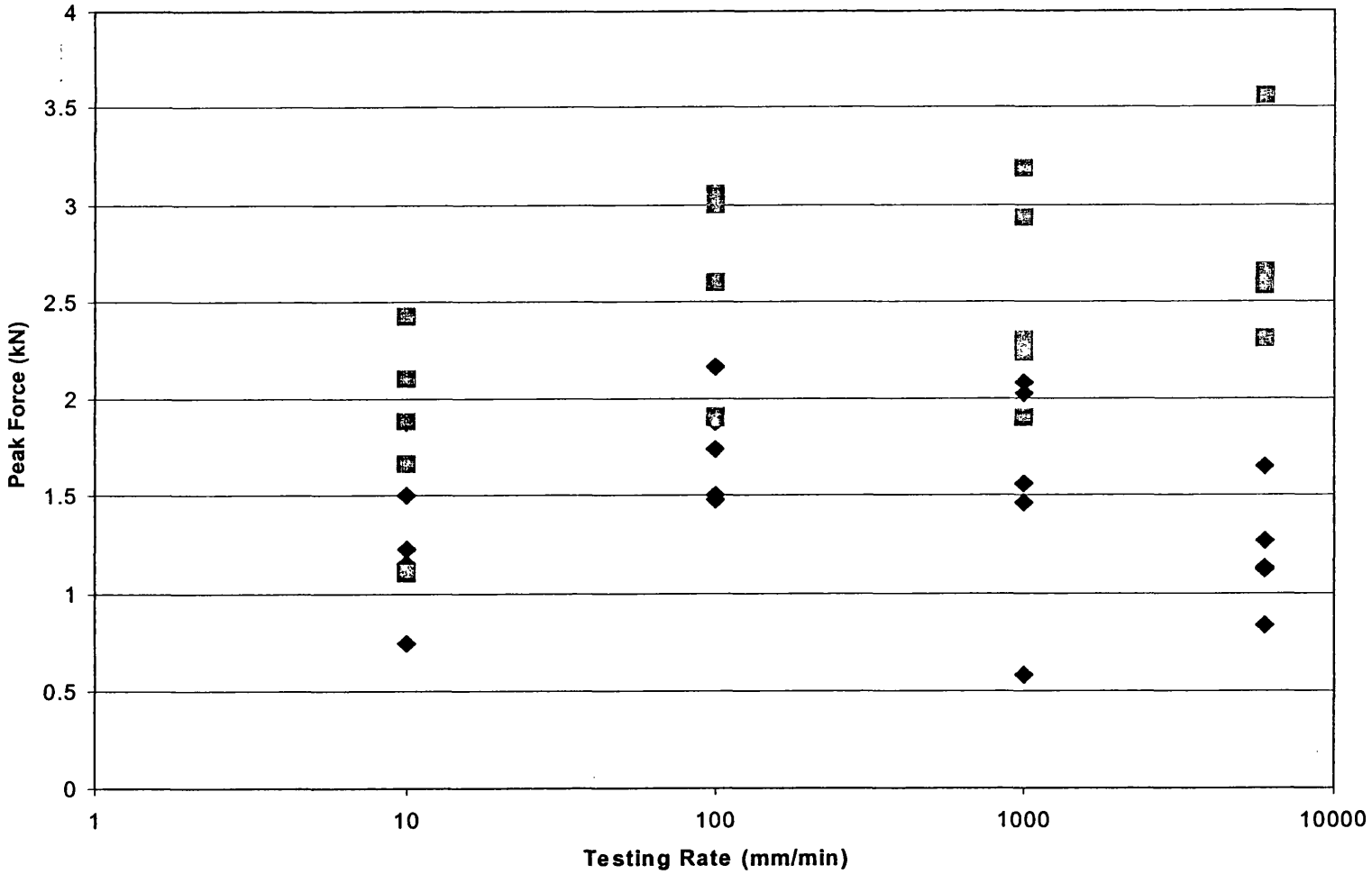

Figure 4.30 The peak force versus testing rate for all tests using both flat (square symbols) and spherical indentors (diamond symbols).

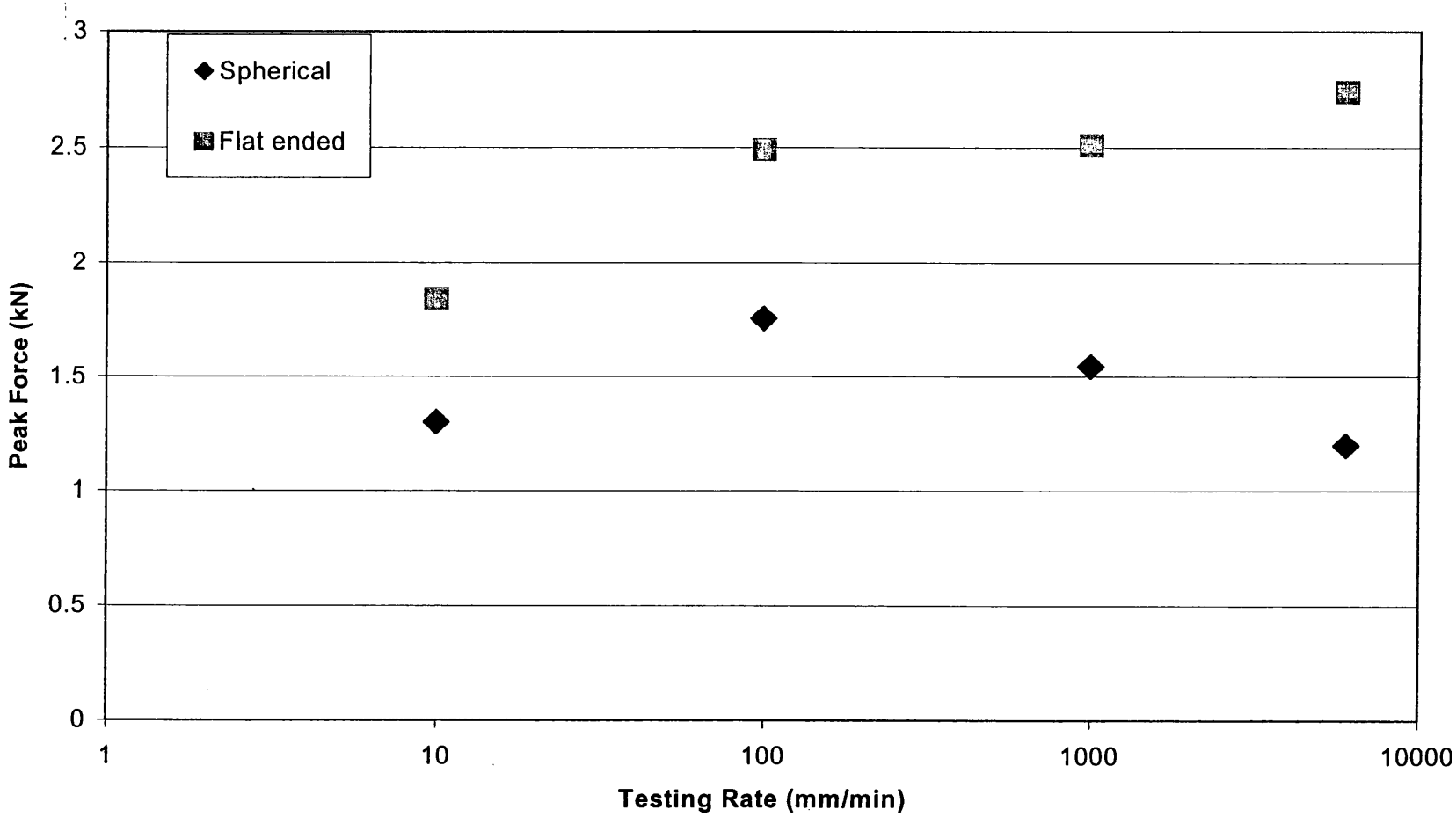

Figure 4.31 The average values of peak force versus testing rate for both flat and spherical indentors

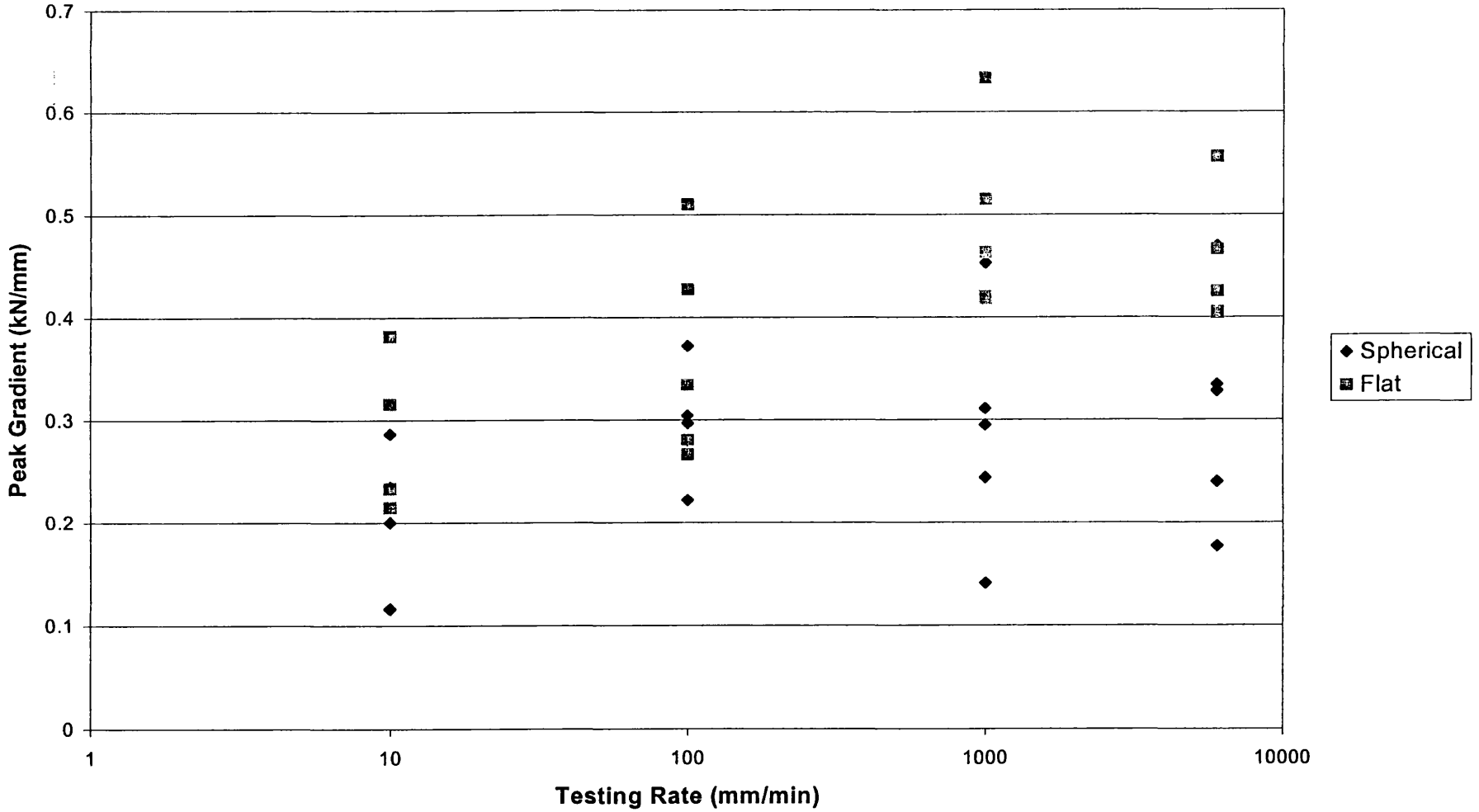

Figure 4.32 The peak gradient versus testing rate for both flat and spherical indentor tests

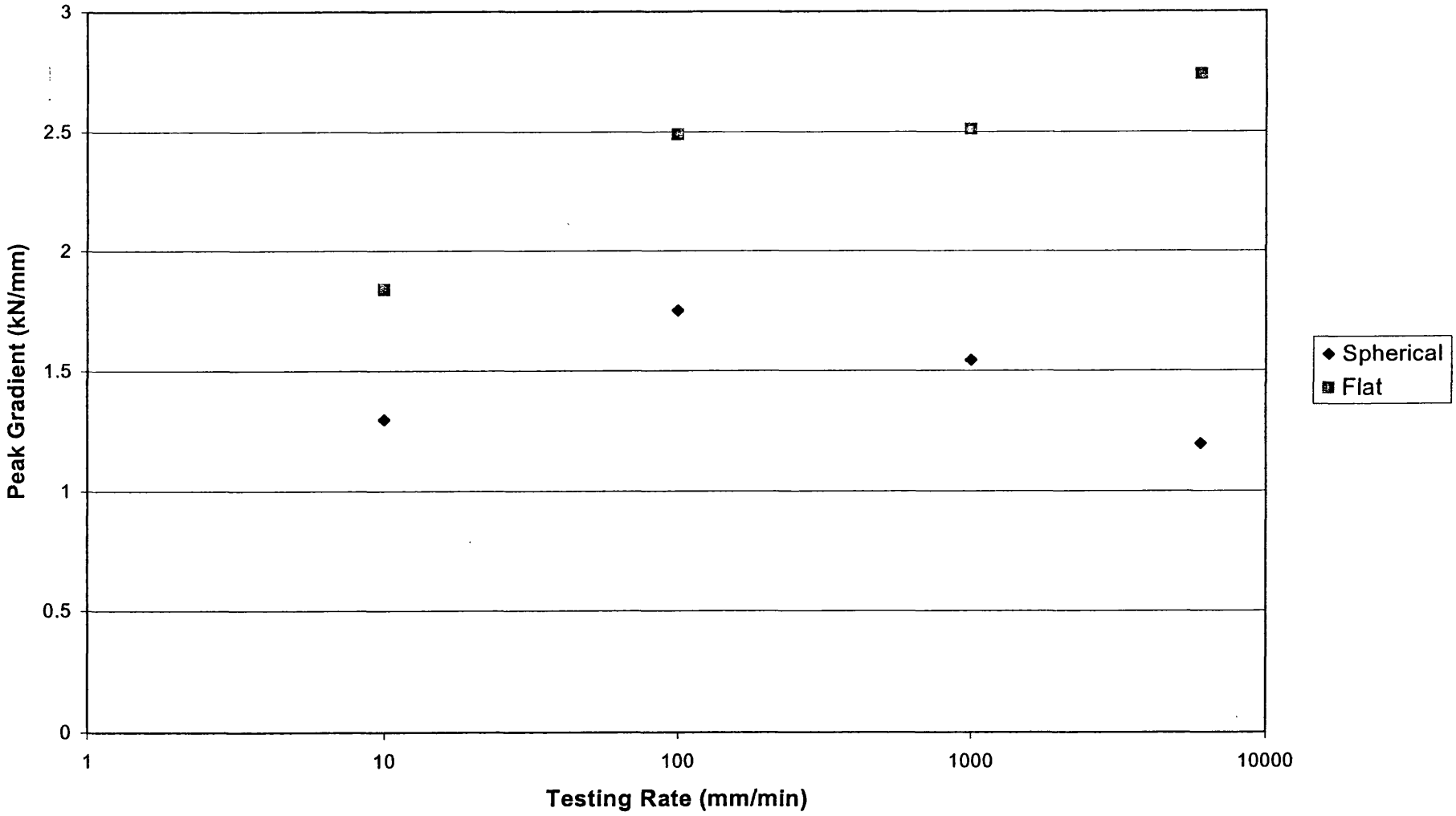

Figure 4.33 The average values for peak gradient versus rate for flat and spherical indentor tests

Table 4.5 The types of fracture behaviour observed with disk tests.

Spherical Indentor	Rate	Type of fracture	Flat Indentor	Rate	Type of fracture
Thickness Group 1 (2.44 - 3.4mm)	6000	b	Thickness Group 1 (2.44 - 3.4mm)	6000	e
	1000	a		1000	e
	100	d		100	b
	10	b		10	e
Thickness Group 2 (3.48 - 4.34mm)	6000	d	Thickness Group 2 (3.48 - 4.34mm)	6000	d
	1000	b		1000	d
	100	b		100	f
	10	a		10	f
Thickness Group 3 (4.54 - 4.74mm)	6000	c	Thickness Group 3 (4.54 - 4.74mm)	6000	a
	1000	b		1000	b
	100	b		100	e
	10	e		10	e
Thickness Group 4 (4.76 - 6.2mm)	6000	d	Thickness Group 4 (4.76 - 6.2mm)	6000	b
	1000	d		1000	b
	100	b		100	b
	10	e		10	d
Thickness Group 5 (6.2 - 7.82mm)	6000	d	Thickness Group 5 (6.2 - 7.82mm)	6000	b
	1000	a		1000	e
	100	a		100	f
	10	e		10	f

4.5.4 DISCUSSION

Firstly, it is noted from Figs 4.22-4.29 that there is an observable, but small variation in force between thickness groups. In general, as the thickness increases, so does the force. This behaviour is expected, but the fact that the peak force only increases slightly with thickness (and not proportionally) is notable.

The differences between the indentors were noticeable. Higher peak forces were produced from the flat-ended indentor (as shown in figs 4.30 & 4.31). These also show that, for the flat-ended indentor, as the rate increases so does the peak force. However, with the spherical indentor an increase is observed until the intermediate rates are reached, and then at the faster rates a drop is seen.

The effects of indentor and rate on the maximum gradient (figs 4.32 & 4.33) showed less differences. The flat indentor produced higher gradients but the difference was less marked. Also, the gradient showed a peak (or plateau) with both indentor shapes. These fairly complicated variations were unexpected, but as the stress pattern produced by the indentor will be complex, they can be rationalised without too much difficulty. As the stress distribution will be determined partly by the sample stiffness (a stiffer sample producing a more concentrated stress pattern), and as both stiffness and strength of bone vary with rate, a complex interaction was not considered unusual. The results of gradient against rate were considered somewhat more surprising, as this was expected to increase continuously with rate. This may have been due to the viscoelastic nature of bone being neglected.

The spherical indentor gives a higher stress concentration under its head, onto the sample due to the small area in contact with the bone samples. The local stresses are higher than for the flat-ended indentor, which is the reason for lower peak forces being observed. i.e less force is required to cause fracture.

As the rate increases the effect of this on the samples will effectively make them stiffer and stronger. It is known that as stiffness increases, a lower peak force is required to cause fracture, and as the strength increases a higher peak force is required. It is the complex relationship between the variations of strength and stiffness with increasing rate that causes the spherical indentor samples to fracture at lower forces at the higher rate than the intermediate rates.

From the photographs of fracture, Figs 4.34 - 4.39, it can be seen that the fractures caused by the flat-ended indentor were considerably more complex and destructive than those of the spherical one. The flat-ended indentor has its peak forces spread out underneath the area of its contact with the bone. Fracture can occur anywhere in this spread out area, which is a reason for the more complex and varied fracture patterns seen with this indentor. Also, the lower concentration of local stresses meant a higher force was required to cause fracture.

Figure 4.34 Failed disk sample showing failure type a): single diametric crack

Figure 4.35 Failed disk sample showing failure type b): single diametric crack through the disk

Figure 4.38 Failed disk sample showing failure type e): complex cracking from diametric crack

Figure 4.39 Failed disk sample showing failure type f): complex cracking from the edge of the indentor

As a summary to the bovine bone disk tests, it can be stated that the method is a convenient one for mimicking some of the biaxial bending loading that would be encountered during an impact, albeit at lower rates. The results demonstrate the complex effects of test rate, with the inter-relationship between the stiffness and strength being important. One of the main aims of this work was to provide experimental data to be used for validating a finite element model (from Fluid Gravity, St. Andrews). Unfortunately, due to funding limitations, this has yet to be performed, however the disk tests have still provided a useful insight into the effects of biaxial loading.

CHAPTER 5 SYNTHETIC BONE SUBSTITUTE MATERIAL

The purpose of this stage of the assessment was to find a synthetic bone simulant material with similar properties to those of human skull. This would then replace bovine scapulae as a test material for determining the effects of baton round impacts on the human skull. The first stage involved a search for suitable synthetic materials that were likely to have similar properties to cranial bone.

5.1 COMMERCIALLY AVAILABLE SYNTHETIC BONE MATERIALS

After an extensive search for producers and suppliers of synthetic bone materials, the following were identified as being commercially available.

SAWBONES

This is a US Company that manufactures bones for surgical training. Their main aim is in anatomical accuracy and realistic sawing behaviour. They produce "composite bones" that are supposed to have same mechanical properties of real live bone.
The materials produced are mainly foams, both rigid and flexible made of polyurethane to represent compact and cancellous bone. There is some use of glass fibre / epoxy composites in some of their composite bones.

SYNBONES

This is a Swiss company manufacturing synthetic bones mainly for surgical training. They use polyurethanes, both foamed and solid. They manufacture spherical shells that have been used for ballistic impact trials.

LAST-A-FOAM

Researchers in Canada (Waterloo) have used this material to mimic the fragmentation of bone. They found that grade FR3740 was most similar in fracture behaviour. Last-a-foam is a polyurethane material (inner foamed, outer solid skin) produced by General Plastics (US), primarily for use in the aerospace industry. They

produce a wide range of materials, and so potentially offer scope as a useful material supplier.

HAPEX

Developed at Queen Mary & Westfield College in London, this material is based on HDPE reinforced with hydroxyapatite (HAP) particles. Although based on biocompatibility, some work on mechanical properties has been done to mimic bone. However, this would only mimic compact bone. It would have potentially been interesting to assess properties, although the use of HAP as a filler (for biocompatibility) would increase the cost; other mineral fillers would do a similar mechanical job at much lower cost.

WRIGHT MEDICAL

This company manufactures Osteoset, a reabsorbable bone scaffold material. This is designed for biocompatability rather than mechanical properties and is therefore, almost certainly unsuitable.

BIOPLANT

Bioplant produces materials for surgical applications, again focussing on biocompatibility and bone-growth promotion. Materials are based on filled acrylic polymers. Fillers include calcium hydroxide and calcium carbonate. The components manufactured are generally small. It was decided this was probably not suitable for the purposes of this project.

US BIOMAT

They produce more surgical graft materials (Bioglas, Novabone, Perioglas), based on filled polymers (no more details specified). Again, their main aim is biocompatibility and they were not considered suitable.

CARNEGIE-MELLON UNIVERSITY

Research here has been conducted on synthetic bone scaffold materials, including HAP-filled polymers, although they do not produce commercial materials.

Most of the commercially available materials listed above are aimed at reconstructive surgery. Therefore it was thought it may be difficult to find materials with suitable mechanical properties, that would be available in large sections. However, requests for suitable samples (representing the temporal skull region) were sent out to Synbones and Sawbones, as potentially the most suitable. The samples that were requested had to be flat samples, typical to skull bone. Once received, the materials were tested to determine modulus and strength at a range of test rates.

5.2 MECHANICAL PROPERTIES OF SYNTHETIC BONE MATERIALS - A COMPARISON WITH BOVINE SCAPULAE

5.2.1 Introduction

This section describes a detailed assessment of the mechanical properties of the two types of synthetic bone substitute materials chosen for testing, and then compares the results to those of bovine scapulae. Testing to determine the mechanical properties of bovine scapulae has already been conducted and has been discussed in detail in Chapter 4.

Initially a single polyurethane foam material, produced by Synbone was assessed. Simple strength and stiffness tests were conducted with this. Following this, a wider combination of materials produced by Sawbones was investigated. Eight separate materials were used, comprising various combinations of three different polyurethane foams and a glass-fibre reinforced epoxy. It was decided to use the same types of testing and conditions for the eight Sawbones materials as for the scapulae to draw as accurate a comparison between the different materials as possible.

5.2.2 Synbone

Three point bending and DMTA tests were carried out on the polyurethane-based synthetic bone, produced by Synbone. The purpose of the tests was to provide information regarding the mechanical properties of the material with specific interest to the strength and stiffness properties.

Firstly, three point bending tests were carried out using a servo-hydraulic testing machine. Strain rates from 0.2 to 200 mm/min were used. At strain rates above this the specimens would be bent too rapidly for the machine to accurately record the data. From these tests graphs were plotted of both flexural strength and modulus against rate. These can be seen in Figures 5.1 and 5.2 below.

It can be seen that there is a clear increase in strength as rate increases. The strength values obtained and the strain rate sensitivity are very similar to that of bone. The modulus shows a degree of scatter but it can be seen that the modulus is far less rate sensitive. There is a small increase in modulus as the rate is increased but not to the same degree as exhibited by real bone. Stiffness values are also approximately one tenth those of bone so this indicates that the properties of this material are not suitable for accurate modelling.

Force against displacement graphs were produced and then converted to graphs of stress versus strain. An example of typical results is shown in Figure 5.3. It can be seen from this that the strain to failure is almost ten percent. This is a factor of ten higher than real bone, which exhibits a typical strain to failure of 0.5 to 1%.

Secondly DMTA tests were carried out in three point bending, over a range of frequencies from 0.1 to 100Hz. The results are plotted as log frequency (rate) against log modulus in Figure 5.4. As with the servo-hydraulic results it is clear that there is very little strain rate sensitivity of modulus exhibited by this material. To mimic bone, the modulus should be seen to rise with an increase in frequency, but instead it remains fairly constant. At the higher frequencies the modulus actually drops, but these inaccuracies can be put down to the machine coming close to its resonant frequency.

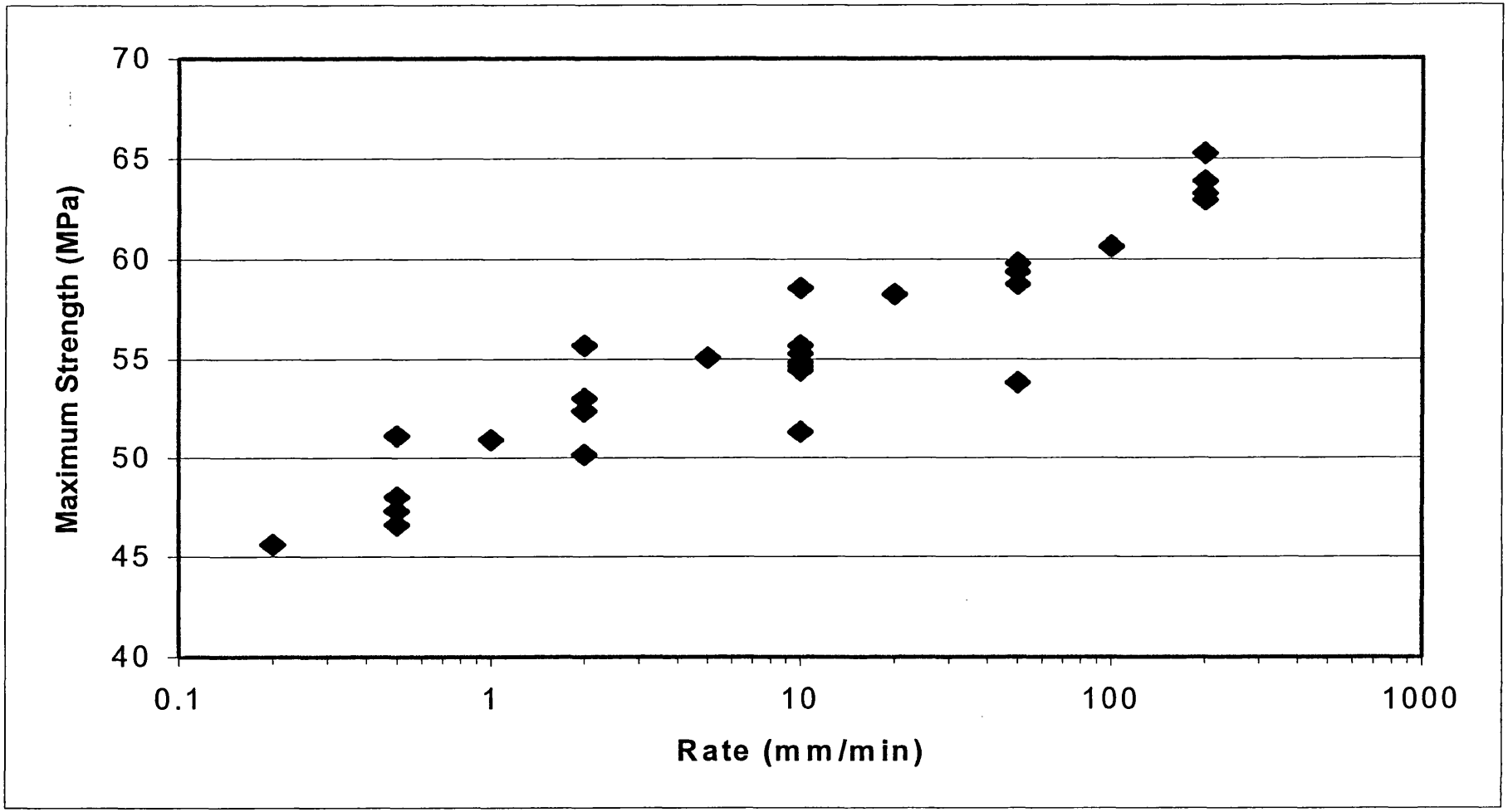

Figure 5.1 Bending test results for Synbone, showing maximum strength versus test rate

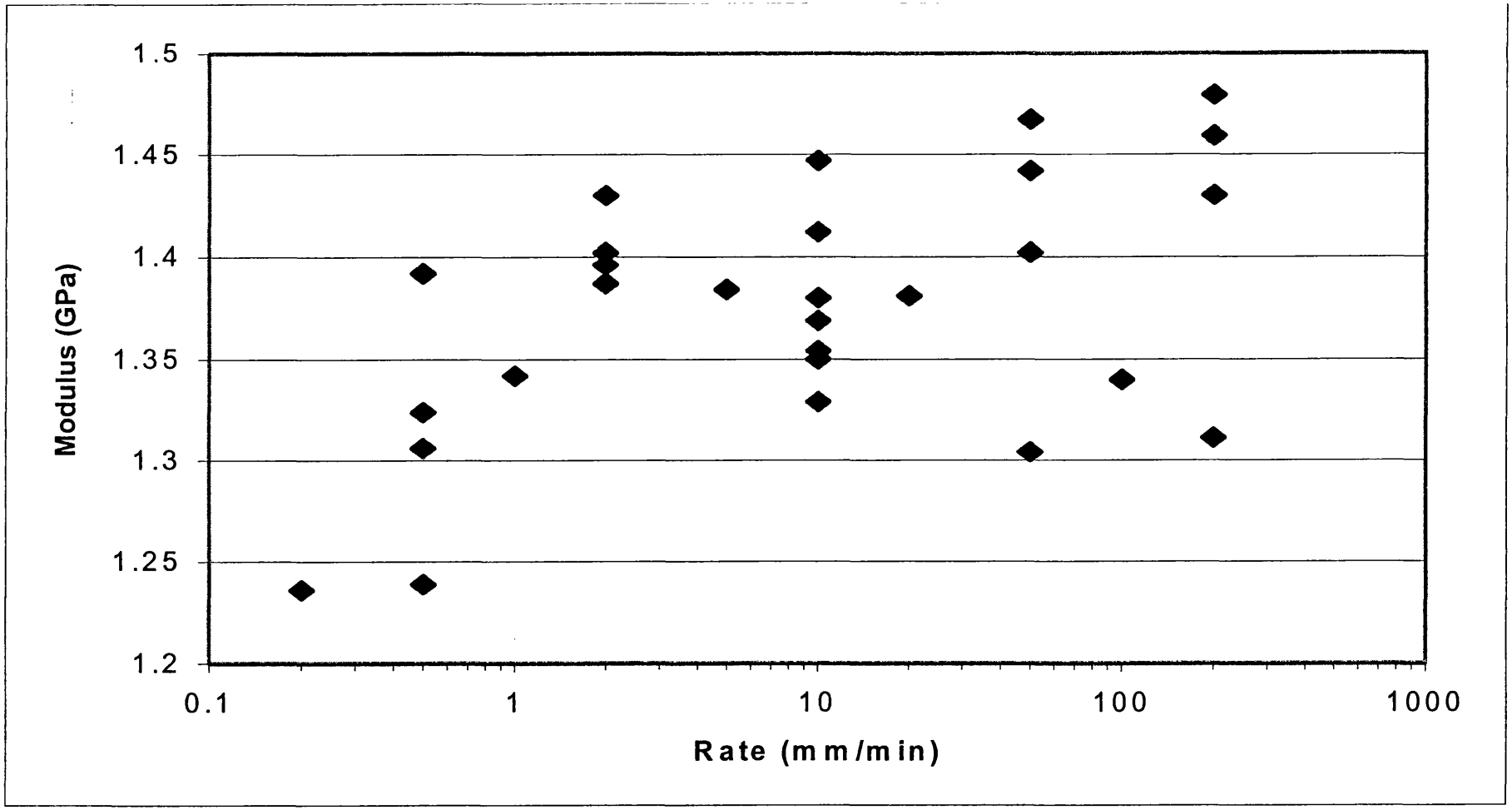

Figure 5.2 Test results for Synbone showing flexural modulus versus testing rate

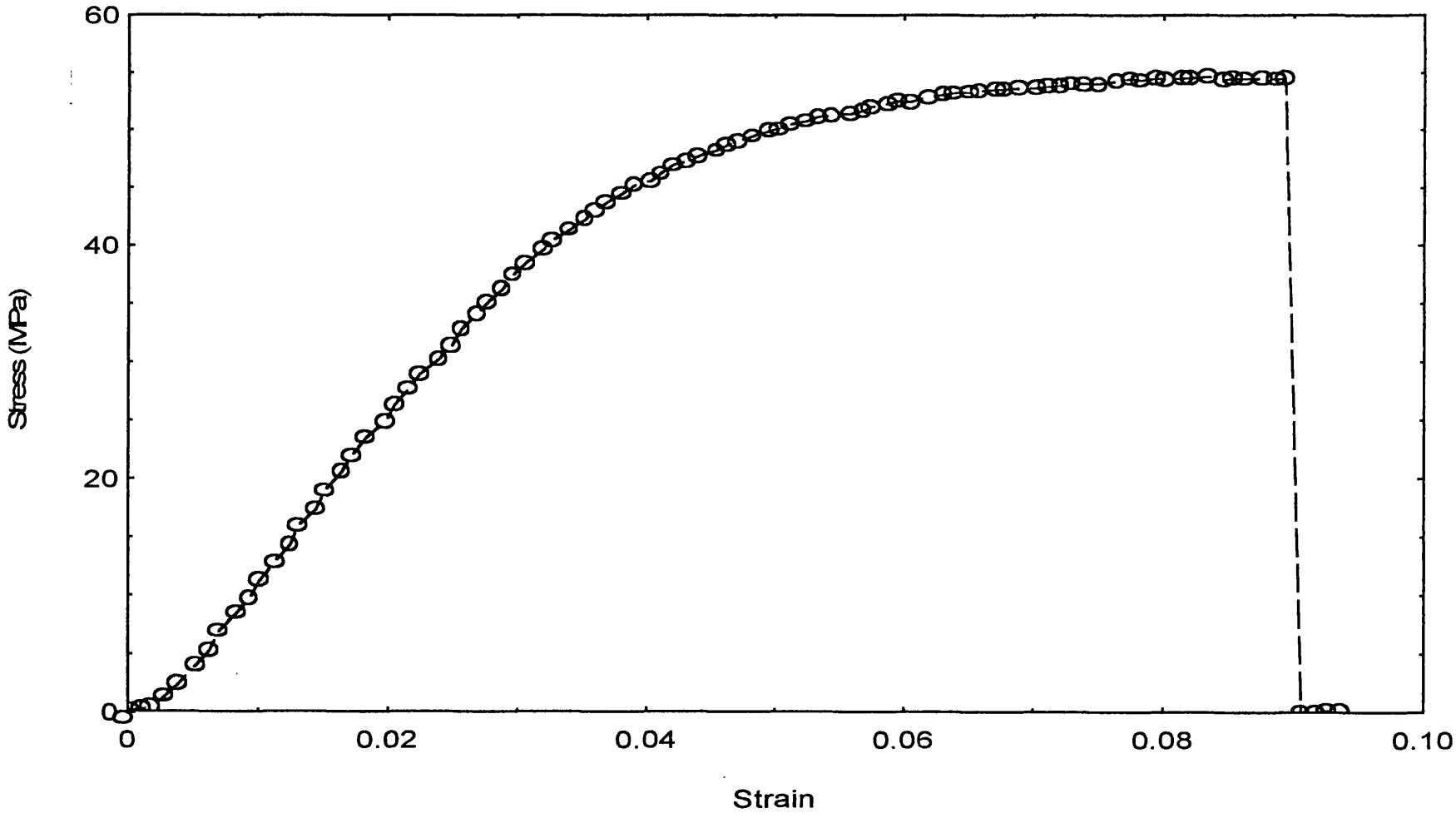

Figure 5.3 Bending test results for Synbone showing stress against strain at a rate of 5 mm/min

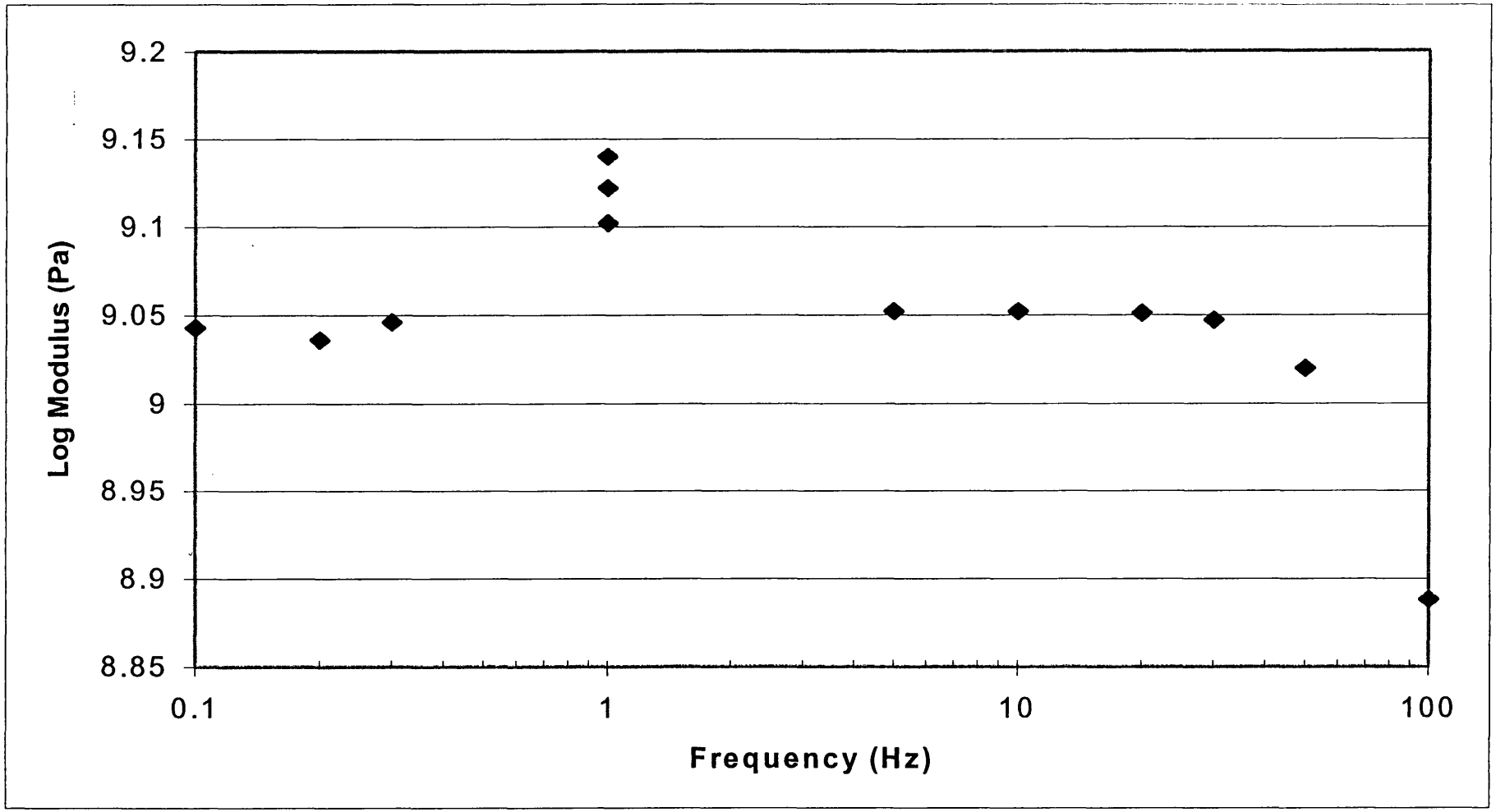

Figure 5.4 The bending modulus against frequency for DMTA tests using Synbone material

In conclusion from the results obtained the strength properties of this material are fairly similar to real bone, but the stiffness and strain to failure differences are significant enough to rule this material out as being suitable for use as a physical human head impact model.

5.2.3 Sawbones

Of this wider range of materials, the methods of testing that were chosen were tensile, torsional and bending tests of strip samples. The tensile and torsional tests allow tensile and shear moduli to be determined at a range of strain rates, and hence allow determination of how Poisson's ratio varies with rate.

The approach that was used was to measure tensional and torsional stiffness at different rates, using small deformations (up to 0.5 %). This permitted several tests to be performed on each sample. After this, the samples were tested to destruction in bending at different rates, to give values of failure strength and flexural modulus as a function of rate.

5.2.3.1 Samples

Eight different types of synthetic bone were produced by Sawbones in sheet form and consisted of varying density polyurethane foams and glass fibre epoxy resins. The different specifications of the eight materials are as follows:

LDF: Low density polyurethane foam
MDF: Medium density polyurethane foam
HDF: High density polyurethane foam
HD1: A layer of 5mm thick MDF in the centre, sandwiched between 1mm thick HDF on the top and bottom surfaces.
HD2: A layer of 3mm thick MDF in the centre, sandwiched between 2mm thick HDF on both top and bottom surfaces.
GFE: Randomly oriented, short glass fibres in epoxy resin.

GF1: A layer of 5mm thick MDF in the centre, sandwiched between 1mm thick GFE on both top and bottom surfaces.

GF2: A layer of 3mm thick MDF in the centre, sandwiched between 2mm thick GFE on both top and bottom surfaces.

The samples were machined into parallel-sided strips of uniform thickness. All samples were 120 mm in length, with a 12 mm width. Thickness of GFE was 3 mm, LDF, MDF and HDF was 5 mm and the HD1, HD2 GF1 and GF2 were between 7 and 8.5 mm thick. The varying thickness of the sandwich materials was due to a layer of bonding material between each of the outer layers and the inner MDF layer.

Three samples of each material were tested in both tension and torsion at three different rates. The samples were designated with the codes, LDF, 1LDF, 2LDF where the numbers refer to the different samples used.

All testing was performed on an ESH servo-hydraulic testing machine at a standard room temperature of 23 C.

5.2.3.2 Tensile Tests

The samples were clamped in the testing machine to give a free gauge length of 100 mm. The samples were then deformed at one of 3 testing rates, to a strain of just under 0.5 %. The testing rates used corresponded to strain rates of $8.3x10^{-4}$, $8.3x10^{-5}$ and $8.3x10^{-6}$ s^{-1}. The testing rate was limited by the speed of accurate data capture, with the fastest tests taking around 6 seconds.

The force was continually recorded from a load cell, and the displacement recorded from the cross-head displacement. The displacement needed to be calibrated to account for machine compliance. It was decided to avoid the use of extensometers or strain gauges, due to the time consumption in fitting them to each sample with almost 150 tension and torsion tests being carried out. It was also considered that the displacement readings from the cross head movement would be sufficiently accurate.

A typical force / displacement graph for a tensile modulus test is shown in Figure 5.5, from which it can be seen that there is a reasonably good straight-line fit to the initial part of the data. The gradient of this line was used to calculate the tensile modulus E as shown previously in equation 4.7.

5.2.3.3 Torsion Tests

Torsional testing was performed on the same samples, using the same grips, but with a rotational displacement. As with the tensile tests the samples were deformed to strains of just under 0.5%. Testing rates used corresponded to maximum strain rates of $1.5x10^{-2}$, $1.5x10^{-3}$ and $1.5x10^{-4}$ s^{-1}.

A typical graph of torque / rotation is given in Figure 5.6. This shows an even better straight-line fit than for the tension tests. The gradient of this line was used to calculate the shear modulus. This, along with equations and further details of test methods has been described previously in Chapter 4.

5.2.3.4 Order of Testing

For each sample, three tension and three torsion tests were performed, each at a different rate. As with the scapulae tests in order to reduce the likelihood of any systematic effects of viscoelasticity, the order of testing was varied with each sample. After each test, the sample was allowed to recover for a short time before the next test.

5.2.3.5 Bending Tests

After tensile and torsional tests, samples were tested in three-point bending mode and taken to failure. This was to provide a measure of the fracture strength of the samples, and incidentally, an additional measure of modulus.

Samples were tested using a three-point bend jig with a span length of 100 mm. Three different testing rates were used, corresponding to strain rates of $8x10^{-5}$, $4x10^{-4}$ and $4x10^{-3}$ s^{-1}. For this geometry, the maximum stress, strain and modulus can be calculated from the equations outlined previously in equations 4.15, 4.16 and 4.17.

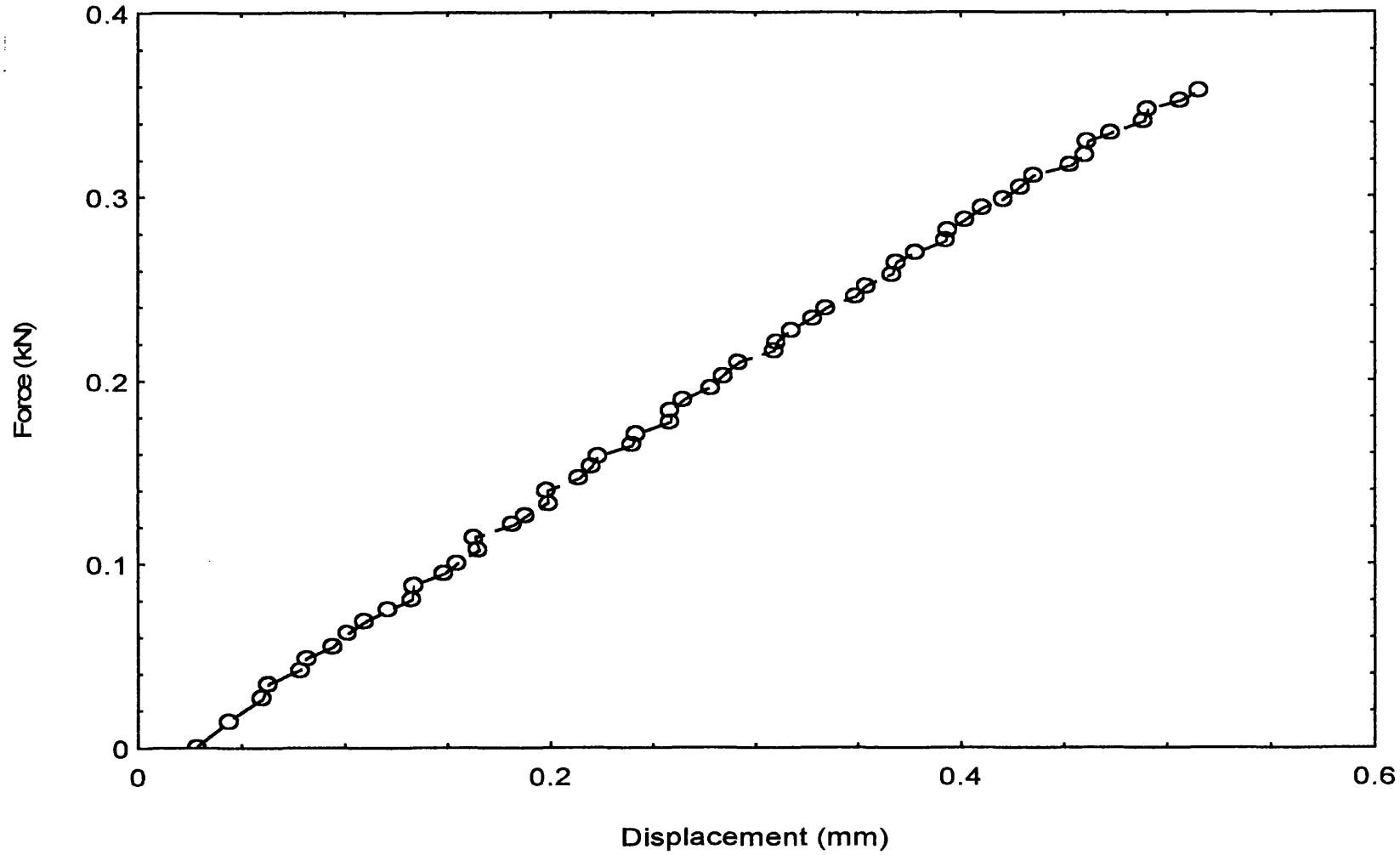

Figure 5.5 A typical plot from a tensile test of the Sawbones samples

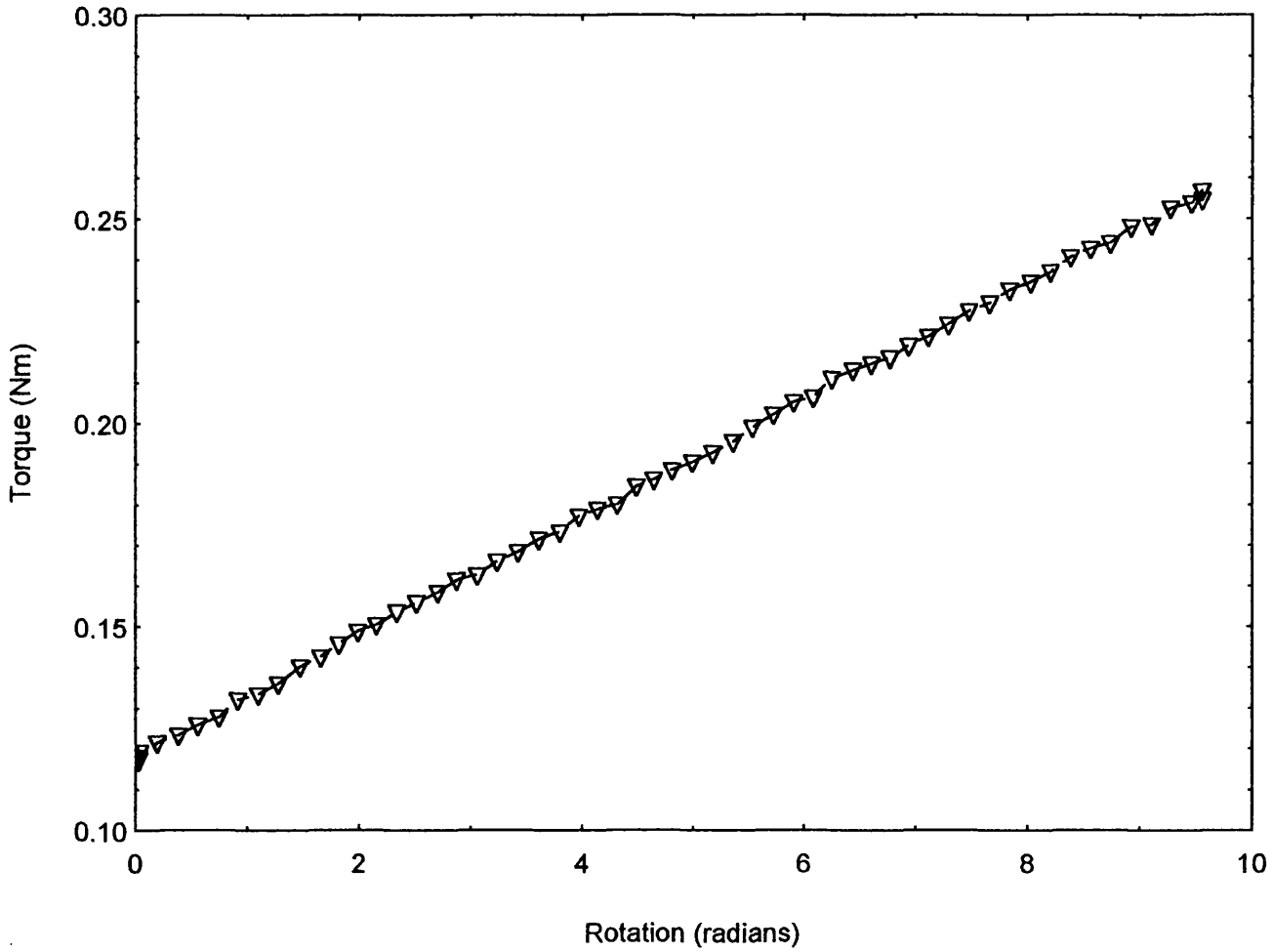

Figure 5.6 A typical plot from a torsion test of the Sawbones samples

A typical Force / Displacement curve for bending is shown in Fig 5.7.

5.2.4 Results for Sawbones

From the force / displacement and torque / rotation data and the relevant stress, strain and modulus equations, a spreadsheet was produced containing values for tensile, shear and bending modulus, failure stress and strain rate for each test. Average values for each material and strain rate were also calculated.

5.2.4.1 Single Material Results

From the spreadsheet data, graphs were plotted for each of the eight sample types showing tensile, shear and bending moduli against strain rate. These can be seen for the four single material samples in Figs 5.8 to 5.11.

For all four single material samples, as expected, the tensile and bending moduli are very similar, with the shear modulus lower. Values of shear modulus for all four samples are approximately half those of the tensile modulus. Shear modulus values are always less than tensile modulus for the same sample. Bending modulus has a mixed mode of stressing, comprising mainly tension and compression but with an element of shear. This is the reason why tensile and bending moduli are generally similar but not always identical.

Apart from the tensile modulus of both HDF and GFE all other values of shear and tensile modulus show a slight increase with rate. Tensile moduli for HDF and GFE show a very slight, and fairly insignificant decrease. For each of the four materials both E and G were fitted to a power law curve (shown in Figures 5.8 – 5.11). The exponent of the resulting power law equation gives an indication of the gradient of the curve, where 0 is horizontal. These values, together with those of E and G for the four materials are shown below in Table 5.1.

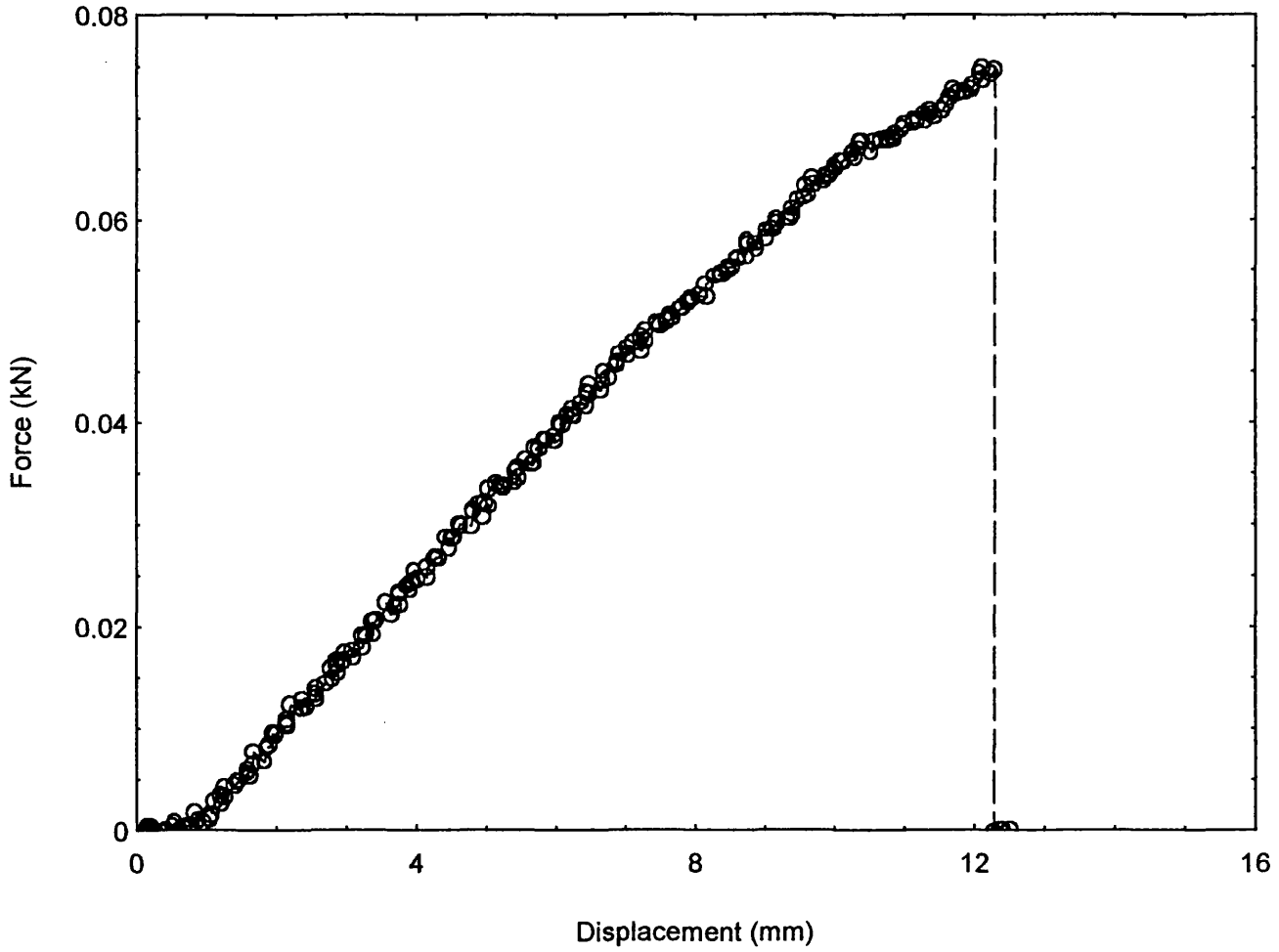

Figure 5.7 A typical plot from a bending test of the Sawbones samples

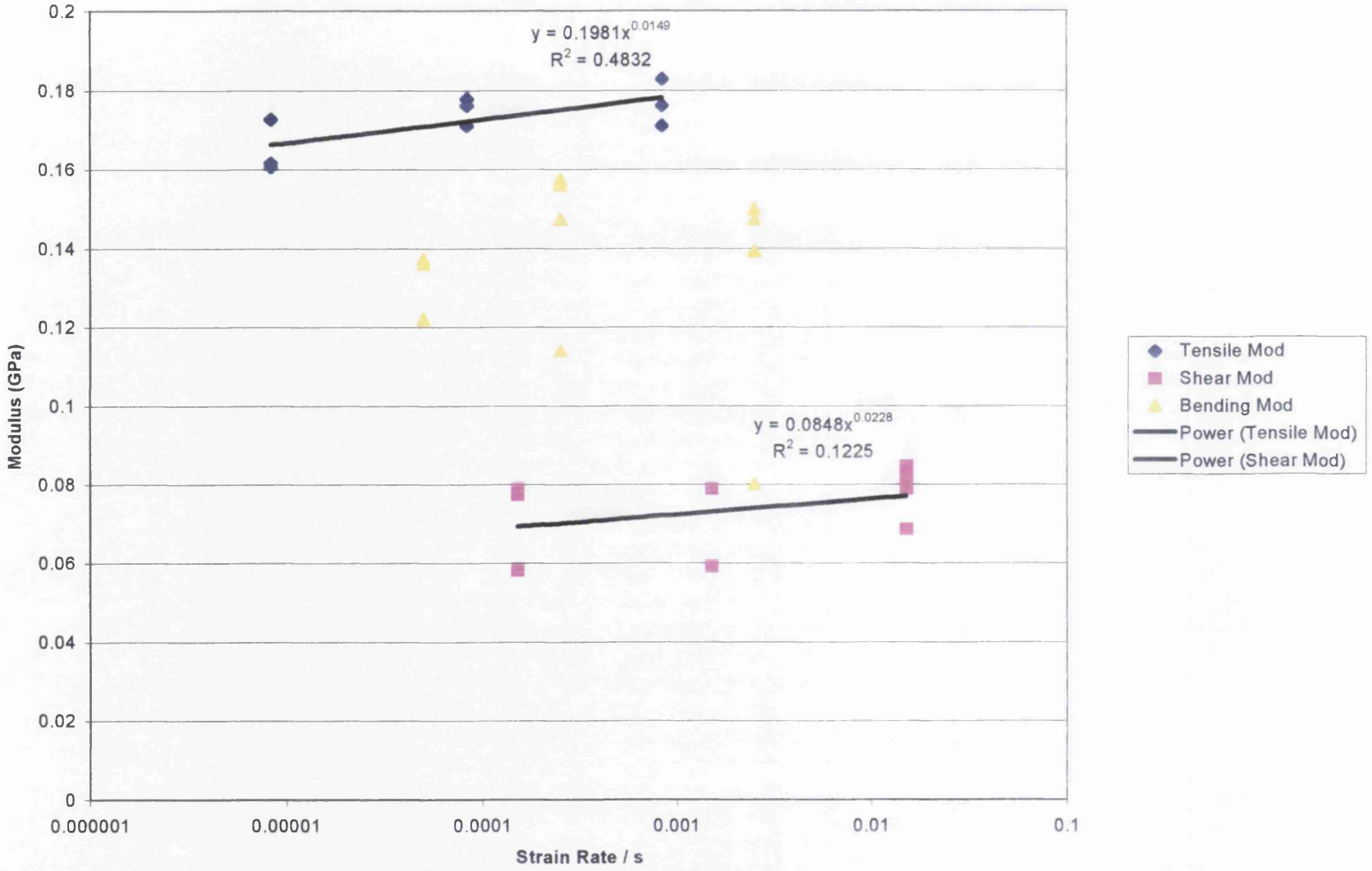

Figure 5.8 Tensile, shear and bending modulus versus rate for LDF

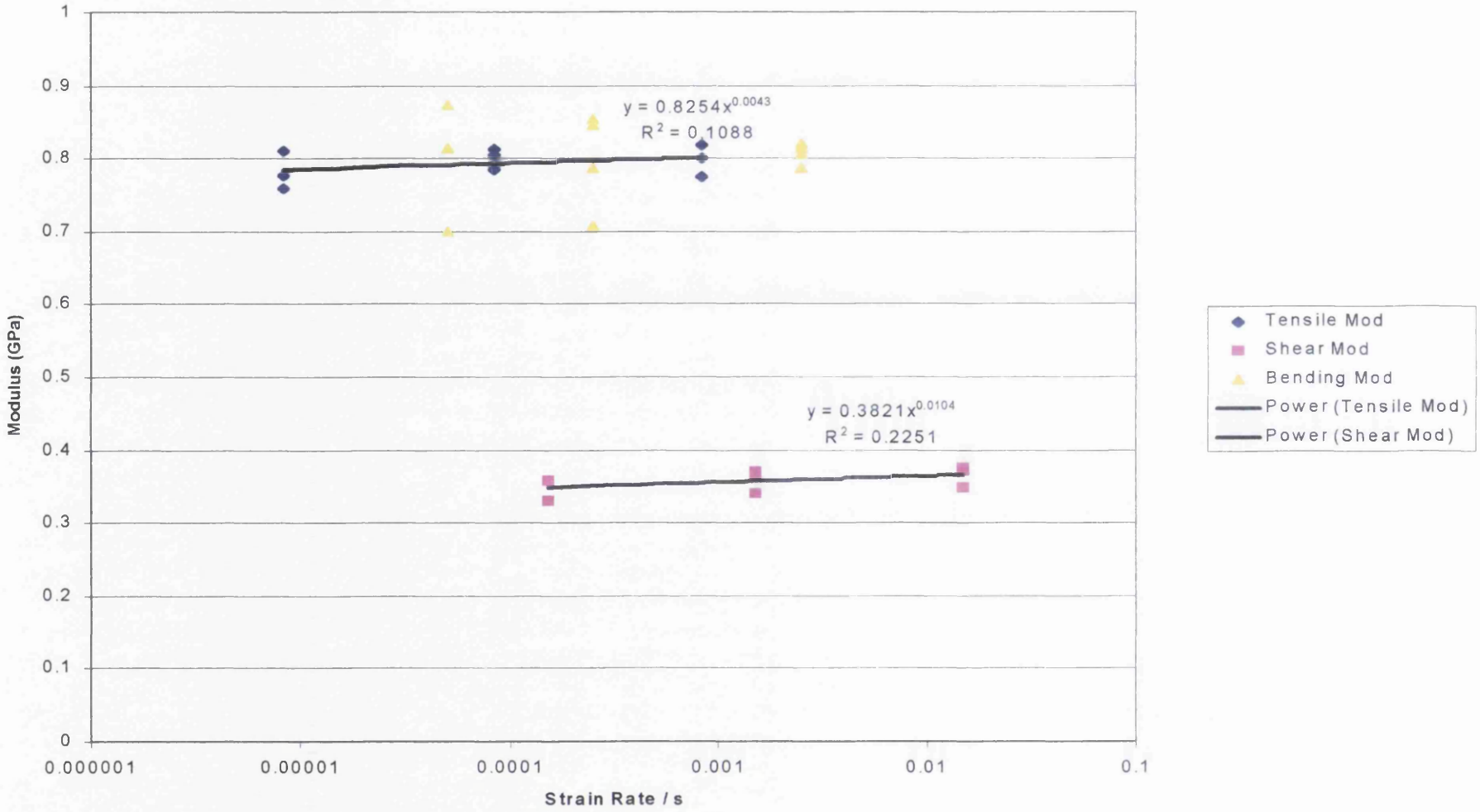

Figure 5.9 Tensile, shear and bending modulus versus rate for MDF

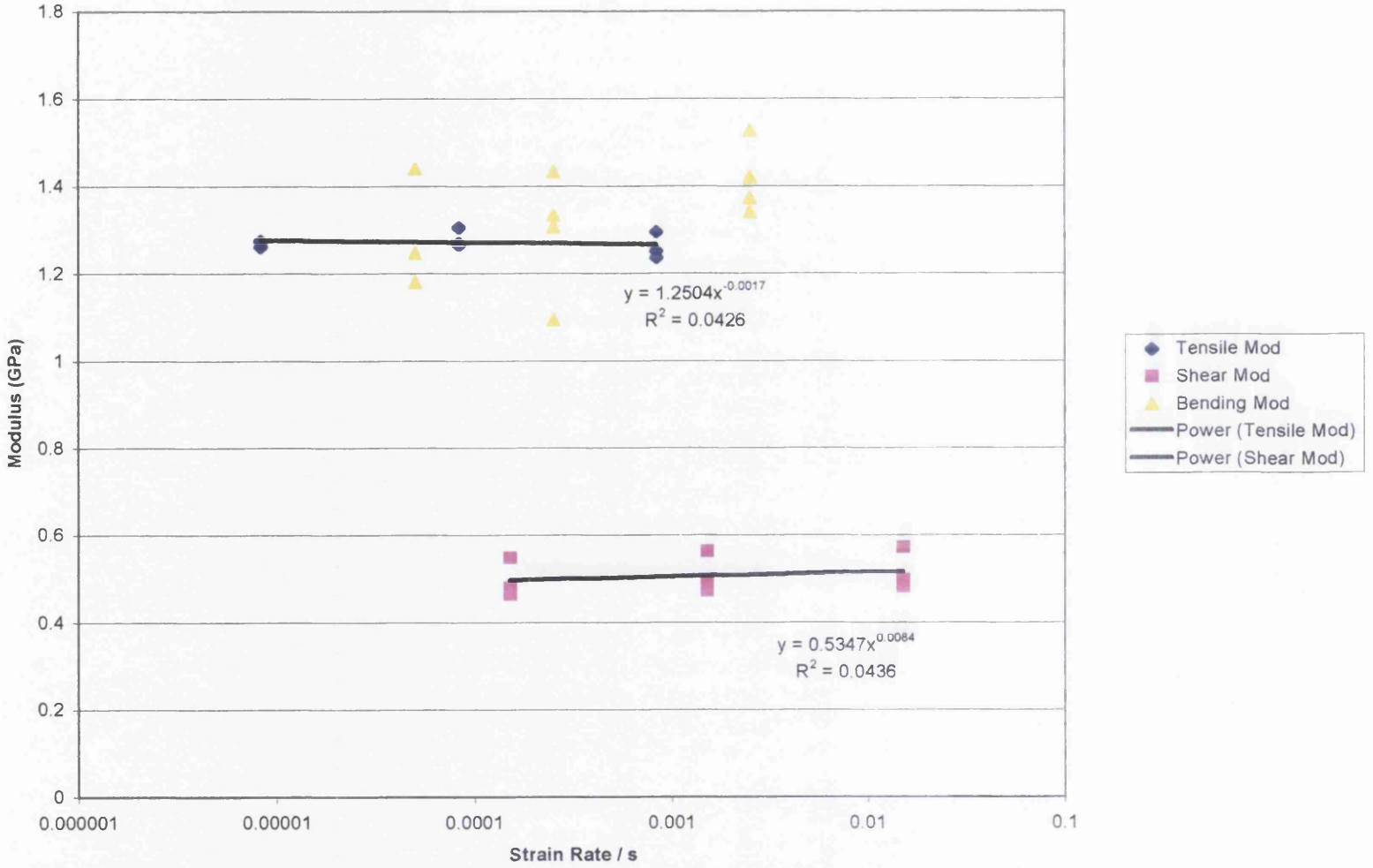

Figure 5.10 Tensile, shear and bending modulus versus rate for HDF

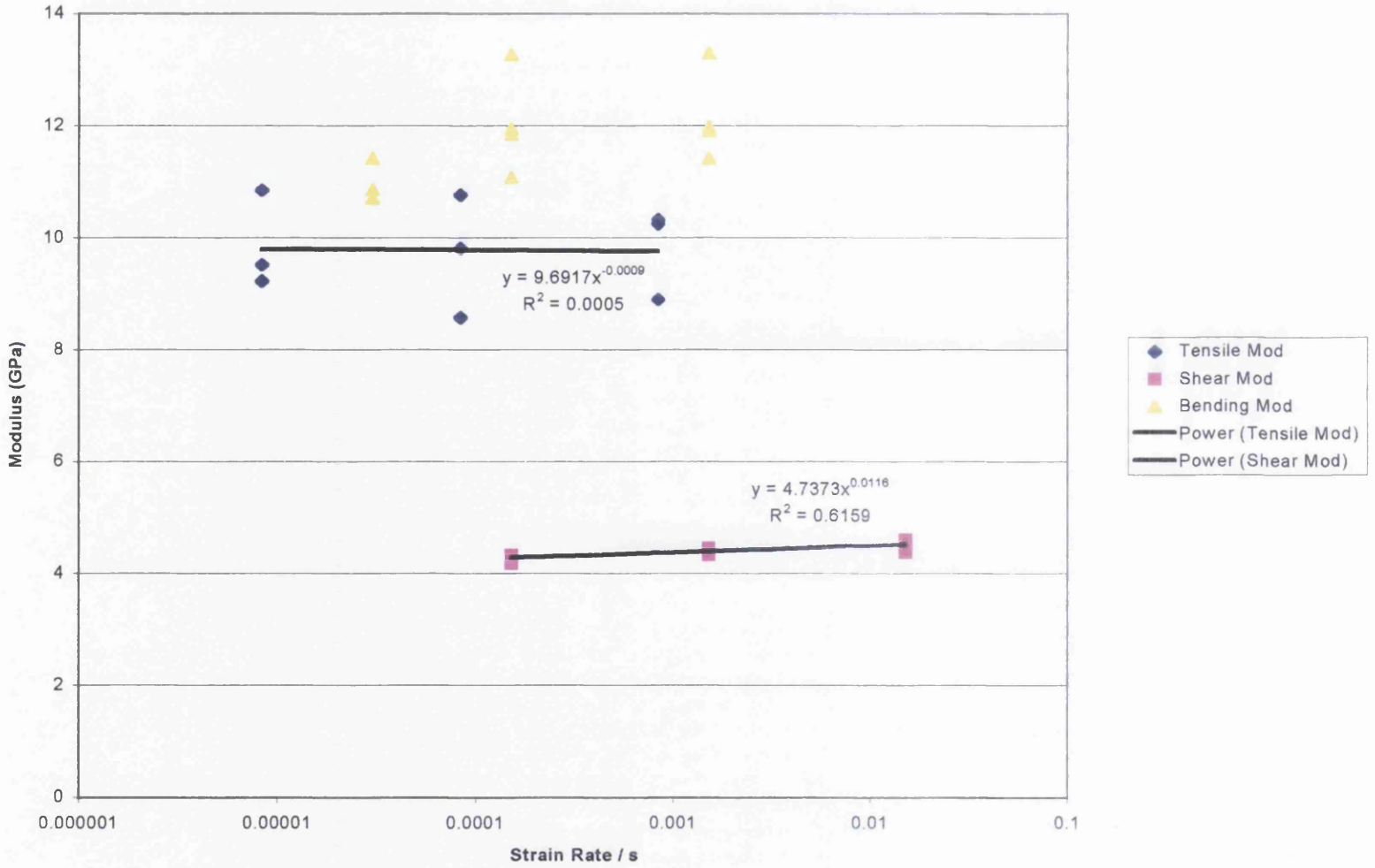

Figure 5.11 Tensile, shear and bending modulus versus rate for GFE

Table 5.1 The modulus values for the single Sawbone materials

Material	Modulus Type	Modulus (GPa)	Power Law Exponent
LDF	E	0.16 - 0.18	0.0149
	G	0.06 - 0.08	0.0228
MDF	E	0.75 - 0.82	0.0043
	G	0.33 - 0.37	0.0104
HDF	E	1.23 - 1.30	-0.0017
	G	0.46 - 0.57	0.0084
GFE	E	8.57 - 10.85	-0.0009
	G	4.17 - 4.60	0.0116

As shown from these values, there is generally little rate sensitivity displayed by any of the four single material samples. The shear modulus has a consistently higher exponent than the tensile modulus. It is possible to compare these values with the exponents found for bovine scapulae samples, where the exponent for tension was about 0.04 and about 0.035 for shear. It is therefore clear that the sawbones samples are less rate-sensitive than bone samples, especially in tension.

Poisson's Ratio

From the values of E and G, it is possible to calculate Poisson's Ratio. Rather than use individual values of tension and torsion modulus for each sample, it was decided to use the average values of E and G, along with the rate-dependence as described above. The reasons for this action are two-fold. Firstly, Poisson's ratio is very sensitive to experimental variations in the values of G and E, and so an averaging process would give more reasonable values. Also, the strain rates of tests performed in tension and in torsion were not identical and so the approach adopted allows comparison of the values at the same strain rate.

As seen from equation 4.13, Poisson's Ratio is given by :

$$\nu = \frac{E}{2G} - 1$$

Therefore, if both E and G can be expressed as a power-law variation, then Poisson's ratio can be given by:

$$\nu = \nu_0 Rate^n - 1$$

5.1

The values of ν_0 and n were calculated from the power-law curves fitted to the tensile and shear modulus for each material and are given below in Table 5.2

Table 5.2 The values of ν_0 and n for each of the individual Sawbone materials.

MATERIAL	ν_0	N
LDF	1.167	-0.0079
MDF	1.080	-0.0061
HDF	1.168	-0.0101
GFE	1.022	-0.0125

From these, it is clear that the Poisson's ratio values are all quite low (generally about 0.2 at the strain rates tested). The values also decrease as the strain rate increases. This is the opposite behaviour from that seen with the bone samples, where there was a slight increase with rate.

5.2.4.2 Sandwich Structure Materials

Figures 5.12 to 5.15 show tensile, shear and bending moduli for the four sandwich structure samples. It is initially clear that, unlike the single material samples where the bending and tensile modulus are very similar, the bending modulus of all four sandwich samples is roughly twice as large as the tensile modulus. This is due to the fact that in

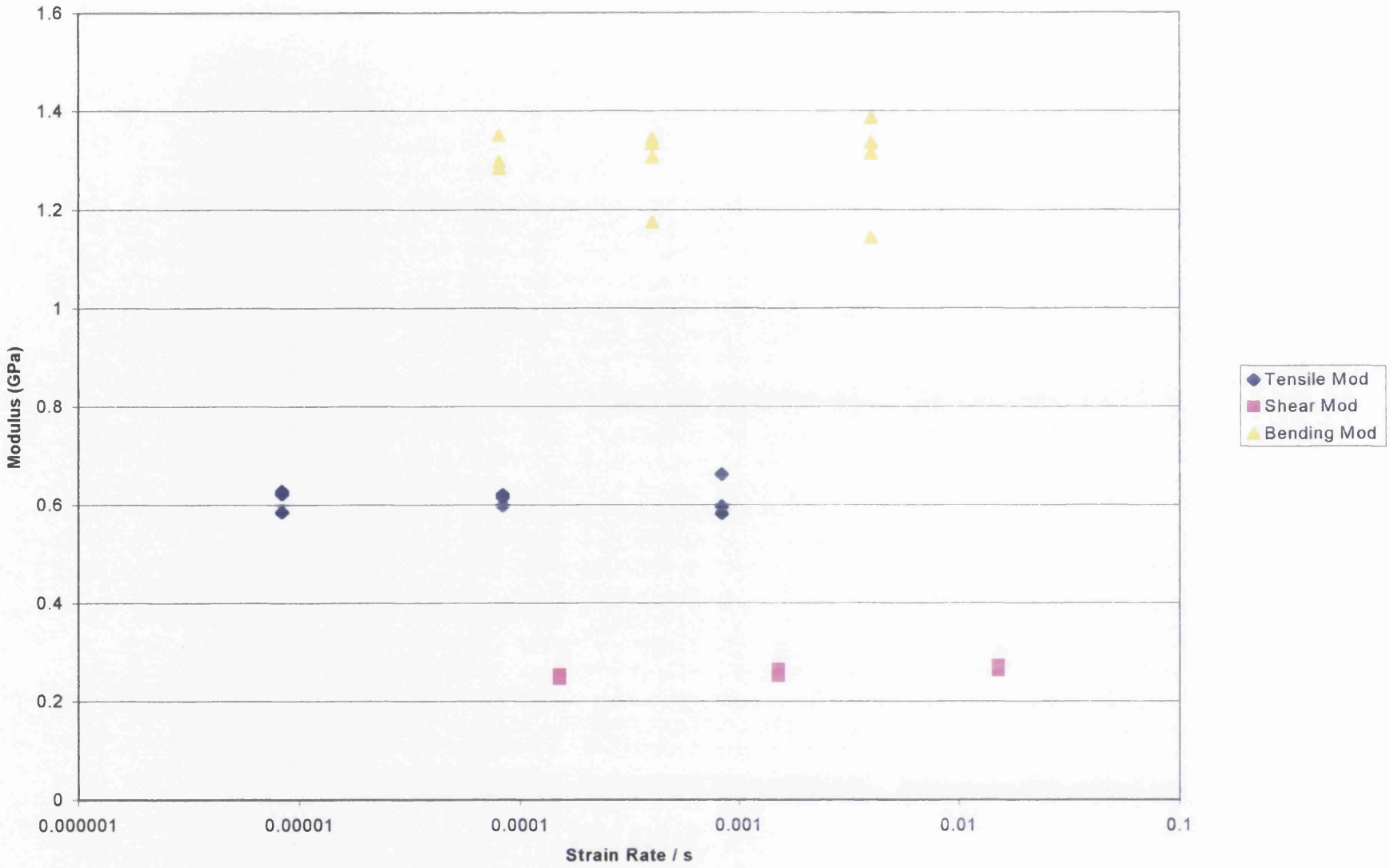

Figure 5.12 Tensile, shear and bending modulus versus rate for HDF1

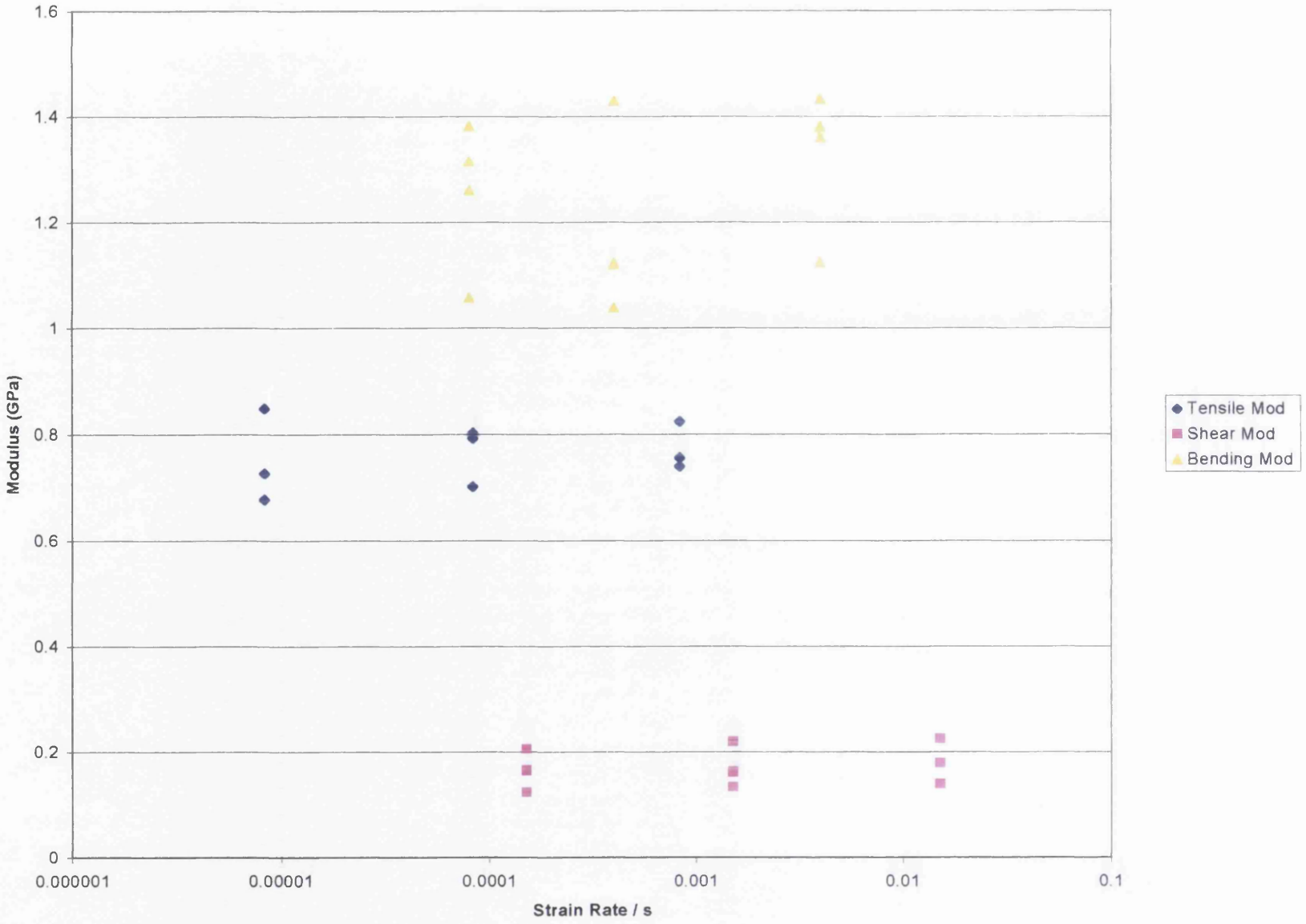

Figure 5.13 Tensile, shear and bending modulus versus rate for HDF2

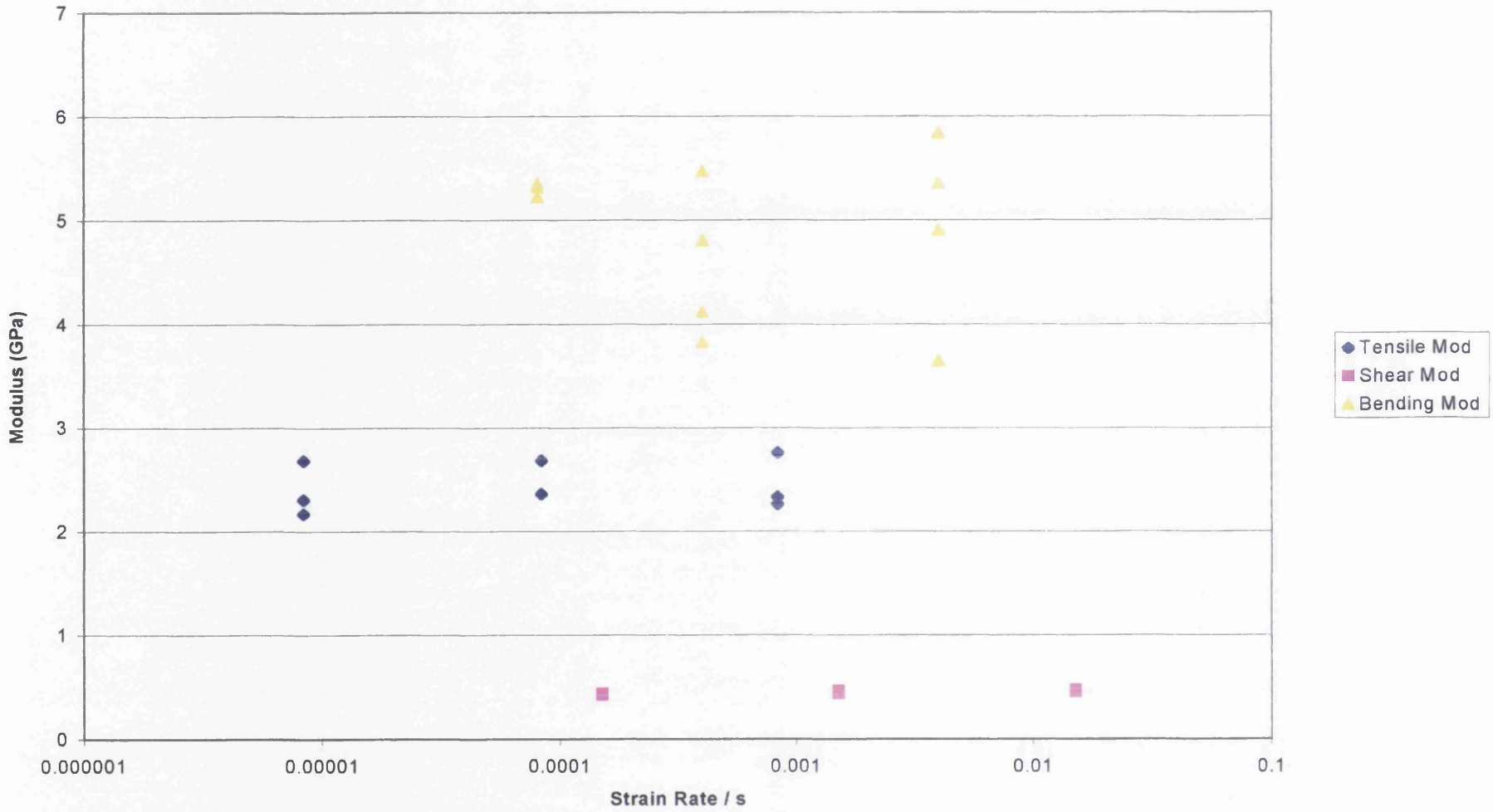

Figure 5.14 Tensile, shear and bending modulus versus rate for GF1

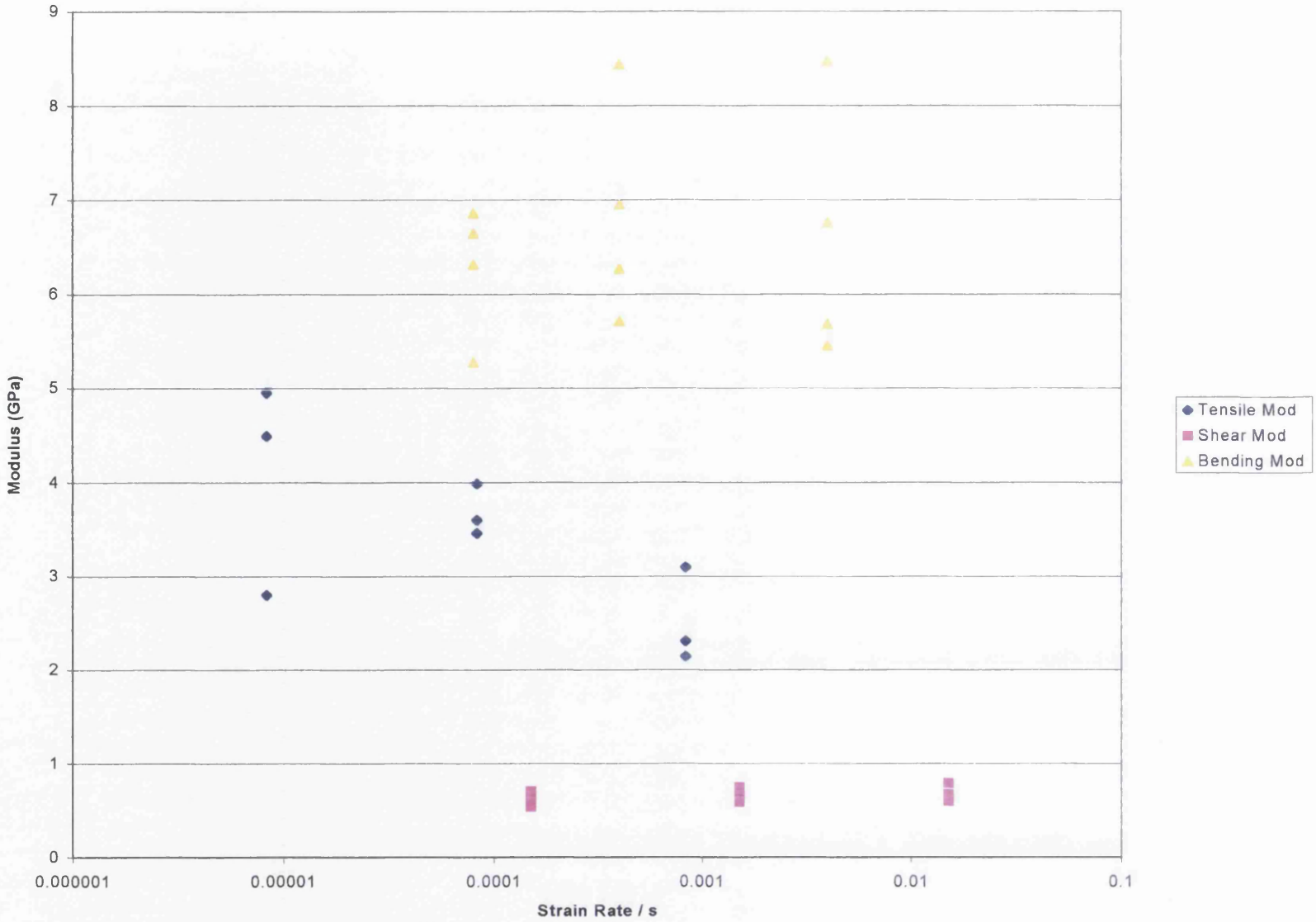

Figure 5.15 Tensile, shear and bending modulus versus rate for GF2

bending the stress and strain are not uniform throughout the sample. They are at a maximum at the edge of the sample and zero in the middle. The modulus in bending is therefore higher than in tension for the sandwich samples due to the stiffer material being on the outer edges and having a greater effect.

Looking at the High Density Foam samples first it can be seen that for both HD1 and HD2 (sandwich) the tensile and shear moduli are reduced to half that of the single HDF material. This is due to the effect of the more flexible MDF in the centre of the samples. The bending modulus, however, remains more or less the same, averaging between 1.25 and 1.3 GPa, again showing the importance of the outer layers in this geometry.

With the Glass Fibre sandwich samples there is a much more marked decrease in modulus compared to that of the single material sample. The tensile modulus for GFE is around 10 GPa, which then falls to only 2.5 GPa for both GF1 and GF2. The shear modulus shows an even greater decrease, falling from 4.5 GPa in GFE to 0.5 and 0.7 in GF1 and GF2 respectively. This time, unlike the HDF samples, the bending modulus does decrease in the sandwich structure samples. There is a large degree of scatter observed, especially at the slower rate tests. The bending modulus for GFE is between 11 and 13 GPa, whereas GF1 falls to between 4 and 6, and GF2 falls to between 5.5 and 8.5 GPa.

5.2.5 Analysis of Sandwich Structure Materials

To validate the accuracy of the tests it was decided to compare the experimental results of the four sandwich structure samples, with theoretical values based on the results of the single material samples. The idea was to see how much individual effect both the inner and outer sections had on the overall properties of the samples. If the theoretical (predicted) results matched the actual experimental results then it would be possible to calculate exactly which combination of sandwich structure would exhibit the same properties as bone.

After a series of initial trial calculations it was decided to calculate predicted values of force / displacement gradient instead of modulus. The mathematics would prove to be less complex and more accurate than if predicting modulus. So for the three testing

geometries, tensile, torsion and bending it was decided to calculate F/δ, T/θ, and F/δ, respectively.

Due to the forces experienced by a material undergoing these kind of deformations it was necessary to consider the influence of the bonding layers between the individual sandwich materials. It was unknown just how stiff these two bonding layers were and how much influence they were having on the experimental values obtained. Therefore three cases were looked at and are outlined below:

Case 1: The first treated the sandwich structure as a whole unit, where the bonding layer was completely solid and joined the two outer parts to the centre part as if it were one rigid structure, experiencing no deformation between the layers during testing.

Case 2: The second treated the structure as five individual sections that had no bonding between them. Each part being free to rotate around its own central axis. The bonding layer only added to the thickness of the sample but did not contribute to the modulus.

Case 3: The third case treated the bonding layer as being so soft that when the sample deformed, the bonding layer transferred no force to the inner MDF. Therefore these calculations only give the effect of the outer layer, and have the two bonding layers and inner MDF contributing to the thickness but not to the modulus.

A labeled diagram of the sandwich structure samples is shown below in Fig 5.16.

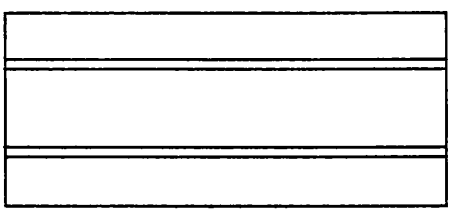

Fig 5.16 A schematic of the sandwich structure

5.2.5.1 Tension

Calculating the predicted Force/Displacement of the four sandwich samples from the single material results in the tension configuration is fairly simple. In a tension test, each individual part of the sandwich structure experiences the same degree of displacement per unit area, ie the middle part is put under the same strain as the outer parts. It is therefore possible to sum the values given by the thickness for each part of the structure.

To calculate values for the three cases, the following formulae were used:

$$E = \frac{\sigma}{\varepsilon} = \frac{F.L}{w.t.\delta} = \frac{L}{w.t}\frac{F}{\delta}$$

$$\therefore \quad \frac{F}{\delta} = \frac{w.t}{L}\mathrm{E}$$

So, for Case 1: $$\frac{F}{\delta} = \frac{w}{L}\left[E_1.t_1 + 2E_2.t_2 + 2E_3.t_3\right]$$

Case 2 is the same as Case 1.

And Case 3: $$\frac{F}{\delta} = \frac{w}{L}\left[2E_3.t_3\right]$$

The results from these calculations came out as shown in the table below in Table 5.3.

Table 5.3 The predicted and measured tensile modulus (GPa) for the sandwich samples

Sample	Case 1 (2)	Case 3	Experimental values
HD1	0.780	0.305	0.589
HD2	0.895	0.610	0.733
GF1	2.828	2.353	2.339
GF2	4.990	4.706	3.290

It can be seen that, for HD1 and 2 the experimental values fall nicely between case 1 (2) and 3. For GF1 and 2 the experimental values are a little lower than case 3. In the case of HD1 and 2 it shows that the bonding layer does transfer a lot of the force to the centre MDF layer, but not all. For GF1 and 2 these results are a little strange to say the least. The results imply that the inner MDF material makes the whole sample softer, as the experimental values are lower than those of Case 3. The only way to explain this is by assuming that the sample is not able to transfer the stress and adopts the following shape:

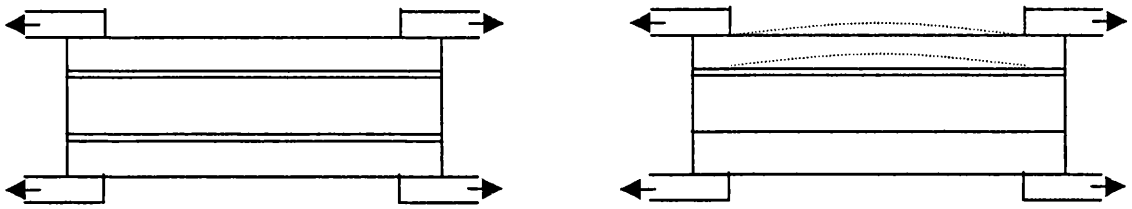

5.2.5.2 Torsion

A similar analysis was carried out on the torsion tests, using the three possible cases. Again it was decided to calculate predicted gradient (Torque/Rotation) values for the sandwich samples using the experimental values from the torsion tests of the single material samples.

For torsion testing the calculation of Torque/Rotation is as follows:

$$\frac{T}{\theta} = \frac{k.G.w.t^3}{L}$$

Once again, k can be approximated to:

$$k = \frac{1}{3}\left[1 - \frac{0.63.t}{w}\right]$$

Due to the fact that the torsion equation comprises of a t^3 function (as opposed to just a t function in tension), the maths now becomes more complex.

For Case 1, the following equation was used:

$$\frac{T}{\theta} = \frac{T}{\theta}(inner) + \frac{T}{\theta}(bonding) + \frac{T}{\theta}(outer)$$, where:

$$\frac{T}{\theta}(inner) = \frac{k_1.G_1.w.t_1^3}{L}$$ Where $k_1 = k$ with $t = t_1$

$$\frac{T}{\theta}(bonding) = \frac{T}{\theta}(bonding\ of\ thickness\ t_1 + 2t_2) - \frac{T}{\theta}(bonding\ of\ thickness\ t_1)$$

$$= \frac{k_2.G_2.w.(t_1 + 2t_2)^3}{L} - \frac{k_1.G_2.w.t_1^3}{L}$$ Where $k_2 = k$ with $t = t_1 + 2t_2$

$$\frac{T}{\theta}(outer) = \frac{T}{\theta}(outer\ of\ thickness\ t_1+2t_2+2t_3) - \frac{T}{\theta}(outer\ of\ thickness\ t_1+2t_2)$$

$$= \frac{k_3.G_3.w.(t_1 + 2t_2 + 2t_3)^3}{L} - \frac{k_2.G_3.w.(t_1 + 2t_2)^3}{L}$$ Where $k_3 = k$ with $t = t_1 + 2t_2 + 2t_3$

Therefore, the final equation for calculating Case 1 is as follows:

$$\frac{T}{\theta} = \frac{w}{l}\left[k_1.G_1.t_1^3 + k_2.G_2(t_1 + 2t_2)^3 - k_1.G_2.t_1^3 + k_3.G_3.(t_1 + 2t_2 + 2t_3)^3 - k_2.G_3(t_1 + 2t_2)^3\right]$$

Case 2

For the second part (treating the material as separate, free sections) the following equation was used:

$$\frac{T}{\theta} = \frac{T}{\theta}(inner) + 2\frac{T}{\theta}(bonding') + 2\frac{T}{\theta}(outer')$$

$$\frac{T}{\theta}(inner) = \frac{k_1.G_1.w.t_1^3}{L}$$

$$\frac{T}{\theta}(bonding') = \frac{k_4.G_2.w.t_2^3}{L}$$ Where k_4 = k with t = t_2

$$\frac{T}{\theta}(outer') = \frac{k_5.G_3.w.t_3^3}{L}$$ Where k_5 = k with t = t_3

Therefore the final equation for calculating Case 2 is as follows:

$$\frac{T}{\theta} = \frac{w}{l}\left[k_1.G_1.t_1^3 + 2k_4.G_2.t_2^3 + 2k_5.G_3.t_3^3\right]$$

Case 3

Only considering the two outer materials was calculated as follows:

$$\frac{T}{\theta} = 2\frac{T}{\theta}(outer)$$

$$\frac{T}{\theta} = \frac{2k_5.G_3.w.t_3^3}{L}$$

The results of both sets of calculations can be seen in the table below (Table 5.4), as well as the actual experimental values (Nm/deg).

Table 5.4 The predicted and measured torsional modulus for the sandwich samples

Sample	Case1	Case2	Case3	Experimental
HD1	4.55	1.356	0.038	3.207
HD2	5.82	0.616	0.291	2.138
GF1	29.29	1.650	0.333	5.939
GF2	47.86	2.841	2.516	8.316

It can be seen from the table above that the predicted values when treating the samples as one rigid structure (Case 1) are higher than those produced experimentally. In contrast, when treating the samples as free-to-move, individual sections (as in Case 2) the predicted values are lower than the experimental ones. Also, it can be seen that all Case 3 values are very low. They are too low to be considered realistic in these tests. All experimental values fall somewhere between Cases 1 and 2.

It is interesting to see that Case 2 predicts HD1 will be stiffer than HD2. This would not be thought of as being realistic on first thought, but it was what was found experimentally too. A reason for this can be attributed to the following:

As you move from HD1 to HD2 the HDF outer layer becomes thicker, and the inner MDF layer becomes thinner, ie the outer parts gain rigidity and the centre part loses rigidity. As the rigidity is proportional to the thickness cubed, the centre losing rigidity becomes more significant than the outer gaining it. The difference between the modulus of MDF and HDF is not that great, so the above effects will be significant. However, these effects are not seen between GF1 and GF2 due to the much bigger modulus difference between MDF and GFE. The GFE modulus is much larger so the outer parts of the structure will have the greater effect.

5.2.5.3 Bending

Once again, predictions for the theoretical outcome of sandwich structure tests in bending were calculated using the values obtained from experiments using the single material samples. As with torsion, the gradient of the bending tests was the value to be calculated and then compared. This time the gradient was for Force/Displacement.

The following equation was used:

$$E = \frac{F.L^3}{4.w.t^3.\delta} \qquad \text{and rearranged to:} \qquad \frac{F}{\delta} = \frac{4.w.t^3.E}{L^3}$$

Case 1:

$$\frac{F}{\delta} = \frac{F}{\delta}(inner) + \frac{F}{\delta}(bending) + \frac{F}{\delta}(outer)$$

$$\frac{F}{\delta}(inner) = \frac{4.w}{L^3} t_1^3 .E_1$$

$$\frac{F}{\delta}(bending) = \frac{4.w}{L^3}\left[(t_1 + 2t_2)^3 E_2 - t_1^3 E_2\right]$$

$$\frac{F}{\delta}(outer) = \frac{4.w}{L^3}\left[(t_1 + 2t_2 + 2t_3)^3 E_3 - (t_1 + 2t_2)^3 E_3\right]$$

Therefore, by amalgamating these the three equations, the final formula for Case 1 is:

$$\frac{F}{\delta} = \frac{4.w}{L^3}\left[t_1^3 .E_1 + (t_1 + 2t_2)^3 E_2 - t_1^3 .E_2 + (t_1 + 2t_2 + 2t_3)^3 E_3 - (t_1 + 2t_2)^3 E^3\right]$$

Case 2:

$$\frac{F}{\delta} = \frac{F}{\delta}(inner) + 2\frac{F}{\delta}(bending') + 2\frac{F}{\delta}(outer')$$

So,

$$\frac{F}{\delta} = \frac{4.w}{L^3}\left[t_1^3 .E_1 + 2.t_2^3 .E_2 + 2.t_3^3 .E_3\right]$$

Case 3:

$$\frac{F}{\delta} = 2\frac{F}{\delta}(outer)$$

So,

$$\frac{F}{\delta} = \frac{4.w}{L^3}.2t^3 .E_3$$

Table 5.5 below shows both predicted and experimental results for F/d values.

Table 5.5 Predicted and measured force / displacement gradients for bending tests on sandwich materials (kN/mm).

Sample	Case 1	Case 2	Case 3	Experimental
HD1	0.02658	0.00494	0.000128	0.03187
HD2	0.03458	0.00207	0.001030	0.03075
GF1	0.1970	0.00594	0.001130	0.12120
GF2	0.2972	0.01010	0.009060	0.16120

Here it can be seen that, in the case of all but HD1, the predicted values for F/d again fall between Cases 1 and 2. The HD samples are closer to Case 1, with HD1 even being higher. The reason for this is that the bonding layer has a finite stiffness, and in the above analysis it was assumed to have zero stiffness.

HD2 is closer to Case 1 as, due to the lower forces involved in testing, the bonding layer is able to transmit the forces better. GF1 and 2 still fall between Cases 1 and 2, but are closer to Case 2 than HD1 and HD2. In contrast to HD1 and 2, there are greater forces involved in the GF1 and 2 tests, and the bonding layer is unable to transmit the forces as well.

Again, as found with torsion, Case 2 predicts that HD2 will be less than HD1, which is also found experimentally.

5.2.5.4 Bending Strength Predictions

In bending the point of first fracture is at the point of maximum stress of the material. The material will fail when the strain at that point reaches the failure strain of the material, regardless of the thickness. Even though the sandwich structure has a soft core, it is the outer surface (in this case the bottom surface) that will fail first. When this happens, the crack will propagate throughout the rest of the sample.

Using the strain to failure (ε_f) of the single (outer) material samples it is possible to predict the bending strength of the thicker sandwich structure materials.

To do this the following equation was used:

$$\varepsilon_{max} = \frac{6.\delta.t}{L^2}$$

For Case 1, with complete bonding, failure occurs when $\varepsilon_{max} = \varepsilon_f$ *(outer material)*, therefore:

$$\delta = \frac{L^2 \varepsilon_f (outer)}{6.t}$$

So the failure strain and deflection are independent of the make-up of the sandwich. HD1 and HD2 would have the same δ_f, as would GF1 and GF2.

For Case 2 where there is no bonding between layers, the strain in the outer material is independent of the rest of the material, so:

$$\varepsilon_{max} = \frac{6.\delta.t_3}{L^2}$$

Again, failure occurs when $\varepsilon_{max} = \varepsilon_f$ *(outer material)*, therefore:

$$\delta = \frac{L^2 \varepsilon_f (outer)}{6.t_3}$$

Case 3 is the same as Case 2.

Table 5.6, below, shows the experimental and predicted values for failure deflections.

Table 5.6 The predicted and experimental values of deflection to failure (mm) for bending tests of the sandwich materials.

Sample	Case 1	Case 2	Experimental
HD1	6.197	52.67	6.37
HD2	6.197	26.33	8.314
GF1	1.659	14.10	1.92
GF2	1.659	7.05	2.216

It can be seen from these results that the Case 2 situation gives overly large predictions, showing that the situation is much closer to Case 1. Case 1 predicts the failure deflection is independent of the relative thickness of inner and outer layers, which is not quite the case. There is obviously some incomplete force transfer across the bonding layer.

It is also possible to calculate the failure forces using the force / displacement predictions for Case 1 or Case 2 appropriately. These are shown in Table 5.7, below (Forces in N).

Table 5.7 The predicted and measured force to failure (N) for bending tests with the sandwich materials.

Sample	Case 1	Case 2	Experimental
HD1	165	26	170
HD2	214	54	156
GF1	327	84	212
GF2	493	71	323

Once again, the values lie between those predicted for Case 1 and Case 2, slightly nearer to Case 1. As with some of the stiffness results, the Case 2 situation predicts that HD1 should be stronger than HD2, as is indeed seen experimentally.

5.3 DESIGNING A BONE SIMULANT

It is clear that neither the Synbone or the Sawbone sample realistically mimic the properties of bone (human skull or bovine scapulae). Despite this, the results with the sandwich materials of the Sawbones show that it should be possible to tailor the properties to match those of bone samples.

The rate dependence is a feature over which it is difficult to have much control; such behaviour is linked to the inherent viscoelastic nature of the material. The modulus and strength of glass fibre epoxy and the polyurethane foams have a slightly lower rate-dependence than is seen with bone samples. The Poisson's ratio also tends to be slightly

lower. As these rate-dependencies are all quite low, the difference between these should not give too much cause for concern. It will be far more important to match the absolute value of stiffness, strength and if possible, thickness.

For the following analysis, the desired properties for a bone simulant are calculated for a strain rate of $1s^{-1}$, which is higher than anything tested, but is realistic to the practical situation. At this strain rate, the following values are required (from tests on bovine scapulae):

Thickness	5 mm
Bending modulus	8.7 GPa
Stress to failure	180 MPa
Strain to failure	2 %.

The bending modulus will be the most important stiffness value that needs to be matched.

The other assumption is to decide whether Case 1 or Case 2 force transfer is appropriate. It will be best to assume that Case 1 applies, with material that has no bonding layer. Certainly, a realistic bone simulant would have to have good bonding between the layers without the need for a bonding layer. For this reason, Case 1 situation with no bonding layer was used for the calculation below.

In this case, the bending modulus is given by:

$$E = \frac{1}{5^3}\left[t_1^3 E_1 + 5^3 E_2 - t_1^3 E_2\right]$$

Where E_1 is the modulus of the inner layer of thickness t_1 and E_2 is the modulus of the outer layers, each of thickness t_2. Using the values of 0.802 GPa and 11.8 GPa for the stiffness of HDF and GFE respectively, it is possible to calculate that t_1 should equal 3.28 mm and t_2 equal 0.86 mm.

The failure strain and hence failure strength will be determined solely by the failure strain of the outer material. For the Case 1 situation, it will be necessary to have the outer

material with the same failure strain as that of the bone samples (1-2%). The failure strain of the GFE material is just over 1%, which is slightly too low. This means that with this material, it will be difficult to obtain exactly the same failure conditions with the same thickness. It would be possible to adjust the material thickness to give the same bending force, but this is not the most desirable option. A better route would be to use a composite with lower glass fibre content for the outer layer. This would give a higher failure strain, and although it would also have a lower stiffness, this could be accommodated by using a larger thickness for the outer layer.

In conclusion, the results and analysis above have shown that neither Synbones nor Sawbones provides a realistic simulant material at present. Despite this, it would be fairly straight-forward to tailor a combination of fibre composite outer and foamed inner to give the required properties. To do this, a tougher fibre composite would be needed than was used for the Sawbones samples.

CHAPTER 6 ENERGY ATTENUATING BATON CONCEPTS

The final part of this study was a brief investigation into the possible structures, design and manufacturing options for the next generation baton round. Also a series of tests were conducted to find the properties of some trial 'energy-attenuating' rounds, which comprised a two-layer polyurethane structure with a hard back end and a softer front end.

6.1 NEXT GENERATION BATON ROUNDS

6.1.1 Introduction

The main aim of producing energy-attenuating rounds must be to reduce the injury potential of a head impact without compromising accuracy. For good firing accuracy, the section of the round that is loaded on impact (end and sides) should be fairly rigid. This will tend to give more injurious head impacts, and so the aim of this work should be to address methods of producing a round that is rigid at the back, but less rigid at the front.

The first method of achieving this will involve slowing down the impact (eg by the use of a softer front end). This will give longer times of impact, and hence lower peak forces. Assuming the baton behaves in a reasonably elastic manner, the total energy and momentum transmitted to the target will be unchanged.

The second involves the baton actively absorbing some energy (eg by permanently deformable crush zones, squirting gel etc). This will reduce the energy and momentum transmitted to the target, as well as slowing the impact and reducing the peak forces.

It is generally thought that the peak forces are most important in determining the impact severity in terms of injury-potential. What factor provides an effective deterrent is less clear. It is possible that the "stopping power" of a round may be determined by peak force, momentum or energy transfer.

Ideally, what would be required is a round that behaves in a similar manner to L5A6 and XL21 rounds if impact occurs to the abdomen; but the energy/force reducing system would come into play if impact occurs to a harder part of the body (chest and especially head).

6.1.2 Composite Design

The basis behind this round is that there is a softer front end, attached to a more rigid back end. This would produce lower peak forces, without changing total momentum or energy transfer. As such, it would certainly achieve the desired aim, at least partially, and has the advantage of simplicity. By using a front-end stiffness of about 5-10 MPa, impacts to the abdomen would be much the same and head impact severity reduced.

There are various methods of achieving this.

i) One option involves a graded stiffness, however this would not be the best way of achieving back-end rigidity and front-end softness. There are likely to be regions in the middle where the properties are not ideal. It would also add complexity to the manufacturing process.

ii) A true composite round involving sections of different materials is more attractive. Technically, several different sections could be employed, however it was thought that a simple front/back split would prove most desirable. In order to have a high enough hardness for the front driving bands, it could require a more complex system, but this would add manufacturing difficulties.

6.1.2.1 Manufacturing Options

i) Using thermosetting polyurethane is possible, and would involve the least change in processing from current methods. This would involve pouring a soft compound into the front of the mould, and then filling up with a harder compound. Some trial rounds were produced in this way by Marbil, which

were then assessed at Swansea. Details on these rounds and the tests carried out on them are highlighted later.

ii) Thermoplastic elastomers (TPE's). These materials are being continually developed and have many favourable manufacturing possibilities. It was thought possible to use a 2-stage injection moulding process with 2 TPE's of different hardness. This would give excellent reproducibility and rapid production, though investment costs would be higher. The bond between different grades can be made very strong and should pose no problem.

An alternative route is to use TPE's that have been developed that can be moulded directly onto thermoplastics. This would allow use of a machined back end (for example, made from LDPE), with a soft end moulded directly onto it. There were, however some concerns regarding the mouldability of TPE's into thick sections. After making enquiries it proved to be unrealistic due to the baton round thickness.

iii) Mechanical assembly. Methods could be devised where a soft polyurethane front end is mechanically fixed to a harder (polyurethane or thermoplastic) back end. This was considered least attractive as it would involve additional manufacturing steps and lead to potential for the two parts detaching on firing.

6.1.3 Crush Zones

There are potentially two variants to this concept. The first would involve an internal cavity (of air or a soft material) that deforms elastically on impact. This would act in a similar manner to the soft front end. The second, true crush zone would use a region that deforms permanently on impact, and would reduce impact energy and momentum as well as peak force. As above, a single crush zone would be sufficient and require least manufacturing steps.

Manufacture may have to involve the crush zone being incorporated as an insert during moulding. This is possible, but difficult, especially as exact axiallity would be needed for aerodynamic stability. A slightly easier compromise would be to have the crush zone extend to the front of the round, so it could be more easily fitted in the mould.

Producing an internally foamed structure is theoretically possible, but would require great control to ensure axial symmetry. There were doubts as to whether this is achievable.

Another option, again using mechanical assembly could use a moulded tube, partially filled with crushable material (or air), with a screwed central part inserted to close the round and provide the back-end rigidity.

6.1.4 Expanding Ogive

The expanding ogive concept could be added to the idea of a soft front end or a crush zone. I.e. either of these could be designed to expand on impact and thereby increase impact area and hence reduce peak force. Manufacturing issues and complexity would be similar to the two above methods, although some extra development work would be needed to determine the optimum geometry. In particular, it would be important to ensure that there was no annular impact from the harder material around the outside of the ogive.

6.1.5 Liquid Gel

This approach would reduce the impact energy as well as the peak force. It can be viewed as the next stage from a crush-zone idea. It also has potential advantages with possible use of staining liquids, etc. Manufacturing issues are similar to the crush zone idea, using either an insert, or a tube to be filled and mechanically assembled. One important aspect here would be ensuring that the liquid capsule burst at appropriate loads. If the capsule did not burst, the round would be as injurious as current designs, however it must be ensured that bursting did not occur on firing.

6.1.6 Quarter-Round

This is an intriguing idea, using a system that splits into four sections at appropriate loads. Moulding in polyurethane, TPE or other materials would be relatively simple. It was suggested that a tie-system at the rear of the round could be used that breaks when the round impacts a target. This tie could have small lugs that insert into holes in the back of the round.

The key issue to be addressed with the tie system would be ensuring that it broke consistently on impact, but not on firing. This should be possible with careful choice of material.

One concern with the design is that it will have 4 points on the front that could be injurious. Also, as the round splits, there is potential for pinching between the four parts. A careful look at the design could address these points.

6.2 INVESTIGATION INTO ENERGY ATTENUATING SOFT-NOSE ROUNDS

6.2.1 Introduction

These were a new type of experimental baton produced by Marbil. The bulk of the material, including the centre and rear driving bands were made of a polyurethane with an IRHD hardness of 92-95. The front end and the front driving band was made from a different polyurethane with an IRHD value of 75-80. The idea behind this was that the rear of the baton will have suitable hardness for a snug fit in the barrel, more precise biting of rifling grooves inside the barrel and suitable level of accuracy. To complement the baton round criteria, the front of the round must be soft enough so as not to cause excessive levels of injury on impact.

A series of experiments was designed and carried out to assess the quality and suitability of these soft-nosed rounds. Firstly, a selection of the rounds were sectioned and examined for voids. This was done visually.

Compression tests were carried out on the nose section, the body section, and the whole round. The whole round tests were identical to those mentioned above. The nose and body tests were performed in the same manner but allowances had to be made for the overall displacement of each section. Therefore the 6mm displacement of the whole round was divided proportionately to the size of the nose and body sections.

Thermal expansion tests were carried out on the nose and body sections using the DMTA. This time the specimens were tested in compression, using creep mode, with a 0.1N static force.

Tension tests were used to determine the interface strength between the nose and body sections. This was carried out on an Instron electromechanical testing machine at room temperature.

Photographs of various sections of the soft nose rounds were taken using digital camera equipment.

6.2.2 Compression Tests

Compression tests, identical to those carried out on the whole round samples, were repeated for the nose and body parts of the soft-nose rounds. From the results of the tests, modulus values could be calculated for both nose and body areas. These were then used to compare with the modulus values of the whole round samples. The results from these tests can be seen below in Table 6.1.

Table 6.1 Compressive stiffness of the soft-nosed rounds.

Sample	Rate (mm/min)	Modulus (MPa)
Soft nose TOP	0.5	7.34
	5	7.83
	50	8.37
Soft nose BOTTOM	0.5	34.58
	5	36.58
	50	38.28
Soft nose WHOLE	0.5	16.75
	5	16.85
	50	17.66

It is clear that the calculated modulus values for the top part of the round are around 4.5 times smaller than those for the bottom part, (7.5 MPa, compared to 36.5 MPa). The modulus values for the whole round fall at around 17 MPa, which is almost twice that of the values for the top part, and almost half that of the values for the bottom part. However, using a mathematical model based on the compression stress, the length, and modulus of both front and rear sections it was possible to predict the value for the whole round. This turned out to be an accurate prediction.

It is also clear from Table 6.1 that as the rate increases, the modulus also increases. The modulus increases for the top and whole round samples are relatively small when compared to the effect of rate on the body section. Over the range of 0.5 to 50 mm/min loading rate both front and whole round samples increase on modulus by around 1 MPa. This compares with the rear sample, which increases by 2 MPa per rate change, i.e by 4 MPa over the whole range. Even though the values of modulus for the rear part are much higher than the other two samples, the effects of rate would not be expected to be so severe.

Even though the rear section was more significantly affected by rate, it is not the part of the round that would be striking the target. It clearly does not affect the modulus increases of the whole round to any significant degree therefore was not to be considered a problem.

The most important consideration is that the front part of the round, which will be striking the target, is not as affected by rate.

6.2.3 Optical Examination

Figs 6.1 and 6.2 below show photographs of the interface of the soft-nose rounds, one cut longitudinally through the sample, and the other cut along the interface. It is clear from Fig 6.1 (showing the nose) that there are a large number of voids both in the nose of the baton, and perhaps more importantly, along the interface. Fig 6.2 (looking down on the interface) shows the voids that have formed at the interface. It is clear once again that there are a very large number of voids. Solely from visual analysis, and before any mechanical testing had been carried out, it would suggest that the processing of the baton is of poor quality and that interface strength is likely to be very weak in comparison to the rest of the round.

Figure 6.1 An end-on view of a section through the soft-nosed round.

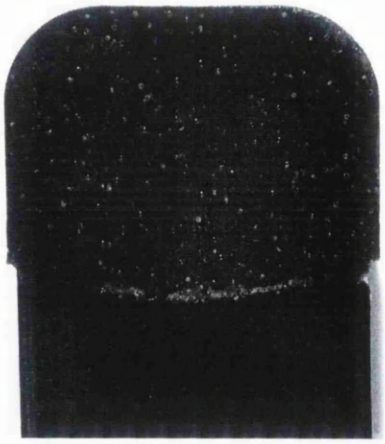

Figure 6.2 The interface section of the soft-nosed round.

The rounds were produced by pouring uncured liquid of the softer polyurethane compound into the mould, then before this had fully cured, pouring in the liquid for the harder body and rear section. The voids have formed in the nose and at the interface due to trapped air and processing gasses in the nose material. The body material was added before the gases could filter through the nose and escape. It was seen that there was more development work needed to optimise this production method. There is potential for improvement by adding the hard compound while the soft compound is still uncured, as long as significant mixing could be prevented. There will be a balance between early pouring of the second polyurethane (to prevent voids at the interface) and delayed pouring (to prevent excessive mixing of the two compounds.

From Fig 6.1, the smooth and shiny surface of the edge of the interface implies that the two materials did not mix at all, leading to a weak bond across the interface. In fact, the interface strength was so low that it was possible to tear the baton apart with bare hands. This is clearly unacceptable for use in the field.

6.2.4 Tensile Tests

Tensile tests were carried out to assess interface strength. Ideally, the round would have a strong enough interface so that it would either take a very large force to break, or, preferably, the interface would not be the central area of weakness, and the specimens would tear at a point at another part of the test piece.

It was found that the interface strength was less than 2 MPa. This is not sufficient to ensure safe use of these rounds. It is possible that the forces of firing may be enough to cause the round to split, even inside the barrel. Certainly, on impact, there is a definite probability that some of the rounds would come apart, which is obviously unacceptable.

6.2.5 Thermal Expansion

Thermal expansion tests were performed on the top and bottom sections of the soft-nosed rounds as described above. Due to the small sample size, it was not possible to test the whole round. The values are shown below.

Specimen	Thermal Expansion Coefficient / °C
Soft nose (top)	123×10^{-6}
Soft nose (btm)	180×10^{-6}

The value of the bottom section compares well with the previous tests on similar polyurethanes. The softer section has a significantly lower value. It is not known whether this difference would cause problems in service, but should be considered.

6.2.6 Summary

Studies on a prototype soft-nosed round have shown that the stiffness of the front section is significantly lower than the back section, as desired. It was also shown that the stiffness of the round as a whole does not increase as markedly with rate as the harder compound

does. The major problem with these rounds was the presence of large numbers of voids at the interface between the two sections, leading to a very weak interfacial strength. Further development is needed with these rounds to address this point.

6.3 CALCULATION OF IMPACT FORCES FROM COMPOSITE ROUNDS

It was identified above that some more information was needed on soft-nosed baton systems; particularly, how much reduction in impact forces could be achieved with certain thicknesses of softer material. To this end, an analysis method has been developed as described below. It should be emphasised that this is a simple approximation, which gives a good indication of the effects of composite rounds, but should not be used for detailed design purposes. For this, a full (finite element) analysis incorporating geometry changes and pressure waves would be needed.

The basis behind this analysis is as follows:

- The aim is to produce force / time profiles during an impact for rounds with composite stiffness (up to four separate sections can be considered).
- Assume the target is completely rigid.
- Assume the force is maximum at the front of the round and varies linearly to zero at the back of the round. This is a reasonable approximation that allows simpler analysis.
- Pressure waves and lateral expansion of the round are neglected.

A computer programme was developed that determines the force / time profile by:

1) Calculating the position of the centre of gravity of the round from equations of motion.
2) Calculating the strain profile through the round at this new position.
3) Calculating the force at the front of the round from this.
4) Repeating this process in time intervals of 1 microsecond until the impact is complete.

Initially, strain-independent modulus values were used. This gave unrealistic situations where the compressive strain became greater than 1. To counter this, a strain-dependent modulus profile was used. Rather than measure this for the different polyurethane grades, a typical response was used, which approximates to real behaviour, but is mathematically simple. The following stress / strain formula was used :

$$\varepsilon = \frac{\sigma}{E + \sigma}$$

Therefore, when the strain is small, $\sigma << E$ and so the modulus equals E. When the strain is large, $\sigma >> E$ and the modulus approaches infinity (with a maximum allowable strain of 1).

This gave much more realistic results, but gave some unexpectedly sharp force-time profiles for very soft rounds. For modulus values of greater than 5 MPa, this was not a feature. It also led to an increase in programme time, as an iteration step was needed, and so the time-interval was changed to 5 microseconds with no loss of accuracy.
Figure 6.3 below shows the variation of modulus with strain.

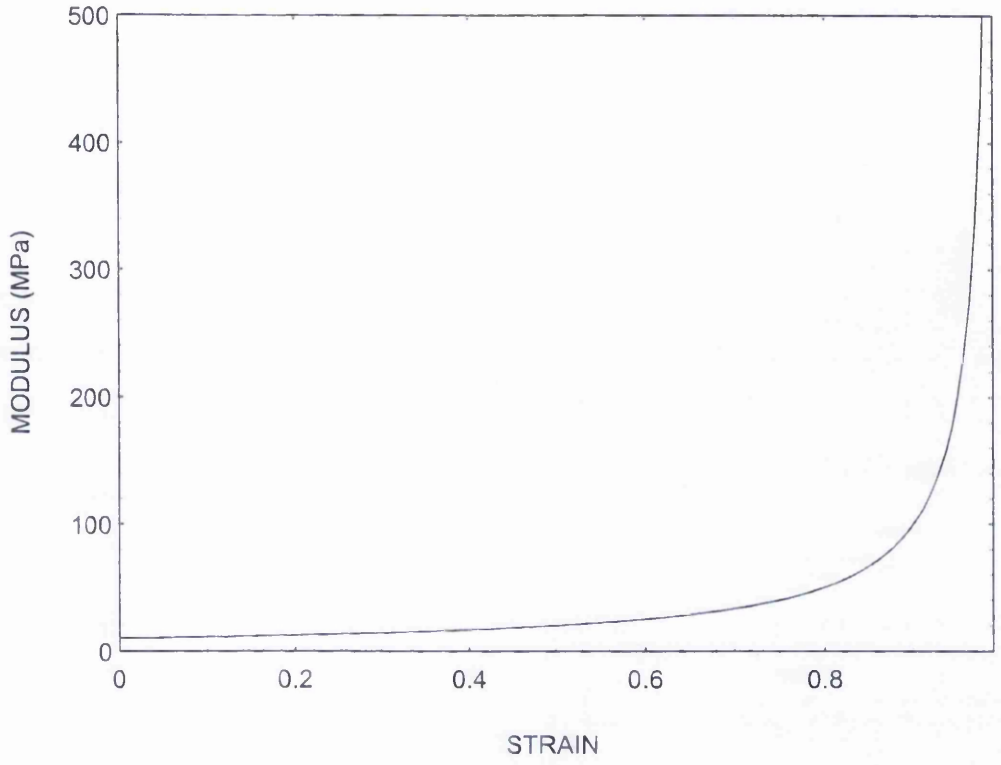

Figure 6.3 The variation of compressive modulus with compressive strain used for modelling composite rounds

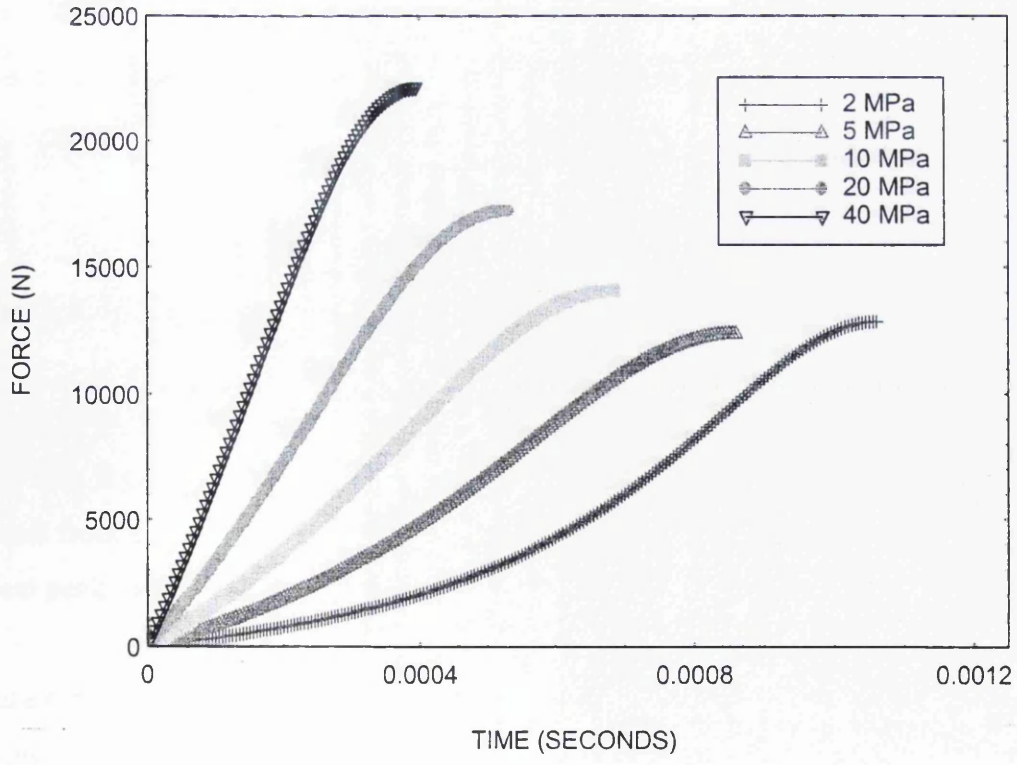

Figure 6.4 The variation of force with time for constant modulus rounds

Figure 6.4 shows the force / time curves for rounds of constant modulus, with an impact velocity of 50 m/s. It can be seen from this that the impact times and peak forces are sensible, but that with the softest round (2 MPa), the degree of compression is such that a significant degree of sharpening is seen.

Figure 6.5 shows the effect of combining two stiffnesses, in this case a soft front end of 5 MPa and a hard back end of 40 MPa. The length of the soft front end has been varied from 0 to 100 mm (full length).

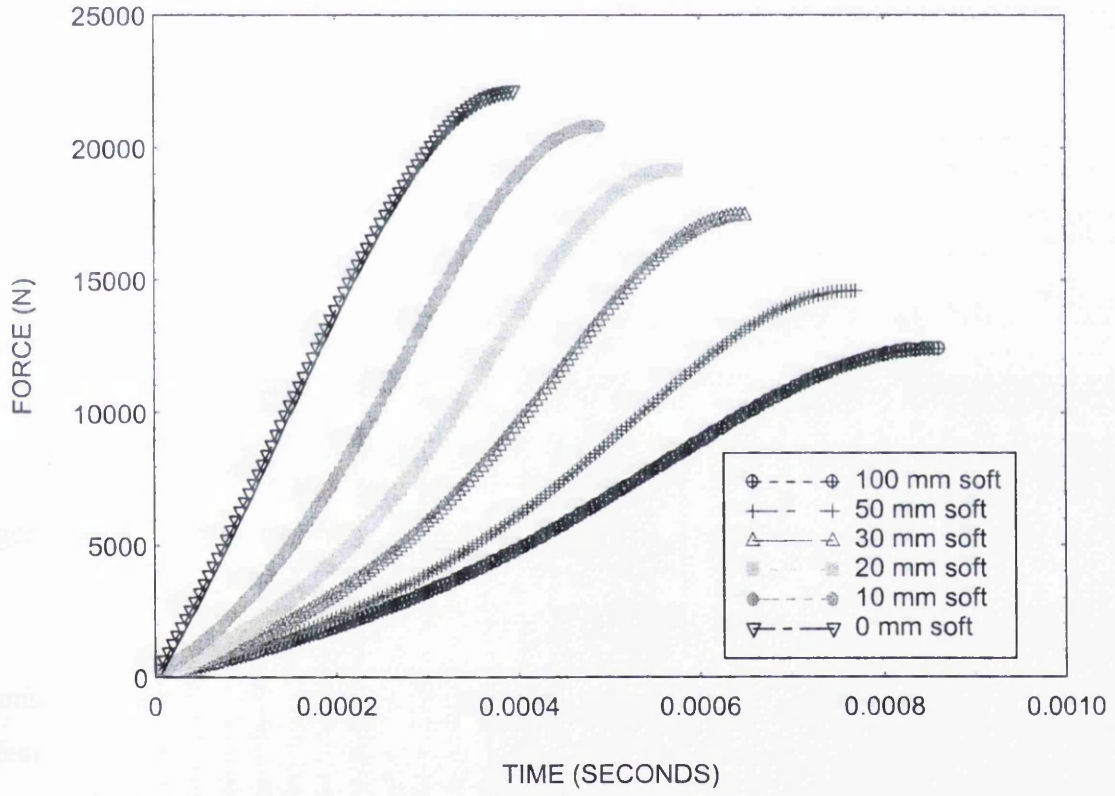

Figure 6.5 The variation of force with time for rounds with soft sections of various lengths

From this, it can be seen that there is a fairly steady reduction in peak force as the size of the soft front end increases. It should be noted that with an impact velocity of 50 m/s, the lowest peak force theoretically achievable would be 5000 N.

Figure 6.6 shows results for a more complex round geometry. This assumes that the front driving bands must be hard. Therefore there is a soft front 10 mm. The next 20 mm is

hard. The rear 30 mm is also hard. The remaining 40 mm just behind the centre is then free to be altered. Figure 6.6 shows the effects of how much of this section is soft.

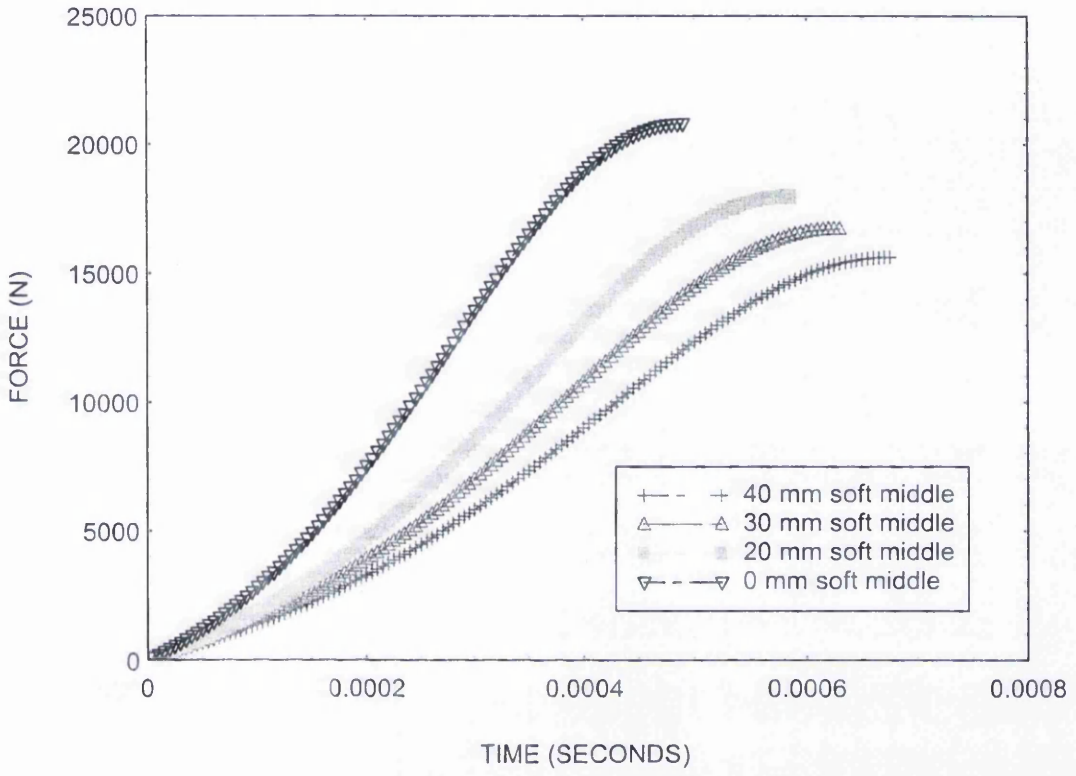

Figure 6.6 The force / time behaviour for rounds with various sized soft middle sections.

From this, it can be seen that the soft middle section does have a significant beneficial effect, with a 40 mm section reducing peak force from over 22 kN to about 15.5 kN.

Figure 6.7 shows the effect of impact velocity on some of the rounds. Round 1 is a constant modulus 40 MPa round. Round 2 has a soft front 10 mm (of 5 MPa). Round 3 has a soft front 10 mm, then a hard 20 mm section, then a soft 40 mm section and a hard 30 mm back end. From this it can be seen that the peak force drops with impact velocity, but slightly more steeply for round 3 (and a little for round 2). This shows that with lower velocities, the stiffening of soft sections due to large compressions occurs less, giving a greater drop in peak force.

From all of the results, it can be seen that there is considerable scope for reducing peak force with soft sections; and that a soft section in the middle of the round does have an

important effect. The analysis method used above has scope for assessing the detailed effects of these changes. Obviously, not all possible variations have been assessed here, for instance the modulus of the soft and hard sections have remained fixed. The analysis method would allow the effects of these detailed changes to be studied.

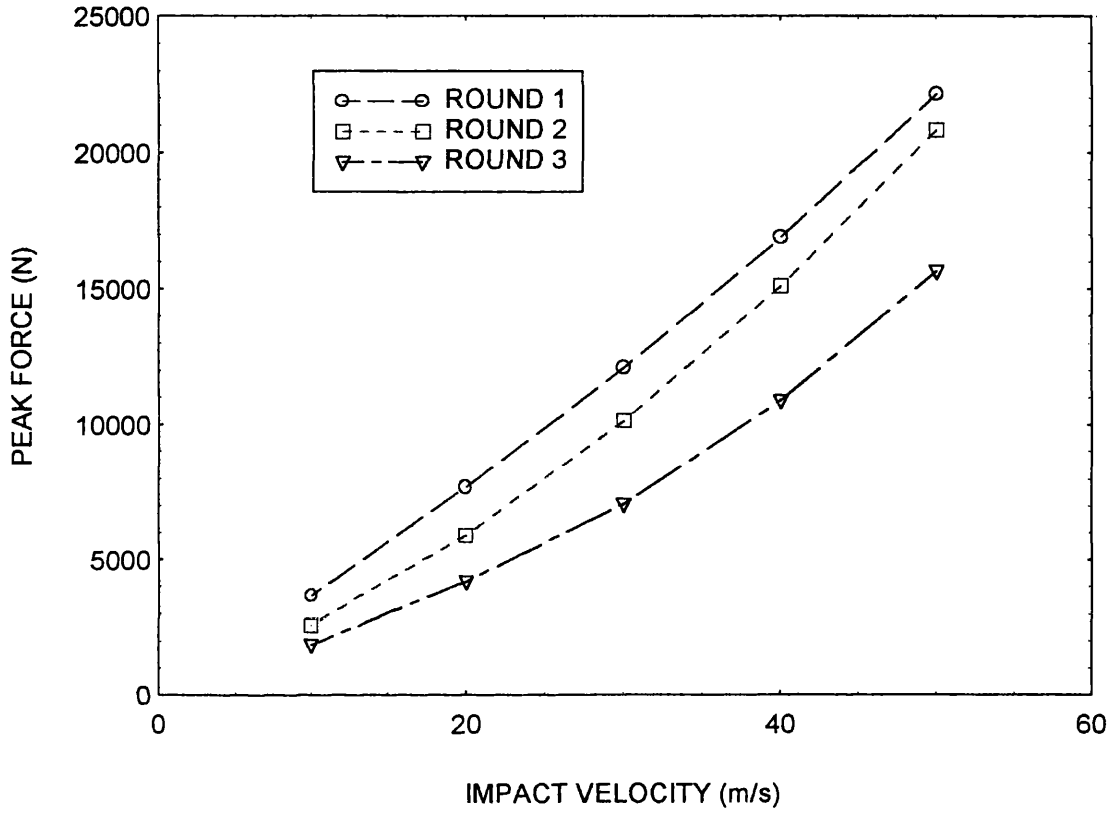

Figure 6.7 The effects of impact velocity on the force / time profiles of the composite rounds

CHAPTER 7 CONCLUSIONS AND FURTHER WORK

- From previous studies Polyurethane has been identified as the most suitable all-round material with which to produce baton rounds. This study furthered this work and identified required properties of the rounds such as stiffness and rebound resilience.

- Rebound resilience is an important property. As rate increases all polyurethanes become stiffer. It was seen that rounds tested with high rebound resilience showed least effects of increased stiffness with rate, whereas some rounds with low rebound resilience produced unacceptably high levels of stiffness at fast rates.

- Rebound resilience did not vary depending on polyurethane type. Therefore any of the polyurethanes tested were acceptable as long as they had high resilience.

- The glass transition temperature can be used as a guide to measure if a material has high or low resilience. Low glass transition temperatures (ie further away from room temperature) will generally give higher resilience.

- Infra red analysis was successful in picking up uncured NCO in the L5A6 rounds which lead to surface hardening. This testing was included as part of the quality control of subsequent L5A7 polyester-based rounds. No NCO was found in the newer XL21 rounds, which were polyether-based.

- Environmental exposure to high temperatures, UV radiation and water immersion produced only slight changes in properties of all polyurethanes tested. These rounds were considered stable and able to be stored for reasonable lengths of time with confidence.

- Thermal expansion tests showed fairly high levels of thermal expansion - in the range 180 to 200 x 10^{-6}. It was thought this may introduce some problems on firing, with increased round-barrel friction at high temperature, but little could be done to reduce the values.

- Following a literature review on bone properties it was possible to assume with reasonable confidence the typical mechanical properties of the human skull.

- It was seen from the literature review and the re-analysis of David Taylor's research that as the sample thickness increased the strength was reduced. This was explained by the thicker samples generally containing the same thickness of cortical bone as the thinner samples, but a greater degree of cancellous bone in the centre. The cancellous bone caused an overall decrease in strength with thickness.

- The thickness of dry bovine scapulae and dry human skull was found to be similar (approximately 4mm).

- Strength values for dry scapulae were found to be higher than dry skull, but the modulus was similar. The strength differences showed that a baton round impact was more likely to cause fracture of the skull than the scapulae. Therefore the scapulae model slightly underestimated the severity of impacts that would be sustained to the human skull.

- No results on wet human skull were available, but the results of dry samples showed that the thickness, strength and stiffness values of bovine scapulae were sufficiently similar to skull.

- A lack of information on the shear modulus of bone was highlighted. This was an important property to be aware of for computer modelling purposes, so a review of methods to obtain shear modulus was conducted. This showed that torsion testing was the most appropriate method and gave shear modulus values of 2 - 3 GPa.

- Testing on strip samples of bovine scapulae showed that both tensile and bending modulus values agreed with previous tests by other workers (5 - 10 GPa). Rate effects were similar too with exponents of 0.03 to 0.04.

- Few previous studies looked at Poisson's Ratio but those that did gave values similar to the tests in this study of 0.29 to 0.36.

- Failure stresses from the bending tests also agreed with the results of David Taylor of 110 MPa. In these tests they proved to be 110 to 130 MPa.

- It was decided to use biaxial disc tests partly to assess the effects of biaxial testing and also to provide data that could be used to validate finite element modelling. These showed that the effects of rate were important, with a complex inter-relationship between the effects on the stiffness and strength.

- The disc tests showed a variety of fracture mechanisms, that to some extent mirror those seen on bullock scapula impact tests.

- A range of synthetic materials have been assessed with the aim of designing a synthetic bone simulant for impact trials. Of the commercial materials tested, those produced by Synbones showed most promise. These consisted of a sandwich structure of polyurethane foam and glass reinforced epoxy.

- An analysis of the behaviour of these sandwich samples indicated how a simulant material could be tailored to mirror the mechanical properties of bone. This could be achieved with outer layers of glass reinforced epoxy (with a lower glass content) and an inner core of medium density polyurethane foam.

- Various energy attenuating baton-round concepts have been examined. The simplest of these comprises a combination of soft and hard polyurethanes. A simple numerical model showed that the peak forces with such rounds would be considerably lower.

- An experimental analysis of some prototype rounds with soft and hard sections showed that the mechanical properties could be predicted fairly well from the constituent materials, however it was found that the integrity of the interface between the two layers was critical.

Future Work

This project has addressed several important issues relating to the design and testing of baton rounds, many of which have been taken up within design specifications. Much of the early work focussed on the XL21 round, which is now in service. The major areas of work that could be extended relate to improved testing of baton rounds and the next generation of rounds that will incorporate some energy attenuating systems to make head impacts less injurious.

The developments in baton round testing will certainly include greater use of finite element modelling, and the data on bone properties generated within this study are key to this. It was a shame that the modelling of the disk tests has yet to be performed as this would prove an interesting test of modelling capabilities. This should be completed within the near future.

The potential use of a synthetic bone simulant could also be extended, and the results of this work would certainly allow a material to be designed with similar mechanical properties. At present, the pressure for a synthetic replacement has been reduced (due to relaxation of the previous "beef on the bone" ban), but in future the use of synthetic material will certainly be explored.

Of the possible energy-attenuating concepts, the simplest involves a combined soft and hard sectioned round, and there is considerable scope for further work within this area. Key to this would be both the dynamic response of the two materials as well as the manufacturing method.

REFERENCES

1. "Plastic Baton Round Injuries", Sean M. Sheridan, Roy I. H-Whitlock, Northern Ireland and Maxillo-Facial Service, Ulster Hospital, Dundonald, Belfast, British Journal of Oral Surgery (1983) **21**, 259-267
2. "The Anatomy of Plastic Bullet Damage and Crowd Control", E. K. Metress, S. P. Metress, Internation Journal of Health Services, **vol 17, No 2**, 1987.
3. Extract from newspaper "An Phoblacht", Thursday 11 July 1996, Thursday 25th July 1996, Thursday 26th September 1996.
4. "Injuries Caused by Plastic Bullets Compared with those Caused by Rubber Bullets", L. Rocke, Royal Victoria Hospital, Grosvenor Road, Belfast, The Lancet, April 23rd 1983, pg 919-920.
5. "Plastic Bullets: Significant Risk of Serious Injury above the Diaphragm", A. J. Richie, Dept of Surgery, Mater Infirmorum Hospital, Belfast, UK. Injury: The British Journal of Accident Surgery, (1992), **vol 23, No 4**.
6. "Advanced Trauma Life Support: Course for Physicians - Student Manual - Committee on Trauma", American College of Surgeons, First Impression, (1993), ISBN 1-880696-01-0
7. "Anatomy and Physiology ABC of Major Trauma", D. Skinner, P. Riscol, R. Earlam. Published by: BMJ, London (1991), ISBN 0-7279-0291-1
8. "Comparison of Head Acceleration Injury Indices in Cadaver Skull Fracture", V. R. Hodgson, L. M. Thomas, Wayne State University, 15th Stapp, Car Crash Conference, Corando, CA, Nov 17-19th, (1971).
9. "Study of Protective Equipment for Baseball", United States Consumer Product Safety Commission, 4th June 1996. Release no. 96-140.
10. "Projectile Trauma: An Enquiry into Bullet Wounds", Robert Scott, Lt.Col, RAMC, University College Hospital, Surgical Thesis (1992)
11. "Mechanics of Head Injuries", A. H. S. Holbourn, University Laboratory of Physiology and Dept of Surgery, Oxford. The Lancet, Oct 9th, 1943.

13. "Human Head Dynamic Response to Side Impact by Finite Element Modelling", J. S. Ruan, T. Khali & A. I. King, Bioengineering Centre, Wayne State University, Detroit, Michigan. Journal of Biomechanical Engineering, **Vol. 113**, (1991)

14. "3-D Anatomical Brain Model for Relating Cortical Strains to Automobile Crash Loading", Dimasi et al, NHTSA, 13th International Technical Conference on Experimental Safety Vehicles, (1991)

15. "An Imaging-Based Computational and Experimental Study of Skull Fracture: Finite Element Model Development", F. A. Bandak, NHTSA, M. J. Van der Vorst, L. M. Stuhmiller, P. F. Mlakar, W. E. Chilton and J. H. Stuhmiller, Applied Science and Engineering, JAYCOR, San Diego, CA. Journal of Neurotrauma, 12, (1995).

16. "The Possible Use of Bovine Scapula as an Analogue for the Human Skull in Experimental Blunt Trauma", D. E. M. Taylor and J. S. Whammond, DERA report DERA/CBDS/MS(T)/H7T/DET (1992).

17. "The Use of Finite Element Analysis of Simulated Skull Impacts in the Assessment of Blunt Trauma". B. J. Broadhouse, AEA Technology plc, DERA internal report DERA/CBDS/MS(T)/TG9/HIMP/EMR (1995).

18 "Material Improvements for Baton Rounds." I. Roberts, University of Wales Swansea MPhil Thesis (1998).

19 "Materials Selection in Mechanical Design." M.F. Ashby, Butterworth-Heinemann, Oxford, (1995).

20 "Theory of Elasticity", S.P. Timoshenko and J.N. Goodier, McGraw-Hill, New York, (1970).

21 "Solid Polyurethane Elastomers", P. Wright and A.P.C. Cumming, McLaren, London, (1969).

22 "Plastics Materials" J.A. Brydson, Butterworth-Heinemann, Oxford, (1995).

23 "Theory and Practice of Engineering with Rubber." P.K. Freakley and A.R. Payne, Applied Science, London, (1978).

24 "Introduction to Polymer Viscoelasticity.", J.J. Aklonis, Wiley, New York, (1983).

25 "The Physics of Rubber Elasticity." L.R.G. Treloar, Clarendon, Oxford, (1958).

26 "Physical Testing of Rubbers." R.P. Brown, Applied Science, London, (1979).

27 "Viscoelastic Properties of Polymers." J.D. Ferry, Wiley, New York, (1980).

28 "Mechanical properties of cranial bone", J.H McElhaney, J.L. Fogle, J.W. Melvin, R.R. Haynes, V.L. Roberts, and M. Alem, Nabih, J. Biomechanics, (1970) **vol 3.** pp 495-511

29 "Flexure of layered cranial bone", R.P. Hubbard, J. Biomechanics, (1970) **vol 4.** pp 251-263

30 "The ultimate properties of bone tissue: the effects of yielding." A.H. Burstein, J.D. Currey, V.H. Frankel, D.T. Reilly, J. Biomechanics, (1972) **vol 5**, pp 35-44

31 "Dynamic response of bone and muscle tissue." J.H. McElhaney, J. Applied Physiology, (1966) **21 (4),** pp 1231-1236.

32 "Dynamic response of human cranial bone." J.L. Wood, J. Biomechanics, (1971) **4,** pp 1-12.

33 "The elastic and ultimate properties of compact bone tissue." D. Reilly and A.H. Burstein, J. Biomechanics, (1975) **7,** pp 393-405.

34 "Anisotropy in the dynamic non-linear viscoelastic properties of bovine compact bone." Y. Tanabe and K. Kobayashi, Journal of materials science: Materials in medicine, (1994) **5,** pp. 397-401

35 "The compressive behaviour of bone as a two-phase structure." D.R. Carter and W.C. Hayes, Journal of bone and joint surgery, (1977) **59-A, No. 7**, pp 954-962.

36 "Mechanical properties of human cancellous bone in the femoral head." C.M. Schoenfeld, E.P. Lautenschlager, and P.R. Meyer Jun, Medical and biological engineering, (1974) **6,** pp. 313-317.

37 "Bone compressive strength: The influence of density and strain rate." D.R Carter and W.C. Hayes, Science, (1976) **194,** pp 1174-1175.

38 "The deformation and fracture of rigid cellular plastics under multiaxial stress." M.R. Patel, PhD dissertation, University of California, Berkeley, (1969).

39 "Postyield behaviour of subchondral trabecular bone." W.C. Hayes and D. R. Carter, J. Biomed. Mater. Res. (1976) **10**, pp 537-544.

40 "A structural model for the mechanical behaviour of trabecular bone." J.W. Pugh, R.M. Rose, and E.L. Radin, J. Biomechanics, (1973) **6,** pp 657-670.

41 "Buckling studies of single human trabeculae." P.R. Townsend, R.M. Rose and E.L. Radin, J. Biomechanics, (1975) **8**, pp 199-201.

42 "Physical properties of trabecular bone." J. Galante, W. Rostocker and R.D. Ray, Calcif. Tissue Res., (1970) **5**, pp 236-246.

43 "Composition of trabecular and cortical bone." J.K. Gong, J.S. Arnold and S.H. Cohn, Anat. Rec. (1964) **149**, pp 325-331.

44 "The effects of geometric feedback in the development of osteoporosis." R.B. Martin, J. Biomechanics, (1972) **5**, pp 447-455.

45 "Elastic and viscoelastic properties of trabecular bone: Dependence on structure." J.W. Pugh, R.M. Rose and E.L. Radin, J. Biomechanics, (1973) **6**, pp 475- 485.

46 "Mechanical properties of cranial sutures." C.R. Jaslow, J. Biomechanics, (1990) **23**, pp 313-321.

47 "Structure and function of mammalian tendon." D.H. Elliott, Biol. Rev., (1965) **40**, 392-421.

48 "Ultimate tensile strength of fetal and adult human tendons." P.L. Blanton and N.L. Biggs, J. Biomechanics, (1970) **3**, pp 181-189.

49 "Mechanical properties of bone tissues with greatly differing functions." J.D. Currey, J. Biomechanics, (1979) **12**, pp 313-319.

50 "Some mechanical properties of goose femoral cortical bone." G.B. McAlister and D.D. Moyle, J. Biomechanics, (1983) **16**, pp 577-589.

51 "Mechanical design in organisms." S.A. Wainwright, W.D. Biggs, J. Currey and J.M. Gosline, Princeton University Press, Princeton, NJ, (1976).

52 "Biomechanics of skull fracture." N. Yoganandan, F.A. Pintar, A. Sances Jr, P.R.Walsh, C.L. Ewing, D.J. Thomas and R.G. Snyder, Journal of Neurotrauma, (1995) **12**, pp 745 – 756.

53 "Head Injuries: Mechanisms, diagnostics, and management." E.S. Gurdjian and J.E. Webster, Brown, Boston, (1958).

54 "Elastic properties of human supraorbital and mandibular bone." P.C. Dechow, G.A. Nail, C.L. Schwarz-Dabney and R.B. Ashman, American journal of physical anthropology, (1993) **90**, pp 291-306.

55 "Dynamic injury tolerances for long bones of the female upper extremity." S.M. Dumas, P.H. Schreiber, J.D. McMaster, J.R. Crandall, C.R. Bass and W.D. Pilkey, J. Anat. (1999) **194**, pp 463-471.

56 "A cumulative damage model for bone fracture." D.R. Carter and W.E. Caler, J. Orthop. Res., (1985) **3**, pp 84-90.

57 "Aging of bone tissue: Mechanical properties." A.H. Burstein, D.T. Reilly and M. Martens, J. Bone joint surg., (1976) **58**, pp 82-86.

57 "Aging of bone tissue: Mechanical properties." A.H. Burstein, D.T. Reilly and M. Martens, J. Bone joint surg., (1976) **58**, pp 82-86.

58 "The response of compact bone in tension at various strain rates." R.D. Crowninshield and M.H. Pope, Ann. Biomed. Eng., (1974) **2**, pp 217-225.

59 "Tensile testing of bone over a wide range of strain rates: Effects of strain rate, microstructure and density." T.M. Wright and W.C. Hayes, Med. Biol. Eng., (1976) **14**, pp 641-679.

60 "Strain rate and mineral content in fracture models of bone." J.D. Currey, Journal of orthopaedic research, (1988) **6,** pp 32-38.

61 "Cycle-dependent and time-dependent bone fracture with repeated loading." D.R. Carter and W.E. Caler, J. Biomech. Eng., (1983) **105**, pp 166-170.

62 "Is bone hydraulically strengthened?" S.A.V. Swanson and M.A.R. Freeman, Med. Biol. Eng., (1966) **4**, pp 433-438.

63 "Elastic and physicochemical relationships within cortical bone " S.S. Kohles and D.A. Martinez, J. Biomedical Materials Research, (1999) **49,** pp 479-488.

64 "Ultrasonic wave velocity measurement in small polymeric and cortical bone specimens" S.S. Kohles, J.R. Bowers, A.C. Vailas, R. Vanderby. Journal Of Biomechanical Engineering-Transactions of the ASME, 1997, Vol.119, No.3, pp.232-236

65 "The role of an effective isotropic tissue modulus in the elastic properties of cancellous bone", J. Kabel, B. van Rietbergen, M. Dalstra, A. Odgaard, R. Huiskes. Journal of Biomechanics, 1999, Vol.32, No.7, pp.673-680

66 "Determination of Poisson's ratio of cancellous bone", B. A. Whitson, B.M. Hillberry, D.C. VanSickle, K.D. Brandt. Journal of Investigative Medicine, 1999, Vol.47, No.2, p.A73

67 Raftopoulos, D. Katsamanis, E. Saul, F. Liu, W. Saddemi, S. An intermediate loading rate technique for the determination of mechanical properties of human femoral cortical bone. J. Biomedical Engineering, 1993, vol 15. January, pp 60-67

68 "Elastic Properties Of Human Supraorbital And Mandibular Bone." P.C. Dechow, G.A. Nail, C.L. Schwartzdabney and R.B. Ashman, American Journal of Physical Anthropology, (1993) **90,** pp 291-306.

69 "Elastic modulus and hardness of cortical and trabecular bone lamellae measured by nanoindentation in the human femur." P.K. Zysset, X.E.

70 "Mechanical And Textural Properties Of Pelvic Trabecular Bone." M. Dalstra, R. Huiskes, A. Odgaard and L. Vanerning, Journal of Biomechanics, (1993) **26,** pp 523-535.

71 "Young's moduli and shear moduli in cortical bone." H.C. Spatz, E.J. Oleary and J.F.V. Vincent, Proc. Roy. Soc. Lond. B., (1996) **263,** pp 287-294.

72 "Elastic Properties Of Human Supraorbital And Mandibular Bone." P.C. Dechow, G.A. Nail, C.L. Schwartzdabney and R.B. Ashman, American Journal of Physical Anthropology, (1993) **90,** pp 291-306.

73 "Parametric Analysis of the Disc Bend Test.", G.E. Lucas, A. Okada and M. Kiritani, J. Nuclear Materials, (1986) **141-143,** pp 532-535.

74 "Small Punch Technique for Measurement of Material Degradation of Irradiated Ferritic Alloys." X. Mao and J. Kameda, J. Materials Science, (1991) **26,** pp 2436-2440.

75 "The use of Miniature Disc Bend Tests with Plastic Materials", J.C. Arnold and J.M. Keeble, Polymer Testing, (1998) **17,** pp 597-611.

76 "An Introduction to the Mechanical Properties of Solid Polymers." I.M. Ward and D.W. Hadley, Wiley, New York, (1993) pp 116- 118.

77 "Theory of Elasticity of an Anisotropic Elastic Body", S.G. Lekhnitskii, Holden-Day, San Fransisco, (1964).

78 M.J. Folkes and R.G.C. Arridge, J. Phys. D., (1975) **8,** pp 1053-1061.

79